PERFORMANCE ENHANCEMENT OF INTEGRATED ANTENNAS USING METAMATERIALS AND CHARACTERISTIC MODE THEORY

Doctoral Thesis

Presented in partial fulfilment of the requirements

for the degree of Doctor of Philosophy

University of Lille

Faculty of Science and Technology

By

CHUKWUKA OZUEM ANTHONY

Defended on 30 November 2020

THESIS COMMITTEE

Aydin Civi OZLEM	Prof. at Middle East Technical university	-Reviewer
Halim BOUTAYEB	Prof. at Université du Québec en Outaouais (UQO)	-Reviewer
Marta CABEDO FABRÈS	Asst. Prof. at the Polytechnic University of Valencia	-Examiner
Eric LHEURETTE	Prof. at IEMN, University of Lille	-Jury President
Jean-Marie BILBAUT	Prof. at University of Burgundy	-Examiner
Divitha SEETHARAMDOO	Researcher at IFSTTAR	-Thesis Supervisor
Marion BERBINEAU	Research Director at IFSTTAR	-Thesis Director
M.Hassanein RABAH	Antenna Expert at Airspan Communication Ltd.	-Invited

AMÉLIORATION DES PERFORMANCES DES ANTENNES INTÉGRÉES À L'AIDE DE MÉTAMATÉRIAUX ET DE LA THÉORIE DES MODES CARACTÉRISTIQUES

Thèse de doctorat

Présenté dans le respect partiel des exigences

pour le diplôme de docteur en philosophie

Université de Lille

Faculté des sciences et de la technologie

par

CHUKWUKA OZUEM ANTHONY

Défendue le 30 novembre 2020

COMITÉ DE THÈSE

Aydin Civi OZLEM	Prof. at Middle East Technical university	-Rapporteure
Halim BOUTAYEB	Prof. at Université du Québec en Outaouais (UQO)	-Rapporteur
Marta CABEDO FABRÈS	Asst. Prof. at the Polytechnic University of Valencia	-Examinatrice
Eric LHEURETTE	Prof. at IEMN, University of Lille	-Président du Jury
Jean-Marie BILBAUT	Prof. at University of Burgundy	-Examinateur
Divitha SEETHARAMDOO	Researcher at IFSTTAR	-Encadrante de thèse
Marion BERBINEAU	Research Director at IFSTTAR	-Directrice de thèse
M.Hassanein RABAH	Antenna Expert at Airspan Communication Ltd.	-Invité

Abstract

The demand for miniaturized mobile wireless systems have increased the need to integrate electrically small antennas which are generally characterized by poor performances and low efficiency. Methods such as the use of dielectric, slots, parasitic components, ... have been applied over the years to enhance the performance of such antennas however, they are empirical and based on time-consuming optimisations. Other methods like antenna current optimization based on modal analysis are systematic methods which have been proposed. It has also been shown that the use of artificial materials known as metamaterial inclusions as parasitic element can help to improve antenna performance at lower cost. The choice of the right inclusion for an antenna design is complicated especially when the antenna is non-canonical and arbitrary. In this thesis, we propose a systematic method for enhancing the performance of antenna using metamaterial inclusion as a parasitic element. The method is used for designing parasitic metamaterial antenna with the potential to analyse both the radiation and scattering properties of the parasitic metamaterial design. It uses the characteristic modal method to evaluate the quantitative stored energy of metamaterial inclusions which provides quantitative information on the near-field behaviour of the inclusion. The modal stored energy method is compared to the effective parameter method for describing inclusions and they both show good qualitative agreement. In the parasitic metamaterial antenna design process, characteristic mode is applied to get an insight into the radiation properties of the structure and an inclusion is chosen to compensate the stored energy of the antenna element based on the quantity of its modal stored energy. The coupling between the antenna and the inclusion is analysed using the inter-modal coupling co-efficient. It represents the scattering between the antenna and the inclusion and defines how the positioning and separation distance between the two elements affect the overall performance of the metamaterial-inspired system. The proposed methodology is validated with a prototype that shows a good agreement between the simulated and measured result. The method is further applied in investigating the enhancement of integrated antenna using electromagnetic cloaking. The cloak couples to the passive element in its vicinity and allows the active antenna element to operate with a better radiation efficiency. The proposed method shows usefulness for future design of parasitic metamaterial systems with enhanced performance.

Key words: integrated antennas, electrically small antennas, metamaterials, inclusions, characteristic modes, electromagnetic cloaking, modal coupling, performance enhancement.

Résumé

La demande de systèmes sans fil mobiles miniaturisés a accru le besoin d'intégrer des antennes électriquement petites qui se caractérisent généralement par de mauvaises performances et un faible rendement. Des approches telles que l'utilisation de diélectriques, de fentes, de composants parasites,... ont été appliquées au fil des années pour améliorer les performances de telles antennes. La plupart des méthodes existantes sont empiriques et basées sur des optimisations chronophages. D'autres approches comme l'optimisation du courant d'antenne basée sur l'analyse modale sont des approches systématiques qui ont été proposées. Il a également été montré que l'utilisation de matériaux artificiels appelés inclusions de métamatériaux comme élément parasite permet d'améliorer les performances de l'antenne à moindre coût. Cependant, le choix de la bonne inclusion pour une conception d'antenne est compliqué, en particulier lorsque l'antenne est non canonique et arbitraire. Dans cette thèse, nous proposons une méthode systématique pour améliorer les performances de l'antenne en utilisant l'inclusion de métamatériaux. La méthode est utilisée pour concevoir une antenne inspirée des métamatériaux avec le potentiel d'analyser à la fois les propriétés de rayonnement et de diffusion de la conception inspirée des métamatériaux. Il utilise l'approche modale caractéristique pour évaluer l'énergie quantitative stockée des inclusions de métamatériaux qui fournissent des informations quantitatives sur le comportement en champ proche de l'inclusion. L'approche modale de l'énergie stockée est comparée à l'approche des paramètres efficaces pour décrire les inclusions et elles montrent toutes deux une bonne concordance qualitative. Dans le processus de conception inspiré des métamatériaux, un mode caractéristique est appliqué pour obtenir un aperçu des propriétés de rayonnement de la structure et l'inclusion est choisie pour compenser l'énergie stockée de l'élément d'antenne en fonction de sa quantité d'énergie stockée modale. Le couplage entre l'antenne et l'inclusion est analysé en utilisant le coefficient de couplage intermodal. Il représente la diffusion entre l'antenne et l'inclusion et définit comment la distance de positionnement et de séparation entre les deux éléments affecte les performances globales du système inspiré des métamatériaux. La méthodologie proposée est validée avec un prototype qui montre une bonne concordance entre le résultat simulé et mesuré. La méthode proposée est en outre appliquée dans l'analyse de l'amélioration de l'antenne intégrée en utilisant le camouflage électromagnétique. Le manteau se couple à l'élément dans son voisinage et permet à l'élément d'antenne actif de fonctionner avec un meilleur rendement de rayonnement. La méthode proposée est donc diverse et utile pour la conception future de systèmes inspirés des métamatériaux avec des performances améliorées.

Mots clés: antennes intégrées, antennes électriquement petites, métamatériaux, inclusions, modes caractéristiques, cloaking électromagnétique, couplage modal, amélioration des performances.

Related publications

Journal papers

- **Chukwuka, Ozuem, Divitha Seetharamdoo, and M. Hassanein Rabah.** "Stored energy of arbitrary metamaterial inclusions." Journal of Physics D: Applied Physics 53, no. 23 (2020): 235501.

- **Chukwuka, Ozuem and Divitha Seetharamdoo.** "Designing of Metamaterial-inspired Electrically Small Antenna Based on Evaluated Stored Energy". Manuscript in Preparation for Submission to IEEE Transactions on Antennas and Propagation.

- **Chukwuka, Ozuem and Divitha Seetharamdoo.** "Theory of characteristic modes analysis of electromagnetic cloaking". Manuscript in Preparation for Submission to Sensors special issue Journal, 2020.

Communications

- **Ozuem, Chukwuka, Divitha Seetharamdoo, M. Hassanein Rabah, and Hedi Sakli.** "Methodology for Quantifying Metamaterial Stored Energy Using Theory of Characteristic Mode". In 2018 IEEE International Symposium on Antennas and Propagation & USNC/URSI National Radio Science Meeting, pp. 1121-1122. IEEE, 2018.

- **Ozuem, Chukwuka, Divitha Seetharamdoo, M. Hassanein Rabah, and Hedi Sakli.** "Stored energy evaluation of metamaterials based on theory of characteristic mode". (2018): 397-5.

- **Rabah, M. Hassanein, Divitha Seetharamdoo, and Chukwuka Ozuem.** "On the Use of Modal Powers and Energies in the Analysis and Design of Metamaterial Structures". In 2018 IEEE Radio and Antenna Days of the Indian Ocean (RADIO), pp. 1-2. IEEE, 2018.

- **Chukwuka, Ozuem, Divitha Seetharamdoo, and M. Hassanein Rabah.** "Coupling Analysis of Metamaterial Inspired Structures using the Theory of Characteristic Modes". In 2019 13th European Conference on Antennas and Propagation (EuCAP), pp. 1-5. IEEE, 2019.

- **Ozuem, Chukwuka, Divitha Seetharamdoo, and M. Hassanein Rabah.** "Electromagnetically Induced Transparency in Metamaterials Using Theory of Characteristic Modes". In 2019 IEEE International Symposium on Antennas and Propagation and USNC-URSI Radio Science Meeting, pp. 1405-1406. IEEE, 2019.

- **Kari, Nadia, Chukwuka Ozuem, Divitha Seetharamdoo, Jean-Marc Laheurte, and François Sarrazin.** "Analysis of a chiral helix metamaterial using eigenmode expansion method and characteristic mode theory". In 2019 IEEE International Symposium on Antennas and Propagation and USNC-URSI Radio Science Meeting, pp. 491-492. IEEE, 2019.

- **Chukwuka, Ozuem, Divitha Seetharamdoo, and Mohammed Kalaagi.** "Analysis of cloaking metasurface using theory of characteristic modes". In 2020 International Workshop on Antenna Technology (iWAT), pp. 1-4. IEEE, 2020.

Table of Contents

List of Figures

Abbreviations

BC-SRR	**B**roadside **C**oupled **S**plit **R**ing **R**esonator
CMA	**C**haracteristic **M**odes **A**nalysis
CMT	**C**oupled **M**ode **T**heory
EC	**E**lectro **D**ynamic
ED	**E**quivalent **C**ircuit
EFIE	**E**lectrical **F**ield **I**ntegral **E**quation
ESA	**E**lectrically **S**mall **A**ntenna
FCC	**F**ederal **C**ommunications **C**ommission
FDTD	**F**inite **D**ifference **T**ime **D**omain
FSS	**F**requency **S**elective **S**urface
GPS	**G**lobal **P**ositioning **S**ystem
GSM	**G**lobal **S**ystem for **M**obile Communications
LTE	**L**ong **T**erm **E**volution
LUT	**L**ook **U**p **T**able
MFIE	**M**agnetic **F**ield **I**ntegral **E**quation
MIMO	**M**ultiple **I**nput and **M**ultiple **O**utput
MoM	**M**ethod **o**f **M**oments
MRTD	**M**ulti **R**esolution **T**ime **D**omain
MTM	**M**etamaterial
MWC	**M**odal **W**eighting **C**oefficient
NF	**N**on **F**oster
NR	**N**on **R**adiating
PEC	**P**erfect **E**lectric **C**onductor
PIFA	**P**lanar **I**nverted **F**-**A**ntenna
$\mathbf{P}_{rad}$	**R**adiated **P**ower
Q-factor	**Q**uality-factor
RF	**R**adio **F**requency
RWG	**R**ao **W**ilton **G**lisson
TCM	**T**heory of **C**harcteristic **M**odes
TE	**T**ransverse **E**lectric
UAV	**U**nmanned **A**rea **V**ehicle
UMTS	**U**niversal **M**obile **T**elecommunications **S**ystem
UWB	**U**ltra **W**ide **B**and
$\mathbf{W}_e$	**E**lectric **E**nergy
WLAN	**W**ireless **L**ocal **A**rea **N**etwork
$\mathbf{W}_m$	**M**agnetic **E**nergy
$\mathbf{W}_{sto}$	**S**tored **E**nergy

General Introduction to Thesis Work

There is a growing need to remotely monitor activities which have led to the increase in the use and development of wireless system technology in areas such as: health structure monitoring, automobile tracking, communication, biomedical, military, transport and safety applications, environmental data gathering and many more. The latest trend is the demand of the Internet of Things (IoT) which have further resulted in increasing research in the area of wireless sensor networks. Wireless sensor network relies on an embedded communication system which makes use of radiating elements or antennas.

Antennas are radiating elements designed for receiving and transmitting electromagnetic waves and conventionally designed to operate in free space when the first one was developed by Marconi in 1901 [13]. Over the years, the design of antennas have evolved from the simple canonical structures to designs suitable for different application, shapes and sizes including the use of materials such as paper, ceramics and even liquid for their design [14]. One of the main challenges in antenna design is the demand for electrically small antennas (ESAs) which are generally characterized by low performances when integrated in small and mobile devices [15]. Indeed, the performances of ESAs are directly proportional to their electrical and physical size and the radiating area. Their radiation properties can be significantly affected by the immediate environment within which they operate as they couple with elements in their immediate vicinity.

Methods developed to enhance the performance of ESAs are usually based on the parameter that need to be enhanced because a compromise between the size, bandwidth, impedance matching and radiation efficiency have to be considered. Most of these methods require a trial and error approach and are based on the understanding of physical mechanism of canonical structures. Unfortunately, ESAs designed and optimized in free space may have their performances degraded after integration if the integration platform is not taken into account in its design.

Integrated antennas: antenna integration is an unavoidable step in the design of wireless systems and require certain technical parameters to be reached for the optimal performance of the system [16]. Some of these parameters include the efficiency, the frequency band of operation where the impedance is matched, the polarisation, directivity which at a given frequency provides a measure of the direction of the antenna's strongest emission, and the gain that describes how well the antenna converts input power to electromagnetic wave in a given direction. The integration platforms affect these parameters especially in modern applications where the platforms can be complex. This makes the integration and deployment of antennas for wireless network expensive as specific antenna need to be modified to adapt to different environment scenario making wireless sensor network design and deployment challenging and time consuming.

An illustration of the challenge in designing integrated antenna is the design of an antenna to be used in a Railway communication system. The antenna is expected to operate efficiently within the assigned frequency band of GSM-R extending from 876-880 to 921-925 MHz while proposing a small footprint. Researchers and engineers have used trial and error optimisations and methods such as inclusion of slots, use of dielectric, geometry optimization... in designing such antennas for optimal performance. Another good method for designing integrated antennas with enhanced radiation properties and improved efficiency is by decoupling it from its environment with different methods such as the intuitive method [17] which requires experience, the systematic method and the use of antenna performance restoration techniques [18] which are difficult to implement without a good knowledge of each component of the antenna and communication system.

Adequate parasitic elements used in the vicinity of an integrated antenna can enhance the performance of the antenna [19] and recent research works have shown that the use of artificial materials such as metamaterials as a parasitic element can provide enhanced antenna impedance matching, efficiency [18] and decouple an antenna from its environment [20]. Metamaterials (MTMs) have the ability to modify the propagation of electromagnetic waves and have unusual physical properties. It is a powerful tool for electromagnetic design because of its potential for unprecedented applications such as perfect lensing beyond diffraction limit, invisibility and transparency, and their ability to exhibit negative effective electrical permittivity (ϵ_{eff}), negative effective magnetic permeability (μ_{eff}) or both simultaneously.

In antenna engineering, metamaterials have been used to decouple antenna elements and excitation ports in multi-port systems, to enhance antenna performances (as parasitic element or as bulk materials) and as cloaks to preserve the radiation properties of antenna in the presence of obstacles. Most of these applications of metamaterials have been demonstrated using canonical structures [21, 22]. In [18], the demonstration of using a single unit cell of metamaterial known as inclusion for antenna design beyond the usual physical limitations of electrical size and performance such as achieving increased bandwidth, gain, and directivity was presented. The challenge in using such inclusions however is that, there is no properly defined method for selecting the appropriate inclusion for a given antenna design if the antenna is arbitrary. This is because metamaterials are generally defined based on far-field quantities (i.e. transmission and reflection coefficients) or their inductive and capacitive properties which are not adequate in completely defining their near-field behaviour. It is even more complicated in the case when the antenna is non-canonical and arbitrary since most analytical methods for analysing antennas are for canonical structures. In this work, we propose the use of theory of characteristic modes based stored energy evaluation and inter-modal coupling analysis for associating an inclusion to an antenna in the design of integrated antennas.

Characteristic modes (CM) are real current modes that correspond to the eigenvectors of a weighted eigenvalue equation involving the generalized impedance matrix of a conducting body. They are relevant to antenna designs because they can be calculated for arbitrary conducting bodies and are issued from a set of orthogonal functions that can be used to expand the total current on the surface of the body. Additionally, they provide physical insight into the radiating and energy storing phenomena taking place in conducting structures. Theory of Characteristic Modes (TCM) has already been demonstrated to be a great tool for designing integrated antennas for positioning of antenna excitation source, for antenna placement on large structures [23], metamaterial design [24] and design of antenna arrays [25] which shows its strong potential for complex antenna related analysis. It was demonstrated in [24] that TCM can also provide an insight into selecting an inclusion to be associated to an antenna based on its intuitive qualitative stored energy however, this qualitative method may not be sufficient in the case of extremely complex antenna design. It also does not provide insight into the coupling between the inclusion and the antenna element which would be useful in positioning the inclusion with respect to the antenna for achieving optimized integrated antenna performance.

Objective of the Thesis

To address the challenge of enhancing the performance of an integrated antenna by selecting a proper inclusion for its association to a particular antenna, the direct use of characteristic modes might be helpful but insufficient in providing accurate analysis for the description of metamaterial inclusions. A systematic approach is needed to provide an accurate description of an inclusion especially based on its near-field behaviour. In this thesis, we focus on the use of stored energy to select an appropriate inclusions for enhancing the performance of integrated antennas.

The stored energy analysis have been a big debate subject in antenna research works [26]. It has been suggested that reducing the stored energy of an antenna structure especially electrically small antennas (ESAs) can help optimize the antenna's quality factor which is a function of the antenna's performance. Gustafsson et al. [27] theoretically showed that equating the electric and magnetic stored energy quantities of an antenna within the required frequency band can increase the bandwidth and performance of the antenna. Also, Erentok et al. [18] proposed the use of metamaterial inclusion as a parasitic element in the near-field of an ESA to enhance its performance and Rabah et al. [24] experimentally showed that the inclusions provide a stored energy matching to that of the antenna structure. Most of the available methods for classifying metamaterial structures are used in describing bulk metamaterials rather than inclusions. They are also based on far-field reflection and transmission quantities which do not precisely describe the near-field behaviour of the structure thus, making them difficult to accurately apply in near-field applications like metamaterial-inspired antenna design.

Our aim in this work is to propose a systematic method based on near-field quantities for enhancing the performance of integrated antenna using metamaterial inclusions. The method should be applicable to antenna radiation and antenna scattering applications and should provide a way to select the proper inclusion as well as its positioning with respect to the antenna element. It is based on the use of modal stored energy evaluation and intermodal coupling coefficient analysis. We believe that this method would provide sufficient insight into systematically selecting inclusions for integrated antenna designs unlike the common trial & error approaches for selecting inclusion in integrated antenna design.

To enhance integrated antennas, we propose to analyse the antenna element for its radiation properties by evaluating its modal stored energy over the frequency band of interest and selecting an inclusion with compensating stored energy. The use of intermodal coupling coefficient is proposed for determining the position of the inclusion with respect to the antenna. This work highlights the comparison between the modal stored energy of inclusions to the common effective parameter approach for describing metamaterials. This is done by applying basic excitation to the inclusion and calculating the modal weighting coefficient. This method that provides a near-field approach for analysing inclusions from an application point of view will be key for designing antenna systems that rely on inclusions to enhance their performance.

Organisation of the dissertation

In chapter 1, the properties that characterise the performance of integrated antennas will be given. The challenges associated with integrated antennas will be explained as well as some of the limitations that affect their performances. These will be classified into the antenna design constraints and the antenna constraints upon integration. In enhancing the performance of integrated antennas, various techniques exist: a literature review on some of the common techniques used in enhancing the performance of integrated antenna will thus be described. They will be divided in two broad categories: empirical and systematic methods.

In chapter 2, limitations to the existing systematic methods are highlighted. Our main motivation is to overcome those limitations through a more complete approach. The proposed approach is presented to show the three distinct analysis that are required to be carried out in enhancing the performance of an integrated antenna. It will be shown that we make use of metamaterial inclusions and it involves evaluating the radiation properties and scattering properties using modal analysis.

In Chapter 3,the description of the stored energy for metamaterial inclusions is described. The mathematical formulation for evaluating the modal stored energy of metamaterial inclusions is based on the theory of characteristic modes. We will show that modal quantities based on stored energy of an inclusion can be evaluated at different frequency points. First, a non-resonant inclusion (rectangular rod) is evaluated to validate the method then, the modal stored energy of two inclusions, the broad-side coupled split-ring-resonator (BC-SRR) and the S-shaped inclusions are evaluated. Furthermore, to classify the inclusion as electric or magnetic, further steps involving the application of an excitation are developed. The result of the classification of the inclusions are compared to that of the effective parameter approach for classifying metamaterials. The obtained result will show that both the modal stored energy method and the effective parameter approach have a good agreement in the qualitative definition of the inclusions.

Chapter 4 focus on the evaluation of the scattering property of antennas and neighbouring obstacles or parasitic elements by the analysis of intermodal coupling coefficient. The chapter gives a brief description of electromagnetic coupling, the mathematical formulation for evaluating the intermodal coupling coefficient and the relationship between intermodal coupling coefficient and modal stored energy. To demonstrate the implementation of the inter-modal coupling coefficient, two scenarios are considered which are when both the antenna and the parasitic elements are resonant and when only the parasitic element is resonant. For the former scenario, it will be shown that the resonant modes of both structures interact while in the later case, the interaction is between the non-resonant modes of the elements. The intermodal coupling coefficient changes with respect to the excitation, position and distance between the antenna and the parasitic element.

In Chapter 5, as an application of the proposed method, we show how we can enhance the performance of an antenna. This is backed with experimental validation. First, a brief description of parasitic metamaterial antenna and the methods employed for the design of such antenna in literature is given. The proposed systematic method is used in designing a parasitic metamaterial antenna consisting of a dipole and a broad-side coupled split ring resonator (BC-SRR) based on stored energy compensation analysis. The simulated and measured results of the fabricated prototype are shown with a good agreement. Important results about the interpretation of the compensation of stored energy for metamaterial antennas are highlighted.

In Chapter 6, the versatility of the proposed systematic method is used in the analysis of electromagnetic cloaking. First we discuss electromagnetic cloaking for antenna application, then we propose the analysis of a passive electromagnetic cloaking scenario found in literature using the proposed systematic method. The method was also used in investigating the cloaking of an active antenna such that the cloaked antenna used the radiation properties of its near-by obstacle in enhancing its performance. The analysis explains the behavioral relationship between the active antenna, the obstacle and the cloaking structure.

Chapter 7 provides a summary of the findings in this thesis. The limitations of the proposed systematic method are discussed and future perspectives of the thesis work are presented.

Chapter 1

Review of existing methods for enhancing integrated antenna performance and their limitations

1.1 Introduction

Generally, the design of antennas are constrained by a physical limitation which requires the balance of three inter-related characteristics which are; size, bandwidth and efficiency. The smaller the size of an antenna, the smaller the achievable bandwidth and an increase in bandwidth would lead to a reduction in efficiency therefore, in enhancing the performance of an antenna, a trade-off between these characteristics have to happen depending on the antenna's application thereby making the enhancing of integrated antenna a challenging task especially with the use of a trial and error approach. Furthermore, since antennas are originally designed to operate in free space, the performance of integrated antennas are also affected by their platform and surrounding environment. The main purpose of antenna integration is to meet the growing consumer's demand of miniaturized wireless system with reliable and efficient performance. To provide a good application example in explaining and demonstrating the challenges of an integrated antenna, one could consider integrated antennas used in the railway industry particularly in train systems where wireless communication is critical with multiple antennas operating at different frequency band and sharing the same platform [28, 29]. These antennas are subject to constantly changing environmental conditions as the train move from one station to another and would be considered here as a case study to provide an understanding into the challenges and limitations of integrated antennas. In order to ensure reliable functioning of wireless systems, researchers are constantly faced with the challenge of enhancing the performance of integrated antennas to meet design and operational specifications with constantly evolving methods.

In this chapter, some of the constraints associated with antenna integration are considered. The physical limitations of antenna are considered and attention is given to the effect of antenna integration on the different antenna performance indicator. In figure 1.1, the relationship between the constraints and limitations of integrated antenna is shown.

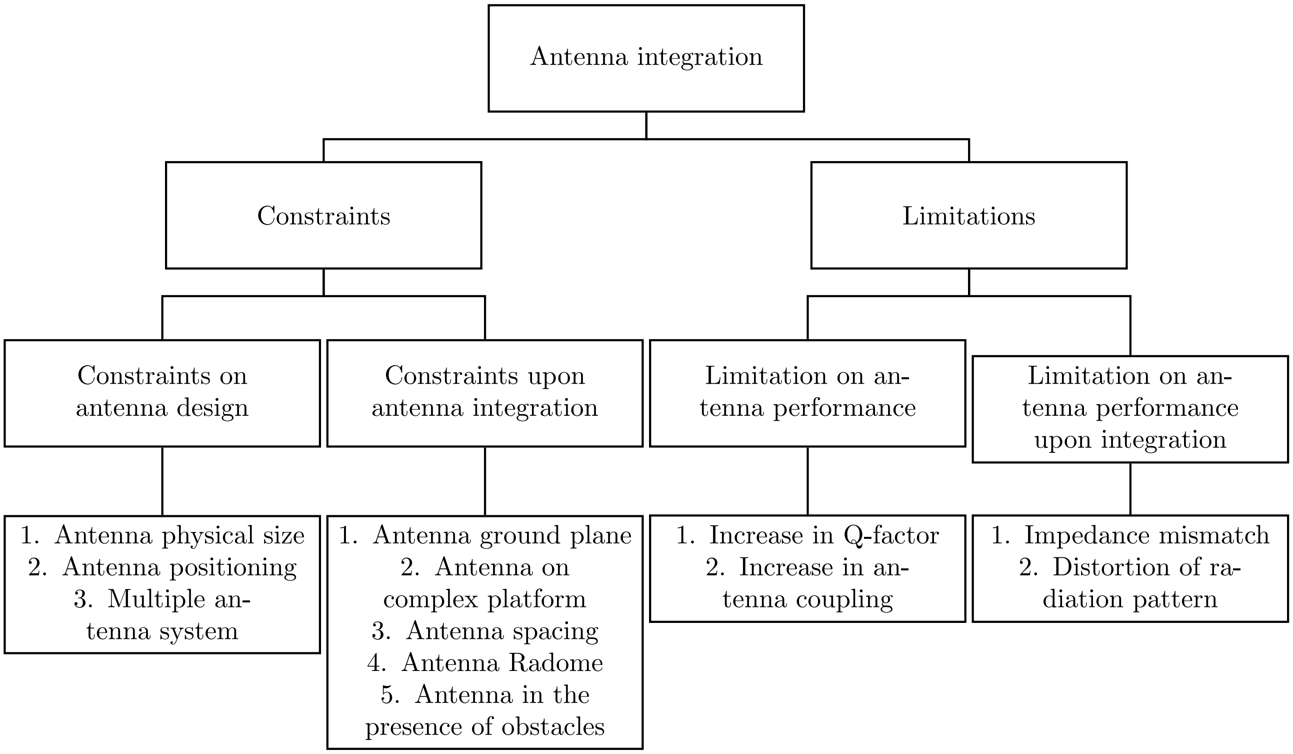

Figure 1.1: Relationship between the constraints and limitations of integrated antenna.

Furthermore, some of the major methods found in literature for enhancing integrated antenna is presented. It is observed from literature that enhancing the performance of integrated antenna can be based on an empirical method or a systematic method done before integration or upon integration. Finally, the limitation of the existing methods and the need to propose a systematic procedure for antenna integration is briefly stated in the conclusion.

1.2 Design constraints of integrated antenna

The need to integrate antennas have led to the design of miniaturized antennas which are characterized by poor performances. The reason for the antenna size reduction is to ensure that the antenna can properly fit into their platforms [28]. Antenna integration involves the design and application of antenna on platforms or in the presence of other antennas and components as compared to their free-space operation that they were originally designed for. It can be a simple integration such as in automotive application where an antenna is placed on a metallic body [30] or a complex integration such as in structural health monitoring applications where antennas have to be integrated into concrete [31] or antenna integration in the human body [32]. To have a better visual understanding of integrated antenna, lets consider a simple antenna integration system of a train shown in figure 1.2 [1]:

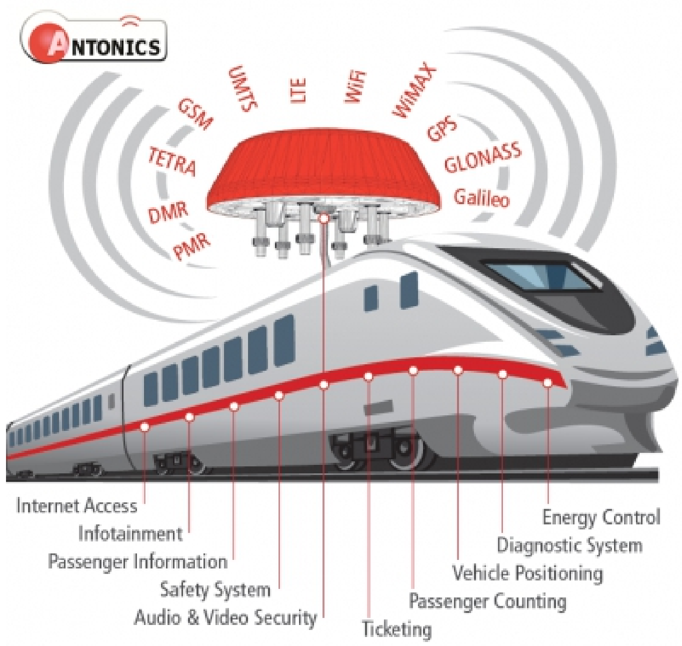

Figure 1.2: Integrated antennas on a train [1].

In the framework of integrated antennas and not being limited to intelligent transport systems (ITS) such as train systems, the increasing wireless functionalities have resulted in complex electronic systems and networks across a wide range of frequencies. The wireless communication system consist of various antennas integrated in different location of the system. Usually, different antennas are designed for different applications and therefore operate at different frequencies [4, 33]. As the number of wireless application increases and the number of antenna increases, it leads to a compact multi-antenna system with strong mutual coupling between antenna radiation paths.

Some of the constraints of antenna integration include:

1.2.1 Constraints on antenna design

Integrated antennas are designed to meet strict antenna parameter specifications in term of operating frequency, bandwidth, polarization, gain and radiation pattern as stipulated by Federal Communications Commission (FCC). They should not only be of a low profile and omnidirectional pattern [29] but also designed to overcome the mechanical constrains like dimensions, weight, ground plane, radome size and material and be easily compatible with other existing RF components. Therefore, they must be compact and conform to the shape, size and location of the integration platform at low production cost [34].

Generally, the specification requirement of integrated antennas are fixed based on the wireless system and not subject to change hence, integrated antennas have to be designed to comply with these requirements. The design of antenna systems are constrained by:

1. **Antenna physical size:** antennas such as those used for railway system communication should have a low profile and an omnidirectinal radiation pattern as compared to that of other automotive applications which can be narrowband, wideband or multiband, have omnidirectional or unidirectional radiation pattern and serve dedicated purpose like LTE, GSM, WLAN systems, etc [29]. One general requirement for most integrated antenna is the miniaturized size. They should be physically small to fit into their integration platform while still retaining its efficiency. Therefore, the antenna's physical dimension is limited by the available space within its device housing [28].

   The electrical size of an antenna is described by its wavelength hence, antenna is physically limited by its electrical size. For high frequency application, the physical size of the radiating element is compatible with the available space however at low frequencies, miniaturization techniques are required to integrate the antenna [28].

   These miniaturized antennas are generally characterized by low radiation efficiency and poor performance. They require the application of various enhancement techniques to operate at the required standard. For example, patch and monopole antennas are printed on 2-D substrates to design miniaturized antenna for automotive applications [35,36] however, the effect of other radiating elements within their vicinity need to be evaluated.

2. **Multiple antenna system:** antennas have to be isolated from other electromagnetic components to function properly. As the number of wireless application increases, several antennas must be accommodated within the same device. These antennas are placed together within the same enclosure. Normally, the presence of close-by radiating elements operating at different frequencies result in strong mutual coupling that affects the performance of the wireless system and distort the antenna's radiation pattern [37]. Separately printed monopole antenna having the same horizontal ground plane and operating at near-by frequencies require a separation distance greater than half wavelength of the operational frequency to achieve a -15 dB isolation [38]. However, the available antenna space for antenna integration is limited thus, the antenna design and arrangement must be carefully optimized to limit the mutual coupling between radiating structures [39].

   Antenna system enhancement involves reducing the mutual coupling between radiating elements. A spacing of about five times the wavelength of the operating frequency is recommended between antenna systems operating in the same frequency band. Also, the design of multiband antenna and single antenna with multiple ports have been proposed as a way of limiting the number of radiating element within wireless systems [4, 36, 40].

1.2.2 Constraints upon antenna integration

The constraints of antenna integration are not only limited to the antenna design but also the integration of antennas to satisfy necessary operational standards. The choice of their mounting location and the continuous mobility of wireless systems mean that the antennas upon integration are exposed to factors that affect their standard performance.

The major constraints faced in the integration of antenna includes:

1. **Antenna ground plane:** in antenna integration, antennas are mostly mounted on ground plane. In train systems for example, the ground plane is usually a flat piece of metal in its simplest form of very large dimension. The shape and size of the ground plane on which the antenna is mounted significantly affect the antenna performance in terms of impedance matching, bandwidth and radiation pattern. In [41], a difference of 8 dB is found between the radiated fields using a finite ground plane compared to those with infinite ground plane. This difference is attributed to high field coupling between the antenna and the device ground plane causing the ground plane to radiate and degrade the radiation characteristics of the antenna. The radiation from the ground plane is however inevitable because electric currents are distributed on both the antenna's radiator and the ground plane. For example when measuring an antenna, currents on the ground plane leak on to the measurement cable causing the cable to radiate and influence the measurement [42].

   To maintain the radiation characteristics, the currents should be controlled since it cannot be completely stopped. By introducing two leakage blocking slots on the ground plane which may be impossible for some antenna integration systems, the current can be controlled [43]. Modifying the antenna's topology could also reduce the current distribution on the ground plane.

2. **Antenna positioning:** in wireless systems, train and other electronic systems, antenna mounting positions are defined by the manufacturer. The rooftop is chosen for most automotive applications because it permit omnidirectionality in azimuth plane [44]. It keep the antennas high above ground which is quite free of any obstacle limiting the radiation pattern and performance efficiency [29, 33]. The near finite dimensions of the surface of the rooftop causes significant shadowing in the direction of travel and induces a ripple in the antenna pattern [45].

   While it is important to ensure that the antenna positioning is done to avoid obstruction, coupling and variation in antenna parameters, the specification of the antenna position and allocated space makes it difficult to simultaneously satisfy all the requirements while maintaining the antenna radiation efficiency. In positioning the antennas, the spacing between the different radiators should also be sufficient enough to reduce coupling and avoid interference [37]. The antenna in its position is also faced with other obstructions such as air-conditioning unit, electronic components, strengthening bars, etc which can cause blocking issues to the antenna radiation.

3. **Antenna on complex platform:** antennas have to be integrated into rigid structures to keep it firmly in place. These structures are mostly platforms that act as mechanical support for the antenna. They are sometimes complex in nature and can include large curved planes, dielectric covers and arbitrary mounting positions. These platforms are within the antenna's near-field hence, they affect the gain and sidelobe levels of the antenna [46]. For instance, antenna's mounted in concrete wall for structural health monitoring and in human body for biomedical application are affected by the dielectric nature of their host [32].

   In train application, the ground plane may sometimes be a curved surface and antennas mounted on the edge of a ground plane have reduced performance [47]. Many research work exploit the resonance of mounting platforms to enhance the performance of integrated antennas [48].

4. **Antenna spacing:** coupling between antennas are evaluated using free-space equations although, the near-field effects become more significant as the spacing between the antennas decrease [39]. The spacing between antennas must be sufficient enough to avoid blocking issues and spurious emissions. However, because of the limited space allocated to the installation of antennas in integrated systems, the positioning of antennas need to be optimized to ensure that each individual antenna can operate without being affected by its neighbouring antenna.

   Many integrated systems adopt the use of multiband and multi-port antennas to reduce the number of radiating element and provide better spacing between antenna elements [4]. Recently, research into cloaking [49] show promising results in solving this challenge.

5. **Antenna radome and shields:** in train systems for example, the antenna may have to be covered with radome to prevent them from damage due to harsh weather conditions. This radome is made of materials with specific permittivity which can affect the performance of the antenna. It distorts the radiation pattern and causes variation in the input impedance due to the modified current distribution of the antenna [50, 51]. In other cases like GPS antenna, an unobstructed view of the sky is required for its proper functioning and the use of radome significantly affect its operation.

   The performance of the antenna in the presence of the radome have to be predicted and the antenna design have to be optimized for efficient performance in such condition [51].

6. **Antenna in the presence of an obstacle:** antenna's free-space radiation characteristics are well known but in reality, the antenna has to operate in the presence of obstacles and other RF circuitry. For example, a shipboard radar antenna operates in proximity to masts, wires and deck-houses [48]. Moreover, the constant motion of of a system such as train means the exposed mounted antenna can come close to objects like tress and wires either due to its transition path or due to improper maintenance of the surroundings.

   Deep multipath fading affect antenna's performance as a result of the reflection and diffraction from surrounding objects [52]. Sometimes, antennas on a train system require a clear line of sight to communicate with other train systems and railway infrastructures which may be hindered by obstacles. Particularly, because the obstacles are within the near-field environment of the antenna, they produce a strong coupling to the antenna element and create blockage effect on the radiation performance of the antenna. Also, the gain and sidelobe level of the antenna is significantly affected [53]. Special techniques such as electromagnetic cloaking can be implemented to reduce the effect of the presence of an obstacle on antenna's performance [49].

1.3 Limitations of integrated antenna

The various challenges of antenna integration discussed in the previous section poses significant limitations to the performance of integrated antennas. An insight into these limitations guide researchers in providing solutions to these constraints thereby enhancing the performance of integrated antennas.

1.3.1 Limitation on antenna performance

Antennas have to be cost effective with a large operating bandwidth, 50 Ohms impedance matched, of a specific pattern (such as omnidirectional or unidirectional) and polarization characteristics (such as elliptical or circular polarization), with good isolation to neighboring radiating systems and high radiation efficiency [52]. They also require easy integration with other RF components.

These antenna design constraints limit antenna performance in two major ways:

1. **Increase in antenna quality factor (Q-factor):** although the increase in Q-factor is also dependent on the size and shape of the integration platform, the antenna size plays a major role. Integrated antennas are compact and miniaturized (i.e. small effective radiating area) due to small available space and result in low radiation resistance (due to short radiating length), significant ohmic loss (due to long current path) and large stored energy (due to complex design structure) [15]. The reduction in antenna's dimension is mostly done by using high permittivity materials or by folding the antenna structure however, both methods lead to a significant increase in the antenna's Q-factor [54]. The radiation efficiency, gain and impedance bandwidth are also affected.

   For all electromagnetic resonators, Q-factor is defined as a figure of merit that determines the ability of the antenna to radiate effectively [55, 56]. It is a measure of the sharpness of antenna's resonance and indicates to what extent the resonator is capable of storing electromagnetic energy at the resonance frequency. It is particularly of interest when designing small antenna because of its relation to antenna performance as its lower bound indicates antenna performance limit in a given volume. However, the physical size of an antenna is related to its electrical size [57] and miniaturized antennas are mostly characterized with narrowband due to its low radiation resistance [58]. The antenna Q-factor is also proportional to the ratio of the energy stored in the antenna to the rate at which the antenna emits radiation and it is given as:

   $$\mathrm{Q} = \frac{2.\omega.\mathrm{W}_{sto}}{\mathrm{P}_{rad}}, \tag{1.1}$$

   where ω is the angular frequency, W_{sto} is the non propagating stored energy of the antenna and P_{rad} is the radiated power. The Q-factor is related to the antenna's near-field considering that stored energy is found in the near field of a radiator thus, the antenna orientation will influence the field distribution in its vicinity. Although, the Q-factor of an antenna is calculated independently of its bandwidth but since Q-factor is calculated at the resonant frequency, its simple relation with the antenna's operating bandwidth can reveal the frequency response of an antenna. The antenna's Q-factor is approximately given by the reciprocal of the antenna's bandwidth:

   $$\mathrm{BW} = \frac{f_0}{Q}. \tag{1.2}$$

   The higher the antenna Q, the smaller the impedance bandwidth. There is a trade-off between the radiation efficiency, the antenna maximum dimension and its bandwidth. It therefore implies that an antenna with a small bandwidth has a high amount of stored energy and a high field concentration in a limited area while an antenna with higher bandwidth has a lower level of stored energy distributed within a larger area around the source. Researchers are constantly looking for ways to enhance the performances of antennas by optimizing the antenna's Q-factor [59].

2. **Increase in antenna's coupling:** when antennas are very close together, the coupling effect is inevitable and cannot be neglected. Antenna coupling arises due to free space radiations, surface currents and surface waves. It describes the energy absorbed by an antenna's surrounding during the antenna's operation. Antenna coupling is also amplified by the choice of the antenna's feeding mechanism. It causes the change in input impedance, reflection coefficient and the radiation pattern [60]. The design of integrated antenna is therefore a process that involves respecting the strong interaction between antenna elements and the components in its surrounding environment. Antennas couple strongly to their near-field environment hence when they are integrated, they couple to complex platforms, near-by obstacles and co-located antennas. The mutual coupling causes increase in the stored energy of the individual antennas, re-distributes the antenna's surface current and changes the input impedance and the radiation pattern [60].

   Finding a solution to the problem of high coupling in integrated antenna is a challenging task [52]. Optimizing the separation distance between the radiating elements reduce the coupling effect therefore, the further the separation of the antenna elements, the less impact the coupling has on the antenna performance. Although, the system performance can be partially improved by calibrating the coupling, a more effective method is to use reliable decoupling techniques.

1.3.2 Limitation on antenna performance upon integration

The performance of integrated antennas are also affected by the integration platform and surrounding environment. The major impact on the antenna performance upon integration include:

1. **Impedance mismatch:** one way to guarantee maximum power transfer between a load and a source is to match their impedance to reduce the reflection loss between the load and the source [61]. In antenna engineering, the impedance varies considerably with frequency and other external circumstances. For example, automotive antennas have a return loss just below –6 dB with insufficient gain at low frequencies however in railway environment, higher requirements for matching and gain are required [29].

   Impedance mismatching result in performance degradation, especially with a huge number of antenna elements placed side by side [60]. The antenna impedance is very sensitive to its surrounding particularly, sudden change in bad weather condition or abnormal connection of antenna port usually amplified by the constant changing position of the wireless system due to its movement. Impedance variation also occur due to presence of other objects within the antenna field (e.g. mounting platform) and aging which de-tunes the antenna resonance frequency. Nominal antennas have an input impedance of 50 Ω and its matching may not be sustained if the antenna was designed and optimised in the free-space [62, 63]. The matching is calculated using the reflection coefficient given as [64]:

$$\Gamma = \frac{\mathrm{Z}_{in} - \mathrm{Z}_0}{\mathrm{Z}_{in} + \mathrm{Z}_0}, \tag{1.3}$$

   where Γ is the reflection coefficient, Z_{in} is the input impedance and Z_0 is the output impedance. Electrically large antenna are less affected by impedance variation because antenna parameters are a function of the antenna size therefore as the antenna gets miniaturized, the quality factor increases, the impedance mismatch increases and the effect of the surrounding becomes more severe [65, 66].

   The individual small antennas employed in wireless system may appear to be matched in free space however when all the antennas radiate simultaneously within the compact design, the combined surface wave, near-field and far-field radiation result in an impedance mismatch. The optimization of some parameters, such as the element length and the feed port enable the input impedance to be adjusted.

2. **Distortion of radiation pattern:** propagation pattern of wireless systems are affected by outside influences such as vegetation, solar radiation, climate conditions, interference from other RF sources and ground reflection. In fact, integrated antennas are significantly affected by their mounting platform, nearby object and surfaces which will reflect or absorb the radiated signal. For example, antennas mounted on large platforms such as ships, aircraft or trains have their radiation pattern affected due to blockage caused by the objects which are part of the host structure [23]. In the case of multiple antenna environment, the near-field mutual coupling severely distorts the radiation pattern of the individual antenna [67]. Some of the antenna's signal will be absorbed by the ground while others would reflect off the ground.

   The size of the ground plane influences not only the radiations pattern of an antenna but the gain, resonance frequency and impedance. This is mainly due to the high field coupling between the antenna, ground plane and surrounding. The coupling causes the ground plane and elements in the surrounding to radiate and degrade the radiation characteristics of the antenna. For instance, the presence of a small wall have a large effect on the radiation pattern considerably [68]. It disturbs the radiation pattern not only under the ground plane but also above it.

   The size constrain of integrated antenna require a trade off between the impedance bandwidth and the far-field radiation pattern. In most cases, the time-varying current on the mounting platform is the primary source of radiation that determines both the antenna's impedance and radiation pattern. It is important to point out that a large ground plane does not necessarily produce a better antenna performance because each antenna element couples to the ground plane in its own unique way. It is the location of the antenna and its feeding point on the ground plane rather than the size of the ground plane itself that primarily establishes the antenna's performance in terms of its impedance, bandwidth, and radiation mode. The ground plane itself becomes an integral component of the radiating structure [69] and should be considered in determining the antenna's effective electrical size. It is therefore important to understand how the antenna couples to its environment and how the current distribution is established on both the antenna and its integration platform.

1.4 Literature review of existing methods for enhancing the performance of integrated antenna

The enhancement of antenna performance is important to ensure that the antenna function within the required standard after its integration. The electrical properties of the antenna such as wide bandwidth, high efficiency and radiation properties must be satisfied for an antenna to function properly [70]. The challenge of blockage due to coupling between antenna elements and between antenna and its immediate environment is also addressed by introducing coupling reduction technique and decoupling methods. Although low coupling is easily achieved when the separation between the antenna elements and between antenna and elements in its immediate environment is of large wavelength, some of the antenna enhancement techniques like cloaking specifically addresses the problem of coupling.

Over the years, various research works have employed various techniques to improve the performance of integrated antennas. Although, some works implement these enhancement techniques upon integrating the antenna [71], others have enhanced the performance of the free space antenna [18] so that its performance after integration is within the required standard. The performance enhancement technique applied to a particular antenna is also dependent on the design of the antenna, application of the antenna and the antenna parameter which need to be enhanced. The commonly used techniques found in the literature are presented in the chart of figure 1.3 and some examples of their implementation are summarized in Table 1.1;

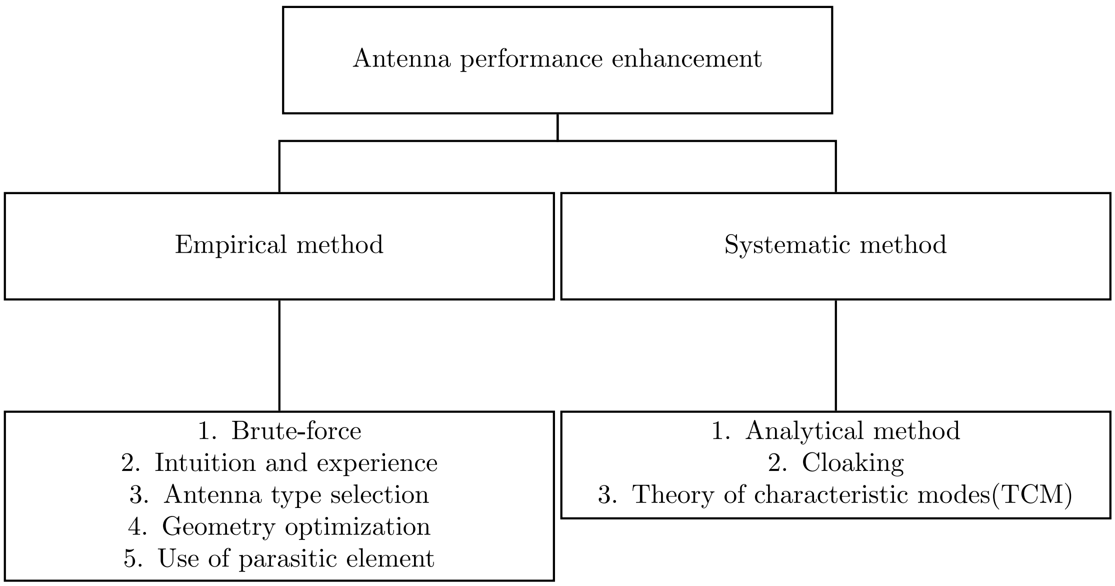

Figure 1.3: Antenna enhancement techniques employed in literature.

Table 1.1: Summary of some of the implemented techniques for enhancing the performance of integrated antenna.

Antenna design	**Year**	**Integration method (method)**	**Enhanced parameter performance**
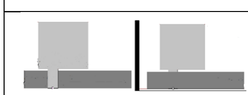 [2]	2012	**Trial and error (Empirical)**	12% increase in 10 dB bandwidth, decrease in antenna width from 0.9 to 0.2
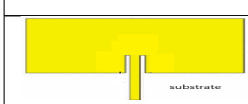 [72]	2017	**Trial and error (Empirical)**	96.97% radiation efficiency, 6.835 dB gain and bandwidth of 102.6 MHz
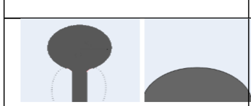 [73]	2015	**Q-factor optimization (Systematic)**	160% increase in bandwidth with significant size reduction
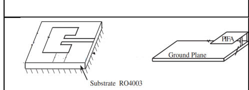 [74]	2010	**Antenna selection analysis (Empirical)**	Bandwidth of 3.65% for Patch and 10.4% for PIFA

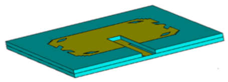 [75]	2018	**Use of parasitic element (Empirical)**	Dual band, gain of 5.035 dB and bandwidth of 97 MHz
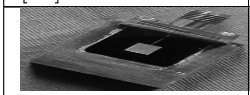 [76]	2010	**Geometry optimization (Empirical)**	50% increase in bandwidth and 25% increase in efficiency
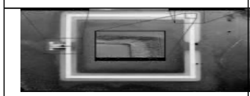 [77]	2006	**Geometry modification (Empirical)**	1.5 dBi gain achieved
 [78]	2013	**Geometry optimization (Empirical)**	Bandwidth of 60% and gain of 6.48 dB
 [79]	2013	**Use of parasitic element (Empirical)**	Peak gain of 3.74 dBi and radiation efficiency of 76%
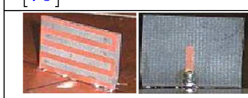 [8]	2008	**Use of metamaterial (Empirical)**	Radiation efficiency of 89.34% and size ka of 0.497
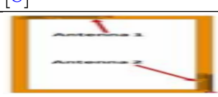 [80]	2014	**Use of metamaterial (Empirical)**	Best positioning of antenna for mobile phone operation
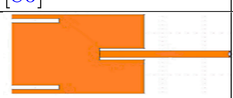 [4]	2010	**Geometry optimization (Empirical)**	Dual band, bandwidth of 33.54 MHz
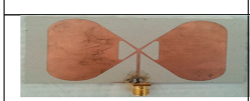 [5]	2020	**Use of dielectric substrate (Empirical)**	Bandwidth of 22% and realized gain of 5.9dB
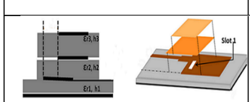 [6]	2016	**Use of multi-layer (Empirical)**	Bandwidth of 35%, peak gain of 8.2 dBi and average gain of 6 dBi
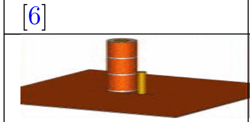 [9]	2016	**Use of electromagnetic cloak (Systematic)**	Recovery of antenna parameter (impedance matching and far-field radiation pattern)

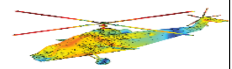 [11]	2018	**Use of CMA analysis (Systematic)**	Current density to show radiation properties
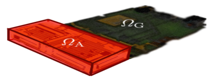 [81]	2016	**Surface current optimization (Systematic)**	Numerical maximum gain
 [82]	2018	**Q-factor optimization (Systematic)**	size ka=0.4 for optimal meander line
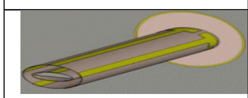 [83]	2017	**Use of electromagnetic cloak (Systematic)**	Recovery of antenna parameter (impedance matching and far-field radiation pattern)

1.4.1 Empirical method to enhancing integrated antenna

The empirical method for enhancing the performance of antenna is one of the methods applied by antenna engineers. It is the process of using brute-force method to achieve the enhancement of antenna performance and require no special knowledge of the system. It can be implemented either before antenna integration or upon antenna integration. Some of the empirical methods include:

1. **Brute-force:** since no knowledge of the antenna system or the integration platform is needed, the engineer goes through a number of trial and error procedure until the desired antenna performance is achieved. Different designs, types and modification of the antennas are tried into the integration platform until the required antenna performance parameters are achieved. A basic knowledge on the working principle of antenna is however needed to minimize the time taken in the trial and error approach. In [2,72], the trial and error approach was employed in the design of micro-strip patch antenna and in [84,85] the method was used for antenna integration. A wide-band patch antenna designed using trial and error approach and its reflection coefficient plot is shown in figure 1.4:

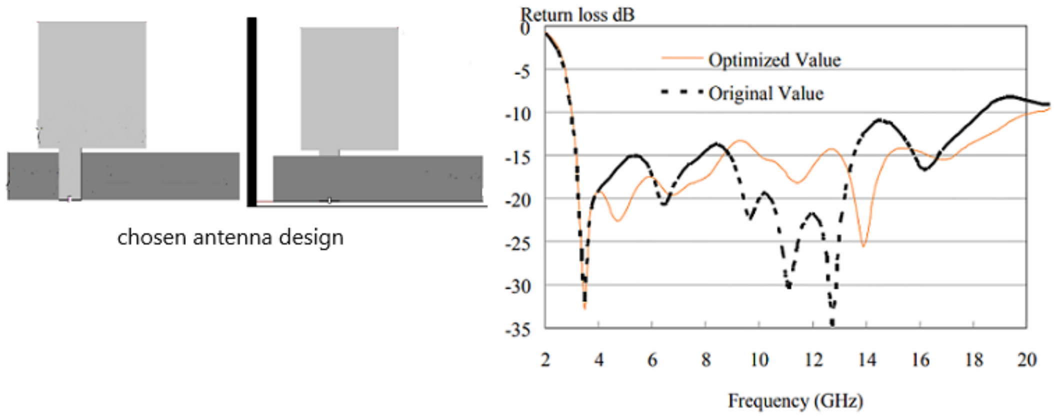

Figure 1.4: Wideband patch antenna designed with trial and error approach [2].

The patch antennas in figure 1.4 are the selected antenna designs from 80 different design trials. Geometry optimization was applied to the selected design to achieve optimal bandwidth. Therefore, the disadvantage of the trail and error approach is that the final design may not produce the optimal performance of the antenna. It requires a lot of time to arrive at the desired performance which could involve irreparable damage to some parts of the antenna or integration platform like the inclusion of slots.

2. **Intuition and experience:** is just like the brute-force method but might take a shorter time because of the experience factor. An engineer who has implemented a similar antenna integration process would find it easier to integrate similar antenna with the required performance [73] since the design parameters and their effect on performances are known over time. However, with a change in the type of antenna or integration platform, the engineer would have to return to the brute-force method. Therefore, the disadvantages faced with the brute-force method would apply with this method for a new antenna design.

3. **Antenna type selection:** antennas are categorized based on its frequency band, its shape and its application [75]. The first point of ensuring that the performance of an integrated antenna is not degraded by its integration platform and surrounding environment is by selecting the proper antenna type suitable for the desired application. Over the years, research works have studied different type of antennas for different applications. For example, a magnetic loop antenna have a better and stable impedance matching when integrated into dielectric medium as compared to an electric antenna [32] however, the magnetic antenna have a poor radiation efficiency. In [74], the PIFA and patch antennas were concluded as the best antennas for reinforced concrete application after performance analysis.

Monopole and dipole antennas have the simplest configuration and are widely employed in broadcasting and wireless communication systems. Its free-space operation is characterized by an omnidirectional radiation pattern and can be equipped with metallic reflector to improve gain and directivity [86]. Planar antennas like slot and patch antennas can be designed using various shapes [87] and exhibit wide impedance bandwidth and omnidirectional radiation pattern. End-fire antennas such as yagi-uda antenna and horn antenna give high gain and are employable for array designs. Microstrip antennas are mostly employed in a variety of applications including handphone, Wi-Fi connection and satellite communication due to their light weight and low profile [75]. Microstrip antennas are an evolution of circuit components with different geometries providing specific antenna performance requirements [87]. Some of the major type of antennas are shown in figure 1.5:

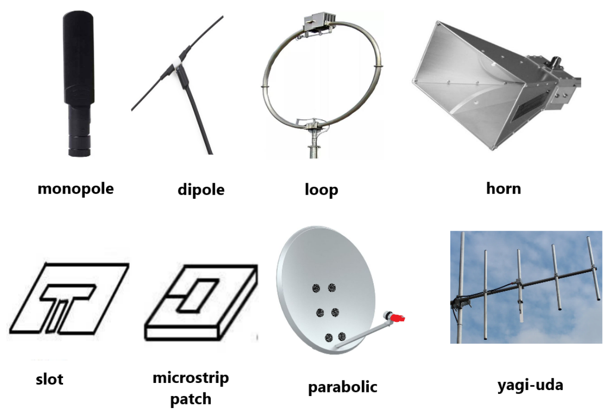

Figure 1.5: Major types of antenna [3].

A good knowledge of the antenna application provide a basis for choosing the right type of antenna and reduces the prospect of having adverse integration effect on the performance of an antenna. However, the brute-force is still applied in conforming the chosen antenna to the integration platform and for the required application.

4. **Geometry optimization:** the geometry of an antenna can be optimized to enhance its performance in term of its impedance matching, bandwidth enhancement and radiation efficiency. It involves modifying the shape and structure of an antenna to increase the bandwidth, efficiency or to modify the radiation pattern. Besides enhancing the impedance bandwidth and gain of an antenna, the geometry optimization technique can also be employed in creating multi-band frequency, enhancing the directivity of array antenna, increasing radiation resistance, improving isolation and reducing mutual coupling [76]. Geometry optimization of antenna to enhance the performance of an antenna can be implemented in three ways:

   - **Modification of antenna geometry:** this involves carrying out modification on the radiating part of the antenna. It includes folding of the radiating elements [88], inserting of slits and slots of various shapes [77,78] and boring of holes into the radiating part of the antenna. The aim of the modified geometry is to create more radiating modes which can be exploited to enhance the bandwidth of the antenna [79]. A patch antenna optimized geometrically using slot to create dual band and its achieved reflection co-efficient graph is shown in figure 1.6:

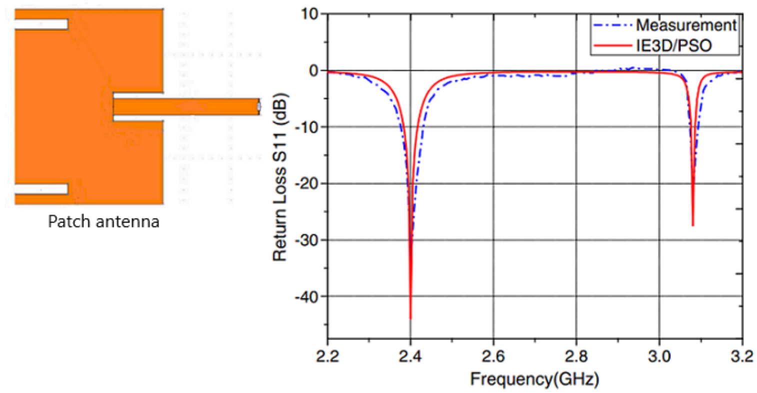

Figure 1.6: Geometrically optimized antenna for achieving dual band [4].

The process of modifying antenna geometry is not straight forward because the size and position of the slots, slits and holes have to be done to achieve performance enhancement. The process is carried out based on parametric studies and application of systematic gradient based algorithms like genetic algorithm and particle swarm method. The particle swarm method often require a lot of function which makes their implementation expensive even for simple designs. The genetic algorithm on the other hand converges quite faster [89]. The implementation of these optimization algorithms usually begin with randomly placing a function in a search space and iterating till an optimum design value is achieved. The number of iteration can vary from a few hundred iterations to million of iterations hence proper consideration of parallelization and the available computer resources available has to be factored [89].

- **Use of dielectric substrates:** antennas like dielectric and microstrip patch are designed using substrates. The use of dielectric substrates are particularly known for achieving miniaturization of antenna. It permits the reduction in the dimension of the radiating element which is approximately proportional to the obtainable bandwidth [90]. The use of dielectric substrate to enhance the impedance matching of an antenna is shown in figure 1.7:

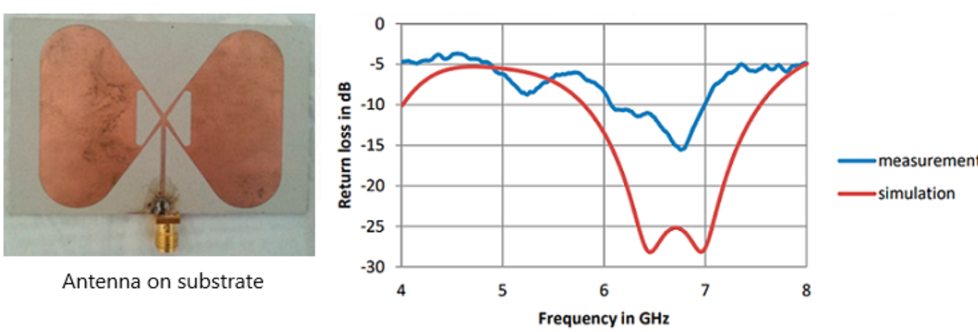

Figure 1.7: An antenna optimized using dielectric substrate [5].

In figure 1.7, RT/Duroid 5880 LZ was employed to provide better impedance matching. The choice of antenna substrate directly affects the performance of antenna hence, the substrate type, permittivity, and thickness are carefully chosen and optimized to enhance the antenna performance. They affect the antenna's input impedance, impedance bandwidth, radiation pattern and radiation efficiency [91]. This technique is however limited to planar antennas which may not be suitable for certain application. Besides direct antenna design, the use of substrates are also employed in the design of artificial surfaces which can be used to replace multi-layered structure with improved antenna performance [92, 93].

- **Use of multi-layered structure:** increasing the layer of patch antennas can enhance antenna's performance. It improves antenna gain, isolation, radiation pattern, directivity and input impedance characteristics [94]. A multilayered structure used to achieve wideband characteristics together with its reflection co-efficient graph is shown in figure 1.8:

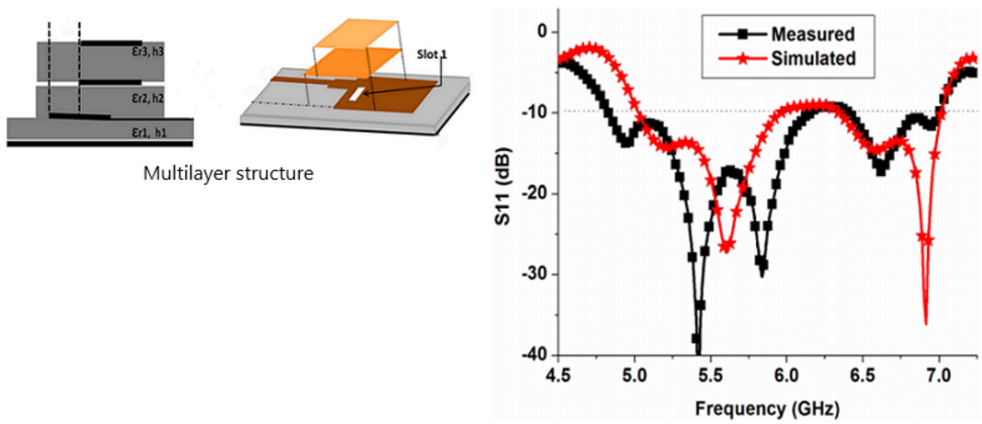

Figure 1.8: Multilayered antenna for achieving wideband performance [6].

The use of multi-layered structure is implemented by optimizing the parameter of the substrate structure, using multiple resonators, using stacked elements, increasing the height and thickness of the substrate, using substrates with high dielectric values and using parasitic patches in multi-layer configuration [6].

5. **Use of parasitic element:** miniaturized antenna are characterized by low radiation resistance and require matching network to increase the power level [95]. Matching network in fact increases the overall size of the antenna and limit the impedance bandwidth of the antenna. Non-Foster (NF) parasitic elements were proposed to overcome these challenges resulting in a matched antenna with optimized output power level [96].

Parasitic elements applied in the design of antennas are passive elements placed within the near-field vicinity of an active antenna elements and coupled either inductively or capacitively to the antenna elements [97]. The parasitic elements provide stored energy sufficient enough to compensate for the antenna and platform's stored energy. The use of parasitic element for enhancing the performance of antenna can be implemented in a variety of form which include:

- **passive electronic components:** parasitic element can sometimes be an electronic component of inductor or capacitor employed to achieve antenna impedance matching. Since small antennas are associated with highly reactive impedance, the matching network can be used to cancel the reactive part of the antenna. The efficiency of the matching network is inversely related to quality factor of the antenna [98]. Tunable impedance matching networks are able to compensate environmental detuning of antenna impedance at fixed frequency which require minor architecture update and only a few additional components [7] as shown in figure 1.9:

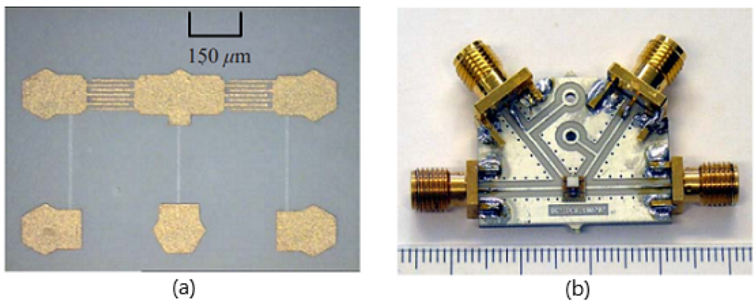

Figure 1.9: Matching network for antenna detuning: (a) varactor (b) matching network module on test board [7].

In [99], a compact LC tank, chip resistors and a double-layer frequency selective surface (FSS) are used to construct a planar dipole antenna for UWB radar and communication systems with enhanced bandwidth. The use of parasitic elements beside a dipole in an open sleeve dipole design was used to enhance the antenna's bandwidth but its limitation was the feeding line between the antenna and RF circuit that could not be printed on the glass together with the antenna because of the physical size limitation of the parasitic element [100].

- **passive structures:** other passive structures are used to create inductance and capacitance with the antenna element. Some of the passive structures used in literature include; directional antenna elements, microwave elements, patch structure, co-planar elements, ring resonators, metallic strips and reflective component [101]. They are placed in the vicinity of the antenna and their interaction with the antenna is used to create the needed inductive and capacitive effect. A good example of a typical passive structure used in antenna design are the reflectors and directors of a yagi-uda antenna.

- **metamaterial structures:** metamaterials are artificial composite engineered materials capable of molding the flow of electromagnetic waves with properties not readily found in nature. It has attracted lot of research works owing to its ability to be used in unprecedented applications [102]. In antenna application, it is used to enhance the performance of antennas [103, 104] in fact in [8], it was demonstrated that a single metamaterial unit cell can enhance the performance of an antenna while maintaining its small size. This has led to the term metamaterial-inspired antenna. An inclusion was used to enhance the performance of a monopole antenna as shown in figure 1.10:

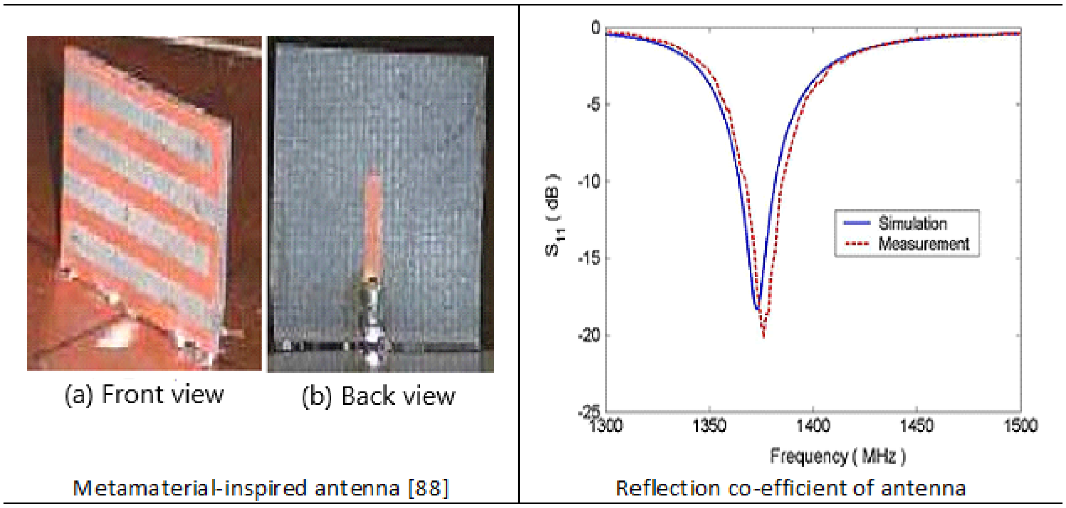

Figure 1.10: Use of metamaterial inclusion to enhance antenna performance [8].

The major challenge with applying metamaterial inclusions in antenna engineering is selecting the proper inclusion with the right characteristics to enhance the performance of integrated antennas. The challenge is more severe when the antenna is electrically small and arbitrary. Although most research works have applied metamaterial to antenna designs, the choice of the inclusion is mostly done by brute force. In [18], the reason for the selection of an inclusion for associating it to a particular small antenna was based on the inductive or capacitive nature of the the antenna structure. This line of reasoning was followed in [24] for the design of ESA for cognitive radio application.

Just like other techniques used to enhance the performance of antennas, the use of parasitic elements besides improving antenna bandwidth can also be employed to enhance the antenna gain, efficiency, isolation, radiation pattern diversity and impedance matching. The parasitic element can also be employed to create multi-band functionality or even design a filter to reject certain frequency band limits [105–107]. The challenge with this enhancement technique however is that if not properly implemented, the parasitic elements may increase the overall size of the antenna and can introduce blocking effect that would affect the antenna's radiation pattern.

1.4.2 Systematic method to enhancing integrated antenna

The systematic method involves having a good knowledge of the system (i.e. antenna and platform) and following a set of procedure to achieve the specified antenna performance requirement. It sometimes involve using analytical and mathematical tools to optimize integrated antenna for enhanced antenna performance. Some of the systematic techniques applied in enhancing the performance of integrated antenna include;

1. **Analytical method:** the behaviour and performance characteristics of an antenna can be expressed by mathematical formulation. They provide a quantitative approach to the process of enhancing antenna's performance. Two of the most recently explored analytical method by researchers for enhancing antenna's performances are:

- **Q-factor optimization:** Q-factor is a good approximation of the bandwidth at a given reflection coefficient. It is inversely related to antenna's bandwidth and performance which is a function of the antenna size. A lower bound on antenna Q for a given antenna shape is a measure of the largest matching bandwidth of any antenna bounded by that shape [108]. Antennas with multi-resonance are usually expected to have high Q-factor which can be achieved by varying the geometry to optimize the Q-factor [109]. The trade-off between performance and size can be expressed as physical bounds based solely on the shape and size of a design [59] and good antenna designs tend to approach these bounds [82].

  Although, optimisation techniques are not limited to antennas and can be applied to find the optimum shape of certain microwave components [110], in antenna engineering it is used in determining optimal maximal gain Q-factor quotient, minimal Q-factor for superdirectivity and minimum Q for given far-fields [59]. The Q-factor optimization for small antennas are formulated as a multi-objective optimization problem. The convex optimization is used in deriving physical bounds for small antennas and their corresponding optimal current densities [111] thereby providing an opportunity for a systematic study of small antenna directivity and optimal current distribution. In optimizing the Q-factor with the convex optimization, the required information are the allowed antenna-size, its position within the device and an estimate of the ohmic loss in the device [112].

  Another technique employed in Q-factor optimization is the time domain technique used to determine the response over an arbitrary frequency band by a Fourier transform. It include techniques like finite-difference time-domain (FDTD) [113] and multiresolution time-domain (MRTD) [114]. Incorporating substrate loss into any of these two technique can accurately predict the Q factor of resonant structures like inductors [115].

  Most recent methods applied in antenna's Q-factor optimization are antenna modelling with electric and magnetic currents. It was shown that magnetic dipole give a lower antenna Q bound than the pure electric dipole and antenna's Q for lossless electrically small antennas can be defined with stored electric and magnetic energies (We,Wm). Thus, the presence of a small magnetic dipole-radiation in addition to the electric dipole lowers the minimal antenna Q bound [116].

- **Antenna current optimization:** is a general methodology used to determine bounds on an antenna [81] and find the best current on a small antenna enclosed within a sphere for providing the optimum directivity [117]. It is used to analyze how small antennas are affected by amplitude constraints on the near field and by lossy background media [118]. It is formulated as a convex optimization problem efficiently solved with a computational cost that can be compared to a Method of Moments (MoM) solution of an antenna in the same geometry [59].

  Although, antenna optimizations are carried out using random search algorithms like genetic algorithms, particle swarm and gradient based algorithms [119], antenna current optimization is different and advantageous because of the many efficient solvers which can provide explicit error estimates and can handle the contradictory requirements on performance and size [120]. It is used to determine optimal current in the antenna design region, physical bound for arbitrary antennas and figure of merit for antenna designs [59, 81]. The physical bounds are found by maximizing a certain performance parameter with freely placed current in the design space [121].

In [122], the theory of non-radiating (NR) source is exploited to modify the current on an antenna surface without introducing modification to the radiated pattern and achieving the desired level of phase smoothness. Also in [123], the Rao-Wilton-Glisson basis representation was used to simplify the underlying algebra while still allowing surface current regions of non-canonical and arbitrary structures to be treated. By switching to another basis generated by a specific eigenvalue problem, it is finally shown that the optimal current can be derived as a combination of a few eigenmodes. Then, the desired current can be determined and the antenna structure that produces the desired current or similar performance can be synthesized.

2. **Electromagnetic cloaking:** aim to reduce the mutual coupling between two closely spaced antenna operating at microwave frequencies. It also conceal an object from an incident electromagnetic wave by reducing the scattered, absorbed, and reflected field by the object thereby making it invisible to external electromagnetic waves. Cloaking is made possible because of the freedom and flexibility of metamaterials in manipulating electromagnetic propagation which represent one of its most powerful feature [124]. The effect of cloaking is observed both in the restoration of the S-parameter of the antenna and the radiation pattern almost similar to that of the free space antennas. In [9], mantle cloaking was employed in the design of two closely spaced monopole antenna shown in figure 1.11:

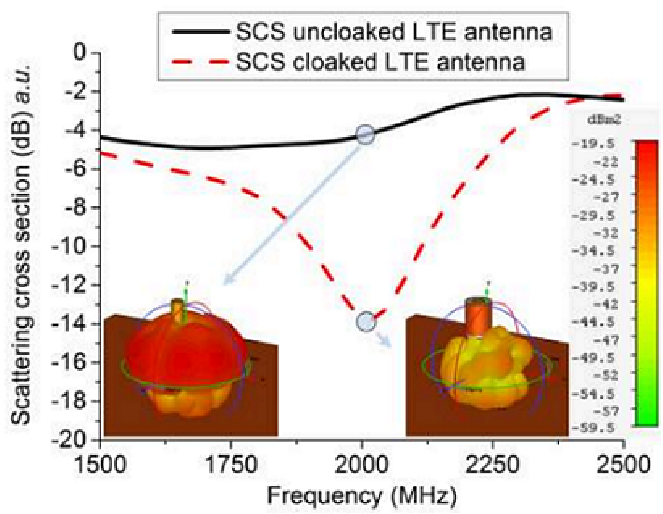

Figure 1.11: Cloaking of two closely spaced monopole [9].

Several methods for cloaking implementation include; transformation optics, transmission-line networks and plasmonic cloaking but these methods require bulk volumetric metamaterials which have a significant thickness compared with the size of the object to be cloaked [125]. An alternative method known as mantle cloaking based on the use of metasurfaces to create anti-phase surface current and enable the suppression of the dominant scattering of the object to be cloaked have been demonstrated to be more effective [9]. Mantle cloaking can be physically understood by considering the destructive interference phenomena between the field scattered by the object and the field radiated by the current induced on the metasurface [49]. The cloak structure is designed such that it provides considerable scattering reduction while preserving the electromagnetic performance of the cloaked surface. Other applications of electromagnetic cloaking include improving sensing [126] and enhancing directivity [127].

Electromagnetic cloaking require proper knowledge and understanding of the antenna structure and its surface impedance. They are mostly designed using analytical formula developed for canonical structures and difficult to implement for non-canonical and arbitrary structures. The size of the object that can be cloaked is also a limiting factor.

3. **Application of theory of characteristic modes:** theory of characteristic modes (TCM) are being applied to antenna designs because of the numerous advantages it bring to the design process. It is applicable to non-canonical and arbitrary structures, independent of excitation and provides insight into the physical behaviour of the design structure [12]. This allows for easy implementation of other existing antenna performance enhancement techniques.

   TCM is a set of surface current and radiated fields that are characteristics of a structure and are dependent on the shape and composition of the structure. Although, it was originally developed for perfectly electrical conductors, it have been extended for use with dielectrics [23]. TCM begins with the surface impedance matrix of the structure given as:

$$\mathrm{Z} = \mathrm{R} + \mathrm{jX}, \tag{1.4}$$

   where R is the real part and X is the imaginary part of the impedance. The impedance, Z is used in finding the solution of the generalized eigenvalue equation given in equation (1.5) as:

$$[\mathrm{X}][\mathrm{I}] = \lambda_{\mathrm{n}}[\mathrm{R}][\mathrm{I}], \tag{1.5}$$

   where λ_{n} is the eigenvalue of each n mode and I is the eigen-current.

   The value of λ_{n} is directly related to the nature of the modal stored energy by the term X with λ_{n} greater than zero indicating a stored magnetic energy, λ_{n} less than zero indicating a stored electric energy and λ_{n} equal to zero indicating total radiation with no stored energy. This modal stored energy deductions are however only qualitative [12]. In [10], TCM was applied to analyze a car structure to determine the best antenna position as shown in figure 1.12:

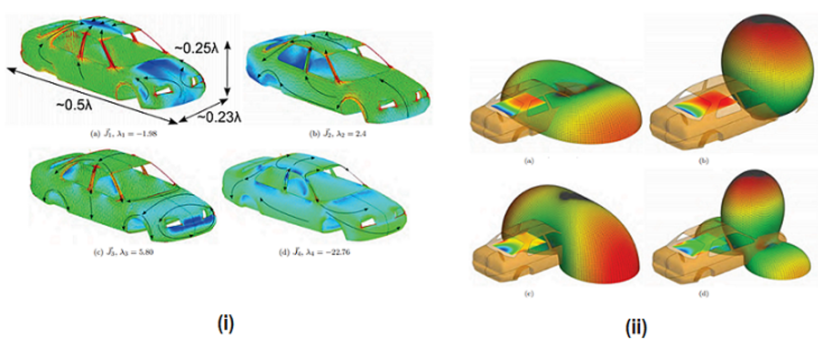

Figure 1.12: Application of TCM to a car design: (a) current distribution of first four modes (b) near field and far field of first four modes [10].

   TCM have been shown to be a very useful tool in many design application, some of which are related to antenna engineering and include:

- Electrically small antenna design: this is the most common use of TCM because it allows for systematic design and understanding of the radiating near and far field behaviour of the antenna structure. It also provides important information which guide the excitation of the antenna structure to achieve the desired radiation pattern [128].

- Antenna placement analysis: TCM have shown to be a useful tool in determining the best position for the placement of an antenna by leveraging the characteristic mode behaviour of the platform. This technique have been extremely useful in design of antennas for moving platforms such as aircraft, ship and unmanned area vehicle (UAV) [23] which require long distance transmission and relatively low frequency bands. The application of TCM to evaluate the surface current density of an helicopter is shown in figure 1.13:

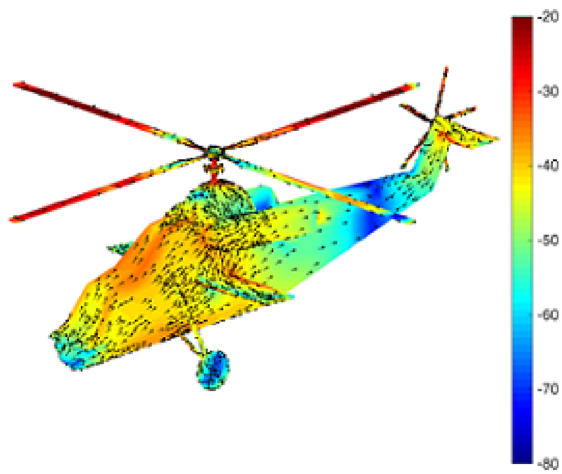

Figure 1.13: Surface current density of an helicopter using TCM to determine its antenna placement [11].

The current density of the helicopter can then be used to determine the best position for the antenna structure based on the available excitation source (capacitive or inductive excitation).

- Antenna shape synthesis: TCM is based on structural geometry and help in optimizing the shape of antennas thereby ensuring efficient radiation and proper impedance matching at a desired frequency [129]. In [12], TCM was used to analyze the physical behaviour of different antenna shapes as shown in figure 1.14:

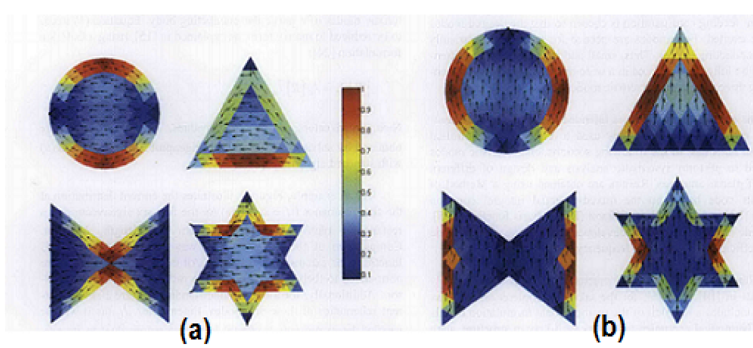

Figure 1.14: Normalized surface current of antenna shapes (a) mode J_O (b) mode J_1 [12].

- Metamaterial inclusion design: TCM have recently been applied to the design of metamaterial inclusion and metamaterial inspired antenna [24,130] thus making it a very versatile tool for electromagnetic synthesis.

- Antenna quality factor computation: this is one of the most studied quantity of antenna design and it is mostly applied in electrically small antenna design for determining the possible bandwidth of the antenna. TCM allow the expansion of the total Q in term of modal Q with two possible methods to evaluate Q which are using the input admittance or using energy and power of the related modes [131].

1.5 Conclusion

This chapter examined the challenges affecting the performance of integrated antennas resulting from the physical limitation of balancing its size, bandwidth and efficiency. An example of installed antenna on a train system was used to provide a pictorial view and understanding of integrated antennas. It was used to provide a baseline on the challenges and limitations on antenna performance upon integration. These include an increase in the Q-factor and antenna coupling, causing impedance mismatch and distortion of the radiation pattern.

A review of the existing methods for enhancing the performance of integrated antennas were given. The methods were divided into two broad categories which are the empirical method which is a brute force method requiring no knowledge of the system and the systematic method requiring sufficient knowledge of the antenna system as a major requirement for its proper implementation. The implementation of these methods require a trade-off among the characteristics for its optimization of another characteristics among the size, bandwidth and efficiency.

One of the drawback to most of the existing techniques for implementing the enhancement of integrated antenna is that they are either limited to radiation problems(i.e. enhancing the radiation properties) or scattering problems(i.e. antenna coupling analysis) but may not apply to the analysis of both scenario. Also, most of the methods are non generic in terms of when they can be implemented. It must either be implemented only before integration or only after integration. To address these drawbacks, it is imperative to develop a more generic approach that can be applied before and after integration as well as applicable to both radiation and scattering analysis.

Chapter 2

Proposed systematic method for enhancing the performance of integrated antennas using parasitic metamaterial inclusion

2.1 Introduction

Modal methods for enhancing the performance of integrated antennas provide several advantages such as providing physical insight into the radiation properties of the antenna structure, obtaining the optimal radiation performance of the antenna and in some cases, evaluating the scattering properties of the antenna. It provide a useful guide to enhancing the design and implementation of an antenna to achieve its optimal performance. Although, most of the existing systematic methods can be applied independently to either radiation or scattering analysis of canonical structures, one of the recent modal method gaining attention by researchers and engineers is TCM because of its independence of excitation and its application to non-canonical and arbitrary structures [12, 23]. TCM allows for systematic implementation of parasitic elements in an antenna design because it gives physical insight into the radiation properties of the antenna element.

Among other parasitic elements, metamaterial inclusions have already been demonstrated theoretically and experimentally to be a good candidate for enhancing the performance of integrated antennas while keeping the antenna within its electrically small regime [24, 132, 133]. This is attributed to their ability to manipulate electromagnetic waves which have made them very popular even in other electromagnetic applications. Their flexibility in electromagnetic applications has made them suitable for the development of our proposed systematic method for the enhancement of integrated antennas. The challenge however is that in antenna applications, the use of metamaterial inclusion require an accurate description of its near-field but the available effective parameter method for defining metamaterials are based on their far-field quantities. In [24], TCM was used in describing the near-field of inclusions for antenna application but these descriptions are only qualitative and might fail to provide adequate description for complex antenna design. The simple analysis of modal fields, eigenvectors and eigenvalues from TCM or other modal methods does not readily provide information on coupling between the inclusion and the antenna element which could aid the optimal positioning of the inclusion with respect to the antenna. Further developments such as the proposal of useful metrics for the analysis of the coupling between an antenna and a nearby structure can be useful.

In this chapter, the challenges of the existing systematic modal methods to enhancing the performance of integrated antenna is addressed with the proposal of a systematic method. First, the limiting factors of the existing methods for enhancing the performance of integrated antennas are given. Furthermore, the motivation which justifies the proposal of a different method and its relevance is explained. Finally, the proposed method for enhancing the performance of integrated antenna is presented. The proposed method consider the use of metamaterial inclusion as either parasitic element or a cloak. It begin with the application of TCM and include the analysis of the radiation and scattering properties. The radiation properties are evaluated using the stored energy while the scattering properties are analysed based on the inter-modal coupling co-efficient. The stored energy of the antenna is used in the selection of an inclusion to compensate for its stored energy at the frequency of interest while the inter-modal coupling determine the configuration of the inclusion with respect to the antenna element. The method is applicable to design of electrically small antenna as well as implementation of electromagnetic cloaking.

2.2 Limitations of existing systematic method for performance enhancement of integrated antenna

There are a number of advantages to the existing systematic methods for enhancing the performance of integrated antennas and also some limiting factors that affect their application and implementation. Some of these limitations are as follows,

- **Restriction to canonical structures:** some of the existing methods like electromagnetic cloaking and many q-factor optimization techniques are only applicable to canonical structures and are complicated to implement when non-canonical and arbitrary structures are involved. Already, the high demand for wireless application require many antenna structures to be non-canonical and arbitrary therefore making the existing methods insufficient for their design and analysis.

- **Needed insight into the properties of the antenna:** one major requirement for the successful implementation of the systematic methods for enhancing the performance of integrated antenna is having sufficient knowledge of the properties of the system. For instance, in the design of vehicular monopole antennas, the type of material and permittivity of the antenna ground have to be known so as to optimize the design for its most efficient performance [33]. In the case of biomedical antenna, the composition of the body have to be predicted and modelled to ensure that the antenna performs efficiently within the human body [32]. Although in the case of simple canonical integrating platforms, the radiation properties can be easily determined by using well known analytical formulations present in literature however for non-canonical structures that cannot be accurately modelled, the challenge is more complicated and a different method is required.

- **Complexity in analysing large integration platforms:** one of the method for enhancing the performance of integrated antenna is the analytical method. It provides exact solutions to enhancing of integrated antennas by representing the problem of antenna integration as a mathematical function. The analytical method have already been employed in the optimization of antenna current and Q-factor for better antenna performance. As noted in [121, 134], these methods are simplified for analysing electrically small radiating structures and gets more complicated as the size of the structure increases. For instance in [26], it was stated that the various analytical methods for evaluating the Q-factor of an antenna tend to agree for electrically small structures but as the structure increases the variation in the result differ and the accuracy of the different formulations can not be ascertained. The use of mantle cloak is also limited by the size of the object that can be cloaked

- **Variation in the antenna performance upon integration:** in implementing the systematic method to enhancing the performance of integrated antennas like the analytical method, some assumptions are made (e.g. the antenna materials are lossless) which do not apply in real scenarios therefore, the antenna performance varies compared to the result obtained from the systematic analysis. Elements in the surrounding also have an impact on the antenna performance and are not taken into consideration in the antenna design process [46]. Although, most of the methods tend to minimize the impact of these variations, they can sometimes limit the optimal performance of the antenna.

2.3 Importance of a proposed systematic method for performance enhancement of integrated antenna

In consideration of the merits and demerits of the existing techniques for enhancing the performance of integrated antennas, the need for a different method is justified. In this section, the justification, relevance and challenge requiring the need for a different method to systematically enhance the performance of integrated antenna are discussed.

2.3.1 Justification for the proposal of a different method

A good number of techniques exist for the enhancement of integrated antennas therefore, for the proposal of a different method, it must be motivated and justified by some factors. The justification and motivation for the proposed method include;

- **Generic technique to antenna enhancement before and after integration:** most of the already existing techniques for antenna integration are limited to either their implementation before integration or their implementation after integration. For instance, the optimization of antenna geometry before integration is difficult to implement after the antenna integration process. Although, after using a particular technique to enhance the performance of an antenna before integration, a different technique can be applied to further enhance the antenna performance upon enhancement.

  Therefore, to provide a more generic technique that can be applied to antenna enhancement before integration and antenna enhancement upon integration, this method is proposed. The method can be used for the free-space optimization of antenna as well as optimization of integrated antenna and provides a link between the antenna enhancement before integration and upon integration.

- **Application to non-canonical and arbitrary structures:** antenna and integration platforms are sometimes designed in canonical form however, with the increasing application of wireless systems, antenna and platform can be non-canonical and arbitrary. Most of the existing analytical methods for designing and analysing antenna's performances are based on formulation for canonical structures [135] which are complicated and require additional complex functions when applied to non-canonical and arbitrary structures hence, limiting their use.

  The need to have a method that is not limited to canonical structure has motivated the proposal of this method in enhancing the performance of integrated antenna. The method should be applicable to canonical structures and non-canonical structures alike.

2.3.2 Relevance of the proposed method

Although, the need for a different method to enhancing the performance of integrated antennas have been justified in the preceding section, the proposed method is of significant relevance to the design of electromagnetic systems because:

- **It provides a link between radiation analysis and scattering analysis:** generally, antenna integration is divided into two sections which are the antenna radiation and the antenna scattering. Antenna radiation deals with the performance of the antenna in terms of the antenna behaviour, radiation pattern and radiation efficiency. It consider the far-field behaviour of the antenna and distinguishes between an omnidirectional or directional antenna. Scattering on the other hand deal with the mutual coupling of antenna to its environment [136]. It considers the antenna surroundings and the impact of the immediate environment on the performance of the antenna.

  Most of the existing methods for enhancing the performance integrated antenna consider the integration problem as either a radiation problem or a scattering problem however in the proposed method, the radiation and scattering of the integrated antenna are considered alike. It analyses the radiation efficiency and the mutual coupling of the antenna in a systematic way using the same impedance matrix data.

- **It is applicable to many antenna integration problem:** the ability of the proposed method to analyze both antenna radiation and antenna scattering makes it a versatile technique. It is applicable to not just free-space antenna optimization but can be used for many antenna integration problems including electromagnetic cloaking and Q-factor optimization. The method is also not limited by the integration platform and can be applied to both simple and complex platform applications such as mobile phones, automobile, aerospace, Internet of Things (IoT), etc.

2.3.3 Challenge for implementing the proposed method

The proposed method for enhancing the performance of integrated antennas follow a modal method which give insight into the physical behaviour of the structure by representing them as a number of modes. Although, a number of modal methods exist such as singular expansion method (SEM) and eigenmode expansion method (EEM), their values are complex which make them difficult to manipulate [137]. TCM whose values are real and easy to manipulate are employed in the modal analysis. The modes are then used to analyze the radiation and scattering properties of the antenna in the following ways;

- **Modelling of antenna radiation:** the radiation of an antenna structure is mainly due to its conductive part [138] therefore in modelling of the antenna radiation, we focus on analyzing the metallic part of the structure. The antenna's radiation efficiency is a function of its stored energy such that the lower the stored energy, the better the radiation of the structure [54, 139]. To model the radiation, we solve for the modal stored energy of the structure which represent how well the different modes will radiate. The larger the stored energy, the less likely the mode is to resonate.

- **Modelling of antenna scattering:** the scattering of an antenna is a function of its mutual coupling to its environment [136]. In many cases, the coupling of an antenna to its environment is reduced to prevent the immediate environment from affecting the antenna's performance. However in our method, we aim at increasing the coupling between the antenna and the inclusion. The inter-modal coupling is used to analyze the antenna's scattering and represent the coupling between the antenna's radiation and the inclusion's radiation by quantifying the interaction between the antenna's mode and the inclusion's mode.

2.4 Description and formulation of the proposed method for enhancing the performance of integrated antenna

A systematic method for enhancing the performance of integrated antenna require insight into the properties of the antenna structure therefore, our proposed method begin with analysing the physical behaviour of the antenna structure. It exploit the advantage of the theory of characteristic modes in providing insight into radiating structures independent of shape and excitation. Furthermore, the derived impedance matrix of TCM are employed in analysing the radiation properties of the antenna structure. They are used in solving for the modal stored energy quantity of the structure which is a near-field quantity that impact the radiation performance of the structure.

By using similar radiation analysis, a set of metamaterial inclusion from either a look-up table (LUT) or existing literature is analyzed. These inclusions have been classified based on their qualitative stored energy analysis using TCM [24] and are known to store compensating energy to that of the antenna structure. The quantitative stored energy analysis of the inclusion is necessary to ensure that the selected inclusion has sufficient stored energy to compensate for the antenna's stored energy without the need for any external matching circuit (i.e. an antenna with dominant electric stored energy is paired to an inclusion with dominant magnetic energy). Although in the case of a non-resonant antenna and a resonant inclusion, the compensating energies will not be equal to each other because the resonant structure would usually store smaller energy compared to a non-resonant structure however, the inclusion with the closest compensating stored energy quantity to the antenna is chosen.

The chosen inclusion is used as a parasitic element for the antenna but the scattering properties will be analyzed to ensure that the coupling between the antenna and the inclusion is strong enough to provide an enhanced performance of the antenna since the positioning of the inclusion with respect to the antenna affect the overall system performance [54]. The scattering properties of the antenna and inclusion are analyzed using the inter-modal coupling co-efficient which uses the TCM impedance matrix in its evaluation such that the higher the value of the inter-modal coupling co-efficient, the better the antenna performance.

An integrated antenna with enhanced performance is therefore achieved when the stored energy of the metamaterial inclusion compensates for the stored energy of the antenna and when the inter-modal coupling between the inclusion and the integrated antenna is strong enough such that the antenna properly excites the inclusion. To summarize the method, consider the chart shown in figure 2.1:

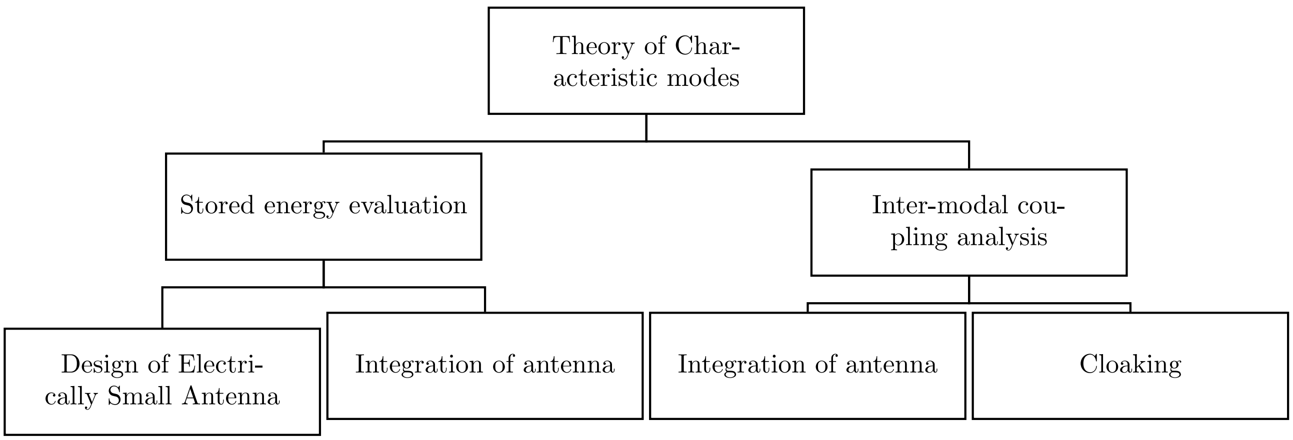

Figure 2.1: Proposed method for enhancing the performance of integrated antenna.

In fig. 2.1, the procedure begins form the application of TCM to the structure. This provides a modal based method focused on the near-field behaviour of the structure. Both the radiation analysis and the scattering analysis are evaluated based on the TCM impedance matrix. Already, the stored energy method have been shown to be useful in the design of ESAs however, the use of quantitative stored energy method and the inter-modal coupling co-efficient enhances the performance upon integration.

The accuracy of the stored energy quantity and the inter-modal coupling co-efficient is dependent on the accurate application of the TCM. The evaluated stored energy provides a more quantitative description of the near-field behaviour of radiating structures and provide a more accurate way to easily select an inclusion for a particular antenna application. When two electromagnetic structures like a radiating antenna and an inclusion are placed in close proximity to each other, the effect of coupling comes to play and has a great impact on the performance of the antenna therefore, the inter-modal coupling co-efficient is important.

For application purpose, the evaluation of stored energy and the inter-modal coupling co-efficient are applicable to the design of parasitic metamaterial ESAs and integrated antennas. They can be applied in determining the best inclusion to associate with a particular antenna and the best configuration of the inclusion with respect to the antenna structure. They are also useful and applicable in antenna integration especially in the design of electromagnetic cloak to shield integrated antennas from being affected by its near-field environment.

2.4.1 Physical insight into the behaviour of a structure using TCM

The use of TCM has been described as one of the existing systematic method for enhancing the performance of integrated antennas with the ability to provide insight into the physical behaviour of radiating structures independent of excitation and applicable to non-canonical and arbitrary structures. As a result of these advantages, it has found usefulness in the proposed method for analysing the physical behaviour of antenna elements.

2.4.1.1 Description of the theory of characteristic modes

TCM show the numerical representation of the current modes supported on a structure which provide physical insight into the radiating properties of the structure. TCM theory was first proposed in 1965 by Garbacz [140] based on the assumption that scattering of an object is a linear combination of modal patterns due to the shape of the object. In 1971, Garbacz [141] used TCM for the problem of scattering of conducting bodies by completing the theory and its expansion method through diagonalizing the corresponding scattering matrix. TCM was thereafter refined by Harrington and Mautz [142] by diagonalizing the operator that relate the current to the tangential electric field on the body. Although, the first development of TCM was applicable to perfectly electric conductors (PEC) [141], it was later extended to dielectric materials [143] making it very useful in many applications especially in the domain of antenna engineering [12, 23, 128, 144].

Theory of characteristic modes is formulated using the surface integral equation [23]. For PEC bodies, electric field integral equation (EFIE) are generally employed but magnetic field integral equation (MFIE) and combined field integral equation (CFIE) can also be used. The surface integral equation is discretized into matrix equation by applying the Method of Moments (MoM). The MoM matrix is then used to develop the generalized eigenvalue equation whose solutions are the characteristic currents and characteristic fields that give physical insight into the radiating properties of the structure.

If one consider an arbitrary shaped conducting structure S, after its illumination by an incident plane wave E^i, it will produce surface current J and scattering field E^s as shown in figure 2.2.

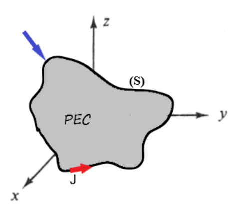

Figure 2.2: Incident electric field E and induced current J on an arbitrary shaped PEC object S.

Based on Maxwell equation and the electromagnetic boundary conditions, the tangential electric field disappear on the surface of the conductor to produce the scattering field E^s. Thus, a relationship between the electric fields and surface currents can be expressed with an operator L:

$$[L(\mathrm{J})]_{tan} = \mathrm{E}^i_{tan}(S). \tag{2.1}$$

The L operator has the impedance property and can be defined by an impedance operator Z as:

$$[L(\mathrm{J})]_{tan} = [\mathrm{Z}(\mathrm{J})]. \tag{2.2}$$

The Z matrix also denotes the MoM matrix and can be written in terms of its real R and imaginary X part as:

$$\mathrm{Z} = \mathrm{R} + j\mathrm{X}. \tag{2.3}$$

Both R and X are real and symmetrical and are used in solving the generalized eigenvalue equation:

$$\mathrm{X}\mathrm{J}_n = \lambda_n \mathrm{R}\mathrm{J}_n. \tag{2.4}$$

λ_n is the eigenvalue and J_n is the eigen-current of the n mode and are both real since R and X are symmetrical

Modal quantities associated with TCM: The solutions of the TCM eigenvalue equation are applied in deriving modal quantities which provide physical insight into the radiating behaviour of the structure. These quantities include:

1. **Eigenvalue (λ):** is the quantity derived directly from solving the eigenvalue equation. Its magnitude is proportional to the stored energy of the radiating structure and its value ranges between -∞ to +∞. The physical interpretation of the eigenvalue is that:
   - $\lambda = 0$ correspond to a case of resonance with no stored energy and the associated modes are referred to as the resonant modes,
   - $\lambda > 0$ correspond to a case of the magnetic stored energy dominating the electric stored energy and the associated modes are referred to as the inductive modes,
   - $\lambda < 0$ correspond to a case of the electric stored energy dominating the magnetic stored energy and the associated modes are referred to as the capacitive modes.
2. **Characteristic angle (α):** is a more intuitive modal quantity from TCM analysis and directly related to λ. The value of λ have a large range between -∞ to +∞ and α help to limit the range to between 90° and 180°. The relationship between λ and α is:

$$\alpha_n = 180^\circ - tan^{-1}\lambda, \tag{2.5}$$

   and the physical interpretation of the characteristic angle is that:
   - $\alpha_n = 180^\circ$, the structure resonate,
   - $\alpha_n < 180^\circ$, the structure store more magnetic energy,
   - $\alpha_n > 180^\circ$, the structure store more electric energy.
3. **Modal significance (MS):** is the normalized amplitude of the current modes which are independent of any specific external excitation source. It show the coupling ability of each mode to an external excitation and it provide convenience for analyzing the resonant behaviour over a large bandwidth. The relationship between λ and MS is:

$$MS_n = \left| \frac{1}{1 + j\lambda_n} \right|, \tag{2.6}$$

   hence, the value of MS ranges between 0 and 1 with the more significant modes identified as those with MS $\geq \frac{1}{\sqrt{2}}$ which are above 0.7.
4. **Modal weighting co-efficient (MWC):** inform on how each current mode respond to an applied external excitation source. It show the level of coupling between the external excitation and the modal current. MWC value depend on the type, position, magnitude, phase and polarization of the external excitation source. Its value also ranges from -∞ to +∞. The MWC is given as:

$$\text{MWC} = \frac{V^i.\text{J}_n}{1 + j\lambda_n}, \tag{2.7}$$

   where V^i is the excitation applied to the structure.
5. **Modal surface current distribution:** show how the current on the structure is distributed for each mode. They provide a basis for selecting and positioning appropriate excitation source to excite a particular mode [145]. A capacitive excitation is used at the position with minimum surface current distribution while an inductive excitation is used at the position with the maximum surface current distribution to excite a particular mode.
6. **Modal far-field distribution:** show the far-field behaviour of each mode such that one could excite a combination of modes to achieve a desired radiation pattern [23]. It could also be used to distinguish one mode from another in analysing the physical behaviour of radiating structures.

Properties of theory of characteristic modes: The properties of the theory of characteristic modes are among the reasons why it is gaining more attention. Characteristic mode values which are real values allow for easy manipulation and interpretation. Characteristic modes also exhibit orthogonality in the following ways:

1. **Characteristic Currents Orthogonality:** in the application of the eigencurrent for characteristic modes, the eigencurrents are normalized to a unit radiation power such that the magnitude of the currents reveal the modal radiation efficiency. The eigencurrent normalization being given as:

$$\text{J.R.}J^H = 1, \tag{2.8}$$

   where J^H is the Hermittan transpose of J. However, R and X of the impedance matrix are real and symmetric and ensures that J remains orthogonal with properties as:

$$\text{J.R.}J^H = \delta, \tag{2.9}$$

$$\text{J.X.}J^H = \lambda\delta, \tag{2.10}$$

$$\text{J.Z.}J^H = (1 + j\lambda)\delta. \tag{2.11}$$

   Hence, current polarization and current magnitude are orthogonal allowing the possibility to excite two modes simultaneously or to suppress the excitation of unwanted modes. This orthogonal current property further help to guide the feeding of a structure to achieve improved isolation performance and desired radiation property [146].

2. **Characteristic Fields Orthogonality:**The electric fields E_n and the magnetic fields H_n produced by an eigencurrent J_n on S are called the characteristic fields or eigen-fields associated to J_n. Characteristic fields polarization and characteristic fields magnitude are also orthogonal allowing the possibility to design structure with multiple radiation properties such as MIMO systems [146, 147]. The orthogonality relationship for the characteristic fields corresponding to the characteristic currents are obtained by means of the complex Poynting theorem [148] and can be represented in terms of the electric field E and magnetic field H:

$$\frac{1}{\eta_s}\,\text{E.}E^* dS = \delta, \tag{2.12}$$

$$\eta_s \text{H.}H^* dS = \delta, \tag{2.13}$$

2.4.1.2 TCM analysis of radiating element

In the design of most integrated antennas, the antenna specifications are pre-defined. The integration platform is defined by the wireless system manufacturer while the antenna is defined based on the integration platform. The physical behaviour of the antenna is analyzed using TCM and evaluated as:

- Resonance: the resonance of the antenna is directly determined from the eigenvalue. It form the basis on which the inclusion will be chosen. In certain cases, the antenna may be non-resonant at the frequency of interest and the eigenvalue provide an insight into the nature of the stored energy at this frequency. All other modal quantities are evaluated around this frequency of interest.

- Bandwidth: show the frequency region where the antenna is matched (i.e. below -10 dB). It is represented with the modal significance above 0.7 and represent the frequency region that contribute to the radiation within which the modal stored energies are compensated for.

- Radiation pattern: inform about the modal far-field behaviour of the structure. One can determine the mode to excite based on the desired far field behaviour. A combination of modes can also be excited by studying the radiation pattern for achieving a hybrid far-field behaviour.

2.4.1.3 TCM analysis of metamaterial inclusion

Inclusions with compensating stored energies are chosen from a list of inclusion LUT. The physical behaviour of the inclusions are studied to ensure that the chosen inclusion matches that of the corresponding antenna. In the design of ESAs with inclusion, the behaviour of the inclusion is imposed on the behaviour of the antenna [24] hence, the inclusion must be carefully chosen to meet the desired radiation properties. Just like the radiating element, the physical behaviour of the inclusion is also analyzed using TCM and it is evaluated as:

- Resonance: the selected inclusion is optimized to resonate at the frequency of interest after its selection from the the inclusion's LUT. The selection is based on the result of the analysis of the antenna structure such that the inclusion compensate for the antenna behaviour. While most antenna application of metamaterial inclusions use the resonant inclusion, the non-resonant inclusion can also be applied and will store electric or magnetic energy.

- Bandwidth: similar to the antenna bandwidth, it show the frequency around which the antenna is matched (i.e. below -10 dB). It is region with modal significance above 0.7 and represent the frequency region that contribute to the radiation. The bandwidth of the inclusion is very important in determining the overall bandwidth of the system and can be optimized to provide a wider bandwidth when used with a resonant antenna structure [149].

- Radiation pattern: inform about the modal far-field behaviour of the structure and determine the mode to be excited depending on the desired far field behaviour. The chosen inclusion should have the radiation pattern of their resonant mode or fundamental mode (i.e. in the case of non-resonant inclusion) similar to the antenna structure or of the desired radiation pattern.

2.4.2 Radiation analysis based on evaluated stored energy

The radiation efficiency of a structure is related to its stored energy therefore, ESAs have low radiation efficiency because of their high amount of stored energy. In the radiation analysis, the evaluation of stored energy is employed since the goal of enhancing the performance of integrated antenna is achieved by minimizing the stored energy of the antenna structure which is a near field quantity concentrated at the source. Usually, the near-field consist of multi-pole type fields considered as a collection of dipoles. The use of the near-field quantity have been of increasing interest especially in the design of capacitive sensing technologies such as in touchscreen of smart phones and computers. In antenna engineering, near-field effect also include energy transfer directly coupled to near-by receivers and affecting the power output of the transmitter. In other words, the near field energy if properly tapped, can be made available to a receiver.

2.4.2.1 Stored energy evaluation

In the electromagnetic fields, stored energy refer to the part of the electromagnetic energy that is not dissipated from the antenna and it is useful in determining performance bound on antennas and in evaluating Quality factor (Q-factor) given as [26]:

$$\mathrm{Q} = \frac{2\pi \mathrm{W}_{\mathrm{sto}}}{\mathrm{P}_{\mathrm{rad}}} \tag{2.14}$$

where $\mathrm{W}_{\mathrm{sto}}$ denote the stored energy and $\mathrm{P}_{\mathrm{rad}}$ denote the dissipated energy. The Q-factor is then used to estimate the fractional bandwidth of the system given as:

$$\mathrm{BW} = \frac{f_0}{Q}. \tag{2.15}$$

The concept of stored energy have been a challenging topic over the years with different methods and no unique definition widely accepted [150]. Although the concept was introduced a long time ago [151,152], the research for the ultimate expression is still an ongoing task [27,118,153,154]. For non-dispersive components, the mean lost energy causes no problem and can be evaluated as the sum of the mean radiated energy and the mean energy dissipated due to material losses. However for non-stationary electromagnetic field associated with radiators, defining the stored electric and magnetic energies present a challenge which comes from the radiation energy that does not decay quickly in the radial direction and instead remain infinite in the stationary state. To overcome the infinite values of total energy, the stored energy in a radiating system is evaluated by a technique of extracting the divergent radiation component from the well-known total energy of the system. Classically, it can be evaluated from either the input impedance of the antenna or the electromagnetic fields around the antenna. While some papers have referred to stored energy as recoverable energy [150,155,156], others consider it as an observable energy [157,158] arguing that, we cannot measure the total stored energy of a structure except that which can be recovered. In [154,159], another method to defining stored energy was proposed. They considered antenna stored energy as the ability of the antenna to perform measurable work when the power supply is switched off. The energy at the port of an antenna was measured just after the antenna source was cut off and considered as the stored energy of the antenna system.

Interestingly, all the various methods to stored energy evaluation are in agreement when applied to electrically small systems (i.e. systems in the quasi-static limit like small antennas) but when large antennas are involved or antennas placed next to large objects are involved, there are large variations in the analysis [26].

2.4.2.2 Stored energy analysis of radiating element

The evaluation of antenna stored energy provide a quantitative basis for selecting an appropriate inclusion as opposed to the TCM direct analysis which is qualitative. In [4], the stored energy was expressed based on antenna current density which showed usefulness for antenna optimization and small antenna analysis however, it gives a negative value for electrically large structures [6]. Already, various formula for the evaluation of antenna stored energy exist which can be classified based on their method of derivation. These includes;

1. Expression based on electromagnetic fields: which is a co-ordinate dependent method and given as:
$$W_{Pr} = \frac{1}{4}\int_{R^3}(\epsilon_0 \mid E \mid^2 + \mu_0 \mid H \mid^2 - 4\sqrt{\epsilon_0\mu_0}\hat{r}.P)dV. \tag{2.16}$$
where W_{Pr} represent the electromagnetic stored energy, E and H are the electric and magnetic fields respectively, ϵ_0 and μ_0 are the permittivity and permeability respectively, R is the region and P is the power flow.

2. Expression based on system: which consider stored energy as recoverable energy given as:
$$W_{rec}(t_0) = -\int_{t_0}^{\infty} u_{in}(t)i_{in}(t)dt \qquad (2.17),$$
where
$$F^{-1}\{\frac{1}{Z_c}(1- \mid \Gamma(\omega) \mid^2)\} * u_{in}^{+}(t) = 0 \tag{2.18}$$
and where $*$ represent convolution, $F^{-1}\{\cdot\}$ is the inverse Fourier transform, u_{in} and i_{in} are the total port voltage and current respectively, Z_c is the port impedance and $\Gamma(\omega)$ is the system reflection coefficient.

3. Expression using currents: which can be based on the system current but also allow for the application of the modal method using the surface current which is given as:
$$W_{reac} = \frac{Z_0}{4\omega}\int_{\Omega}\int_{\Omega}((k^2 J_1.J_2^* + \nabla_1.J_1\nabla_2.J_2^*)\frac{cos(kr_{12})}{4\pi r_{12}} - k(k^2 J_1.J_2^* - \nabla_1.J_1\nabla_2.J_2^*)\frac{sin(kr_{12})}{4\pi})dV_1 dV_2 \tag{2.19}$$
where J represent the current density and the modal method is given as:
$$\mathrm{W_{sto}} = \mathrm{W_m} + \mathrm{W_e} = \frac{1}{4\omega}\mathrm{I^H X' I}, \tag{2.20}$$
where
$$\mathrm{W_m} = \frac{1}{8\omega}\mathrm{I^H X_m I} \tag{2.21}$$
and
$$\mathrm{W_e} = \frac{1}{8\omega}\mathrm{I^H X_e I}. \tag{2.22}$$

In [154], it was suggested that in evaluating antenna stored energy, one should consider time-evolution of total reactive energy within a given volume around the antenna, visualize reactive energy distributions around an antenna system, the connection between an antenna's localized electromagnetic energy and its re-radiated energy, and the exchange of energy between non-propagating and propagating antenna modes in time-domain.

In our proposed method, the modal method for evaluating stored energy of an antenna is applied to allow for its application to non-canonical and arbitrary structures and independent of excitation. It allow the use of the impedance matrix derived from the TCM analysis thereby providing consistency in the analysis of the structure.

2.4.2.3 Stored energy analysis of metamaterial inclusion

Generally, electromagnetic field energy density of materials such as metamaterials are defined using their effective material parameters which are the ϵ and μ values that are derived from far field quantities [160]. In literature, the stored energy density of metamaterial inclusions are derived using either the electrodynamic (ED) approach or the equivalent circuit (EC) approach which require the power loss and a knowledge of the dynamic equations of the electric and magnetic dipoles in the medium. The ED approach derive its energy density formula as a by-product of the Poynting theorem and it is inherently a time domain approach. In the EC approach, the material is transformed to a corresponding electric circuit where the arrangement and the value of the capacitances, inductances and resistances are derived and the electric and magnetic energies stored in the circuit system can be evaluated [161]. Other known methods applied in evaluating metamaterial stored energy density includes; Brillouin Approach, Landau Approach and Loudon Approach.

These energy density evaluation methods are only useful within the frequency range where the effective theory is accurate and gives unreliable results beyond this frequency range. They are also fully developed for canonical structures but becomes challenging when the metamaterial is non-canonical and arbitrary therefore, it does not provide physical insight into the near-field behaviour of the inclusion. The stored energy density of inclusions can be splitted into the near-field electric energy density and near-field magnetic energy density given as;

$$< W_e >= \frac{\epsilon_0 \mid E \mid^2}{4}(1 + \frac{\omega_p^2}{\omega^2 + v^2}) \tag{2.23}$$

and

$$< W_m >= \frac{\mu_0 \mid H \mid^2}{4}[1 + F\frac{\omega^2(3\omega_0^2 - \omega^2)}{(\omega_0^2 - \omega^2)^2 + \omega^2\gamma^2}] \tag{2.24}$$

with the total stored energy represented as;

$$< W_{sto} >= W_e + W_m \tag{2.25}$$

To gain physical insight of the near-field behaviour using the stored energy quantity of metamaterials, we follow a modal method based on the theory of characteristic modes. It provide an opportunity to directly evaluate the near-field stored energy quantity without the necessary application of an excitation source and can be used to classify metamaterial inclusions as either magnetic or electric. The stored energy of the inclusion is used to select an inclusion with compensating energy to that of the radiating element (i.e. if the antenna has dominant electric energy, an inclusion with dominant magnetic energy is chosen and vice versa).

2.4.2.4 Stored energy application

Some of the commonly used applications of the stored energy quantity include:

1. Antenna bandwidth enhancement: antenna's Q-factor is inversely proportional to its bandwidth and can be used as a direct measure of its bandwidth. However, the methods to compute antenna's Q require the evaluation of its stored energy quantity which can be integrated into a global optimization algorithm to reduce the optimization time. To enhance an antenna's bandwidth, the Q factor is minimized by reducing the stored energy of the antenna [162].

2. Antenna size optimization: antenna performance deteriorate as the antenna's physical size in wavelength decreases. The trade-off between performance and size is expressed by physical bounds which are based on the shape and size of the design. Physical bounds used as stopping criterion for an optimization process require a linear combination of the Q-factor, the difference between the stored electric and magnetic energies, and the metallic area [121, 162]. The Q-factor bounds can be applied to determine total directivity while the stored energy-based physical bounds for arbitrary small antennas provide interesting and useful information about the antenna design possibilities [163].

3. Small antenna analysis: usually the stored energies of a small antenna are quasistatic and similar to the stored energies in a static field. The physical limitation of electrically small antennas (ESAs) have always been used to evaluate such antenna's performance so as to develop an optimal designs. The minimum Q provide a benchmark on the possible maximum impedance bandwidth for an ESA. This require the stored energy evaluation which also allow the study of the effect of the shape on the performance [163].

4. Inclusion classification: recently, the stored energy have been shown to be a good tool for classifying inclusions in antenna application based on the qualitative stored energy analysis of the inclusion [131]. As would be later demonstrated, the use of the modal stored energy can provide an alternative way to defining inclusions for near-field application.

2.4.3 Scattering analysis using inter-modal coupling co-efficient

An antenna is a scatter whose scattering is related to its impedance. The impedance and radiation pattern are both frequency-dependent quantities relevant for defining an antenna. Describing an antenna by its radiation is incomplete because antennas with identical amplitude and phase patterns can scatter differently. These scatterings depend on the reactance and occur due to the interaction of an electromagnetic wave with surfaces due to mutual coupling between the wave and the surfaces [164]. It can also be referred to as the coupling which quantifies the transfer of energy from one system to another [165]. These coupling most times affect the electromagnetic system efficiency and the antenna radiation pattern hence, most systems try to limit its effect.

Coupling occur when there is another object in the vicinity of the antenna therefore the near-field configuration is different from that of the isolated antenna in free space. As a result, the current distribution, the antenna radiation pattern and input impedance changes. It varies by the number and type of antenna elements, spacing, relative orientation, radiation characteristics of the radiators, bandwidth, and the feed network. Neighboring objects can also be considered as part of an antenna thereby giving it a new radiation characteristics. The use of MTM have been shown to mitigate the effect of coupling and improve the return loss and gain with materials such as electromagnetic bandgap (EBG), split-ring resonators (SRR) and frequency-selective surfaces (FSS) [166].

In parasitic metamaterial antenna design, the goal is to optimize the coupling between the antenna element and the inclusion for performance enhancement. Therefore, to ensure consistency with the modal method in our proposed method, the inter-modal coupling analysis is used to evaluate the scattering properties.

2.4.3.1 Inter-modal coupling

Although there are a number of coupling theories and analysis for antenna designs [167] [168] and MTM designs [169], we follow the TCM based method [170] [149] in this work owing to the numerous advantages of TCM including the fact that the impedance matrix takes into account the effect of coupling, the physical insight given into the radiation properties of the element, independence of excitation and its applicability to arbitrary structures [12].

A method to evaluate the inter-modal coupling was proposed by S. Ghosal et al in [171] which expressed inter-modal coupling as a linear combination of the isolated modes. However in our proposal, a direct method for the evaluation of inter-modal coupling co-efficient proposed in [149] is followed. The antenna structure consisting of the radiating element and the metamaterial inclusion is taken as a single unit with different modes representing the different behaviours of the the individual structure. The coupling between the modes show how the different elements couple together to affect the performance of the antenna.

2.5 Conclusion

In this chapter, the limitations to the existing systematic techniques for enhancing the performance of integrated antennas were discussed. The motivation for the proposal of a different method which is the need to have a generic enhancement technique applicable to arbitrary-shapes and applicable before and upon integration was also discussed. The relevance of our proposed method in providing a link between radiation and scattering analysis was explained. Furthermore, the proposed method was presented and explained.

The proposed method is based on using metamaterial inclusions to enhance the performance of the integrated antenna. The proposed method involves the analysis of the radiation properties using stored energy and scattering properties using inter-modal coupling analysis. The stored energy of the antenna form the basis for the selection of an inclusion which aim is to compensate for the antenna's stored energy at the frequency of interest. The inter-modal coupling determine the configuration of the inclusion with respect to the integrated antenna such that the configuration with the highest inter-modal coupling is selected.

The method will be shown to be useful for enhancing electrically small antenna in both free-space and as integrated antenna. As will be shown in subsequent chapter, the method is also used in investigating the design of mantle cloaks to reduce blocking of antenna.

Chapter 3

Modal stored energy by metamaterial inclusions

3.1 Introduction

Our proposal for systematically enhancing the performance of integrated antenna involves the use of an accurate metamaterial inclusion to compensate for the modal stored energy of an antenna structure. Since these inclusions are used in the near-field of the antenna, the challenge in selecting these inclusions are compounded by the fact that metamaterials are generally defined from their far-field quantities (transmission and reflection co-efficient) using the classical method of the common effective parameter which do not accurately describe their near-field behaviour [172]. In fact, most of the analytical formula to describe metamaterials are only applicable to canonical structures. TCM has been demonstrated to be useful for non-canonical and arbitrary structures and provide a qualitative description of the near-field behaviour of inclusions [24] which may not be sufficient for an application involving complex structures since its relationship to the classical method cannot be accurately determined.

With the growing application of metamaterial inclusions to electromagnetic designs such as cloaking [173], antenna [18] and sensor design [174, 175], an evaluation of the near-field quantity of a metamaterial inclusion is significantly important to accurately describe its near-field behaviour and for accurately selecting and matching the proper metamaterial to the right electromagnetic structure to ensure an optimized performance. We believe the use of the TCM based modal stored energy provides an opportunity to be able to evaluate this near-field behaviour.

In [176], it was concluded that the general reactive field concept is inadequate to generally characterize the near-field of a radiator because when the excitation is unknown, one can use an abstract level of theory to formulate general propositions that include all antennas of interest which is only mathematical and does not provide insight on the inner structure of the antenna's near-field. However, one can derive enough useful information on the near-field behaviour which is relevant to its application with external structures.

The reactive component is represented by the imaginary part of the impedance matrix Z:

$$\mathrm{Z} = \mathrm{R} + \mathrm{jX}, \tag{3.1}$$

where R is the resistive part that denotes the radiation and X is the reactive part that denotes the stored energy. X is a combination of the capacitive and inductive part given as:

$$\mathrm{X} = \mathrm{X_L} + \mathrm{X_C}, \tag{3.2}$$

where

$$\mathrm{X_L} = \omega \mathrm{L} \ = 2\pi \mathrm{fL}, \tag{3.3}$$

and

$$\mathrm{X_C} = \frac{-1}{\omega C} = \frac{-1}{(2\pi \mathrm{fC})}. \tag{3.4}$$

In this chapter, we provide an overview to stored energy of metamaterial inclusions. We demonstrate a modal method to evaluating the stored energy quantity of metamaterial inclusion in details. The mathematical formulation for the modal stored energy evaluation is demonstrated and applied to well known inclusions (i.e. Broadside coupled split-ring resonator (BC-SRR) and S-shaped inclusion). We use the characteristic mode method which provide an opportunity to ensure that the method is applicable to arbitrary shaped inclusion. The relationship between the common effective parameter method and the proposed modal stored energy method is represented in figure 3.1:

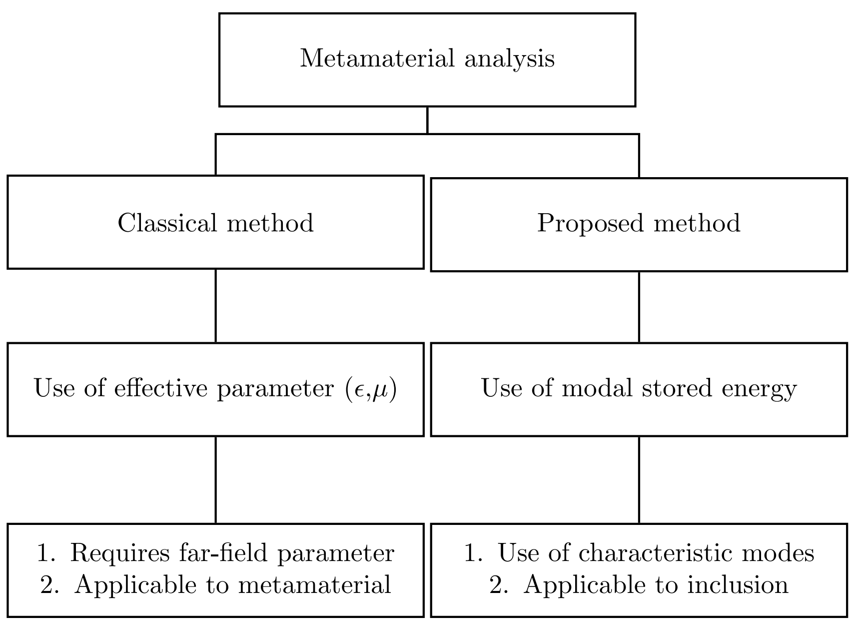

Figure 3.1: Relationship between the classical method and proposed method for describing metamaterials.

The modal stored energy can aid the classification of inclusions for near-field application purpose and it is qualitatively comparable to the common effective parameter method for describing metamaterial structures. To demonstrate this, new steps involving the excitation of the inclusions are added to the modal stored energy evaluation. A comparison of the modal stored energy method with respect to the known classical effective parameter method for describing metamaterial (MTM) structures is shown with the physical and qualitative analysis based on the modal stored energy method showing a good agreement to that of the effective parameter method.

3.2 Stored energy for metamaterials

There is an increasing interest in the properties of metaterial because of the need to explore its application. For this reason, their electromagnetic field energy density have been explored using different methods [177]. The stored and dissipated energy define the efficiency, performance bounds and bandwidth of electromagnetic systems like antenna [178, 179]. Unfortunately, there are no general formulation valid for arbitrary-shaped metamaterials. Infact, the use of the common effective parameter of permittivity and permeability functions are insufficient to provide an expression for evaluating the stored electromagnetic energy in the case of dispersion and losses except in the case of a known internal structure of the medium where a specific dispersion model (e.g. Lorentz or Drude dispersion) can be applied. In that case, the stored energy can be formulated in terms of the dispersion model parameters using the resonant frequency, the plasma frequency and the damping factor [160].

It is also true that the evaluation of the stored energy for metamaterials can be evaluated if the operational frequency is far away from the resonant frequencies and its absorption can be neglected however, most of the useful information for electromagnetic systems can be extracted at the region of resonance [160,180] where effective parameters are not always valid. An example is the association of the negative index of a metamaterial with a resonance in the magnetic polarizability. In [181], Q-factor of metamaterial was evaluated as the ratio between the resonance frequency and the full-width at half maximum of the resonance dip in the reflectance spectrum despite the fact that the Q-factor really means the ratio between the amount of energy stored to the amount of energy lost through dissipation.

A better approach to stored energy evaluation is to consider a modal solution since many small scatterers including metamterial unit cells can be modeled in terms of their mode. Although modal solutions may pose some numerical difficulties in solving eigenvalue problems for open systems with strong radiative losses, the modes of individual resonators allows for easier study of the behavior of the resonators as only few modes are required to give a highly accurate description of the structure over a very broad bandwidth range [12]. They also give account for the coupling interaction between elements.

A simple way to apply the modal method is to illuminate the structure at its resonance frequency and observe the fields but this is only effective if the modes are well separated in frequency. Unfortunately, many systems operate with overlapping modes making it difficult to separate the contribution of individual mode to the total response. Another technique is the application of equivalent circuit models [182] which provide simplicity by building on its well known application in antenna theory. A more advantageous method will be the scattering method that give the solution in terms of the conduction or polarization current [183]. It provide a useful description of the mode with a natural method to the current evaluation using integral equation methods like boundary element method, integral equation method or the method of moments [**?**] which is followed in this work. The current is expanded and the green's function is used to evaluate the interaction between the current elements. A solution is then found for any external exciting field using the derived impedance matrix with the radiation boundary conditions automatically accounted for. The model of resonant scatterers based on their complex singularities is an ideal tool to study coupling [184] .

In previous work, the qualitative insight of stored energy from the theory of characteristic modes was extended to design MTM inclusion [185]. It was shown that one of the challenge with metamaterial inclusions especially magnetic inclusion is that their magnetic properties are exhibited when excitation is placed in a specific polarization. Thus, excitation and polarization effect should be considered for accurately describing the modal stored energy of MTM inclusion.

3.3 Modal stored energy formulation

Unlike effective parameters which are valid in far-field, stored energy quantities define near-field interaction of electromagnetic systems [154]. The modal stored energy formulation is based on the Theory of Characteristic Modes (TCM) which represent a structure in terms of its surface impedance Z [12]. The surface impedance Z is given in equation (3.1) as:

$$\mathrm{Z} = \mathrm{R} + \mathrm{jX}. \tag{3.1}$$

Using the derived impedance Z, a solution is found for the generalized eigenvalue equation given in equation (3.11) as:

$$[\mathrm{X}][\mathrm{I}] = \lambda_{\mathrm{n}}[\mathrm{R}][\mathrm{I}], \tag{3.11}$$

where λ_{n} is the eigenvalue of each n mode and I is the eigencurrent.

The method of moments as applied in the theory of characteristic modes (TCM) bring physical insight through intuitive knowledge into the electromagnetic energy of radiating structures [12]. It is based on the surface current distribution which would address the challenge of near-field evaluation. It expand the current as a number of basis function and green function and by solving the derived impedance matrix as a generalized eigenvalue equation, electromagnetic energy can be calculated for any external exciting field. In other words, the TCM method is independent of excitation, applicable to non-canonical and arbitrary structures, takes into account the nature of the material and require only few modes to describe the global behaviour of an electrically small structure [12]. Thus, TCM stored energy method can be applied for the design of many electromagnetic systems especially antenna design [23, 48, 186] for various applications.

Although this modal stored energy formulation uses TCM-based method for its formulation, TCM have already been presented in the previous chapter. The value of λ_{n} is directly related to the nature of the modal stored energy by the imaginary part of the impedance matrix X with λ_{n} greater than zero indicating a stored magnetic energy, λ_{n} less than zero indicating a stored electric energy and λ_{n} equal to zero indicating that both the magnetic energy and electric energy are of equal magnitude which result in total radiation with no stored energy [23, 179]. The TCM modal stored energy deductions are however only qualitative [12]. Modal quantitative stored energy value of MTM inclusion provide a new way to reliably analyze artificial materials. This would aid their choice for specific application especially in cases where the near-field behaviour need to be predicted such as its association to antennas [132] and sensors.

Using the surface impedance Z derived from TCM, the modal stored energy operator ($\mathrm{W_{sto}}$) derived in [118, 162] and as applied to antenna design [179] is:

$$\mathrm{W_{sto}} = \mathrm{W_m} + \mathrm{W_e} = \frac{1}{4\omega}\mathrm{I^H X' I}, \tag{3.12}$$

where ω is the angular frequency, I is the eigen-current from the generalized eigenvalue equation, $\mathrm{I^H}$ is the Hermitian transpose of the eigen-current and $\mathrm{X'}$ is given in [179] as equation (3.13):

$$\mathrm{X'} = \omega\frac{\partial \mathrm{X}}{\partial \omega}. \tag{3.13}$$

The electric energy ($\mathrm{W_e}$) and magnetic energy ($\mathrm{W_m}$) component are represented individually by equation (3.14) and (3.15) [179]:

$$\mathrm{W_m} = \frac{1}{8\omega}\mathrm{I^H X_m I}, \tag{3.14}$$

and

$$\mathrm{W_e} = \frac{1}{8\omega}\mathrm{I^H X_e I}, \tag{3.15}$$

where,

$$\mathrm{X_m} = \mathrm{X}' + \mathrm{X}, \tag{3.16}$$

and

$$\mathrm{X_e} = \mathrm{X}' - \mathrm{X}. \tag{3.17}$$

X being a 3D matrix complicate the implementation of X', thus further simplification is carried out by splitting the impedance Z into its inductive and capacitive component as:

- For X as an inductive impedance:

$$\mathrm{X} = \omega L, \tag{3.18}$$

differentiating both sides with respect to ω,

$$\frac{\partial \mathrm{X}}{\partial \omega} = L. \tag{3.19}$$

But from equation (3.19),

$$\mathrm{X}' = \omega \frac{\partial \mathrm{X}}{\partial \omega}$$

substituting equation (3.19) into equation (3.13),

$$\mathrm{X}' = \omega \frac{\partial \mathrm{X}}{\partial \omega} = \omega L, \tag{3.20}$$

therefore substituting equation (3.18) into equation (3.20),

$$\mathrm{X}' = \mathrm{X}. \tag{3.21}$$

- For X as a capacitive impedance:

$$\mathrm{X} = \frac{-1}{\omega C}, \tag{3.22}$$

differentiating both sides with respect to ω,

$$\frac{\partial \mathrm{X}}{\partial \omega} = \frac{1}{C\omega^2}. \tag{3.23}$$

But from equation (3.13),

$$\mathrm{X}' = \omega \frac{\partial \mathrm{X}}{\partial \omega}$$

substituting equation (3.23) into equation (3.13),

$$\mathrm{X}' = \omega \frac{\partial \mathrm{X}}{\partial \omega} = \omega \frac{1}{C\omega^2} = \frac{1}{C\omega}, \tag{3.24}$$

therefore substituting equation (3.22) into equation (3.24),

$$\mathrm{X}' = -\mathrm{X}. \tag{3.25}$$

The conclusion therefore is that X' equal $|X|$ and the two possible analytical solution for X' depend on the nature of W_{sto} as either electric or magnetic. This conclusion has been qualitatively concluded using the first derivative of λ_n with respect to the frequency [131].

To ensure uniformity of the modal stored energy value, just as it is done for W_{sto} in antenna application for Q-factor evaluation, W_m and W_e are normalized with respect to the radiated power (P_r) [179, 187] given in equation (3.26):

$$P_r = I^H R I. \tag{3.26}$$

The transition from the qualitative modal stored energy method to the quantitative stored energy method based on TCM is represented in figure 3.2:

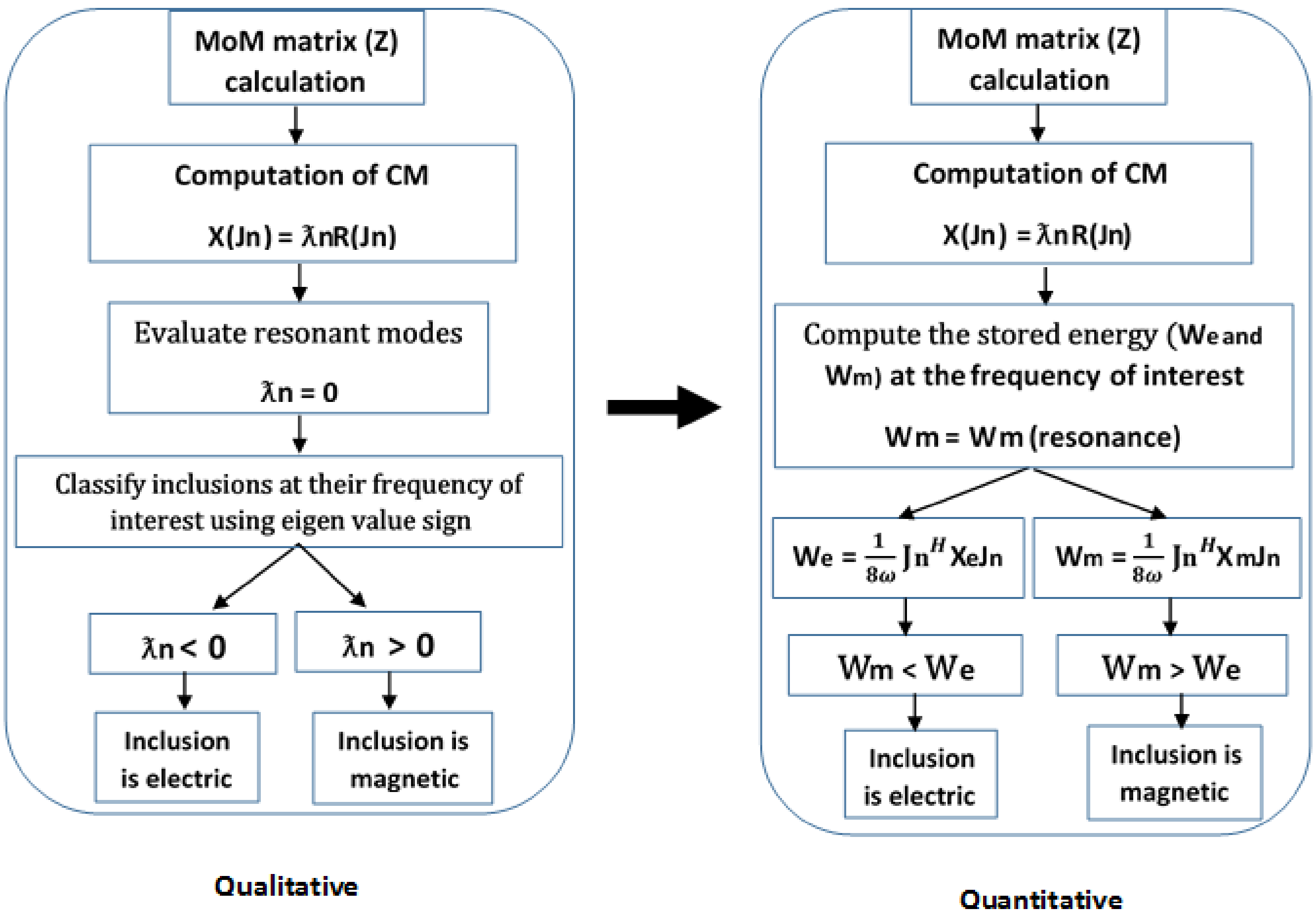

Figure 3.2: Summary of transition from qualitative to quantitative stored energy evaluation.

The chart in figure 3.2 show that both the qualitative and quantitative analysis result in the same conclusion. They both start from solving the MoM impedance matrix however, while the qualitative method intuitively draw its conclusion from the eigenvalue (λ) sign, the quantitative method evaluate the energies and thus provide a path to a more accurate and detailed analysis for application purpose.

3.4 Evaluation and analysis of modal stored energy of MTM inclusion

In this section, the W_{sto} formulation is applied to MTM inclusions to determine their modal magnetic and electric energies. The difference between the magnetic and electric energy (W_m - W_e) is used to determine the dominant energy with zero value indicating a vanishing energy (resonance) [188]. The non-resonant and resonant inclusions are analyzed. For the non-resonant case, a rectangular strip structure is considered while for the resonant case, two elementary inclusions with known effective parameters are considered; the Broadside-Coupled Split-Ring Resonator (BC-SRR) and the S-shaped inclusion. The BC-SRR is a well known and extensively studied magnetic MTM inclusion while the S-shaped inclusion exhibit both the electric and magnetic behaviour at different resonant frequencies. The analysis for the structures are done in the frequency range of 1 GHz to 4 GHz to cover the resonance of both resonant inclusions. The commercial method of moment (MoM) based characteristic modes analysis tool (FEKO) [189] is used to evaluate the eigenvalue, modal surface current distribution and modal weighting coefficient. The impedance matrix is then extracted and used to evaluate the stored energy on matlab.

3.4.1 Non-resonant inclusion

Although most MTM design applications are based on resonant MTMs [132,190,191], non-resonant MTMs also find usefulness in few applications [192,193]. Therefore to show that the stored energy formulation is generally applicable to all metamaterial structures, we consider the evaluation of the stored energy of a non-resonant unit cell. We consider a non-resonant rectangular strip line of 8 mm by 1 mm as shown in figure 3.3:

Figure 3.3: Rectangular strip line with dimensions: L = 8 mm, W = 1 mm.

The behaviour of this structure can be likened to the metal rod used together with the ring structure for the demonstration of metamaterial properties by pendry et al. [194]. In [194], a structure of infinite length was shown to possess an electric behaviour because of its permittivity value defines its dominant behaviour when applied to electromagnetic design. To evaluate the stored energy of the strip line structure, we first carry out the qualitative stored energy evaluation based on TCM analysis. The TCM commercial software was used for the modal analysis of the strip line structure by solving the generalized eigenvalue equation and the obtained result of the TCM analysis for the structure is represented by the plot of λ_n with respect to frequency. The frequency band for the analysis is chosen between 1 GHz and 4 GHz to ensure that the structure is far enough from its resonance frequency while covering the resonance frequency of the resonant inclusions. Figure 3.4 show the eigenvalue curve against frequency of the non-resonant strip line.

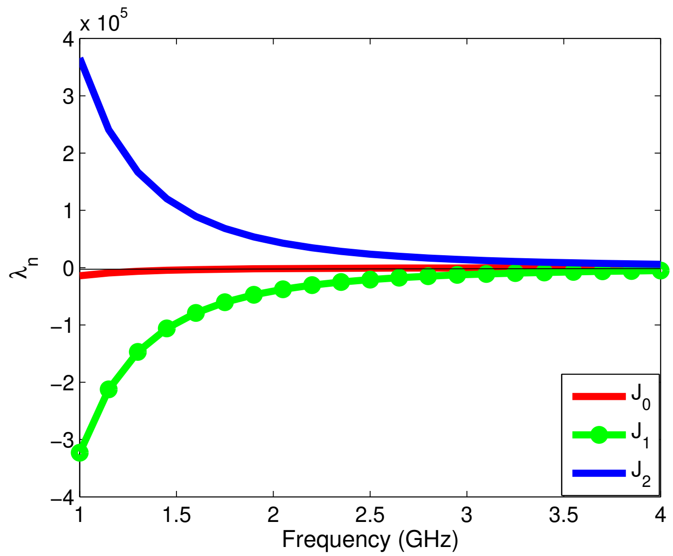

Figure 3.4: Rectangular strip line eigenvalue (λ_n) with respect to frequency.

The structure is non resonant since none of the modes cross the eigenvalue at 0. The first two modes J_0 and J_1 given by the red and green curve respectively show an electric behaviour because its value remains in the negative region of the eigenvalue while the third mode J_2 represented by the blue curve show a magnetic behaviour with its value in the positive region of the eigenvalue curve. In order to understand how the different modes can be applied in a design application, we look at the modal surface current distribution of the structure. The modal surface current distribution of the rectangular strip line is shown in figure 3.5.

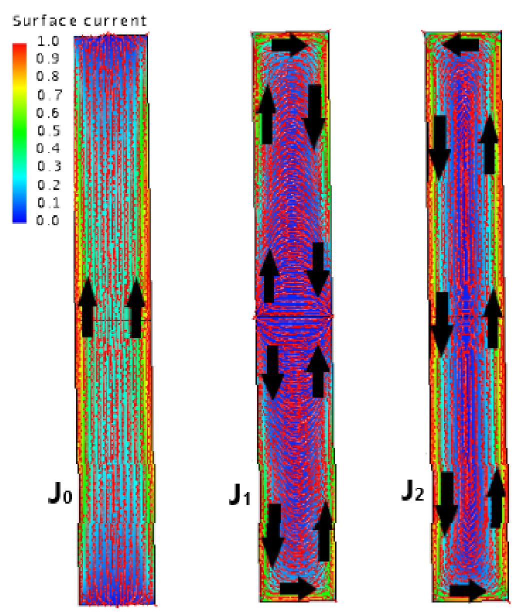

Figure 3.5: Rectangular strip line: Normalized surface current distribution at 2.4 GHz.

The current distribution is a reflection of the eigenvalue deduction of the structure and give an insight to how the modes can be excited in a design applications [195, 196].

From the current distribution of mode J_0, the mode is an electric mode as the current distribution follow that of an electric dipole. In order to excite this mode, the excitation should be placed at the centre where the current distribution is at its maximum. Mode J_1 is also an electric mode with a half loop current flow. The current maximum is at the edge and the current flow in opposite direction at both end of the strip line. To excite this mode, the excitation port need to be placed at the centre of any half of the strip line. The third mode J_2 is a magnetic mode as indicated by the eigenvalue curve. The current distribution show a resemblance to that of a loop antenna with a constant current flow around the strip line. Exciting mode J_2 will require placing the port at one of the edge of the structure.

The eigenvalue and surface current distribution can help define the modes of the structure as being electric or magnetic and provide qualitative information on the nature of the stored energy, the quantitative stored energy provide design accuracy. Therefore, using the modal stored energy formulation of the previous section, the quantitative stored energy represented by normalized $(\mathrm{W_m} - \mathrm{W_e})$ against frequency is given in figure 3.6:

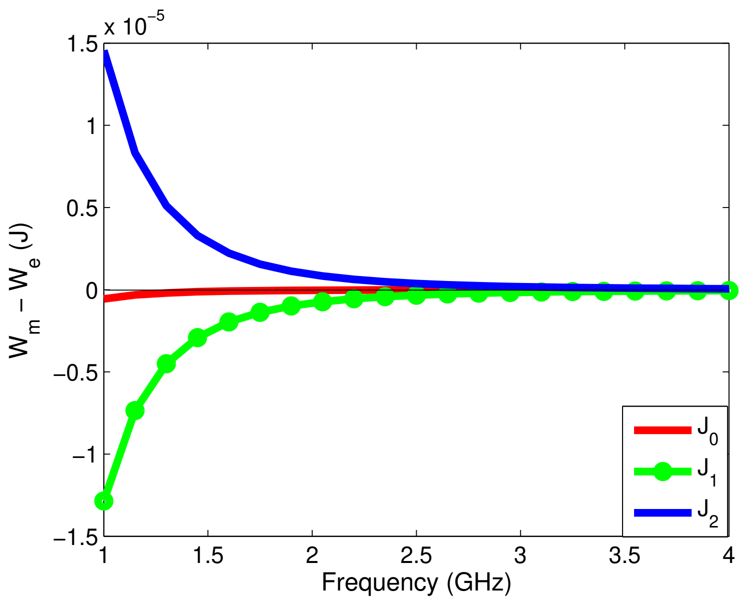

Figure 3.6: Normalized $(\mathrm{W_m} - \mathrm{W_e})$ with respect to frequency of non-resonant rectangular strip line.

The $(\mathrm{W_m} - \mathrm{W_e})$ curve in figure 3.6 follow the same pattern of the eigenvalue curve except for the fact that the values of the $(\mathrm{W_m} - \mathrm{W_e})$ are the modal stored energy value of the structure. Therefore, modes J_0 and J_1 shown in red and green curve respectively show an electric behaviour because its value remain in the negative region while the third mode J_2 represented by the blue curve show a magnetic behaviour with its value in the positive region of the $(\mathrm{W_m} - \mathrm{W_e})$ curve. For application purpose, the energy values of the desired modes and within the desired frequency bandwidth can be summed up to classify the stored energy of a non-resonant MTM.

3.4.2 Resonant inclusion

In this section, the W_{sto} formulation is applied to resonant MTM inclusions. Resonant MTM are the most commonly used MTM structure for near-field applications which include antenna design [8, 104], cloak design [173], sensor design [175] and many other applications. The stored energy analysis is therefore useful for evaluating the near-field behaviour of MTM structure which can aid its manipulation to achieve desired response.

Two elementary inclusions with known effective parameters are considered; the Broadside Coupled Split Ring Resonator (BC-SRR) and the S-shaped inclusion. While the BC-SRR is a well known and extensively studied magnetic MTM inclusion, the S-shaped inclusion exhibit both the electric and magnetic behaviour at different resonant frequencies. The analysis for the structures is done in the frequency range of 1 GHz to 4 GHz to cover the resonance of both inclusions.

3.4.2.1 Broadside Coupled Split Ring Resonator (BC-SRR)

The BC-SRR which is known to exhibit artificial magnetism is made up of two circular symmetric loops of PEC material and placed on the two opposite side of a teflon substrate of effective permittivity, ϵ_r 2.2. It resonate at 2.35 GHz and its dimension is given in figure 3.7:

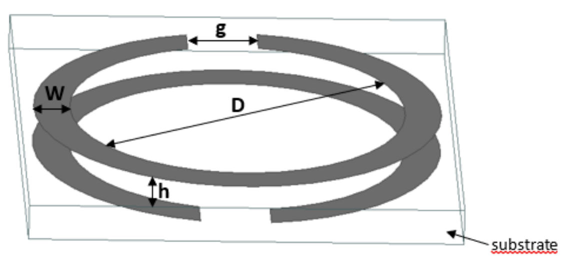

Figure 3.7: BC-SRR with dimensions: D = 11.25 mm, W = 1 mm, g = 1.95 mm, h = substrate height = 1.08 mm.

The artificial magnetic behavior of this BC-SRR was shown by Rabah et al. [185] using characteristic modes and static polarizability. The TCM commercial software is used for the modal analysis of the structure to solve the generalized eigenvalue equation and the obtained result of the TCM analysis for the structure is represented by the plot of λ_n with respect to frequency in figure 3.8 and the surface current distribution in figure 3.9.

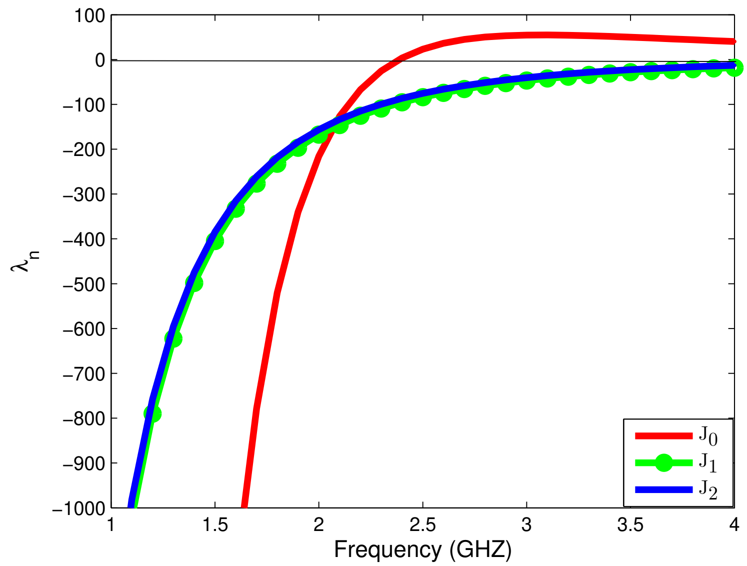

Figure 3.8: BC-SRR inclusion eigenvalue (λ_n) with respect to frequency.

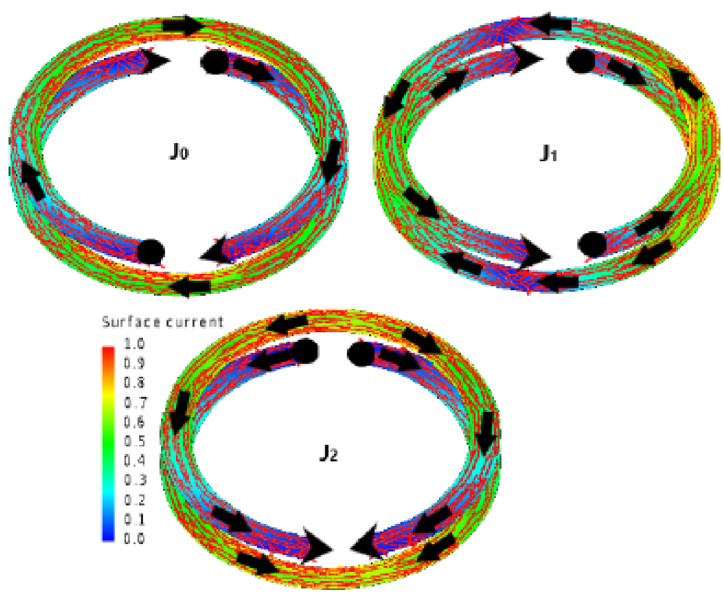

Figure 3.9: BC-SRR inclusion: Normalized surface current distribution at 2.4 GHz.

Only the fundamental mode J_0 in red cross the zero mark at 2.35 GHz as shown in figure 3.8 hence, only one resonance occur. The $\mathrm{W_e}$ and $\mathrm{W_m}$ are of equal magnitude and no energy is stored at this frequency of 2.35 GHz. Also, this resonance frequency of 2.35 GHz is close to that of the BC-SRR analyzed by Rabah et al. [185] which was referred to as the fundamental DC mode of a circular loop. The other modes J_1 and J_2 in green and blue have negative values of λ_n through out the considered frequency band and indicates that they store more $\mathrm{W_e}$. From the current profile shown in figure 3.9, the black arrow head show the direction of the current flow, the black dot show the starting point of the current flow. The behaviour of the modes can be easily described as magnetic or electric. J_0 show a magnetic current distribution with both loops having similar direction of current flow while J_1 and J_2 show a current distribution pattern similar to that of an electric dipole with the current flowing in the opposite direction on both loops.

To quantify the energies with respect to frequency for each mode, the impedance matrix is extracted from the commercial software and the $\mathrm{W_{sto}}$ formulation of section II is applied to determine the modal magnetic and electric energies. The result of the dominant energy is represented by the normalized $(\mathrm{W_m} - \mathrm{W_e})$ with respect to frequency in figure 3.10.

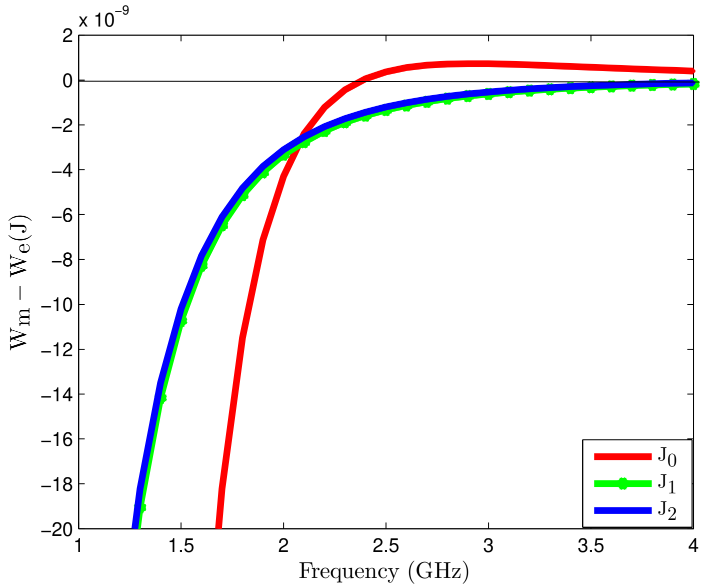

Figure 3.10: Normalized $(\mathrm{W_m} - \mathrm{W_e})$ with respect to frequency of BC-SRR.

The value of $\mathrm{W_e}$ and $\mathrm{W_m}$ are equal at 2.35 GHz for mode J_0 in red thus, the value of normalized $(\mathrm{W_m} - \mathrm{W_e})$ is 0 J at this frequency. J_1 and J_2 in green and blue both have negative values of $(\mathrm{W_m} - \mathrm{W_e})$ within the considered frequency band and implies that $\mathrm{W_e}$ remains greater than $\mathrm{W_m}$. The $(\mathrm{W_m} - \mathrm{W_e})$ quantity agree with the qualitative deductions of the eigenvalue (λ_n) curve.

3.4.2.2 S-shaped MTM inclusion

The S-shaped inclusion exhibit both the electric and magnetic behaviour due to its bianisotropic character [197]. It is made of a PEC sheet forming an S-shape and its dimension is shown in figure 3.11.

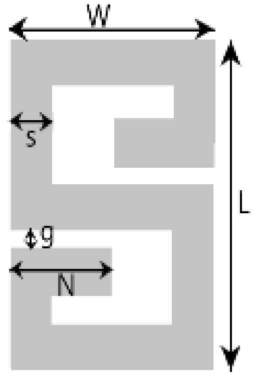

Figure 3.11: S-shaped inclusion with dimensions: L = 27 mm, W = 13 mm, g = 1.1 mm, N = 4 mm, s = 1.5 mm.

The S-shaped structure has its fundamental resonance at 1.92 GHz. The same analysis followed for the BC-SRR inclusion was carried out for the S-shaped inclusion. The TCM commercial software is used for the modal analysis of the structure and the obtained result of the TCM analysis is represented by the plot of λ_n with respect to frequency in figure 3.12 and the surface current distribution in figure 3.13.

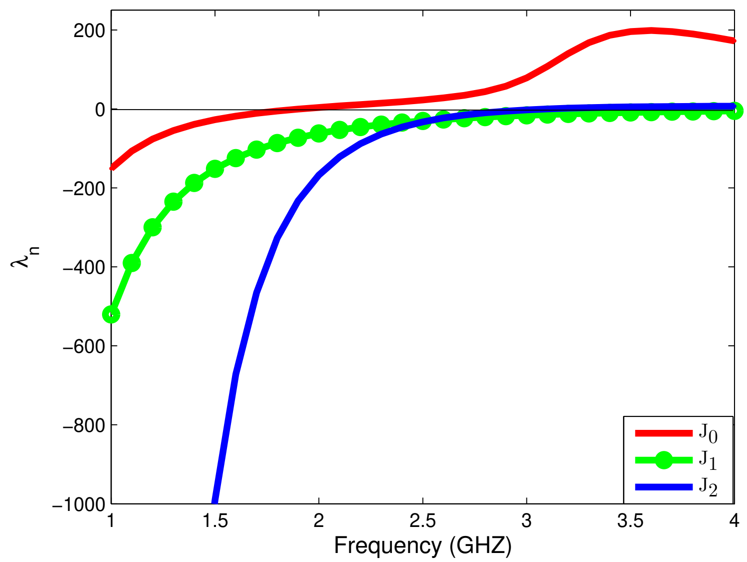

Figure 3.12: S-shaped inclusion eigenvalue (λ_n) with respect to frequency.

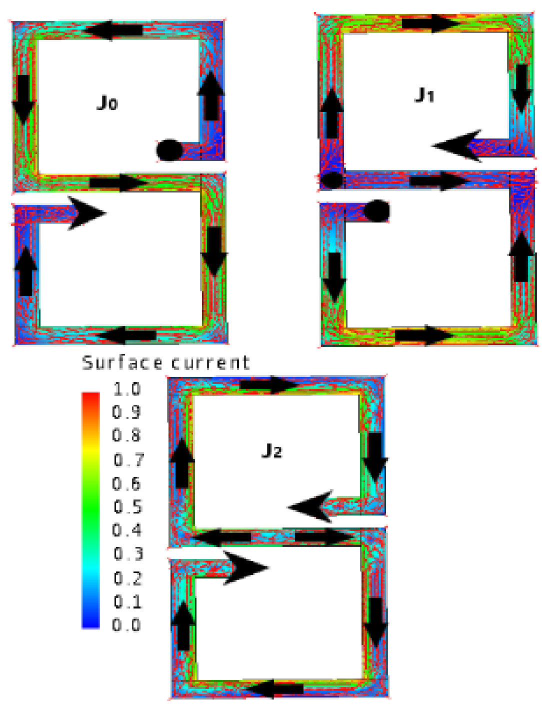

Figure 3.13: S-shaped inclusion: Normalized surface current distribution at 1.92 GHz.

J_0 and J_2 of figure 3.12 in red and blue cross the zero mark at 1.92 GHz and 3.1 GHz respectively. This correspond to its resonance frequencies and indicate that W_e and W_m are of equal magnitude at these frequencies and no modal stored energy at these points. J_1 on the other hand remain with negative values of λ_n with respect to the considered frequency band implying that W_e is dominant. The behaviour of the modes as electric or magnetic can also be analyzed using the surface current distribution in figure 3.13. The black arrow head show the direction of the current flow and the black dot show its starting point. The current distribution of J_0 is similar to that of an electric dipole with the current flowing in one direction. J_1 also show an electric dipole current distribution splitted into two halves with the current flowing in opposite direction on the two halves. J_2 show a magnetic current distribution with the current flowing in the same direction when the S-shape is split into two equal halves.

To quantify the modal energies with respect to frequency for each mode, the impedance matrix is extracted from the commercial software and the W_{sto} formulation of section II is applied to determine the modal magnetic and electric energies. The result of the dominant energy is represented by the normalized $(W_m - W_e)$ with respect to frequency in figure 3.14.

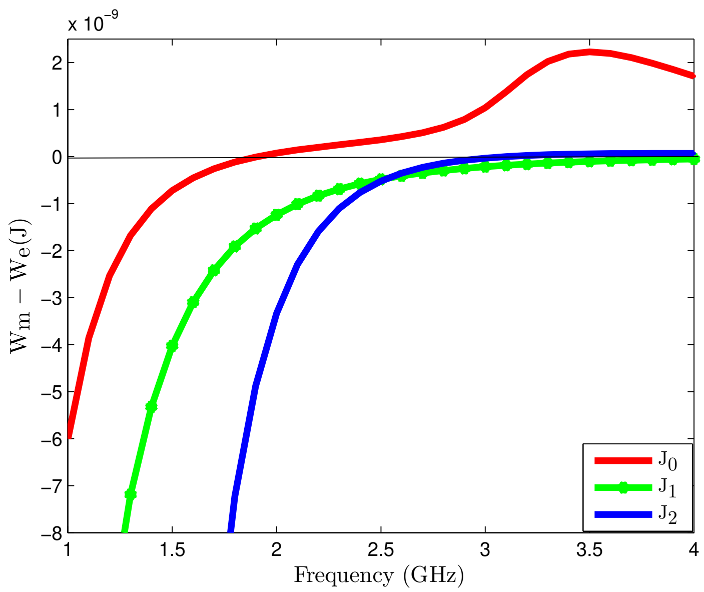

Figure 3.14: Normalized $(W_m - W_e)$ with respect to frequency of S-shaped inclusion.

J_0 and J_2 of figure 3.14 in red and blue show that at the resonance frequency of 1.92 GHz and 3.1 GHz respectively, (W_e - W_m) is 0 J and the magnitude of W_m and W_e are of the same value. The region of the curve that lie in the negative part indicate that W_e is dominant while the region in the positive part indicate that W_m is dominant. J_1 in green has negative values across the considered frequency band hence, W_e is dominant across the considered frequency band. The $(W_m - W_e)$ quantity agree with the qualitative deductions of the eigenvalue (λ_n) curve.

3.5 Comparative analysis between metamaterial stored energy and conventional metamaterial analysis

Generally, the physical behaviour of MTMs are described in terms of effective parameters [102, 198, 199] which are represented as the permittivity ε and permeability μ values describing it as an electric or a magnetic MTM [200]. They are calculated from far-field complex reflection and transmission co-efficient [102] using classical technique of extraction [199, 201] given as:

$$\varepsilon = \frac{n}{z}, \tag{3.27}$$

$$\mu = nz, \tag{3.28}$$

where n is the refractive index given as:

$$n = \frac{1}{kd} cos^{-1}\left(\frac{1 - \mathrm{S}_{11}^2 + \mathrm{S}_{21}^2}{2\mathrm{S}_{21}}\right), \tag{3.29}$$

and z is:

$$z = \pm\sqrt{\frac{(1+\mathrm{S}_{11})^2 - \mathrm{S}_{21}^2}{(1-\mathrm{S}_{11})^2 - \mathrm{S}_{21}^2}}, \tag{3.30}$$

given that S_{11} is the reflection co-efficient, S_{21} is the transmission co-efficient, k is the wavenumber and d is the maximum length of the unit element

If ε and μ provide physical insight, the association of MTM to devices at microwave frequencies in the near-field region can not be studied in a reliable manner based on these parameters.

Modal stored energy is quantity is derived from modal current and account for near-field effects [178]. The modal stored energy being quantitative and independent of excitation is believed to be a more reliable analysis of MTM.

In this section, we present a comparative analysis between the effective parameter and the dominant stored energy such that within a given frequency band, one can appreciate the convergence in terms of physical and qualitative analysis. Most inclusions especially magnetic inclusions have their magnetic properties exhibited when excitation is placed in a specific polarization [185]. The TCM based energies $\mathrm{W_m}$ and $\mathrm{W_e}$ are excitation and polarization independent whereas, the effective parameters are excitation and polarization dependent. To enable a comparison between the two methods, new steps are introduced to the calculation of the differential stored energies (i.e. $\mathrm{W_m}$ - $\mathrm{W_e}$) to account for the polarizability of the inclusions. Additional steps are introduced to the calculation of ($\mathrm{W_m}$ - $\mathrm{W_e}$) given in figure 3.15.

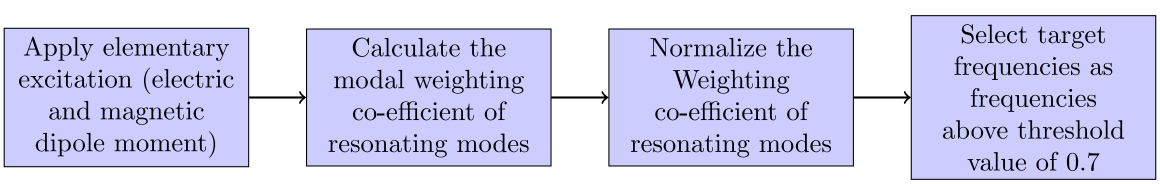

Figure 3.15: Additional steps for calculating ($\mathrm{W_m}$ - $\mathrm{W_e}$).

The block diagram in figure 3.15 describe the procedure that take into account the effect of excitation and polarization in the modal stored energy analysis of MTM inclusion. First, an elementary excitation (electric and magnetic dipole moment) is applied to the structure and the modal weighting coefficient $\mathrm{MWC_n}$ [12] is derived from the TCM based commercial software where $\mathrm{MWC_n}$ is given as:

$$\mathrm{MWC_n} = \frac{\mathrm{V^i J_n}}{1 + j\lambda_\mathrm{n}}, \tag{3.31}$$

where $\mathrm{V^i}$ is the applied excitation, λ_n is the eigenvalue and $\mathrm{J_n}$ is the surface current of the n^{th} mode.

The $\mathrm{MWC_n}$ provide information of the modal response to the applied excitation. The $\mathrm{MWC_n}$ of the resonant modes are normalized with their maximum value. Stored energy is related to bandwidth by Q-factor definition [26, 202] hence, we evaluate the modal half power bandwidth using the TCM bandwidth definition. This represent the region of frequencies that participate in radiation and it is given as frequencies with a modal significance above 0.7 [23]. The dominant energy within the modal bandwidth (i.e. having a value above 0.7 of the normalized $\mathrm{MWC_n}$) are considered and referred to as target frequencies. They account for the behaviour before and after the resonance frequencies which are important for electromagnetic applications. To quantitatively describe an inclusion, the dominant energy ($\mathrm{W_m}$ - $\mathrm{W_e}$) within the target frequencies are summed up and the sign of the summation indicate the dominant energy within the modal bandwidth of the structure. It tells if the inclusion is electric or magnetic. A positive value indicate dominant $\mathrm{W_m}$ and the inclusion is magnetic while a negative value imply that $\mathrm{W_e}$ is dominant and the inclusion is electric.

This procedure is applied to the resonant inclusions whose dominant modal energy values ($\mathrm{W_m}$ - $\mathrm{W_e}$) were evaluated in the previous section.

3.5.1 Resonant magnetic metamaterial

3.5.1.1 Broadside Coupled Split Ring Resonator (BC-SRR)

The BC-SRR is excited with a magnetic dipole moment and only the resonant mode J_0 is considered. The normalized $\mathrm{MWC_n}$ with respect to frequency extracted from the TCM based simulation software is shown in fig. 3.16.

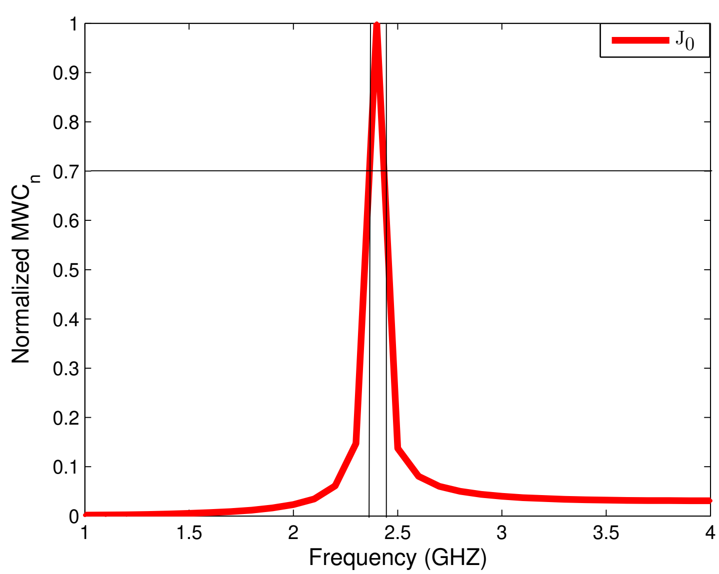

Figure 3.16: Normalized $\mathrm{MWC_n}$ with respect to frequency of BC-SRR.

The horizontal thin black line in figure 3.16 show the threshold value of 0.7 which indicate the region of the target frequencies between 2.35 GHz and 2.43 GHz. The shift of the centre frequency from the resonance is due to the coupling of the excitation with the structure. The summation of the normalized ($\mathrm{W_m} - \mathrm{W_e}$) at the target frequencies from the BC-SRR modal stored energy analysis is 4.1969×10^{-10} J. The value is positive hence, one can conclude that J_0 of the BC-SRR exhibit a magnetic behaviour and therefore it is a magnetic inclusion. This analysis agree with the current profile of BC-SRR. In comparison to the classical method of effective parameters of the BC-SRR, the plot of effective parameters (ε and μ) with respect to frequency is shown in figure 3.17.

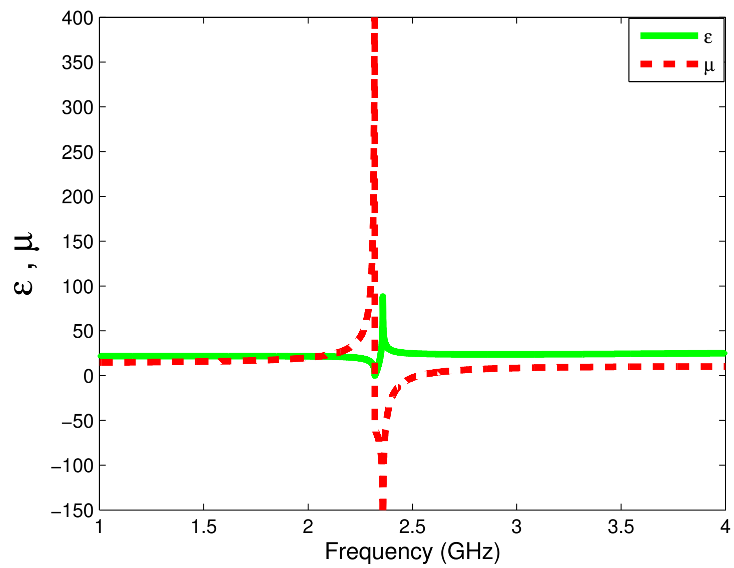

Figure 3.17: ε and μ with respect to the frequency of BC-SRR.

ε and μ in green and red respectively give information of the dominant property of the BC-SRR. Around the resonance frequency of 2.35 GHz, the values of μ are higher than that of ε and the magnetic behaviour of the structure dominate thus, the inclusion is magnetic. This qualitative description is in agreement with that of the dominant stored energy analysis.

3.5.2 Resonant electric metamaterial

3.5.2.1 S-shaped MTM inclusion

The S-shaped inclusion has two resonant modes J_0 and J_2 with different behavior. The S-shaped inclusion is excited with an electric dipole moment and the normalized $\mathrm{MWC_n}$ with respect to frequency which has been extracted from the TCM based simulation software is shown in figure 3.18.

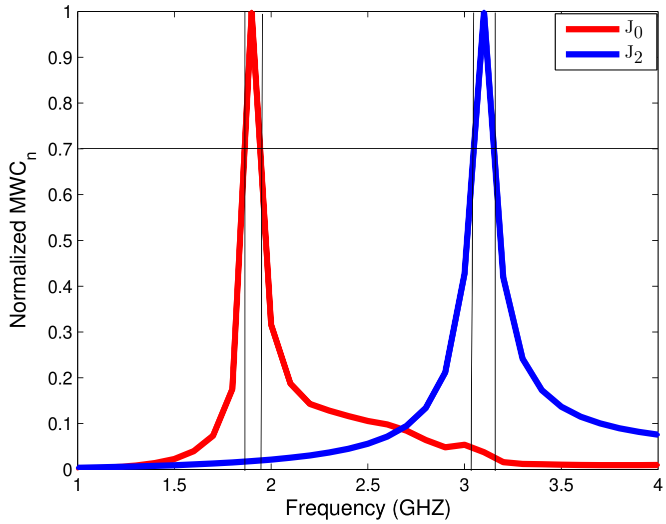

Figure 3.18: Normalized $\mathrm{MWC_n}$ with respect to frequency of S-shaped inclusion.

The horizontal thin black line in figure 3.18 show the threshold value of 0.7 which indicate the region of the target frequencies between 1.86 GHz and 1.94 GHz for mode J_0 in red and between 3.05GHz and 3.2 GHz for mode J_2 in blue. The shift of the centre frequency from the resonance frequency is due to the coupling of the excitation to the structure. The summation of the $(\mathrm{W_m} - \mathrm{W_e})$ values at the target frequencies from the S-shaped inclusion modal stored energy analysis is -1.2×10^{-10} J and 2.5545×10^{-11} J for J_0 and J_2 respectively. The value for J_0 is negative indicating that the inclusion behave as an electric structure around the first resonance. J_2 has a positive value which imply that the inclusion behave as a magnetic structure at its second resonance. This analysis agree with the current profile of the S-shaped inclusion. In comparison to the classical method of effective parameters of the S-shaped inclusion, the plot of effective parameters (ε and μ) with respect to frequency is shown in figure 3.19.

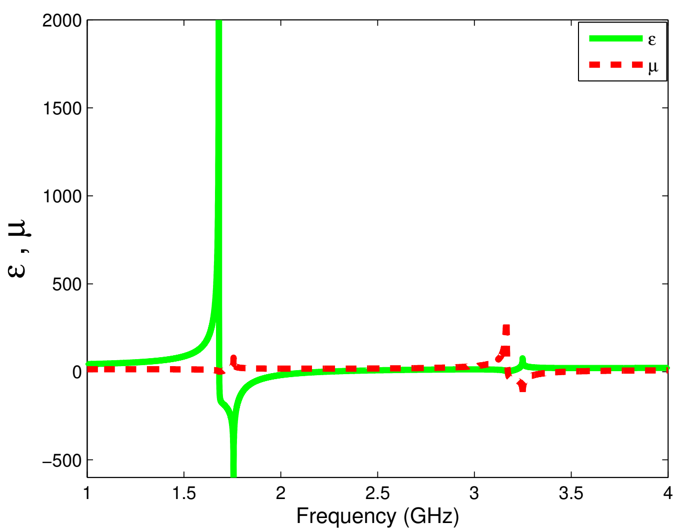

Figure 3.19: ε and μ with respect to the frequency of S-shaped inclusion.

ε and μ in green and red respectively give information of the dominant property of the S-shaped inclusion. Around the fundamental resonance frequency of 1.92 GHz, the values of ε are higher than that of μ and the electric behaviour dominate the magnetic behaviour hence, the structure behave as an electric inclusion. On the other hand, the values of μ are higher than that of ε at the second resonance of 3.01 GHz and the structure behave as a magnetic inclusion at this frequency. This qualitative description is in agreement with that of the dominant stored energy analysis for the S-shaped inclusion.

3.6 Conclusion

The effectiveness of the proposed method for enhancing the performance of integrated antenna is dependent on selecting the proper metamaterial inclusion with the right near-field behaviour. It is therefore important to accurately describe the near-field behaviour of metamaterial inclusion. Although, it was concluded that the general reactive field concept used in antenna design is inadequate to generally characterize the near-field of a radiator because with an unknown excitation, one has to use an abstract level of theory to formulate general propositions and the evaluation of the modal stored energy provided a solution to those challenges. In comparison to the effective parameter method of defining metamaterial inclusions which are valid in the far-field region and may not be reliable for near-field analysis, this chapter presented a method to evaluating the stored energy of metamaterial inclusions by application of the modal method which is based on modal current and account for near-field effects. The method can be applied to both non-resonant and resonant metamaterial structures. It is based on theory of characteristics modes which independently of excitation, bring physical insight into the resonant property of a structure.

A non- resonant rectangular strip line and two resonant elementary inclusions, BC-SRR and S-shaped were considered for demonstration. For one to appreciate the usefulness of the method, the convergence in terms of physical and qualitative analysis is shown with the comparison of the effective parameter to the modal stored energy method by introducing additional steps into the calculation of stored energy which take into account the polarization and excitation dependence of the inclusions. The both method show a good agreement in their physical and qualitative analysis. This method is useful in designing metamaterial inspired structures especially when the near-field quantity is of paramount importance including in antenna, sensor and cloak design. Its application in the design of metamaterial-inspired antenna and electromagnetic cloaking will be demonstrated in subsequent chapters.

Chapter 4

Inter-modal coupling analysis

4.1 Introduction

The coupling of an antenna is an important antenna behaviour that cannot be overlooked because it determine the antenna performance upon integration. It represent the scattering characteristics of an electromagnetic system when an element is placed within its near-field [164]. The coupling define the interaction between the stored energy of the electromagnetic system and other elements in its vicinity. In fact antenna systems such as MIMO try to minimize the coupling between antenna elements to achieve efficient performance [203]. For metamaterial design, its behaviour is a function of the coupling between the elements hence, the coupling between metamaterial elements are modified to achieve a particular electromagnetic response [184]. In a similar way, the coupling between inclusions and electromagnetic system can be modified to enhance the performance of the system like in parasitic metamaterial antenna design.

The performance of metamaterial inspired antenna strongly depend on the coupling between the inclusion and the antenna element. They can be modified to obtain different responses and achieve particular parameter enhancement of an antenna. This can be done by changing the configuration and separation distance between the inclusion and the antenna element since both factors affect the coupling [204]. However, the method for analysing coupling depends on the goal of either reducing or enhancing the coupling. The modal coupling analysis provide an opportunity to achieve both goals.

The modal stored energy and the inter-modal coupling are representations of the near-field behaviour of the structure and thus are related. When combined in an analysis, they could provide a better analysis by ensuring that all the near-field factors relating to the antenna design are accounted for and therefore, providing a complete description of the near-field behaviour.

In this chapter, the evaluation of the scattering properties through the inter-modal coupling analysis is explored in detail. First, the description of modal electromagnetic coupling is described to provide a framework for the TCM based inter-modal coupling. The inter-modal coupling is presented to provide insight into the modal stored energy coupling phenomenon between the antenna elements. The relationship between stored energy and inter-modal coupling can be traced to their dependence on the imaginary part of the impedance matrix thus, giving a complete near-field account of the structure. For demonstration on the application of the inter-modal coupling analysis, the inter-modal coupling between resonant antenna and non-resonant inclusion is first considered using two dipole structures and two I-shaped structures. Then, a non-resonant antenna and resonant inclusion is considered using a monopole-meander-line antenna and a dipole-BC-SRR antenna.

4.2 Modal electromagnetic coupling

Electromagnetic coupling can be described as the transfer or interaction of energies between two medium. It represent the level of interaction between electromagnetic systems and their immediate surrounding [165]. Although in most applications, coupling are unwanted phenomenon such as in MIMO system, antenna array system and closely spaced antenna [203, 205], various methods have been developed to minimize or eliminate coupling including the use of electromagnetic cloaks. In few applications like metamaterial design [206, 207], refractive index sensor design [208] and parasitic metamaterial antenna design [8, 209], a strong coupling is highly desired for efficient performance.

Coupling play an important role in the design of metamaterials which consist of patterned unit cells mostly resonators, arranged such that the spacing between the unit cells are sufficient enough to ensure strong interaction and substantially change the media property [210, 211]. In electromagnetic applications where coupling is highly required, insufficient coupling could present challenges such as impedance mismatch, narrow bandwidth, unstable radiation pattern and reduced efficiency. Despite this fact, only few research works on electromagnetic design give attention to the effect of coupling particularly in research works relating to the application of metamaterials in antenna design [149, 212].

The modal method is one of the available method employed in research works for analysing the coupling between resonators because of the absence of limiting factors present in classical methods (like cavity-model or the Transmission-line model) , factors such as the need for sophisticated excitement method that require rigorous numerical method and its unsuitability for arbitrary structures [213]. Modal method allow coupling co-efficient to be obtained in the power expansion form [**?**]. One of the modal method, coupled mode theory (CMT) when applied mostly to weakly coupled systems [214, 215] have demonstrated the efficacy of the modal method to reducing computational complexity by reducing computational domain to a number of relevant modes.

The CMT method follow from expressing the coupled fields as a linear superposition of the uncoupled fields [215]:

$$\mathrm{E} = \sum_{i=1}^{\mathrm{N}} a_i \mathrm{E}_i, \tag{4.1}$$

$$\mathrm{H} = \sum_{i=1}^{\mathrm{N}} b_i \mathrm{H}_i, \tag{4.2}$$

and the current density over the surface of the conductor is expanded in terms of the uncoupled fields as:

$$\mathrm{J}_s = \sum_{i=1}^{\mathrm{N}} b_i \mathbf{n} \times \mathrm{H}_i, \tag{4.3}$$

given that a_i and b_i are the expansion coefficients of the electric and magnetic fields respectively and N is the mode number.

In antenna engineering, among the various ways of increasing the operational bandwidth of an antenna, the effect of coupling can be employed by placing a resonant parasitic structure with a resonance frequency close to that of an antenna in the vicinity of the antenna such that the there is a strong coupling between the antenna and parasitic element. The antenna is then able to excite the parasitic element to achieve increased bandwidth [96, 149]. However, the strength of the coupling between the antenna and the parasitic element is a function of the size of the parasitic element, the position of the parasitic element and the distance between the parasitic element and the antenna structure.

With the growing application of TCM to antenna design and engineering, research work on TCM based electromagnetic coupling is gaining attention, one of which evaluates electromagnetic coupling of an antenna using the modal mutual admittance given as [170]:

$$\mathrm{Y}_{11} = \frac{\mathrm{I}_1}{\mathrm{V}_1} = \sum_{n=1}^{\infty} \mathrm{Y}_{11}^{\mathrm{n}} = \sum_{n=1}^{\infty} \frac{\mathrm{I_n(p)I_n(p)l_pl_p}}{1 + j\lambda_{\mathrm{n}}}, \tag{4.4}$$

and

$$\mathrm{Y}_{21} = \frac{\mathrm{I}_2}{\mathrm{V}_1} = \sum_{n=1}^{\infty} \mathrm{Y}_{21}^{\mathrm{n}} = \sum_{n=1}^{\infty} \frac{\mathrm{I_n(p)I_n(q)l_pl_q}}{1 + j\lambda_{\mathrm{n}}}, \tag{4.5}$$

where λ_{n} is the eigenvalue of the $\mathrm{n_{th}}$ mode, $\mathrm{Y}_{11}^{\mathrm{n}}$ and $\mathrm{Y}_{21}^{\mathrm{n}}$ are the modal source admittance and modal mutual admittance respectively of one of the resonators, p and q are the non-boundary edge indexes of the feeding point for both resonators, $\mathrm{l_p}$ and $\mathrm{l_q}$ are the lengths of the corresponding edges of the feeding points and $\mathrm{I_n(p)}$ and $\mathrm{I_n(q)}$ are the coefficient of the basis function. The application of this method is limited to reducing coupling between electromagnetic systems therefore to enhance electromagnetic coupling based on TCM, a different method is followed.

4.3 Inter-modal coupling analysis based on TCM

The study of coupling enhancement using TCM was demonstrated in [149] while showing the link between the use of excitation and parasitic element for enhancing the bandwidth of an antenna. It was shown that the TCM metric of modal weighting co-efficient ($\mathrm{MWC_n}$) is a representation of coupling. It represent the coupling between an excitation source and a resonator's mode (source-mode coupling) and as applied in TCM, it is given as:

$$\mathrm{MWC_n} = \frac{\mathrm{V^iJ_n}}{1 + j\lambda_{\mathrm{n}}}, \tag{4.6}$$

where $\mathrm{V^i}$ is the applied excitation, λ_{n} is the eigenvalue and $\mathrm{J_n}$ is the surface current of the n^{th} mode.

The $\mathrm{MWC_n}$ show how the different modes which represent the different behaviour of a structure respond to a given excitation source therefore, a stronger coupling between a mode and the excitation source will produce a high value for the $\mathrm{MWC_n}$ while a weak coupling will produce a lower value.

The behaviour of the various elements of a structures are represented in the different modes of the TCM analysis. These different modes of the structure (e.g. the mode of an antenna and a parasitic element) can couple together to affect the overall performance of the system. This coupling involve the interaction between two modes of a design (mode-mode coupling) and is referred to as the inter-modal coupling (M_{ij}) [149]. It was demonstrated in [149] that the source-mode coupling can be optimized and adjusted using the mode-mode coupling while the mode-mode coupling can be adjusted to optimize antenna's bandwidth.

The formulation of M_{ij} was motivated by [216] which showed that coupling exist between different modes. These couplings are related to the cross terms of electric and magnetic energies. It start from the computation of the MoM matrix derived from TCM given in equation (3.1) as:

$$\mathrm{Z} = \mathrm{R} + \mathrm{jX}, \tag{3.1}$$

and solving the generalized eigenvalue equation given in equation (3.11) as:

$$[\mathrm{X}][\mathrm{I}] = \lambda_{\mathrm{n}}[\mathrm{R}][\mathrm{I}]. \tag{3.11}$$

Considering that mode-mode coupling is related to the cross term of electric and magnetic energies between two modes, therefore given two modes (i.e. mode i and mode j), the inter-modal coupling between the two modes M_{ij} as given in [149] can be written as:

$$\mathrm{M_{ij}} = \frac{\mathrm{I_i}^{\mathrm{H}}\mathrm{X}'\mathrm{I_j}}{\sqrt{\mathrm{I_i^H X' I_i . I_j^H X' I_j}}}, \tag{4.7}$$

where I is the eigencurrent, I^H is the hermitan transpose of the eigencurrent and $X^{'}$ is given in (3.13) as;

$$\mathrm{X}' = \omega\frac{\partial \mathrm{X}}{\partial \omega}. \tag{3.13}$$

with ω as the angular frequency and X as the imaginary part of the impedance matrix of equation (3.1) for the structure.

Considering the modal stored energy formulation for metamaterial inclusions, equation (3.13) contain the inductance and capacitance term of the structure hence, the electric and magnetic stored energy term of the structure are represented in its value. However the value of M_{ij} could be negative or positive, therefore the absolute value of M_{ij} ($|M_{ij}|$) is used in normalizing its value such that it only vary between 0 and 1. The closer $|M_{ij}|$ is to 1, the stronger the inter-modal coupling however to ensure consistency with the TCM modal bandwidth applied to modal significance [23], as a way of convention, the $|M_{ij}|$ value of 0.7 and above is taken to represent the presence of significant coupling which has an effect on the system's performance while $|M_{ij}|$ value below 0.7 demonstrate a weak coupling with less significance on the system's performance.

4.4 Relationship between modal stored energy and inter-modal coupling co-efficient

The modal stored energy and inter-modal coupling have a direct relationship. Besides the fact that both quantities are related to the near field behaviour of a structure, the formulation for their evaluation are also linked to the same imaginary part X of the generalized impedance matrix Z as given in equation (3.12) and equation (4.7) which represent the stored energy and inter-modal coupling formulation respectively:

$$\mathrm{W_{sto}} = \mathrm{W_m} + \mathrm{W_e} = \frac{1}{4\omega}\mathrm{I^H X' I} \tag{3.12}$$

and

$$|\mathrm{M_{ij}}| = \frac{\mathrm{I_i}^{\mathrm{H}}\mathrm{X}'\mathrm{I_j}}{\sqrt{\mathrm{I_i}^{\mathrm{H}}\mathrm{X}'\mathrm{I_i}.\mathrm{I_j^H}\mathrm{X}'\mathrm{I_j}}}. \tag{4.7}$$

The $|\mathrm{M_{ij}}|$ can therefore be computed by the imaginary part of the generalized impedance matrix even without evaluating the stored energies.

Just like the stored energy evaluation, the $|\mathrm{M_{ij}}|$ is applicable to lossy media structures because the losses are accounted for in the value of X [23,149]. The orthogonality property of characteristic modes do not apply to the inter-modal coupling as they are associated to stored electric and magnetic energy rather than the modes. The relationship between the magnetic and electric energies are already presented in the previous chapter thus, $|\mathrm{M_{ij}}|$ relate to the near-field like the modal stored energy.

4.5 Evaluation of inter-modal coupling co-efficient

In this section, the $\mathrm{MWC_n}$ and $|\mathrm{M_{ij}}|$ are applied in two different scenarios. The first scenario is similar to the one found in literature [149] and involve two resonant structures with one of them being the source and the other a parasitic element. For the second scenario, the case of parasitic metamaterial antennas are considered. The radiating elements are non-resonant while the inclusions are resonant. The $\mathrm{MWC_n}$ show how the excitation source affect the modes while $|\mathrm{M_{ij}}|$ represent how the modal energies of the antenna and the parasitic element interact.

A strong $|\mathrm{M_{ij}}|$ ensure that the $\mathrm{MWC_n}$ excite the parasitic element to produce enhanced bandwidth for the case of two resonant structures and an improved performance for the case of parasitic metamaterial antenna.

4.5.1 Coupling analysis between a resonant antenna and a resonant parasitic element

The TCM based inter-modal coupling is a useful tool for evaluating the coupling between two resonant structures because the behaviour of the individual elements are represented by modes thus, we can evaluate how the elements couple with each other just by analysing the inter-modal coupling between their resonant modes. The distance between the two resonators are varied to show how distance affect both the $\mathrm{MWC_n}$ and the $|\mathrm{M_{ij}}|$. Two design examples are considered; two resonant dipole structures and two I-shaped structures.

4.5.1.1 Two dipole elements

The two dipole elements were already considered in [149] however, we re-analyze the structure to validate our method since the derivation for $X^{'}$ is different. One of the dipole element is the driven element excited at the centre while the second one is the parasitic element. The resonance of the elements are at 2.3 GHz and 2.85 GHz respectively. In contrast to the analysis done in [149] which showed the effect of changing length of the parasitic resonator on MWC_n and $|M_{ij}|$, we evaluate the coupling with respect to the change in distance between the driven and the parasitic element. The dimension and arrangement of the two dipole elements are shown in fig. 4.1:

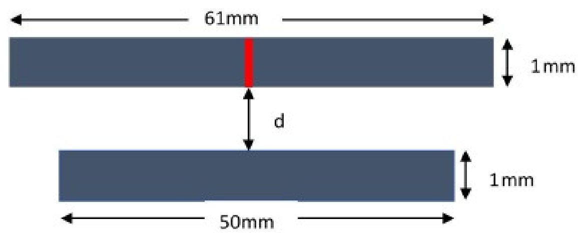

Figure 4.1: Dipole structures.

In fig. 4.1, the parasitic element is placed at two different distances d to the driven element corresponding to $\frac{\lambda}{59}$ and $\frac{\lambda}{5.2}$ where λ is the wavelength at 2.3 GHz. These distances are represented in the presented results as design 1 and design 2 respectively. They show the effect of distance between the two resonators on MWC_n and $|M_{ij}|$. The driven element is excited with an edge port at the centre and the combined structure of the parasitic and driven element is analyzed between 1 GHz to 4 GHz. The TCM commercial software is used for the modal analysis of the structure to solve the generalized eigenvalue equation. The obtained result of the TCM analysis for the elements are represented by the plot of the characteristic angle in degree against frequency and MWC_n against frequency for design 1 and design 2. The plot of the characteristic angle in degree against frequency is shown in fig. 4.2:

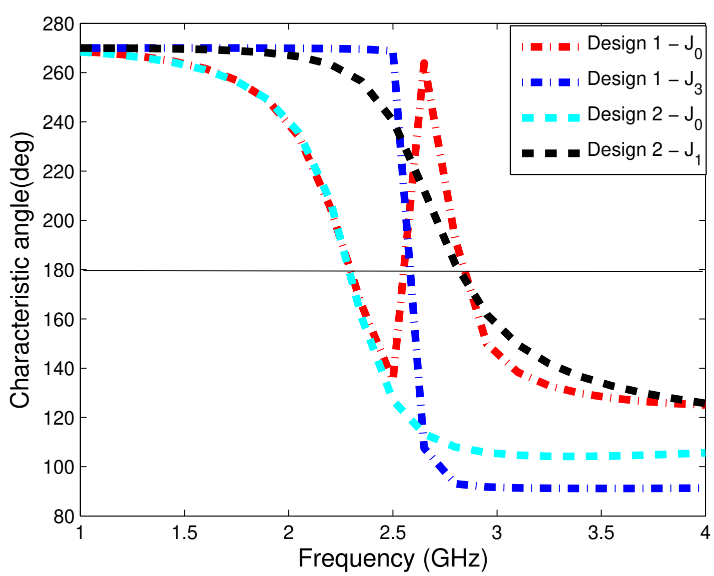

Figure 4.2: Dipole structures: Characteristic angle against frequency.

In fig. 4.2, the characteristic angle against frequency show the resonance of the elements. The resonance appear at the frequency where the curve cross the 180° [23]. The resonance of the individual elements are represented on the graph irrespective of the distance between the two elements. However for design 1, the resonance of the two elements combine into one mode (i.e. design 1- J_0) as shown by the red curve and a new mode (i.e. design 1- J_3) as shown by the blue curve at 2.6 GHz appear. The significance of the new resonant mode at 2.6 GHz can be explained by the $\mathrm{MWC_n}$ and $|\mathrm{M_{ij}}|$. For design 2, the resonance of the individual element appear on separate modes shown by the cyan and black curve (i.e. design 2- J_0 and design 2- J_1 respectively).

For the relationship between the excitation source and the resonant modes, the plot of $\mathrm{MWC_n}$ against frequency is shown in fig. 4.3:

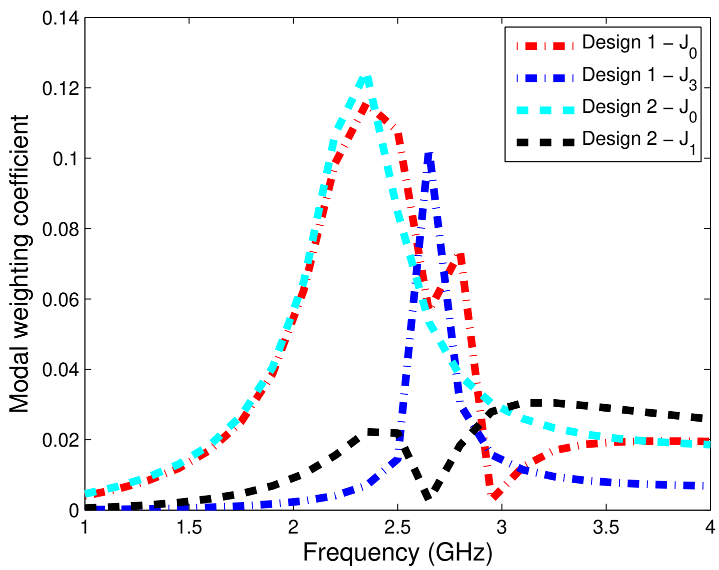

Figure 4.3: Dipole structures: Modal weighting coefficient against frequency.

In fig. 4.3 which show $\mathrm{MWC_n}$ and represent the source-mode coupling, the driven element is excited irrespective of the distance because it contain the excitation source. Therefore, $\mathrm{MWC_n}$ has a relatively higher value at the first resonance of 2.3 GHz for both design 1 and design 2 represented by the red and cyan curves respectively. The second resonance at 2.85 GHz for the parasitic dipole is excited for only design 1 as shown by the red curve. It can be concluded that as the separation between the source and a parasitic element increase, the source-mode coupling reduces which is observed by the reduction of the $\mathrm{MWC_n}$ magnitude at the second resonance for design 2 as shown by black curve.

The new resonance at 2.6 GHz which appear for design 1 and represented by the blue curve also get excited. It links the resonance of the driven dipole to that of the parasitic dipole and it is at this frequency point that the excited driven dipole couple to the parasitic dipole. This conclusion can also be verified by the $|\mathrm{M_{ij}}|$ analysis in fig. 4.4:

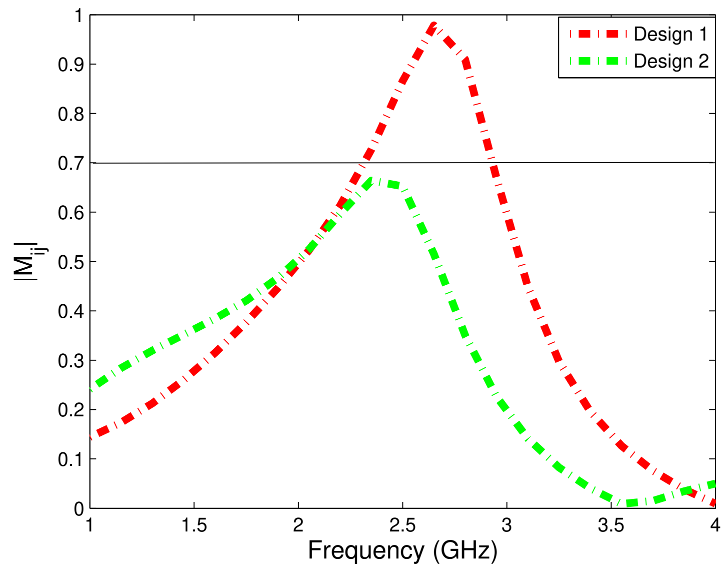

Figure 4.4: Dipole structures: $|M_{ij}|$ against frequency.

In fig. 4.4, the $|M_{ij}|$ represent mode-mode coupling between the resonating modes. Design 1 as shown by the red curve have a value closer to 1 around 2.6 GHz hence, the mode-mode coupling is strong and significant. This confirm that, the new resonance at 2.6 GHz represented the point where the coupling is strongest. Design 2 as shown by the green curve have a value lower than 0.7 therefore the coupling is weak and insignificant. The effect of this mode-mode coupling on the performance of the structure can be observed using the reflection co-efficient curve shown in fig. 4.5:

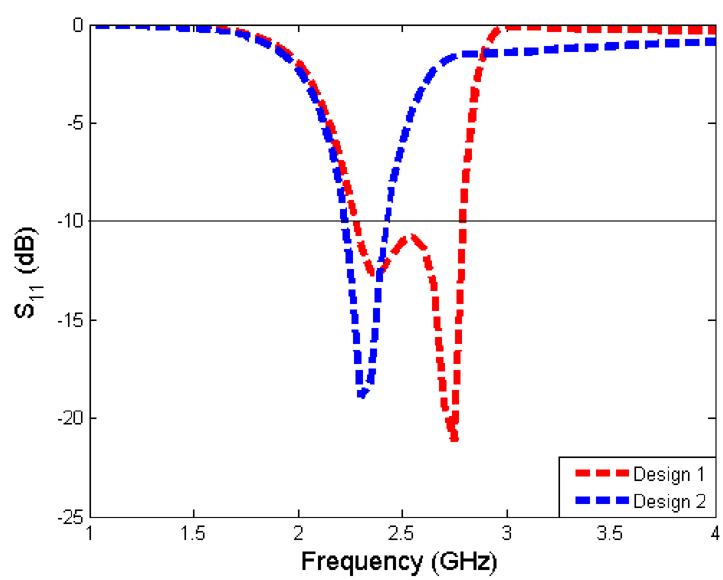

Figure 4.5: Dipole structures: Reflection coefficient (S_{11}).

The reflection co-efficient for design 1 and design 2 is shown in fig. 4.5. For design 1 as shown by the red curve, the inter-modal coupling is significant and result in an extended bandwidth of the design. For design 2 shown by the blue curve, it has an insignificant inter-modal coupling hence only the driven element affect the performance of the design thus a smaller bandwidth.

This result is in agreement with the result found in [149] and therefore, validate the method using our $X^{'}$ derivative.

4.5.1.2 Two I-shaped elements

A similar configuration to the two dipole structure is considered. The structure consist of two resonant I-shaped elements with one being the driven element and the other as the parasitic element. The driven element is excited at the centre with both the driven and parasitic element having their individual resonance at 2.4 GHz and 3.04 GHz respectively. The dimension and arrangement of the two I-shaped elements are shown in fig. 4.6:

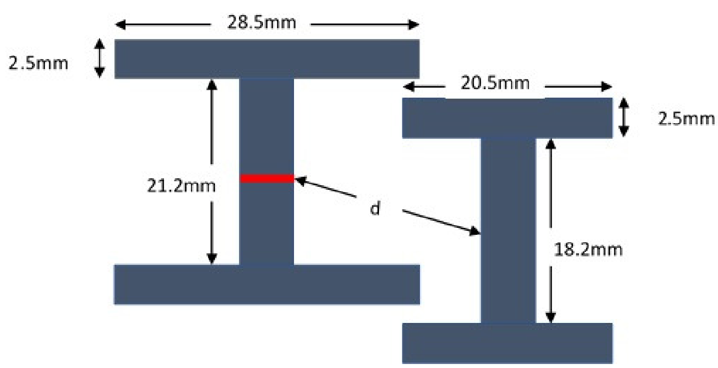

Figure 4.6: I-shaped structures.

Just like the two dipole elements, the two I-shaped elements are placed at two different distances d apart corresponding to $\frac{\lambda}{56.6}$ and $\frac{\lambda}{5}$ and represented in the result as design 1 and design 2 respectively. The driven element is excited with an edge port at the centre and the analysis is done within the frequency range 1 GHz and 4 GHz. The TCM commercial software is used for the modal analysis of the structure to solve the generalized eigenvalue equation. The obtained result of the TCM analysis for the elements are represented by the plot of the characteristic angle in degree against frequency and $\mathrm{MWC_n}$ against frequency for design 1 and design 2. The plot of the characteristic angle in degree against frequency is shown in fig. 4.7:

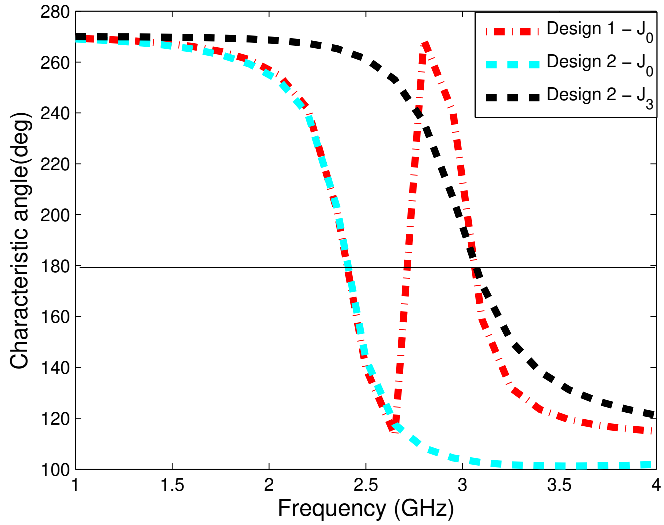

Figure 4.7: I-shaped structures: Characteristic angle against frequency.

In fig. 4.7, the characteristic angle against frequency show the resonance of the elements. The resonance appear at the frequency where the curve cross the 180°. The resonance of the individual elements are represented on the graph irrespective of the distance between the two elements. For design 1, the resonance of the two elements combine into one mode (i.e. design 1- J_0) as shown by the red curve and a line linking the two curve pass through 180° at 2.8 GHz. The significance of this line is similar to the new mode of the two dipole elements which represent the frequency of coupling between the two structures. For design 2, the resonance of the individual element appear on separate modes shown by the cyan and black curve (i.e. design 2- J_0 and design 2- J_3) respectively.

The relationship between the excitation source and the resonant modes are shown in the plot of $\mathrm{MWC_n}$ against frequency in fig. 4.8:

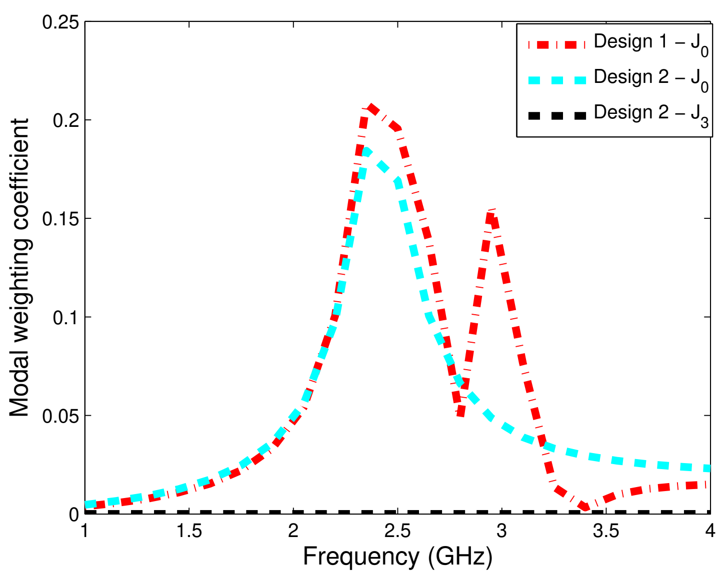

Figure 4.8: I-shaped structures: Modal weighting coefficient against frequency.

In fig. 4.8 which show MWC_n and represent the source-mode coupling like the analysis of the two dipole, the driven element is excited irrespective of the distance because it contain the excitation source. The MWC_n value at the first resonance of 2.4 GHz appear for both design 1 and design 2 and it is represented by the red and cyan curve respectively. The second resonance at 3.04 GHz for the parasitic I-shaped element is only excited by the source for design 1 as shown by the red curve. Therefore, the separation distance between the excitation source and the resonator is inversely proportional to the source-mode coupling which is observed by the reduction of the MWC_n magnitude at the second resonance for design 2 shown by black curve.

The dip at 2.8 GHz for design 1 links the resonance of the driven I-shaped element to that of the parasitic I-shaped element and it is at this frequency point that the excited driven I-shaped element couple to the parasitic one. This conclusion can also be verified by the $|M_{ij}|$ analysis in fig. 4.9:

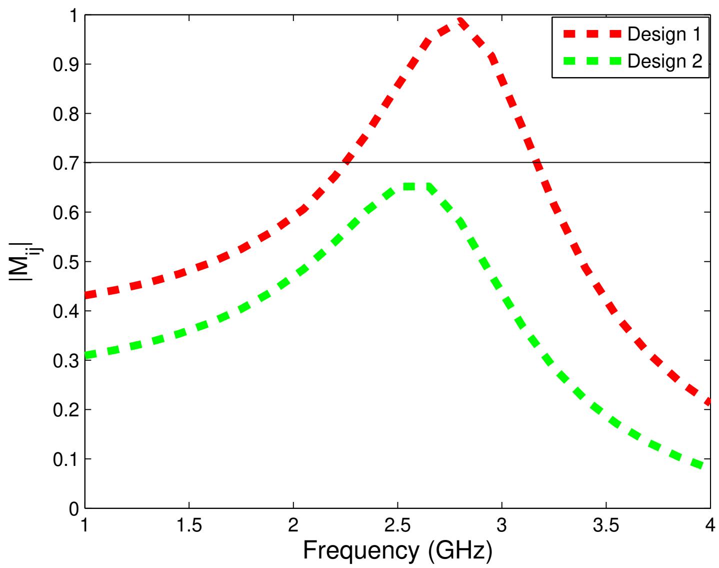

Figure 4.9: I-shaped structures: $|M_{ij}|$ against frequency.

In fig. 4.9, the $|M_{ij}|$ represent mode-mode coupling between the resonating modes. Design 1 as shown by the red curve have a value closer to 1 around 2.8 GHz hence the mode-mode coupling is strong and significant. The dip at 2.8 GHz represent the point where the coupling is strongest. Design 2 shown by the green curve have a value lower than 0.7 therefore the coupling is weak and less significant. The effect of this mode-mode coupling on the performance of the structure can be observed using the reflection co-efficient curve shown in fig. 4.10:

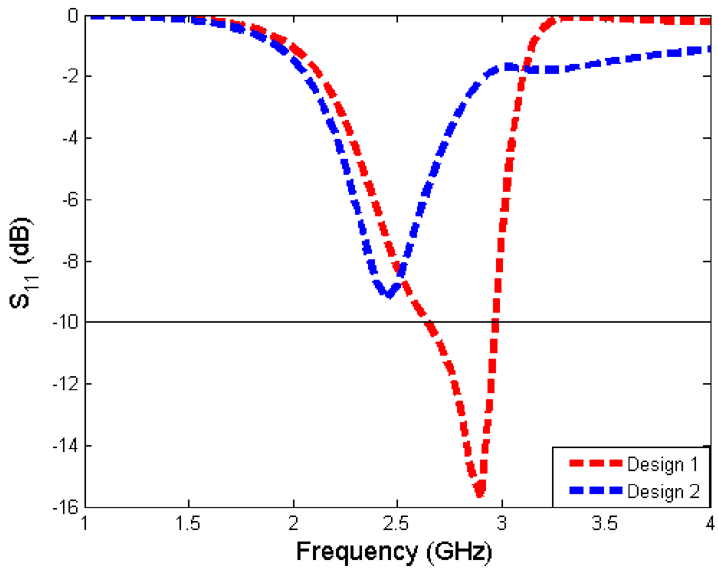

Figure 4.10: I-shaped structures: Reflection coefficient (S_{11}).

The reflection co-efficient for design 1 and design 2 is shown in fig. 4.10. For design 1 as shown by the red curve, the inter-modal coupling is significant and result in a -10 dB impedance-matched design. On the other hand for design 2 shown by the blue curve, it has an insignificant inter-modal coupling hence only the driven element affect the performance of the design and the design is mismatched at -10 dB.

For the case where one of the element is non-resonant, the analysis differ since only the resonance of one of the element is available.

4.5.2 Coupling analysis between a non-resonant antenna and a resonant parasitic element

In the previous section, the source-mode and mode-mode coupling are evaluated for design consisting of two resonant elements. In some cases however, one of the element may be non-resonant like in parasitic metamaterial antenna design [96, 217]. This section consider the coupling analysis of a different scenario, metamaterial-inspired antenna. The result will show that a different analysis apply when one resonant element couple with a non-resonant element. Two antennas are considered, monopole-meanderline antenna and dipole-BC-SRR antenna.

4.5.2.1 Monopole-meander-line metamaterial-inspired antenna

The monopole-meander-line antenna was considered and designed in [18, 209] using the inductive and capacitive compensation approach but with no particular mention on the effect of the coupling between both elements. It is an electrically small antenna consisting of a monopole antenna which is non-resonant between 1 GHz to 2 GHz and with a dimension of $\frac{\lambda}{23.8}$. The meander-line is a metamaterial inclusion which has its fundamental resonance at 1.48 GHz.

When the monopole antenna which is the driven element is excited and placed in close proximity to the meander-line which is the parasitic element, the monopole-meander-line antenna resonate at 1.45 GHz due to the impact of the coupling between the two structures. The reason for the shift in frequency and the explanation for the resonance of the combined structure was the complementing of the monopole's behaviour by that of the inclusion [18, 209].

The dimensions and arrangement of the monopole-meanderline antenna is shown in fig. 4.11:

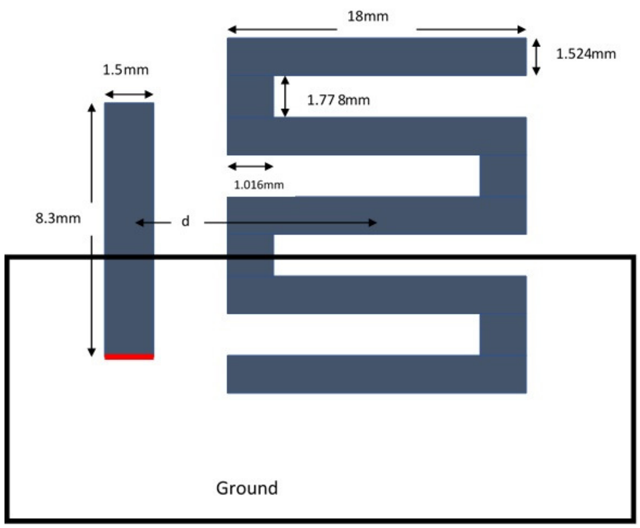

Figure 4.11: Monopole-meanderline antenna.

The same analysis done for two resonant elements is replicated. The meander-line is placed at two different distances d away from the monopole element corresponding to $\frac{\lambda}{338}$ and $\frac{\lambda}{4}$ and represented in the presented result as design 1 and design 2 respectively. The monopole is connected to an infinite ground plane and excited with an edge port between the monopole rectangular strip and the ground. The infinite ground plane is used to reduce computational complexities that result in modal tracking issues. The monopole-meander-line antenna is analyzed within the frequency range of 1 GHz and 2 GHz to cover the resonance of the meander-line. The TCM commercial software is used for the modal analysis of the antenna to solve the generalized eigenvalue equation. The obtained result of the TCM analysis for the antenna is represented by the plot of the characteristic angle in degree against frequency and MWC_n against frequency for design 1 and design 2. The plot of the characteristic angle in degree against frequency is shown in fig. 4.12:

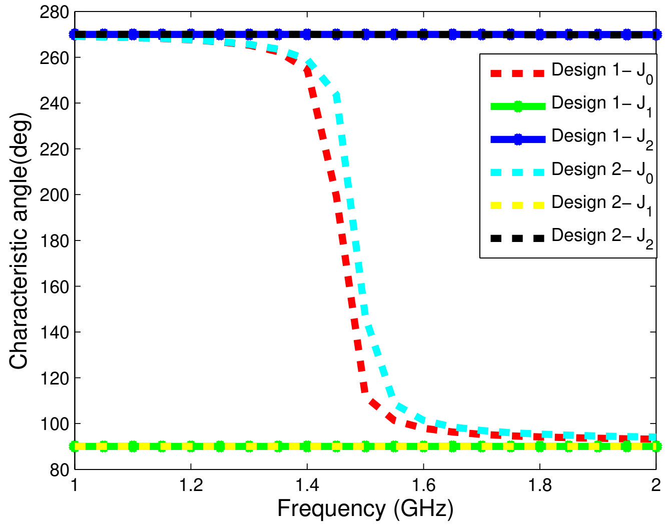

Figure 4.12: Monopole-meanderline antenna: Characteristic angle against frequency.

In fig. 4.12, the characteristic angle against frequency show the resonance of the structure. The resonance appear at the frequency where the curve cross the 180°. Since only the meander-line resonate among the two elements, only one resonance occur at the first mode for design 1 (i.e. design 1- J_0) and design 2 (i.e. design 2- J_0) represented by the red and cyan curve respectively. The second mode for design 1 (i.e. design 1- J_1) in green and design 2 (i.e. design 2- J_1) in yellow store magnetic energy throughout the studied frequency band since their curve remain below 180°. The third mode for design 1 (i.e. design 1- J_2) in blue and design 2 (i.e. design 2- J_2) in black store electric energy throughout the studied frequency band since their curve remain above 180°. The relationship between the modes of the meander-line element and the monopole element of the antenna will be established with the coupling analysis and modal surface current distribution.

The relationship between the excitation source and the resonant mode is shown with the plot of $\mathrm{MWC_n}$ against frequency in fig. 4.13:

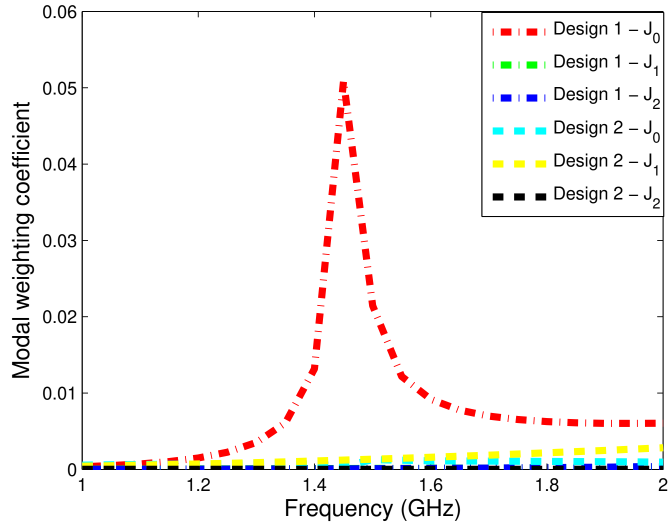

Figure 4.13: Monopole-meanderline antenna: Modal weighting coefficient against frequency.

In fig. 4.13 which show $\mathrm{MWC_n}$ and represent the source-mode coupling, only the first mode at 1.45 GHz of design 1 as shown in red is sufficiently excited. This is because the excitation source is on the non-resonant element. The coupling between the excitation source of the monopole element and the meander-line element is not sufficient enough to excite the meander-line for design 2 shown in blue. The second and third mode for design 1 and design 2 are also not excited since they are non-resonant.

To understand how the modes of the monopole and that of the meander-line couple to each other, the $|\mathrm{M_{ij}}|$ is evaluated and its result is presented in fig. 4.14:

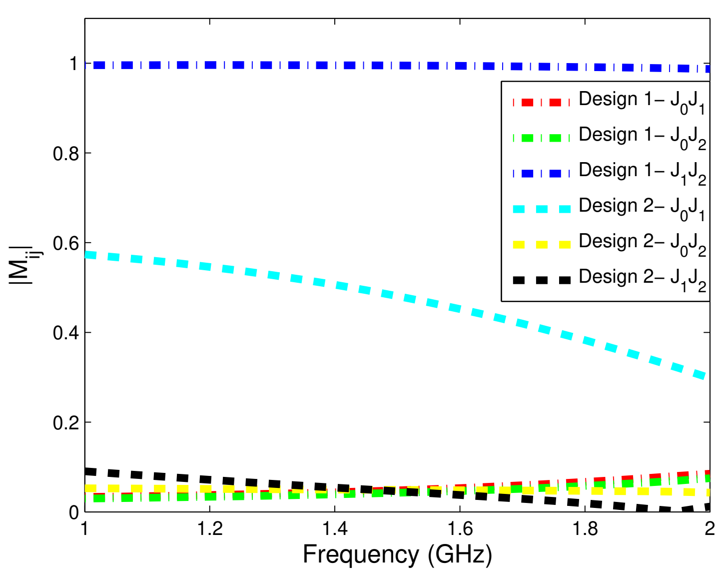

Figure 4.14: Monopole-meanderline antenna: $|\mathrm{M_{ij}}|$ against frequency.

In fig. 4.14, the $|M_{ij}|$ represent mode-mode coupling between modes. Design 1 has the magnetic mode J_1 coupling to the electric mode J_2 shown by the blue curve. The value remain 1 throughout the considered frequency band of 1 GHz to 2 GHz. On the other hand, coupling between the modes of design 2 have values lower than 0.7. The coupling between other modes for design 1 are also below 0.7 and insignificant.

To get more clarity, a visual analysis of the inter-modal coupling is done using the modal surface current distribution of design 1 as shown in fig. 4.15:

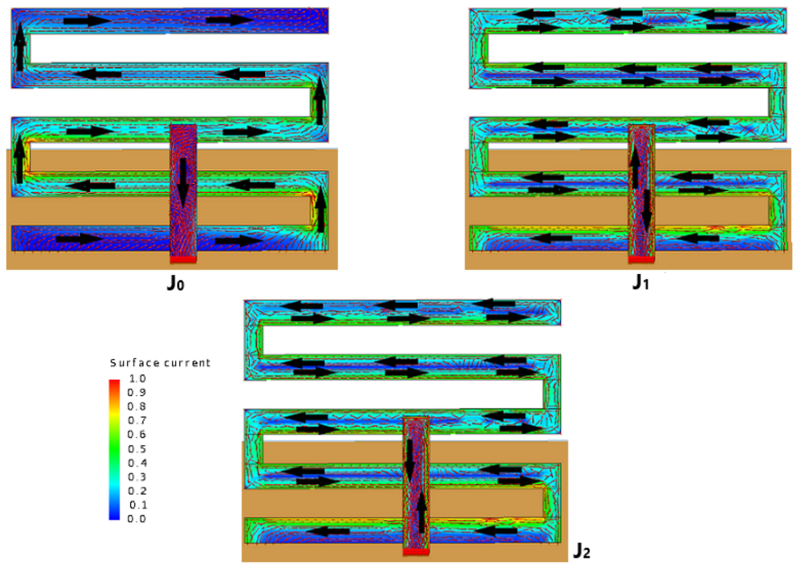

Figure 4.15: Monopole-meanderline antenna: Modal surface current analysis.

The current distribution in fig. 4.15 is similar to what is found in [209] which show that the resonant mode J_0 of the meander-line in the antenna maintain its current distribution as when it operates alone. The current profile on the monopole follow that of the meander-line for the resonant mode of the monopole-meander-line antenna. For the other modes J_1 and J_2, their current profile is a combination of the magnetic mode of the monopole element and the electric mode of the meander-line element.

The conclusion is that in the case of a resonant and a non-resonant element placed in very close proximity to each other, coupling happen as a result of the compensation of energy (i.e. electric energy of one structure couple and compensate the magnetic energy of the the other structure and vice versa). This conclusion is in agreement with the explanation given in the literature for this type of antenna [18, 209] where the compensation of qualitative modal stored energy is required to enhance the performance of the antenna. In contrast to the case of two resonant elements, the inter-modal coupling occur between non-resonant modes when placed in close proximity.

4.5.2.2 Dipole-Broadside-Coupled Split Ring Resonator (Dipole-BC-SRR) metamaterial-inspired antenna

The Dipole-BC-SRR antenna is an ESA consisting of a dipole element which is non-resonant between 0.2 GHz to 1.6 GHz and with a dimension of $\frac{\lambda}{33}$. The BC-SRR is an inclusion which has a fundamental resonance at 0.48 GHz and 1.35 GHz without the use of a substrate.

When the dipole element which is the driven element is excited and placed in close proximity to the BC-SRR, the dipole-BC-SRR antenna resonate at 1.35 GHz due to the impact of the coupling between two elements. The first occurring resonance of 0.48 GHz is not excited because it has a low modal significance and a low inter-modal coupling.

The dimensions and arrangement of the dipole-BC-SRR antenna is shown in fig. 4.16:

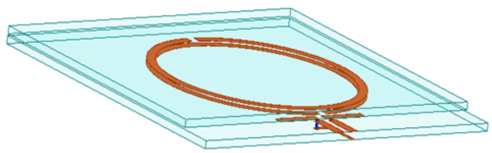

Figure 4.16: Dipole-BC-SRR.

In the design of fig. 4.16, the BC-SRR is placed at an optimized distance of $\frac{\lambda}{1110}$ away from the dipole antenna. The dipole is a printed one with the port placed between the dipole structure and a balun. The use of substrate is ignored to reduce computational complexity that result from modal tracking issues. The dipole-BC-SRR antenna is analyzed within the frequency range of 0.2 GHz and 1.6 GHz to cover the resonance of the BC-SRR inclusion. The TCM commercial software is used for the modal analysis of the antenna to solve the generalized eigenvalue equation. The obtained result of the TCM analysis for the antenna are represented by the plot of the characteristic angle in degree against frequency and $\mathrm{MWC_n}$ against frequency. The plot of the characteristic angle in degree against frequency is shown in fig. 4.17:

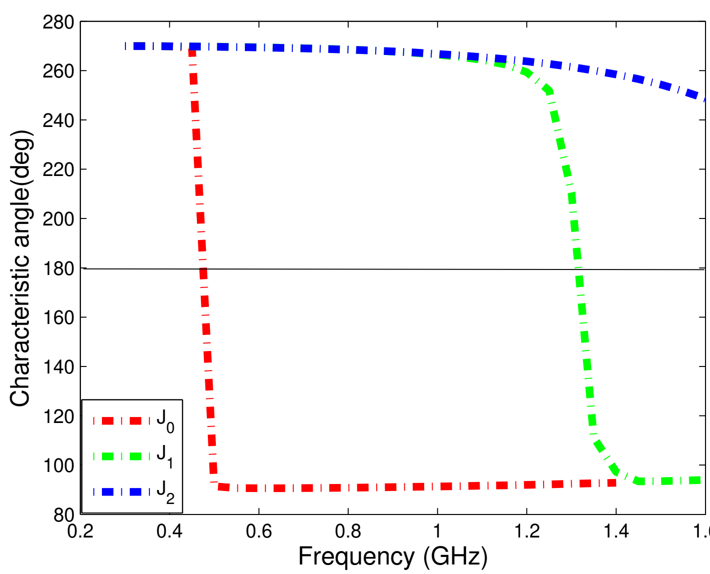

Figure 4.17: Dipole-BC-SRR: Characteristic angle against frequency.

In fig. 4.17, the characteristic angle against frequency show the resonance of the structure. The resonance appear at the frequency where the curve cross the 180°. Since only the BC-SRR inclusion resonate among the two elements, the two resonances of the BC-SRR in mode 1 (i.e.J_0) and mode 2 (i.e.J_1) represented by the red and green curve respectively are seen. The third mode (i.e.J_2) store electric energy throughout the studied frequency band since the curve remain above 180°. J_0 and J_1 represent the resonant behaviour of the BC-SRR (i.e. J_0 and J_2 of the BC-SRR alone) and J_2 represent the non-resonant behaviour of the dipole (i.e. J_0 of the dipole alone).

The relationship between the excitation source and the resonant mode is shown with the plot of $\mathrm{MWC_n}$ against frequency in fig. 4.18:

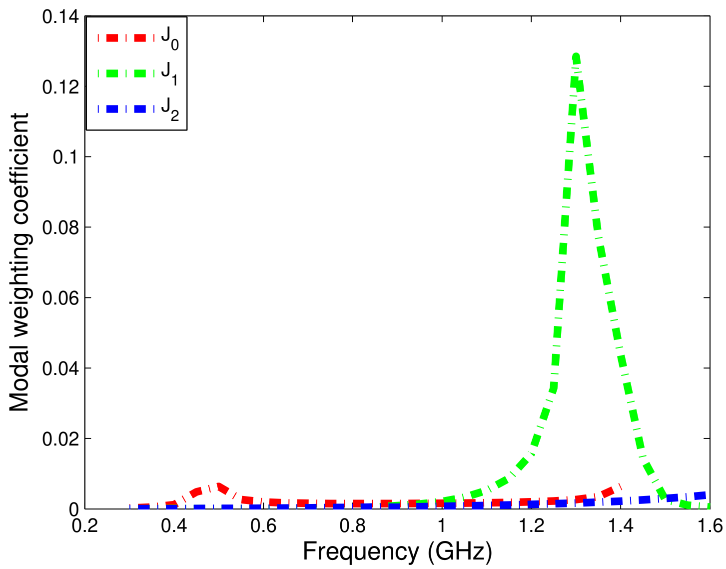

Figure 4.18: Dipole-BC-SRR: Modal weighting coefficient against frequency.

In fig. 4.18 which show $\mathrm{MWC_n}$ and represent the source-mode coupling, only the second mode (i.e.J_1) of the antenna at 1.35 GHz is sufficiently excited. Mode 1 (i.e.J_0) is not excited because it has a modal significance below 0.7, mode 3 (i.e.J_2) is not excited since it stores electric energy throughout the considered frequency band and the distance between the dipole and the BC-SRR is only sufficient to ensure that the coupling between the excitation source on the dipole can excite J_1 of the BC-SRR. To excite J_0, a magnetic excitation or a different configuration and separation distance between the dipole and BC-SRR can be implemented.

To understand how the dipole and BC-SRR couple to each other, the $|\mathrm{M_{ij}}|$ is evaluated and its result is presented in fig. 4.19:

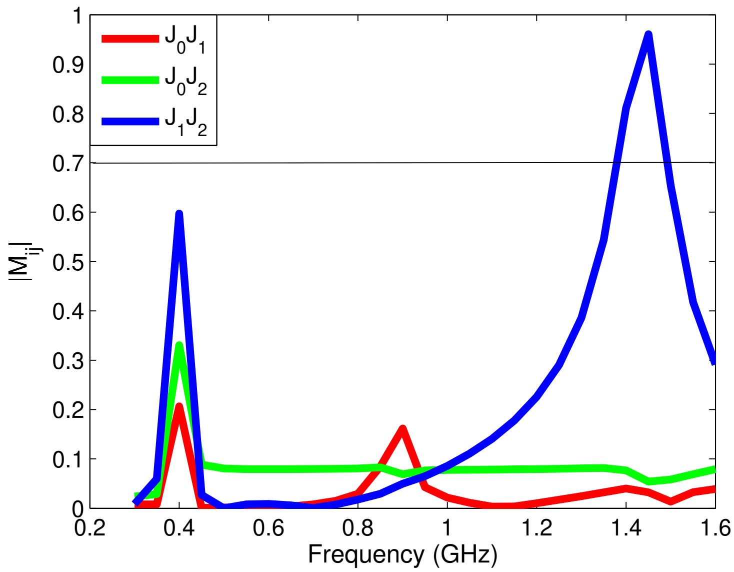

Figure 4.19: Dipole-BC-SRR: M_{ij} against frequency.

In fig. 4.19, the $|M_{ij}|$ represent the mode-mode coupling between modes. The coupling between the two resonant modes J_0 and J_1 in red are insignificant because they have a value below 0.7. For the coupling between J_0 and J_2 in green, the coupling is insufficient because it has a value below 0.7 and this is because J_0 have a low modal significance despite the coupling of the dipole mode and the BC-SRR mode.

The $|M_{ij}|$ value for the coupling between J_1 and J_2 is above 0.7 between 1.35 GHz and 1.46 GHz. The coupling at this region is strong and significant. The electric energy of the dipole couple with the magnetic energy of the BC-SRR that appear after its modal resonance hence the bandwidth of coupling between the two elements are limited.

To get more clarity, a visual analysis of the inter-modal coupling is viewed using the modal surface current distribution as shown in fig. 4.20:

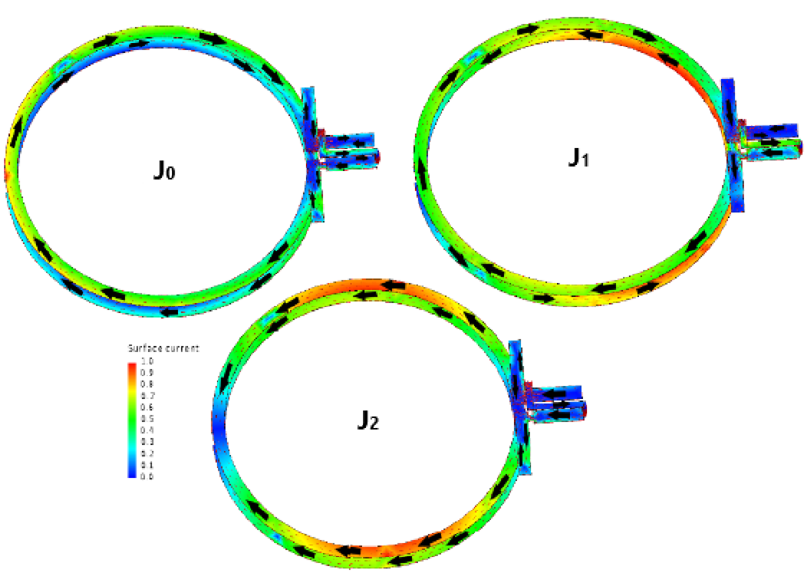

Figure 4.20: Dipole-BC-SRR: Modal surface current analysis.

In fig. 4.20, J_1 which is the only mode to be sufficiently excited by the source excitation and have its resonance at 1.35 GHz show that its modal surface current distribution is a combination of the J_2 surface current of the BC-SRR alone which store magnetic energy after resonance and J_0 surface current of the dipole alone storing electric energy. The coupling occur between the resonant mode of the BC-SRR and the non-resonant mode of the dipole structure which is a compensation of energy between the BC-SRR which store magnetic energy after resonance and the dipole structure which store electric energy at the considered mode.

The design process, the choice of the BC-SRR and the effect of the inter-modal coupling on the performance of the dipole-BC-SRR antenna is discussed in another chapter.

4.6 Conclusion

In this chapter, the evaluation of the scattering using coupling analysis is presented. The coupling affecting the performance of integrated antennas were considered in two part which are the source-mode coupling and the inter-modal coupling. While the source-mode coupling describe how the excitation source couple to the various modes to affect the overall performance of the system, the inter-modal coupling describe how the different mode representing the behaviour of the different antenna elements interact to affect the performance of the system. An insight into modal electromagnetic coupling was given before the presentation of the formula for the evaluation of modal coupling (source-mode and inter-modal coupling). Although these formulation was developed and used in literature, it was only applied to two resonant structures. The relationship between modal stored energy and inter-modal coupling analysis was also explained based on their dependence on the imaginary part of the impedance matrix of the structure.

The application of TCM based coupling analysis was then carried out with the formulation. To give a uniform comparison of the effect of the inter-modal coupling on the antenna performance, 0.7 was considered as the minimum threshold to consider a coupling as significant. First, the case of a resonant driven element and resonant parasitic element was considered and compared to the literature since the derivation process for the $X^{'}$ is different. The analysis showed that the modal coupling occur between the resonant modes of the two structure and compare to result found in literature. A different scenario was then analysed consisting of a non-resonant driven element and a resonant parasitic element (metamaterial inclusion). The obtained result show that a compensation of energy happened in this case. The electric energy of one structure combine with the magnetic energy of another structure and the compensation was not dependent on if the modes are resonant or non-resonant but rather on the stored energy within a specific frequency band.

The obtained result also confirmed that the distance between elements affect the source-mode coupling and the inter-modal coupling which has a direct effect on the overall performance of the system in terms of impedance matching and impedance bandwidth. This analysis complement the modal stored energy of a system in describing its near-field behaviour. We believe it is a useful tool in designing metamaterial-inspired antenna especially in designing the configuration of the inclusion with respect to the antenna structure.

Chapter 5

Design of an ESA with enhanced performance based on the proposed systematic method

5.1 Introduction

Some of the reasons why electrically small antennas are useful despite its physical size constrain, very small bandwidth, low radiation resistance and large reactance are its mechanical strength in wind, obstacle clearance on mobiles and field-probing application [15]. Electrically Small Antennas (ESAs) perform well under matched conditions but achieving a good matching is quite often very challenging because the size, bandwidth, gain, quality factor and radiation efficiency of an antenna are interrelated. With antenna's miniaturized size, there is only a limit to the optimization of the performance parameters [61]. This implies that researchers have to constantly work on developing methods for enhancing different performance parameter of ESAs depending on the application requirement critical for the system's operation. Some of the existing methods include; good antenna choice, geometry optimization, q-factor optimization, use of parasitic elements among others.

Most of the methods for enhancing the performance of ESAs are only intuitive and require a brute force method. The use of metamaterial as a parasitic element is one of the promising method for enhancing ESA and it is mostly implemented based on intuition without having knowledge on its electromagnetic behaviour. In fact in [24], an method based on TCM was applied in using metamaterial to enhance the performance of antennas however in complex design, the choice of the inclusion and its configuration would be difficult without completely analysing the near-field behaviour of the inclusion. A better method would be to quantitatively evaluate the near field behaviour of the inclusion to use it as a parasitic element of an antenna to achieve enhanced performance.

This chapter present the design of a parasitic metamaterial antenna for railway application. The antenna is designed using the proposed systematic method for enhancing the performance of integrated antenna. It takes into account the radiation properties and scattering properties of the antenna whose source of excitation could be a monopole [8], printed monopole [24], loop [8], patch [218] or even a dipole [18]. For the design presented here, a printed dipole is used as the excited element because of the ease of fabrication and the available testing procedure. It is non-resonant and used with a resonant metamaterial inclusion which is chosen based on its modal stored energy quantity.

A briefly review on the use of inclusion as parasitic element for antenna is given and the proposed method applied in the design of the antenna is presented. The method involve using TCM to evaluate the physical behaviour of the excited element, then determining its radiation properties using modal stored energy. An inclusion (i.e. broadside coupled split ring resonator) is selected to compensate for the stored energy of the excited element based on the modal stored energy. The scattering properties are also evaluated with inter-modal coupling to determine the configuration and spacing between the excited element and the chosen inclusion. Finally, the practical implementation of the proposed method is applied in the design of an antenna, the antenna prototype is realized and tested. The result show that both the simulated result and the measured result are in good agreement for the reflection co-efficient and far-field radiation pattern.

5.2 Parasitic metamaterial ESA

Among the many methods for enhancing the performance of ESAs, the use metamaterial have been shown to be a good choice [18]. Metamaterials (MTMs) are artificially engineered materials with properties not readily found in nature thus making them have flexible control of electromagnetic wave propagation. They are useful in antenna application for radiating and scattering problems including enhancing radiation properties and decoupling antenna from its near-field surrounding [219]. The earlier use of metamaterial in the design of antennas were referred to as metamaterial-based antennas [220] but these antennas had a large size because of the metamaterial structure. Ziolkowski et al. later demonstrated both theoretically and experimentally that a single unit-cell of a metamaterial can improve the performance and efficiency of ESA while maintaining the antenna size within its electrically small limit [8, 18]. These type of antennas are nowadays referred to as metamaterial-inspired antenna and are becoming quite popular with lot of research interest. A comparison between the metamaterial-based antenna and metamaterial-inspired antenna is shown in figure 5.1:

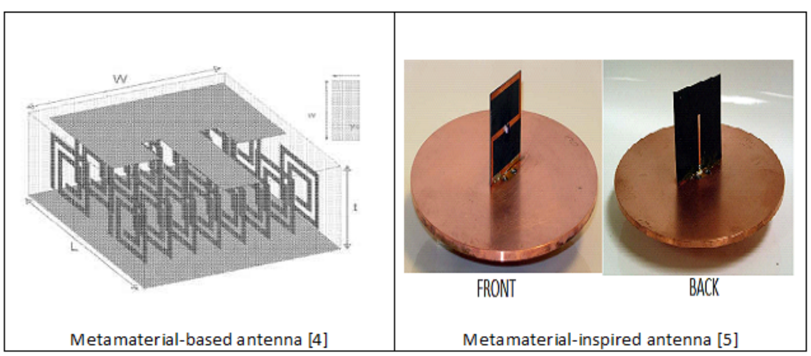

Figure 5.1: Design comparison between metamaterial-based antenna and Parasitic metamaterial antenna.

The parasitic metamaterial antenna (or metamaterial-inspired antenna) use less elements and therefore have a smaller size compared to the metamaterial-based antenna. Many literature works have applied the use of parasitic metamateriakl inclusion in the design of ESAs for achieving the enhancement of different antenna parameter [18, 24, 218] but the method for the selection a particular inclusion for a given antenna has not been addressed. The challenge is more significant for the case of non-canonical and arbitrary antennas with no sufficient knowledge and insight into its radiating properties and physical behaviour. In [18], the principle of selecting an inclusion in the case of canonical antenna structure was based on the compensation of the inductive nature of the antenna by a capacitive inclusion and vice versa. For arbitrary antennas, Rabah et al. employed the use of qualitative analysis of stored energy derived directly from theory of characteristic mode (TCM) [24] in selecting an inclusion for the design of an arbitrary antenna. However in the case of complex antenna design, the qualitative stored energy may be insufficient to describe the inclusion's near-field behaviour.

The advantage of the TCM method is not only its excitation independence but also the insight gotten on the physical behaviour, radiation properties and intuitive nature of the modal stored energy of the structure which are qualitative [12, 24]. The stored energy quantity is useful for easy classification of inclusions (see chapter 3) and for selecting a proper inclusion for a given antenna in the design of a parasitic metamaterial antenna. It ensure that the electric stored energy of the antenna is compensated by the magnetic stored energy of the inclusion and vice versa. We therefore follow a systematic method based on the quantitative stored energy of the metamaterial inclusion in selecting the proper inclusion for the design of parasitic metamaterial ESA.

5.3 Design method for a parasitic metamaterial ESA based on the proposed method

In this section, the proposed method for enhancing the performance of integrated antenna is summarized and provide an insight into its application for the design of ESA. It involve the implementation of the procedure already discussed in previous chapters which include; application of the theory of characteristic modes in evaluating the physical behaviour, evaluation of radiation properties using modal stored energy and evaluation of the scattering properties with inter-modal coupling co-efficient. It start from the extraction of the impedance matrix used in solving the generalized eigenvalue equation as shown in the chart of figure 5.2:

In the first step of evaluating the physical behaviour, the TCM method is used to determine the resonance frequency and gain an intuitive knowledge on the stored energy. The characteristic angle (θ_n) and modal surface current distribution of TCM are used in this evaluation. At the frequency where θ_n is 180°, the structure resonate. When θ_n is greater than 180°, the structure store electric energy while when θ_n is less than 180°, the structure store magnetic energy at these frequencies.

The second step of evaluating the radiation property use the qualitative stored energy method since the stored energy is related to the radiation by the Q-factor [26]. It focuses on the near-field of the structure and in comparison to the intuitive stored energy knowledge derived from TCM, the stored energy quantity at each frequency point can be evaluated. The difference between the magnetic and electric energy (i.e. (W_m - W_e) is used in determining the quantity of the dominant stored energy. At the frequency when (W_m - W_e) is 0, the structure resonate. When (W_m - W_e) is negative, the structure store electric energy while when (W_m - W_e) is negative, the structure store magnetic energy at these frequencies.

The final step of evaluating the scattering property is done with the inter-modal coupling analysis. It show how the antenna elements couple to their immediate environment. In comparison to antenna

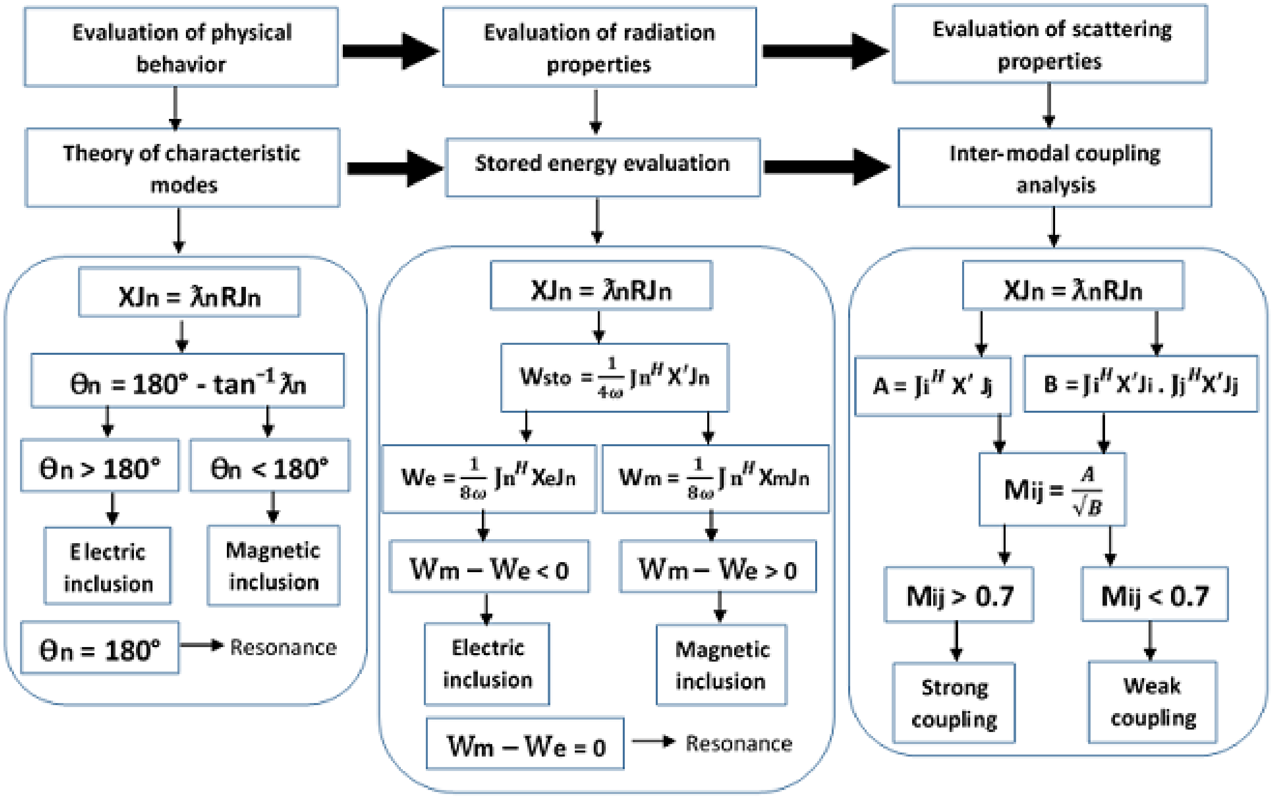

Figure 5.2: Chart showing the components for the implementation of the proposed method to antenna design.

applications like MIMO system where coupling negatively affect performance and need to be reduced, the coupling is needed and should be enhanced. The evaluated coupling is between the modes that represent the behaviour of the different elements. To remain consistent with the modal bandwidth definition since the TCM impedance matrix is used in the inter-modal coupling analysis, 0.7 is taken as the threshold. The modes which have their inter-modal coupling co-efficient greater the 0.7 have significant coupling and affect the performance compared to modes which have their value lower than 0.7.

5.4 Application of the proposed systematic method to antenna design

In this section, the proposed method is applied in the design of parasitic metamaterial ESA. The antenna consist of a dipole antenna and a metamaterial inclusion. The antenna which is a printed non-resonant dipole act as an exciter and is chosen because of the ease of fabrication. Its evaluated stored energy was considered for choosing it from a group of inclusions in an MTM inclusion LUT. The chosen inclusion of Broadside-coupled split-ring resonator (BC-SRR) have sufficient stored energy to compensate the stored energy of the antenna. The configuration of the parasitic metamaterial ESA was chosen due to the inter-modal coupling value being greater than 0.7 around the frequency of interest. The overall size of the MTM inspired-antenna is 0.133λ by 0.133λ with a resonance at 0.88 GHz and a bandwidth of 14 MHz.

The analysis of the antenna is done using the same assumption in [24] where the substrate is taken to be a mechanical support hence only the PEC part of the structures are considered while the substrate is added for the full wave simulation.

5.4.1 Selection of radiating element

The chosen antenna element is a printed dipole antenna referred to as an exciter because it does not radiate or resonate within the frequency band of interest (i.e. 0.2 GHz to 1.6 GHz). It only contain the feeding port which capacitively excite the chosen inclusion. The dipole antenna is chosen to be a printed dipole because of the ease of fabrication and measurement. Its design dimension is shown in figure 5.3:

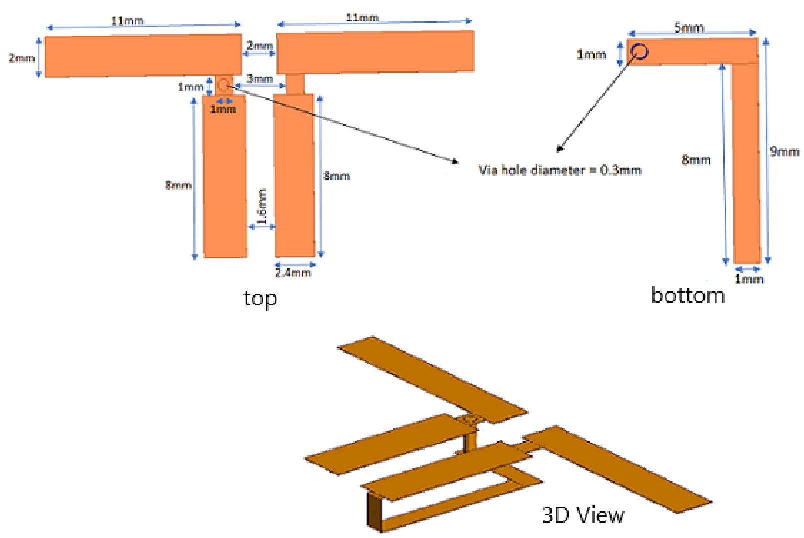

Figure 5.3: Printed dipole structure.

The dipole antenna presented in figure 5.3 consist of the top part which is the main dipole structure and the bottom part which is a balun 1.6mm apart and linked together by a via. The balun is necessary to allow for a balanced current flow between the two legs of the dipole after an excitation is applied [221]. To get a proper understanding of the physical behaviour of the dipole element and to evaluate the modal surface current distribution, the TCM analysis is carried out.

5.4.1.1 TCM analysis

TCM which is independent of excitation and applicable to arbitrary structures give an insight into the physical behaviour of the dipole antenna [23] by providing information on which mode resonate and the qualitative nature of the stored energy for the various mode at different frequencies [12]. The modal surface current distribution derived from the TCM analysis is used as a guide for placing the excitation port to excite the required mode of the dipole element [145].

The TCM analysis for the dipole antenna is represented with the first three modes since they are sufficient to represent the global behaviour of small structures [12]. The result is given in the characteristic angle against frequency curve in figure 5.4 and the modal surface current distribution diagram in figure 5.5:

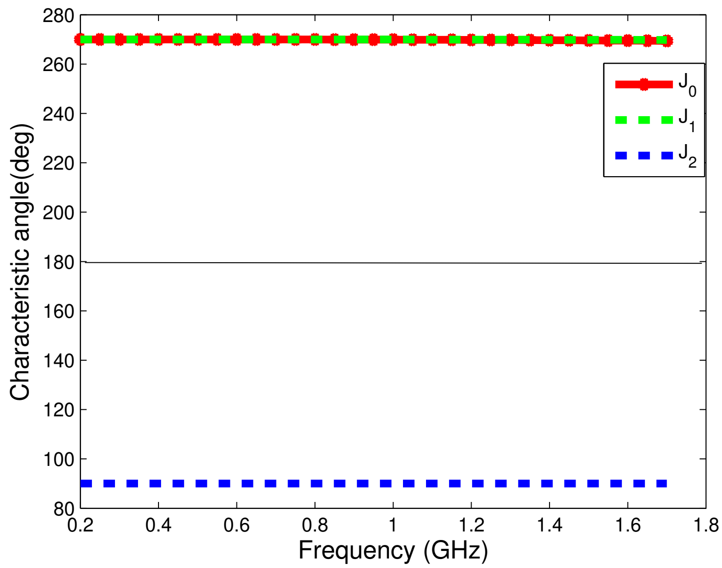

Figure 5.4: Printed dipole: Characteristic angle against frequency.

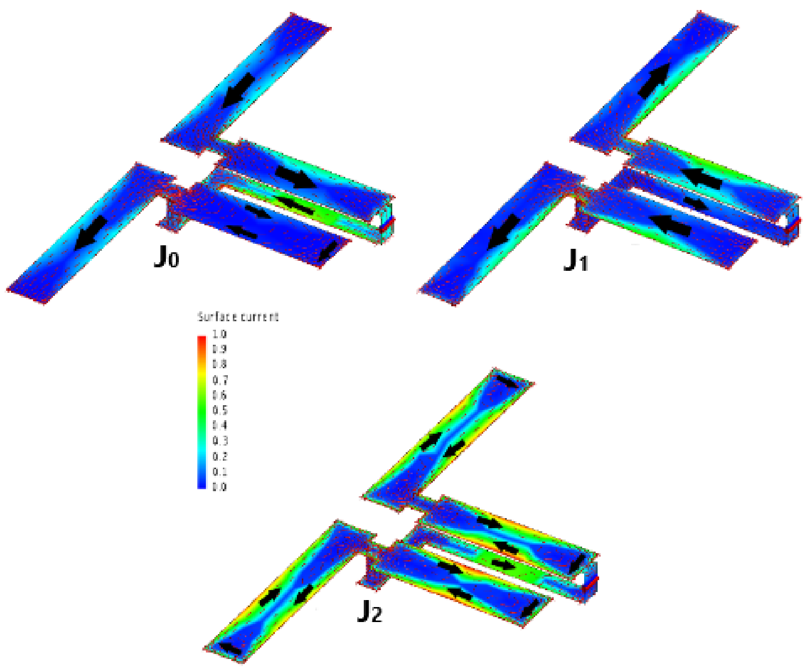

Figure 5.5: Printed dipole: Modal surface current distribution.

From figure 5.4, the dipole does not radiate and it has no resonance because none of the mode cross the 180° of the characteristic angle curve. The first two modes J_0 in red and J_1 in green are above the 180° which indicate that they store electric energy throughout the considered frequency band. J_2 in blue is below the 180° and therefore store magnetic energy. The characteristic angle curve confirm that the dipole is non resonant and only store energy at the various mode. This stored energy deduction is only qualitative in nature.

The same stored energy conclusion can be the derived from the modal surface current distribution in figure 5.5. In figure 5.5, the surface current distribution of J_0 and J_1 are similar to that of an electric dipole structure with the current flowing in a single direction for J_0 and in opposite direction for J_1 on the different part of the structure. In J_2, the surface current distribution is in a loop-like form similar to a magnetic loop antenna. Hence one can draw the same conclusion as that of the characteristic angle (i.e. J_0 and J_1 store electric energy while J_2 store magnetic energy).

The modal surface current distribution also provide an insight into the port placement and feed excitation. For an inductive excitation source, the port is placed on the area with maximum surface current distribution while a capacitive excitation source have its port on the the area with the minimum surface current distribution [145, 222]. In the case of our dipole with the balun, the port is placed between the dipole and the balun to balance the current distribution of the dipole.

In selecting the proper inclusion to be associated with the printed dipole, the radiation properties based on the qualitative stored energy are evaluated.

5.4.1.2 Stored energy analysis

Although the characteristic angle and modal surface current distribution of the TCM analysis provide an insight into the stored energy of the dipole element in a qualitative manner [24]. Evaluating the stored energy quantity help to select the best inclusion capable of adequately compensating for the stored energy of the dipole. It focuses on the near-field quantity of the structure thus has the ability to provide sufficient impedance matching to the antenna if the right inclusion is selected.

The impedance matrix of the dipole is extracted from the CMA simulation tool and the TCM-based stored energy evaluation method presented in previous chapter (see chapter 3) is applied to the impedance matrix of the dipole element. The dominant stored energy of the dipole is represented by the curve of normalized $(\mathrm{W_m} - \mathrm{W_e})$ against frequency of the first three modes shown in figure 5.6:

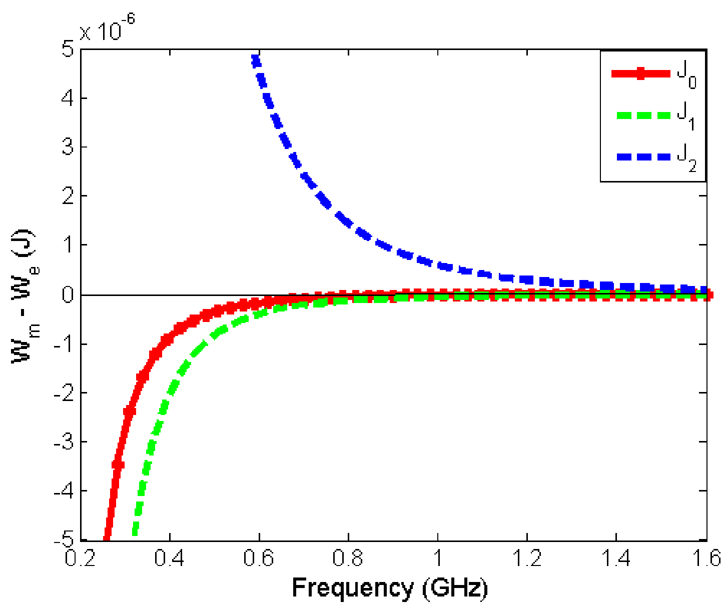

Figure 5.6: Printed dipole: Normalized $(\mathrm{W_m} - \mathrm{W_e})$ against frequency.

From figure 5.6, the same qualitative stored energy deduction derived from the TCM analysis are attained however, the normalized $(\mathrm{W_m} - \mathrm{W_e})$ curve provide the quantitative values of the dominant modal stored energy at various frequencies. J_0 and J_1 in red and green have electric stored energy since they have negative values throughout the considered frequency band. They have their values between $-3.3X10^{-05}$ J and 0 J much closer to zero and easier to compensate compared to the J_2 which predominately store magnetic energy with values between 0 J and $3.6X10^{-04}$ J since it have positive values throughout the considered frequency band.

Therefore, an inclusion which dominantly store magnetic energy in its resonating mode with an energy quantity as close as possible to that of the dipole's J_0 or J_1 is required for the design of a well matched parasitic metamaterial ESA.

5.4.2 Selection of metamaterial inclusion

To choose the best inclusion, a group of inclusion already studied by Rabah et al. [24] using the TCM method was considered based on their classification as either electric or magnetic inclusion. Among these metamaterial inclusions, the Broadside Coupled Split Ring Resonator (BC-SRR) was chosen because it has been well studied and its magnetic properties have been established (see [223] and chapter 3). It was also chosen because of its dominant magnetic stored energy on its resonant mode which is sufficient to compensate the electric stored energy of the dipole (see chapter 3).

The group of considered inclusion from which the BC-SRR was chosen is shown in figure 5.7a but only the results from the BC-SRR analysis is presented. The design and dimension of the BC-SRR inclusion is shown in figure 5.7b:

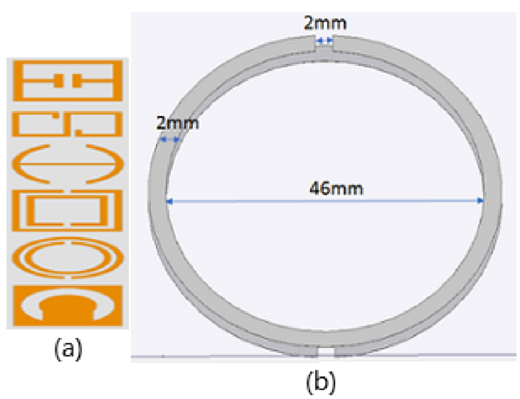

Figure 5.7: Metamaterial inclusion: (a) inclusion list (b) BC-SRR.

The inclusion in figure 5.7b is a well studied inclusion [223, 224] which was shown to exhibit artificial magnetism [223]. The BC-SRR consist of two circular symmetric loops of PEC material placed 1.6mm apart. The BC-SRR has two resonances within the considered frequency band of 0.2 GHz to 1.6 GHz. The first resonance occurs at 0.5 GHz and the second resonance at 1.5 GHz.

The behaviour of the BC-SRR inclusion which made it suitable for association to the printed dipole is first demonstrated using the TCM analysis of the structure to determine its physical behaviour and resonance frequency. The TCM analysis is done using the CMA tool.

5.4.2.1 TCM analysis

Just like the TCM analysis of the printed dipole, the TCM analysis provide information on the resonance frequency and give a qualitative idea on the nature of the modal stored energy of the inclusion. It also provide a guide to exciting the desired mode based on the modal surface current distribution.

The TCM analysis for the BC-SRR inclusion is represented with the first three modes since they are sufficient to represent the global behaviour of the inclusion [12]. The result is represented by the characteristic angle against frequency curve in figure 5.8 and the modal surface current distribution diagram in figure 5.9:

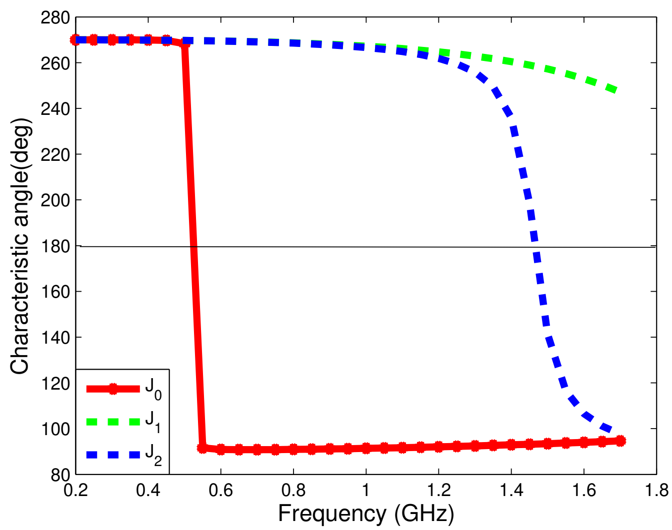

Figure 5.8: BC-SRR: Characteristic angle against frequency.

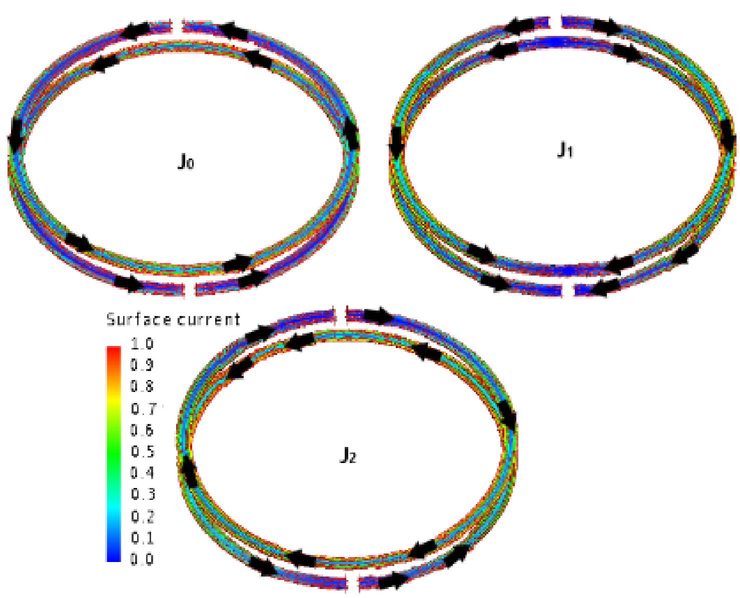

Figure 5.9: BC-SRR: Modal surface current distribution.

The BC-SRR is a resonant structure as shown in figure 5.8. It has two resonances which are at 0.5 GHz for J_0 in red and 1.5 GHz for J_2 in blue. J_0 and J_2 are resonant modes because their curve cross 180° of the characteristic angle plot. The two resonant modes go from storing dominantly electric energy to resonance. After resonance they store magnetic energy for the remaining part of the considered frequency band. J_1 in green store electric energy throughout the considered frequency band since it has its curve above 180°.

Although the evaluation of the resonance frequency and the qualitative nature of the stored energy is derived using the characteristic angle plot, the same stored energy deduction can be deduced from the modal surface current distribution of the inclusion.

The modal surface current distribution of the BC-SRR in figure 5.9 show the current distribution of J_0 and J_2 being similar to that of a magnetic loop antenna. J_0 was also referred to as the fundamental direct current mode [223] and have its current distribution on the two loops flowing in the same direction. J_2 have its current distribution on both loop flowing in the opposite direction while J_1 have its current flowing in two opposite direction on each half of the loop similar to the current distribution on an electric dipole.

It can therefore be concluded that J_0 and J_2 store magnetic energy while J_0 store electric energy based on their current distribution pattern. This conclusion is in accordance with the conclusion from the characteristic angle plot where only J_0 and J_2 store magnetic energy after resonance. The interesting modes of the BC-SRR are J_0 and J_2 needed for the compensation of the stored electric energy of the dipole. The inclusion is a resonant structure which will make the antenna radiate and store magnetic energy which is required for compensating the electric energy of the printed dipole.

The modal surface current distribution provide information on the position for the excitation port in order to excite the required mode of the inclusion structure. For instance, an inductive excitation is placed on the area with maximum surface current distribution while for a capacitive excitation source, the area with the minimum surface current distribution is used [145, 222]. Since the BC-SRR will be excited by the dipole in a capacitive manner, the inclusion is excited by placing the centre of the dipole close to the gap of the rings where the minimum surface current distribution.

To understand the energy compensation phenomenon between the inclusion and the printed dipole, the stored energy quantity is evaluated using the TCM-based modal stored energy procedure (see chapter 3).

5.4.2.2 Stored energy analysis

The evaluation of the modal stored energy is necessary to ensure that the stored magnetic energy of the BC-SRR is sufficient enough to compensate for the stored electric energy of the dipole. The same procedure employed in the stored energy evaluation of the dipole is followed. The impedance matrix of the BC-SRR is extracted from the CMA tool and the TCM-based stored energy evaluation procedure is applied. The modal stored energy of the BC-SRR is represented by the curve of normalized $(\mathrm{W_m} - \mathrm{W_e})$ against frequency of the first three modes shown in figure 5.10:

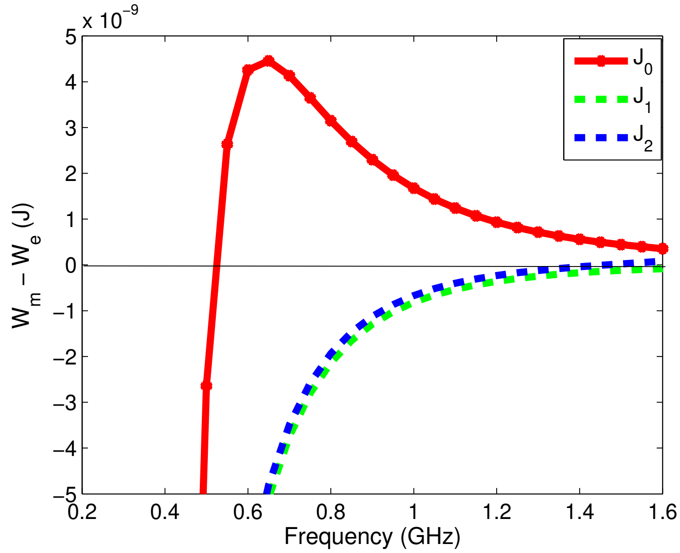

Figure 5.10: BC-SRR: Normalized ($\mathrm{W_m} - \mathrm{W_e}$) against frequency.

The dominant stored energy curve of the BC-SRR inclusion represented in figure 5.10 provide the same qualitative stored energy deduction as that of characteristic angle plot and modal surface current figure. The quantity of the dominant modal stored energy at the various frequency points can be extracted. The inclusion being a resonant inclusion has two of its modes (i.e. J_0 and J_2) crossing zero joule which indicate that the magnetic stored energy and electric stored energy are of the same quantity at the frequency point of 0.5 GHz and 1.5 GHz respectively. J_0 and J_2 in red and blue respectively are therefore the resonant modes and have no stored energy at their resonant frequencies while J_1 in green store electric energy throughout the considered frequency band between 0.2 GHz to 1.6 GHz.

Our interest is in ensuring that the magnetic stored energy of the inclusion is sufficient to compensate for the electric stored energy of the dipole, however since the inclusion is resonant and have zero joule of energy at its resonance frequency, the stored energy classification of metamaterial inclusion is used to quantify the dominant stored energy (see chapter 3). The modal weighting co-efficient of the BC-SRR is shown in figure 5.11:

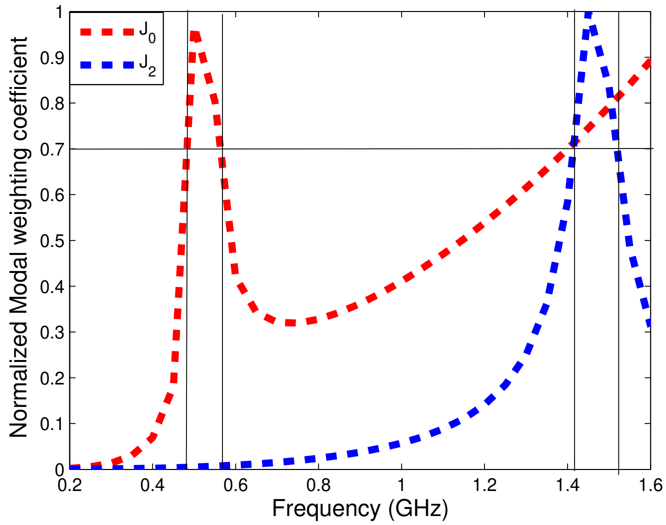

Figure 5.11: BC-SRR: Normalized modal weighting co-efficient (MWC_n) against frequency.

Applying the stored energy classification method which involve exciting the structure with a magnetic point excitation, normalizing the modal weighting co-efficient and summing up the energies at the frequency of interest between 0.48 GHz and 0.56 GHz for J_0 in red and between 1.42 GHz and 1.52 GHz for J_2 in blue as shown in figure 5.11, the modal stored energies are 4.24 x 10^{-09} J and 6.33 x 10^{-11} J for J_0 and J_2 respectively. Figure 5.11 show that J_0 have an effect on J_2 therefore taking into consideration the effect of J_0 and J_2 between 1.42 GHz and 1.52 GHz, the stored energy value is 1.40 x 10^{-09} J. The stored energies have positive values which validate the magnetic nature of the inclusion. At the frequency region of J_2 there is more magnetic energy to compensate the electric stored energy of the printed dipole compared to other frequency region.

5.4.3 Design of parasitic metamaterial ESA

The metamaterial-inspired ESA is a combination of the printed dipole and BC-SRR inclusion placed at $\frac{\lambda}{1110}$ apart. The optimized spacing between the dipole and BC-SRR as well as its configuration is based on the inter-modal coupling co-efficient. The modal surface current distribution also play a role in the configuration since it guides on the excitation of J_2 of the BC-SRR. Although the behaviour of the ESA follow the behaviour of the resonant element and has properties dominated by that of the resonant element [24], the coupling of the non-resonant element affect the behaviour such that the resonance frequency could be shifted upward or downward. For instance, using an electric inclusion on a magnetic exciter will shift the resonance upward while in our case the resonance is shifted downward. The final design and arrangement of the metamaterial-inspired ESA is shown in fig. 5.12:

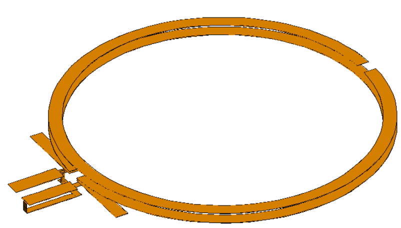

Figure 5.12: Parasitic metamaterial ESA structure.

The TCM stored energy analysis and inter-modal coupling analysis are carried out for the PEC part of the ESA structure but the final design and fabrication is done with an FR-4 substrate of ϵ_r 4.4 to provide for mechanical support. The substrate size is also extended to 0.23λ X 0.21λ to aid the drilling of nylon hole for support during measurement.

The physical behaviour of the final metamaterial-inspired ESA is demonstrated with the TCM analysis of the structure using the CMA tool.

5.4.3.1 TCM analysis

As explained in [24], the ESA antenna usually follow the behaviour of the resonant structure which is the BC-SRR inclusion. The TCM analysis of the ESA is similar to that of the BC-SRR except for the downward shift in the resonance frequency which is an effect of the coupling between the inclusion's magnetic stored energy and the dipole's electric stored energy. The TCM analysis of the ESA is represented by the characteristic angle against frequency curve of the first three modes in figure 5.13 and the modal surface current distribution diagram of the first three modes in figure 5.14:

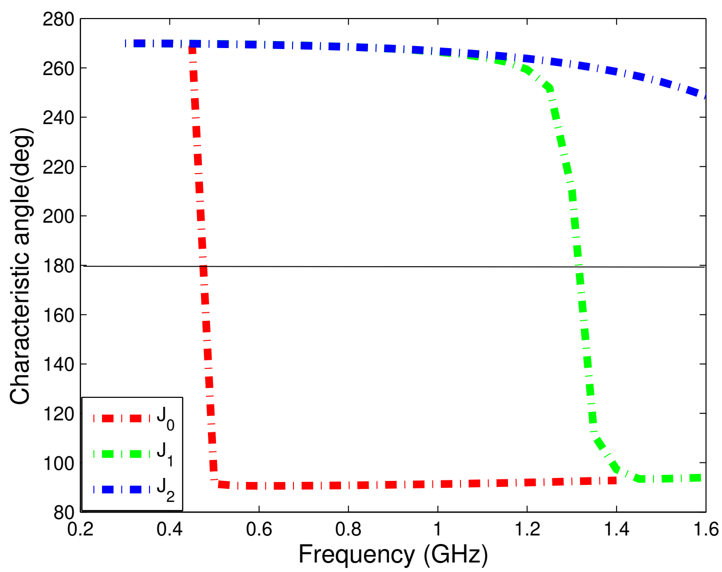

Figure 5.13: Parasitic metamaterial ESA: Characteristic angle against frequency.

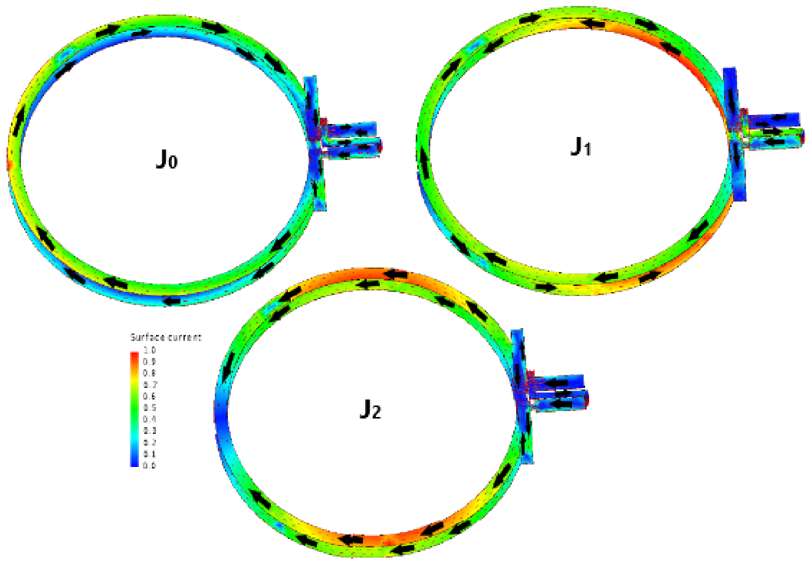

Figure 5.14: Parasitic metamaterial ESA: Modal surface current distribution.

The ESA behaviour in figure 5.13 is very similar to that of the resonant BC-SRR inclusion except for the mode switching between J_1 and J_2 due to the influence of the dipole element. It still has two resonances which are now at 0.48 GHz for J_0 in red and 1.35 GHz for J_1 in green. J_0 and J_1 are the resonant modes because their curve cross 180° of the characteristic angle plot. They go from storing dominantly electric energy to resonance. After resonance they store magnetic energy for the remaining part of the considered frequency band. J_2 in blue store electric energy throughout the considered frequency band since it has its curve above 180°.

The evaluation of the resonance frequency and the qualitative nature of the stored energy is derived using the characteristic angle plot, the same stored energy deduction can also be deduced from the modal surface current distribution of the inclusion. It also provide an insight into how the modes of the inclusion and dipole element interact. The modal surface current distribution of the antenna in figure 5.14 show the current distribution for J_0, J_1 and J_2. The current distribution of J_0 is a combination of J_2 of the dipole element and J_0 of the BC-SRR element, the current distribution of J_1 is a combination J_1 of the dipole element and J_2 of the BC-SRR element and that of J_2 is a combination of J_2 of the dipole element and J_1 of the BC-SRR element.

To quantify the modal stored energy, the modal stored energy is evaluated using the TCM-based stored energy formulation.

5.4.3.2 Stored energy analysis

This analysis is done to quantitatively evaluate the stored energy of the antenna as compared to its TCM qualitative stored energy analysis given by the characteristic angle curve and the modal surface current distribution. The impedance matrix is extracted from the CMA tool and the TCM-based stored energy evaluation procedure is applied to the impedance matrix. The modal stored energy of the antenna is represented by the curve of normalized $(\mathrm{W_m} - \mathrm{W_e})$ against frequency for the first three modes shown in figure 5.15:

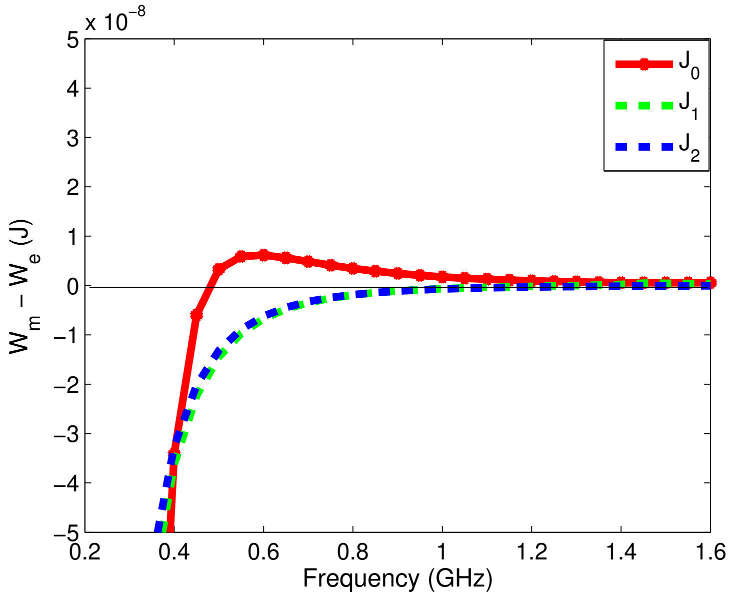

Figure 5.15: Parasitic metamaterial ESA: Modal stored energy.

The dominant stored energy curve of the antenna represented in figure 5.15 provide the same qualitative stored energy deduction as that of characteristic angle plot. The quantity of the dominant modal stored energy at the various frequency points can be extracted in this case. The antenna resonate and has two of its modes (i.e. J_0 and J_1) crossing zero joule which indicate that the magnetic stored energy and electric stored energy are of the same quantity at the frequency point of 0.48 GHz and 1.35 GHz respectively. J_0 and J_1 in red and green are the resonant modes and have no stored energy at their resonant frequencies while J_2 in blue store electric energy throughout the considered frequency band of 0.2 GHz to 1.6 GHz.

To know how the various modes couple to affect the performance of the antenna structure, the inter-modal coupling analysis is carried out.

5.4.3.3 Inter-modal coupling analysis

The inter-modal coupling provide complementary information on the description of the near-field behaviour. It account for the energy quantity needed to create a balance between the stored energy of the dipole element and that of the BC-SRR inclusion. It vary based on spacing and configuration. The inter-modal coupling of this antenna has been explained in previous chapter (see chapter 4) and it is represented by the curve of $|\mathrm{M_{ij}}|$ against frequency shown in figure 5.16:

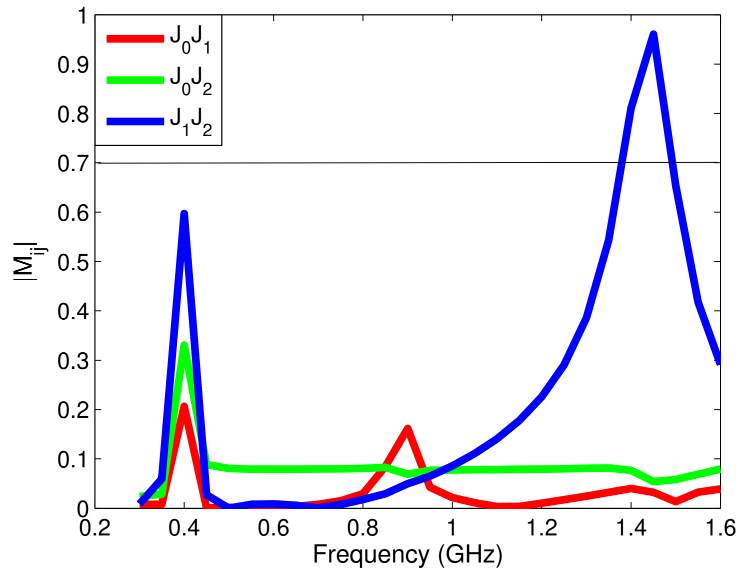

Figure 5.16: Parasitic metamaterial ESA: Inter-modal coupling.

The $|M_{ij}|$ represent the mode-mode coupling between modes. The coupling between the two resonant modes J_0 and J_1 in red are insignificant because they have a value below 0.7. For the coupling between J_0 and J_2 in green, the coupling is insufficient because it has a value below 0.7. This is because J_0 has a low modal significance despite the coupling of the dipole element to the BC-SRR inclusion. The value for the coupling between J_1 and J_2 is above 0.7 between 1.35 GHz and 1.46 GHz. The coupling at this region is strong and significant. It is the electric energy of the dipole coupling to the magnetic energy of the BC-SRR which appear after its modal resonance.

5.4.4 Measurement and result

To validate the application of the proposed method in the design of the parasitic metamaterial ESA, a prototype is fabricated and tested. A FR4 substrate of ϵ_r 4.4 is used as a mechanical support for both the the BC-SRR and the dipole. The substrate is 1.6 mm thick and used between the dipole and the balun for the exciter structure. For the BC-SRR structure, it is placed between the two circular rings. The different view of the fabricated prototype are shown in figure 5.17:

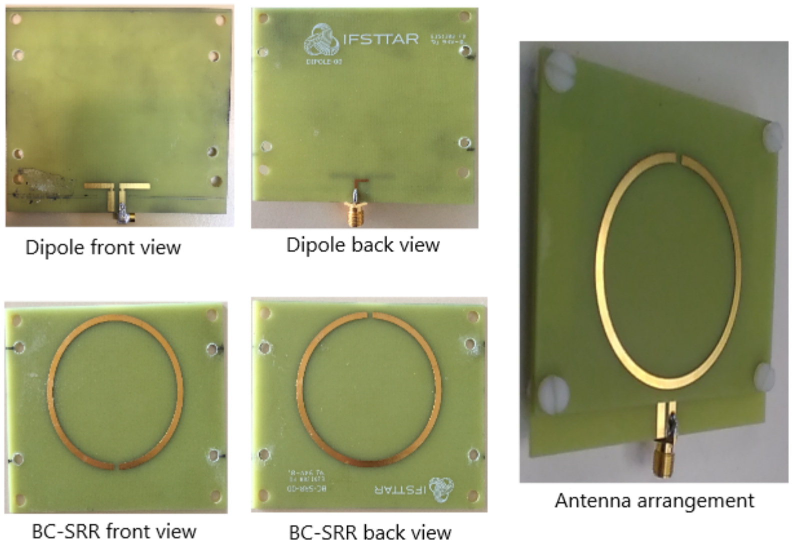

Figure 5.17: Parasitic metamaterial ESA prototype.

The full wave simulation of the antenna is carried out and the design prototype is measured with a VNA to validate the impedance matching with the use of the reflection co-efficient. The measurement setup involves soldering a 50 Ω SMA 3.5 mm port to the dipole element, calibrating the VNA between 0.2 GHz and 1.6 GHz and carrying out the measurement of the S_{11} parameter using a 50 Ω matching cable. The measurement setup for the reflection co-efficient measurement and the obtained result are shown in figure 5.18 and figure 5.19 respectively:

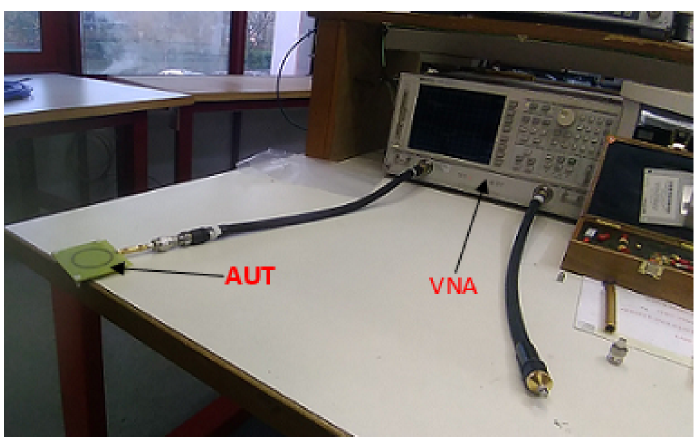

Figure 5.18: Parasitic metamaterial ESA: Reflection co-efficient measurement set-up.

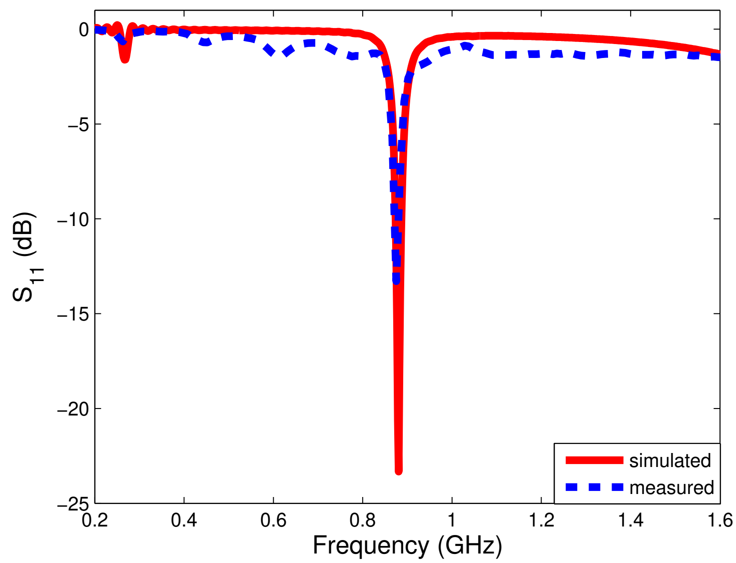

Figure 5.19: Parasitic metamaterial ESA: Reflection co-efficient.

Figure 5.19 show that both the simulated result and the measured result are in good agreement. The antenna resonate at 0.88 GHz and has a bandwidth of 14 MHz between 0.873 GHz and 0.887 GHz. The resonance frequency is shifted from its original 1.35 GHz to 0.88 GHz because of the substrate effect however the analysis still remains consistent with that of the antenna's PEC structure analysis. The far-field radiation pattern of the antenna was also obtained from the full wave simulation and compared to that of the antenna's measurement. The radiation pattern measurement was done in an anechoic chamber. The metamaterial-inspired antenna was placed as the emitting antenna while a horn antenna was used as the receiving antenna. The antenna being an electrically small antenna and susceptible to interference from its cable, a choke was used on the input cable which was isolated by covering it with an absorber. The measurement set-up for the far-field radiation pattern is shown in figure 5.20 and the obtained radiation pattern shown in 5.21

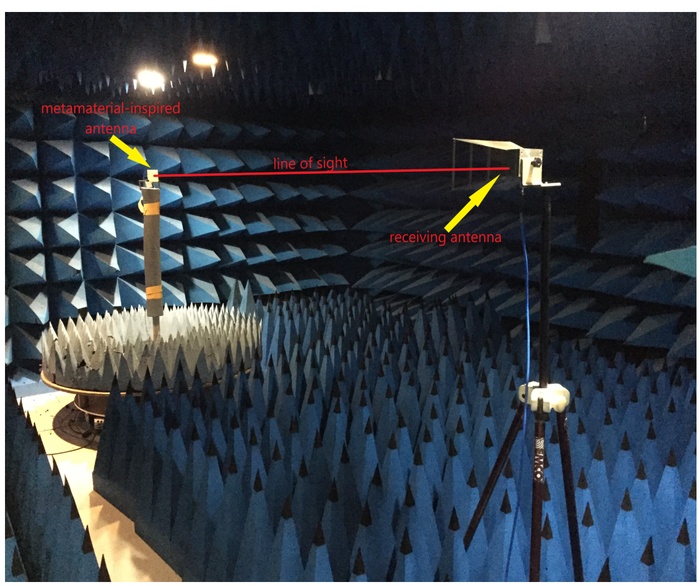

Figure 5.20: Parasitic metamaterial ESA: Radiation pattern measurement set-up.

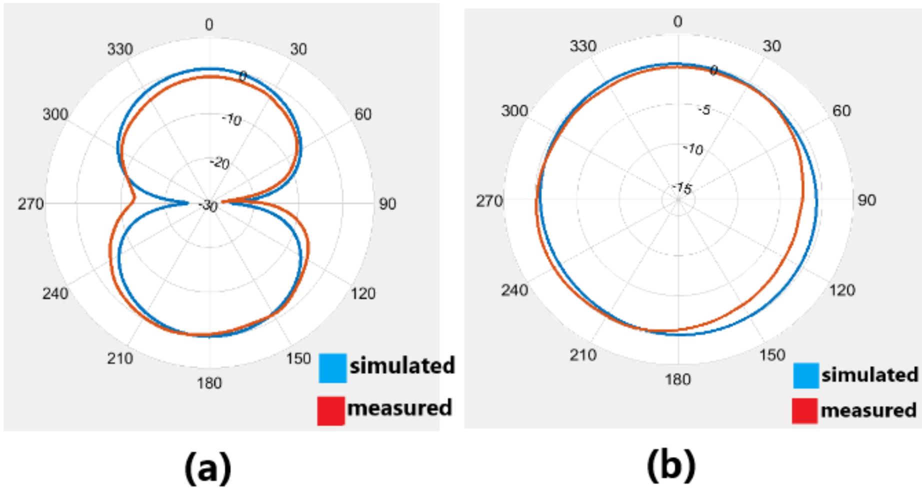

Figure 5.21: Radiation pattern of Parasitic metamaterial ESA: (a) xz-plane (b) yz-plane.

The radiation pattern of the simulated antenna and the measured prototype agree. The antenna has the pattern of a dipole antenna both in the YZ-plane and the XZ-plane partly owing to the fact that the BC-SRR inclusion also has similar radiation pattern to a dipole antenna.

5.5 Conclusion

In this chapter, the proposed systematic methodology was applied for the design of a metamaterial-inspired ESA. The choice of an inclusion to associate to an ESA is not straight forward especially when the antenna is of an arbitrary shaped hence accurately defining the near-field behaviour of the inclusion was critical to the design. The chapter began with a brief insight into the background of metamaterial-inspired ESAs, then a summary of our proposed systematic method for enhancing the performance of antenna was presented. The method involved three major steps which included; evaluation of the physical behaviour of the structure using TCM, evaluation of the radiation properties of the structure using quantitative modal stored energy evaluation and the evaluation of the scattering properties of the system using the inter-modal coupling analysis. The designed antenna consisted of a printed dipole as an exciter and a BC-SRR inclusion chosen based on its near-field behaviour. The dipole is a non-resonant structure while the inclusion is a resonant structure.

In the design process, TCM was first used to evaluate the physical behaviour of the exciter structure, then its radiation properties were evaluated using modal stored energy. An inclusion (i.e. broadside coupled split ring resonator (BC-SRR)) is selected to compensate for the stored energy of the exciter structure based on the evaluated stored energy. The BC-SRR store dominant magnetic energy in its significant modes and compensate the electric energy of the dipole structure. The scattering properties is also evaluated with inter-modal coupling to determine the configuration and spacing between the exciter and the BC-SRR. A full-wave simulation of the antenna is carried out, the antenna prototype is realized and tested to confirm the application of the proposed systematic method. The realised antenna prototype resonates at 0.88 GHz with a bandwidth of 14 MHz. The result showed that both the simulated result and the measured result are in good agreement for both the reflection co-efficient and far-field radiation pattern.

The proposed systematic method is therefore a useful tool in the design and enhancement of the performance of antennas. It helped in selecting the proper inclusion for enhancing the performance of the antenna and can be applied to complex integrated antennas. The systematic method can also be applied in the analysis of electromagnetic cloaking of passive structure.

Chapter 6

Cloaking of integrated antenna based on the proposed systematic method

6.1 Introduction

The demand for reliable antenna system with low-interference can be traced to the design of minimum scattering receiving antenna [225]. Since the discovery of metamaterial and some of its rarely found properties such as its ability to manipulate electromagnetic wave, there is a growing interest in electromagnetic invisibility and cloaking [226]. Antenna performances are affected by near-field elements [133, 227] hence electromagnetic cloaking, particularly for antenna application help to preserve the antenna performance including its impedance matching and radiation properties in complex environment. It reduce the mutual coupling between an antenna and other elements found in its vicinity such that the antenna operate almost like it would in free space [9]. In the context of antenna integration, cloaking is useful in applications where there is a limit to the degree of freedom for example, an antenna designed to be integrated in a complex platform where the platform or surrounding element cannot be modified to accommodate the antenna properties.

Antenna cloaking is either passive or active depending on the element on which the cloak is placed around. For passive cloaking, a non-radiating element in the presence of an active antenna is cloaked but for an active cloaking, the cloaked element radiate. It is important to point out that from the fundamental cloaking theory, cloaks are designed to operate outside its operating frequency band because an antenna cannot operate at its resonant frequency when cloaked at the same frequency [228]. Cloaks are generally designed with 2D and 3D metamaterials using different techniques to achieve electromagnetic invisibility of the antenna properties. Technique such as transformation optics [229] and plasmonic cloaking based on using bulk material to suppress scattering modes are among the techniques being used in literature however they have sizes which are difficult to practically realize [226]. A different technique which is based on scattering cancellation have recently been presented. This technique also known as mantle cloaking aims at reducing the scattering width of the radiating element using antiphase surface current of metasurfaces that cancels the dominant scattering mode of the radiating antenna [9, 226].

The scattering cancellation is a more desirable method for antenna cloaking despite its limitation of the size of material that can be cloaked because of its practical realization and the available analytical formulation. The surface impedance of the cloak is designed to match the radiating antenna (i.e. $Z_s = Z_s^{cloak}$) but its global application is for planar and canonical object and based on plane wave excitation [230]. In-fact antennas and elements within antenna vicinity are not limited in shape and can be arbitrary which would require new method for their cloaking implementation.

In this chapter, we investigate the application of TCM in the design of antenna cloak based on the scattering cancellation method. We show how the insight gotten from the radiating properties of a structure can help model cloak for future application. TCM have been demonstrated as a useful electromagnetic tool for designing arbitrary antenna. It provide insight on the radiation properties of a radiating element using its surface impedance hence it can provide insight into how cloaking of arbitrary structure can be done. We briefly describe a state-of-the-art for electromagnetic cloaking of antenna, the proposed systematic method for enhancing the performance of integrated antenna is applied for two cloaking scenario. First scenario which is an example found in literature [9] is cloaking of an obstacle in the presence of a radiating antenna and the second scenario is cloaking of a radiating antenna in the presence of an obstacle. The result show that in both cases, modal coupling occur which permit the antenna to radiate effectively. The insight gotten from the analysis of cloaking using the proposed systematic method provides a pathway to generalizing the method for modelling cloak for arbitrary structure.

6.2 Electromagnetic cloaking for antenna application

The concept of electromagnetic cloaking in antenna application has gained more interest since the practical realization of the mantle cloak and has found application in multi antenna environment. It is an innovative way to reduce the mutual coupling between an antenna element and other elements within its vicinity. It involve making an object invisible to an antenna electromagnetic wave [133,227] by controlling the scattering of the object to reduce its scattering cross section ($\mathrm{C_s}$) given as [230]:

$$\mathrm{C_s} = \frac{\pi}{\mathrm{K}^2} \sum_{l=1}^{\infty} \sum_{m=-l}^{l} (2l+1)[\mid \alpha_E(l,m) \mid^2 + \mid \alpha_M(l,m) \mid^2] \tag{6.1}$$

where k is the wave number; $\alpha_E(l,m)$ and $\alpha_M(l,m)$ are the multipole scattering coefficients. The electromagnetic wave emitting from the object is equal to that from the incoming wave and cancel out thus making the object invisible to the incoming wave. If you consider the scattering coefficients of long infinite cylinders with mantle cloak, they are analytically calculated by ensuring a discontinuity of the tangential magnetic field on the surface of the cloak. Mantle cloaking is not limited to cylinder as it has been implemented for elliptical, spherical and even rectangular shape. It depend on the frequency, surface impedance of the cloak, the thickness and dielectric constant of the material between the cloak and the object [230].

Research into mantle cloaking of antenna have progressed from cloaking at a single frequency with plane wave [231] to cloaking co-sited antennas [9], achieving dual-band cloaking [136] and also achieving broadband cloaking [232]. Mantle cloaking have also been implemented in antenna arrays [227] where two yagi-uda antennas operating at two different frequency bands and placed in close proximity were able to function without interfering with each other. In-fact, mantle cloaking have been implemented not only in the GHz frequency band but also in the THz frequency band where single layer graphene was used as the metasurface [233]. More complex implementation of cloaking involving the use of foster element to achieve wideband, the use of loaded metasurface for non-linear cloaking based on its power-dependency [234] and tunable cloaks for re-configurable application [235] based on changing potentials have also been demonstrated. Recently, the fundamental limitation of cloaking that prevent an antenna from being cloaked at its resonance frequency [236] was turned around in the implementation of a waveform selective cloak [228]. The cloak operate at the resonance frequency of the antenna but only switches on if the illuminating signal is a pulse wave.

One of the challenge of designing a mantle cloak is finding the optimal parameter of the unit cell that determines the cloak performance. In [237], it was shown that by properly tailoring the surface reactance of the unit cell, one can achieve reduction on the total scattering of an object. Alessio Monti and co. [9] using this principle designed a mantle cloak for co-site radio frequency antenna based on the analytical formulation given as [237, 238]:

$$\mathrm{Z_s^{rect\ TM}} = \frac{-j\eta_0(ac_0f)ln[\csc^2(\frac{1}{2a})]}{abf(1+\epsilon_r)ln[\csc^2(\frac{1}{2a})]ln[\sec^2(\frac{2}{2b})] - 2c_0^2}$$

where η_0 is the free space impedance, c_0 is the speed of light in vacuum and f is the frequency. Also, in the case of a TE incidence wave, $\mathrm{Z_s^{rect\ TM}}$ is found by interchanging a and b with w_1 and w_2.

Most mantle cloaks are designed using the available analytical model which were developed for canonical structures [225, 238] however antennas and obstacles can also be non-canonical and arbitrary where such analytical formula do not apply. Considering that scattering cancellation technique is based on the proper modelling of the metasurface surface impedance to match that of the radiating element and its implementation is in the near-field of the cloaked structure, TCM can be applied to the analysis and design of mantle cloak. TCM rely on the surface impedance of the elements and provide physical insight into the radiating behaviour of the structure therefore it becomes a good tool for investigating the interaction between antenna element and cloak. The application of TCM to the design of unit cells has already been demonstrated for planar structure [25] and it shows how metamaterial unit cells are analyzed for absorption application. TCM is the representation of the current distribution supported on a radiating surface and derived from the discretization of the surface impedance of a structure to provide physical insight into the radiation properties of the structure independent of an excitation source. TCM is applicable to non-canonical and arbitrary structure and provide information on the near-field behaviour of a structure making them very useful and desirable for cloaking application.

6.3 Description of the proposed systematic method in the analysis and design of cloak

In implementing the TCM method for cloaking, the evaluation of the three major quantities are necessary which are;

- Theory of characteristic modes: that provide insight into the physical behaviour of a structure using a modal method. It give intuitive knowledge of the resonance and qualitative stored energy of the structure thereby providing near-field information. It begin from discritizing the surface of the structure into small triangle blocks represented by the surface impedance Z given as:

$$\mathrm{Z} = \mathrm{R} + \mathrm{jX}, \tag{3.1}$$

where R is the real part and X is the imaginary part of the impedance. The impedance Z is used in solving the generalized eigenvalue equation given in equation (3.11) as:

$$[\mathrm{X}][\mathrm{I}] = \lambda_{\mathrm{n}}[\mathrm{R}][\mathrm{I}], \tag{3.11}$$

where λ_{n} are the eigenvalues of each n mode and I are the eigen-currents.

The value of λ_{n} can be large and ranges from -∞ to +∞ hence, to get an intuitive knowledge into the behaviour and resonance of the structure, the characteristic angle α_n which ranges between 90° and 270° is used. α_n is derived directly from λ_{n} as:

$$\alpha_n = 180° - \tan^{-1}\lambda_n. \tag{6.1}$$

The value of λ_{n} and α_n provide information on the modal behaviour of the structure such that with λ_{n} greater than zero and α_n less than 180°, the mode is magnetic and when λ_{n} is less than zero and α_n is greater than 180°, the mode is electric. A resonant mode has λ_{n} equal to zero and α_n equal to 180°. More information about the formulation and application of TCM can be found in the literature [12, 23].

- Quantitative stored energy evaluation: that provide precise modal stored energy value of the structure at different frequencies as compared to TCM that provide qualitative stored energy information. Its derivation, formulation and application are detailed in chapter 3 and it is evaluated using [179]:

$$\mathrm{W_m} = \frac{1}{8\omega}\mathrm{I^H X_m I}, \tag{3.14}$$

and

$$\mathrm{W_e} = \frac{1}{8\omega}\mathrm{I^H X_e I}, \tag{3.15}$$

where,

$$\mathrm{X_m} = \mathrm{X'} + \mathrm{X}, \tag{3.16}$$

$$\mathrm{X_e} = \mathrm{X'} - \mathrm{X}. \tag{3.17}$$

and

$$\mathrm{X'} = \omega\frac{\partial \mathrm{X}}{\partial\omega}. \tag{3.13}$$

ω is the angular frequency, $\mathrm{W_m}$ is the magnetic energy, $\mathrm{W_e}$ is the electric energy and X is the imaginary part of the TCM impedance matrix. The dominant stored energy is derived using $(\mathrm{W_m} - \mathrm{W_e})$ so that a positive value indicates magnetic energy and a negative value indicate electric energy. This stored energy value quantify the near-field behaviour of the structure.

- Inter-modal coupling analysis: provide information of the coupling between the antenna element, the obstacle and the cloak. It compliment the near-field information derived from the stored energy evaluation. Its derivation, formulation and application are given in chapter 4 and it is evaluated using [149]:

$$|\mathrm{M_{ij}}| = \frac{\mathrm{I_i}^{\mathrm{H}}\mathrm{X'}\mathrm{I_j}}{\sqrt{\mathrm{I_i^H X' I_i . I_j^H X' I_j}}}, \tag{4.7}$$

when $|\mathrm{M_{ij}}|$ is above 0.7, the coupling is significant enough and affect performance but when the value is below 0.7, the effect of the coupling can be neglected.

The procedure for the implementation of the evaluated quantities and how they apply to the analysis of electromagnetic cloaking is represented by the flow chart in figure 6.1:

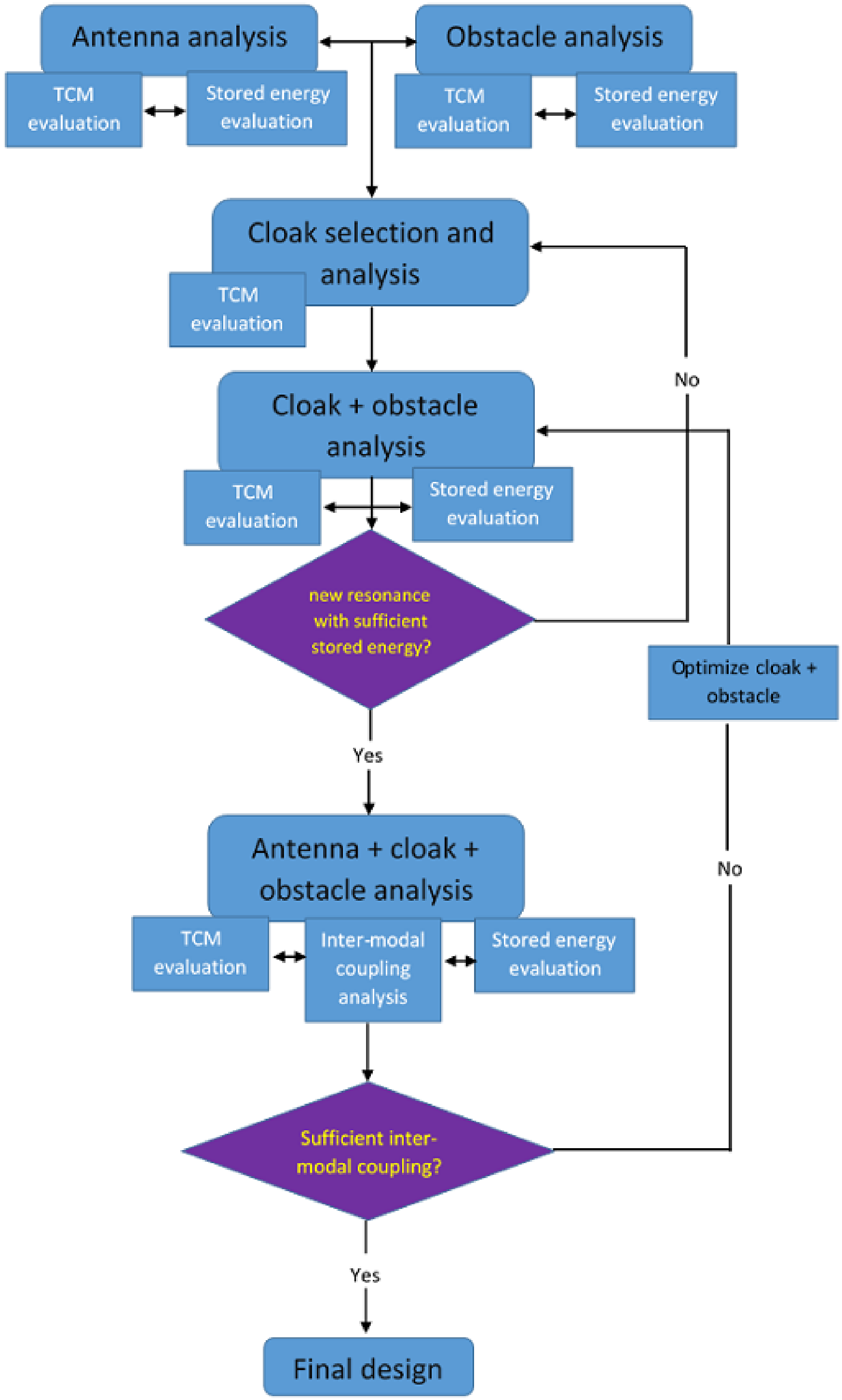

Figure 6.1: Flow chart for the implementation of proposed method to electromagnetic cloaking.

From the flow chart in figure 6.1, the antenna element and the obstacle are analyzed individually. The TCM analysis is used to provide insight of the physical behaviour of the structure and the stored energy analysis provides information on the near-field behaviour of the structure. The derived information can be used to design a cloak structure that provide a new resonance at the upper frequency band of the antenna. This resonance appear due to the interaction between the cloak and the obstacle.

If no new resonance is achieved, the cloak structure have to be modified or changed. The combination of the cloak and obstacle should also have sufficient electric energy before resonance to compensate for the magnetic energy of the antenna structure.

In the final step, the antenna element and the cloaked obstacle is analyzed as a single unit. The inter-modal coupling co-efficient is evaluated to ensure that there is sufficient coupling between the antenna and the cloaked obstacle. The coupling ensure that the antenna propagates through the obstacle hence, making it appear invisible to electromagnetic wave. In the case where the inter-modal coupling co-efficient is insufficient (i.e. below 0.7), the cloaked obstacle structure is optimized by changing the position or configuration of the cloak with respect to the obstacle.

6.4 Application of the proposed systematic method to cloak design

In this section the proposed method for enhancing the performance of antenna is used to investigate the design and implementation of mantle cloak. Two scenarios are considered, the first one which is based on an example in literature is cloaking of an LTE antenna in the presence of a UMTS antenna [9]. The second scenario is cloaking of an active antenna in the presence of an obstacle.

6.4.1 Cloaking of an obstacle in the presence of a UMTS antenna

To evaluate the application of the proposed method to electromagnetic cloaking, a cloaked UMTS antenna found in the literature [9] is investigated. This cloaking scenario is chosen rather than another example in literature because of the problem simplicity.

The UMTS antenna functions in the presence of an obstacle (an LTE antenna). The LTE antenna is not affected because of its size but the UMTS antenna is affected by the LTE antenna. Its impedance matching and radiation pattern are both affected but by the introduction of the cloak, the impedance matching and radiation pattern of the UMTS antenna is restored to almost its free space operation.

6.4.1.1 Analysis of the UMTS antenna operating alone

It is important to understand the properties of the UMTS antenna because the cloak would be designed based on its surface impedance properties. The UMTS antenna used in the design is a simple monopole antenna operating within the frequency range of 1900 MHz and 2200 MHz. The antenna and its dimension is shown in figure 6.2:

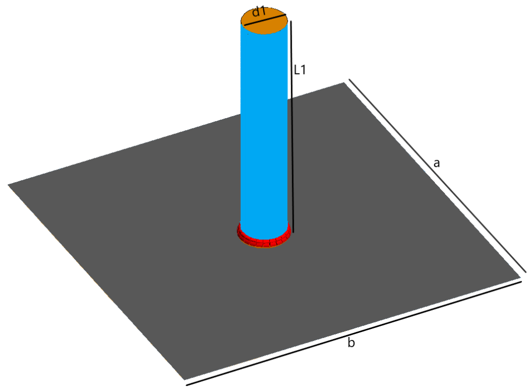

Figure 6.2: UMTS monopole antenna with dimensions: a = 307 mm, b = 307 mm, L1 = 35mm and d1 = 3 mm.

Although the length of the ground plane a by b in figure 6.2 is used in the full wave simulation, an infinite ground plane is applied in the TCM analysis to avoid computational complexity that lead to modal tracking issues. The structure is analyzed to understand its physical behaviour between the frequency range of 1.7 GHz and 2.6 GHz to cover the UMTS band. The TCM commercial software FEKO [189] was used for the modal analysis of the structure to solve the generalized eigenvalue equation and the obtained result of the TCM analysis for the structure is represented by the plot of the characteristic angle with respect to frequency for the first three modes in figure 6.3:

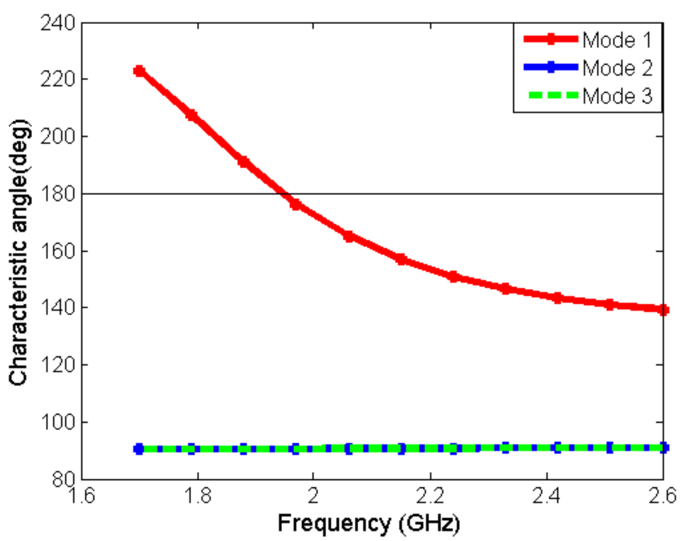

Figure 6.3: Characteristic angle against frequency of UMTS monopole antenna.

In figure 6.3, information on the resonance of the structure can be derived. Only mode 1 in red resonate at 1.95 GHz where it cross the 180°. The monopole being symmetric have mode 2 in blue and mode 3 in green as degenerate modes with the same behaviour but with a phase shift. They store magnetic energy throughout since they stay below 180° throughout the considered frequency band. Thus mode 1 is the resonant mode while mode 2 and mode 3 are high order non-radiating modes. The behaviour of this UMTS antenna can be better visualized using the modal far-field in figure 6.4:

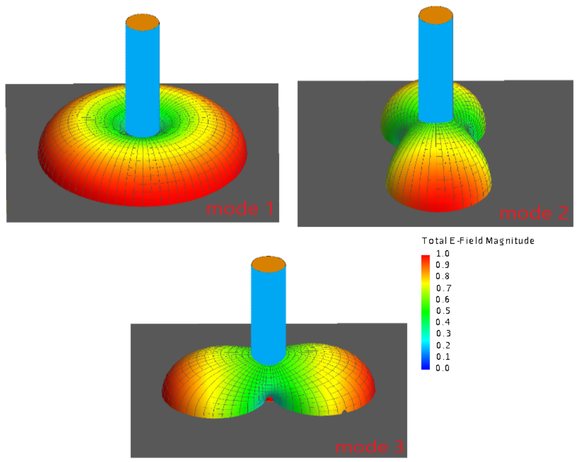

Figure 6.4: Modal far-field of UMTS monopole antenna.

The far-field in figure 6.4 show that while mode 1 has the pattern of a monopole, mode 2 and mode 3 being degenerate modes have similar far-field pattern with equal magnitude however there is a 90° shift in the position of their far-field pattern. The far-field pattern showing the 90° position shift can also be visualized with the modal surface current distribution. The far-field pattern is chosen to be displayed to allow for better understanding of the evolution of the UMTS antenna behaviour.

The modal stored energy of the UMTS antenna derived using the formulation in chapter 3 is presented with the graph of normalized $(\mathrm{W_m} - \mathrm{W_e})$ against frequency in figure 6.5.

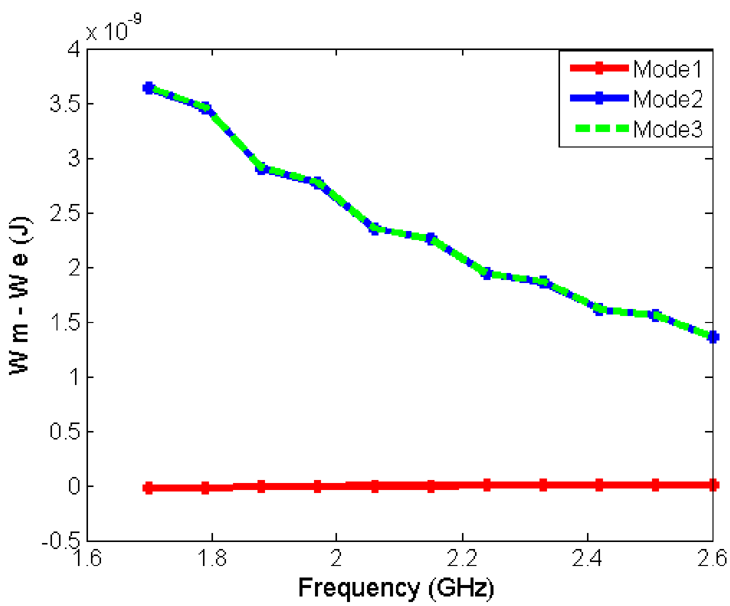

Figure 6.5: Normalized $(\mathrm{W_m} - \mathrm{W_e})$ of UMTS monopole antenna.

The curve in figure 6.5 represent the dominant modal stored energy of the UMTS antenna. Mode 1, mode 2 and mode 3 are represented by the red, blue and green curve respectively. They provide the same qualitative stored energy conclusion similar to the characteristic angle curve. The modal surface current also provide similar qualitative stored energy analysis. Mode 1 has no stored energy at 1.95 GHz which is resonance however mode 2 and mode 3 both store the same amount of dominant magnetic energy. In contrast to the characteristic angle and modal stored energy which provide qualitative stored energy information, the modal stored energy value can be extracted from the $(\mathrm{W_m} - \mathrm{W_e})$ curve.

When an obstacle is placed in the vicinity of the the UMTS antenna, the antenna encounter blocking issues which affect the impedance matching and the far-field radiation pattern.

6.4.1.2 Analysis of the UMTS antenna in the presence of an obstacle

In the design, the obstacle is placed in close proximity to the UMTS antenna is an LTE antenna operating at a much lower frequency band of 790 MHz to 860 MHz. Both antennas share the same ground plane however, the LTE antenna is not affected by the UMTS antenna because of its size [9] but the UMTS antenna is affected by the LTE antenna. The UMTS in the presence of the LTE antenna and its dimension is shown in figure 6.6:

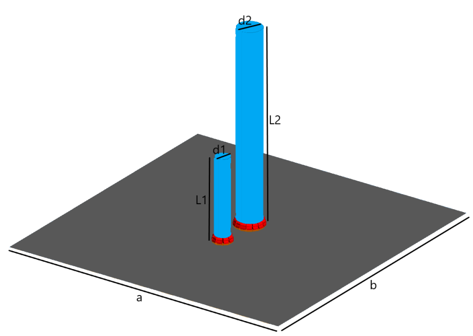

Figure 6.6: UMTS and LTE antenna on the same platform with dimensions: a = 307 mm, b = 307 mm, d1 = 3mm, d2 = 5 mm, L1 = 35 mm and L2 = 80 mm.

Just as was done for the analysis of the UMTS antenna alone, the ground plane in figure 6.6 is set to infinity for the TCM analysis. The distance between the UMTS antenna and the LTE antenna is $\frac{\lambda}{10}$ where λ is the wavelength of the UMTS antenna. The TCM analysis for understanding the physical behaviour is done between the frequency range of 1.7 GHz and 2.5 GHz to cover the UMTS band. The TCM commercial software is used for the modal analysis to solve the generalized eigenvalue equation and the obtained result of the TCM analysis for the structure is represented by the plot of the characteristic angle with respect to frequency in figure 6.7:

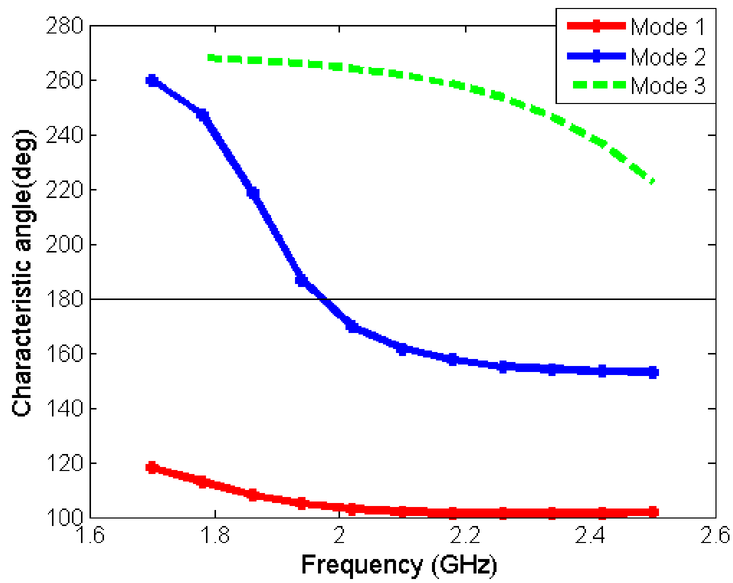

Figure 6.7: Characteristic angle against frequency of UMTS antenna in the presence of LTE antenna.

In figure 6.7, mode 2 in blue resonate at 1.95 GHz where it cross the 180° and it is the resonance is of the UMTS antenna alone. The resonant mode switch from being the fundamental mode to a higher order mode. Mode 1 in red and mode 3 in green store dominant magnetic and electric energy respectively. They are the non-resonant modes of the LTE antenna which affects the performance of the UMTS antenna. The degenerate modes of the UMTS antenna are distorted and do not appear because of the presence of the obstacle which changes the surface current distribution of the UMTS antenna. The evolution in the behaviour of this UMTS antenna in the presence of the LTE antenna can be better visualized using the modal far-field in figure 6.8:

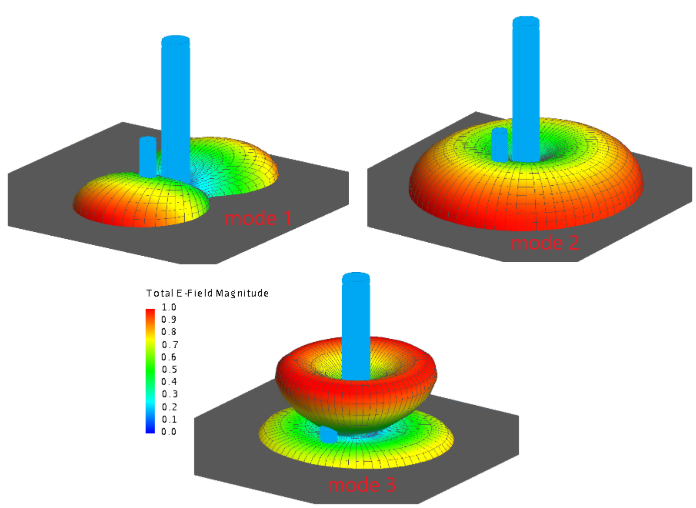

Figure 6.8: Modal far-field of the UMTS antenna in the presence of an LTE antenna.

The far-field in figure 6.8 show that mode 2 has a similar pattern to mode 1 of the UMTS antenna alone. Mode 1 and mode 3 have different pattern which can be attributed to the presence of the

LTE antenna. The far-field is chosen to be displayed instead of the surface current to allow for better understanding of the evolution of the UMTS antenna behaviour. It is clear that while the resonant mode of the UMTS antenna alone still remain despite the presence of the LTE antenna, the degenerate modes does not exist any more and the radiating properties of the UMTS antenna is affected.

The modal stored energy of the UMTS antenna in the presence of an LTE antenna, derived using the formulation in chapter 3 is presented with the graph of normalized $(\mathrm{W_m} - \mathrm{W_e})$ against frequency in figure 6.9.

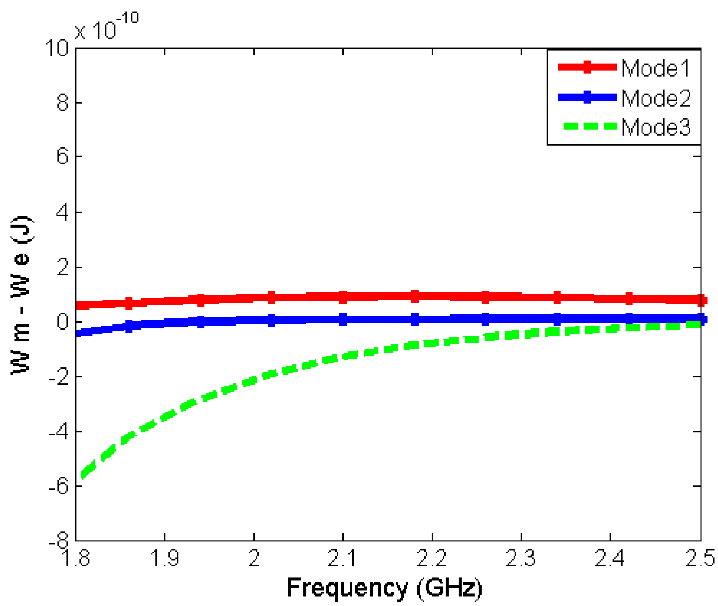

Figure 6.9: Normalized $(\mathrm{W_m} - \mathrm{W_e})$ of the UMTS antenna in the presence of an LTE antenna.

The curve in figure 6.9 represent the dominant modal stored energy of the UMTS antenna. Mode 1, mode 2 and mode 3 are represented by the red, blue and green curve respectively. They provide the same qualitative stored energy conclusion similar to the characteristic angle curve. The modal surface current can also provide similar qualitative stored energy analysis. Mode 2 has no stored energy at 1.95 GHz which is resonance however, mode 1 and mode 3 both store energy. In comparison to the behaviour of the UMTS antenna alone where among the three modes, no mode store electric energy throughout the considered frequency band, the introduction of the obstacle causes mode 3 to store electric energy because of the increased electric path of the current while mode 1 store magnetic energy. In contrast to the characteristic angle and modal stored energy which provide only qualitative stored energy information, the modal stored energy values can be extracted from the $\mathrm{W_m} - \mathrm{W_e}$ curve.

6.4.1.3 Analysis of the cloak structure alone

According to the literature [9], the cloak structure is designed based on the surface impedance of the UMTS antenna. It consist of three hollow cylinders spaced equally and placed on a teflon substrate of ϵ_r 4.4. The cloak structure and its dimensions are shown in figure 6.10:

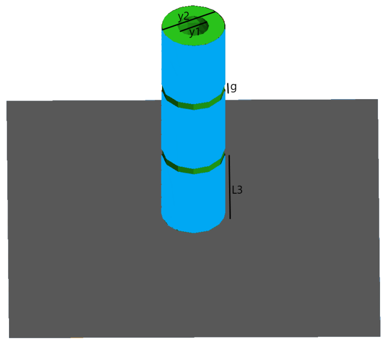

Figure 6.10: Cloak structure with dimensions: y1 = 5 mm, y2 = 10 mm, g = 2.6 mm and L3 = 24.07 mm.

The cloak structure is analyzed using infinite ground plane to avoid computational complexity and ensure consistency with the UMTS design. It is analyzed to understand its physical behaviour between the frequency range of 1.7 GHz and 2.1 GHz. This frequency range was chosen in order to cover the known resonance of the UMTS antenna of 1.95 GHz. The TCM commercial software was used for the modal analysis of the structure to solve the generalized eigenvalue equation and the obtained result of the TCM analysis for the structure is represented by the plot of the characteristic angle with respect to frequency in figure 6.11:

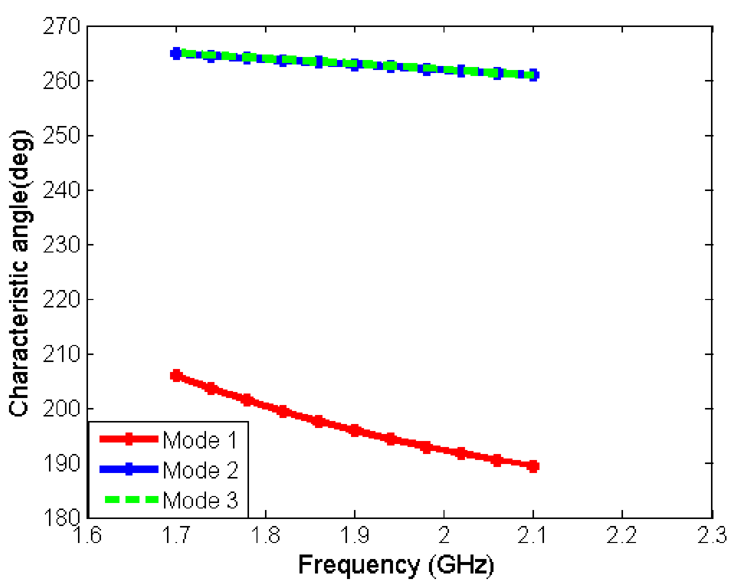

Figure 6.11: Characteristic angle against frequency of cloak structure.

In figure 6.11, none of the mode cross 180° hence no mode resonate. Mode 1 in red, mode 2 in blue and mode 3 in green all store energy. Mode 1, mode 2 and mode 3 all store electric energy throughout since they stay above 180° throughout the considered frequency band. While mode 1 is a mode closer to resonance, mode 2 and mode 3 are degenerate modes having the same behaviour but with a phase shift because of their structural symmetry. The behaviour of this UMTS antenna can be better visualized using the modal far-field in figure 6.12:

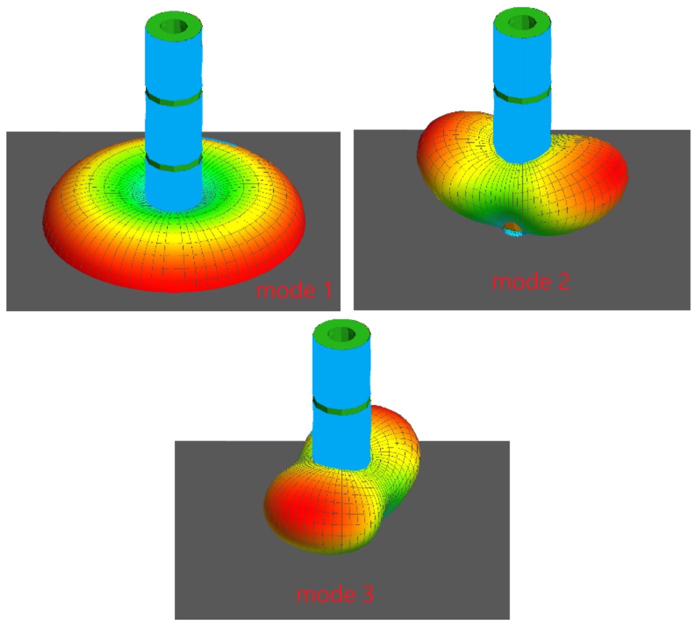

Figure 6.12: Modal far-field of cloak structure.

The far-field in figure 6.12 show that while mode 1 has the pattern of a monopole, mode 2 and mode 3 being degenerate modes have similar pattern with equal magnitude however there is a 90° shift in the position of the far field. The far-field pattern of mode 1 is similar to that of the UMTS antenna's mode 1 while mode 2 and mode 3 pattern differ to that of the UMTS antenna although, they are degenerate modes just like the UMTS antenna. The far-field pattern showing the 90° position shift can also be visualized with the modal surface current distribution. The far-field however is chosen to be displayed to allow for better understanding of the effect of the cloak on the UMTS antenna in the presence of the LTE antenna.

The modal stored energy of the cloak structure derived using the formulation in chapter 3 is presented with the graph of normalized ($W_m - W_e$) against frequency in figure 6.13.

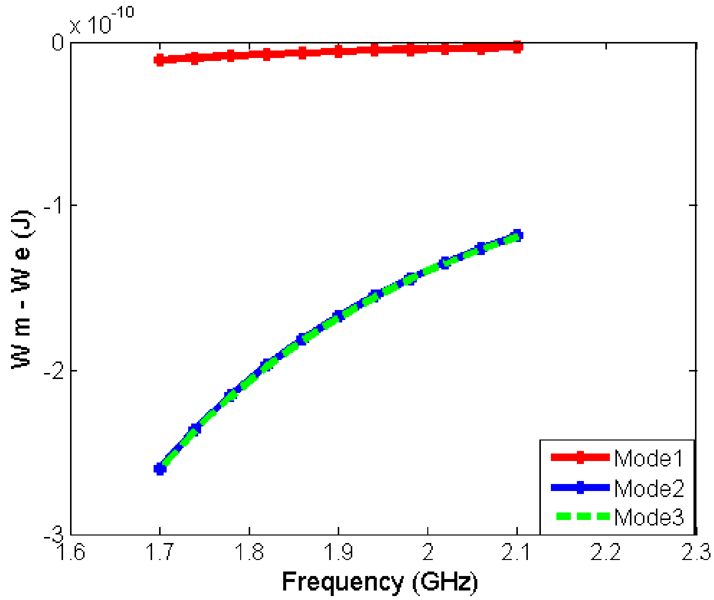

Figure 6.13: Normalized ($\mathrm{W_m - W_e}$) of cloak structure.

The curve in figure 6.13 represent the dominant modal stored energy of the cloak structure. Mode 1, mode 2 and mode 3 are represented by the red, blue and green curve respectively. They provide the same qualitative stored energy conclusion similar to the characteristic angle curve. The modal surface current can also provide similar qualitative stored energy analysis. Mode 1, mode 2 and mode 3 all store electric energy however, mode 2 and mode 3 are degenerate modes and store the same amount of dominant electric energy. Mode 1 on the other hand stores lesser energy and is closer to resonance. In contrast to the characteristic angle and modal stored energy which provide only qualitative stored energy information, the modal stored energy value can be extracted from the $\mathrm{W_m - W_e}$ curve.

It can be quickly inferred that Mode 1 of the UMTS antenna alone which store magnetic energy after resonance will be compensated by the electric energy of the cloak structure which is closer to resonance and store electric energy after that same frequency point of 1.95 GHz. Also, while the UMTS antenna has two degenerate modes storing magnetic energy, the cloak structure has two degenerate modes storing electric energy.

Therefore, in the use of the TCM stored energy method for cloak design, the choice of the cloak should have compensating energy (i.e. if the antenna has non-resonating modes storing magnetic energy, the cloak should have modes storing electric energy at the same frequency region and vice versa).

Next, we consider the analysis of the UMTS in the presence of the LTE antenna after the introduction of the cloak on the LTE antenna.

6.4.1.4 Analysis of the UMTS antenna in the presence of the cloaked obstacle

The cloak structure is placed on the obstacle which is the LTE antenna. The aim of the cloak on the LTE antenna is to prevent the LTE antenna from affecting the performance of the UMTS antenna while ensuring that the LTE antenna still functions as expected. The configuration of the UMTS antenna in the presence of the cloaked LTE antenna is shown in figure 6.14:

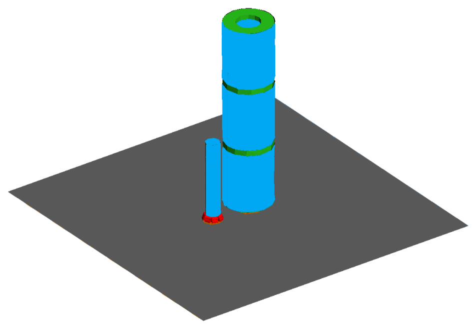

Figure 6.14: UMTS antenna in the presence of a cloaked LTE antenna.

All the conditions with regard to the ground plane are applied in this scenario as well. The analysis is done within the frequency range of 1.75GHz to 2.1 GHz to cover the known resonance of the UMTS antenna of 1.95 GHz. The cloak structure on the LTE antenna affects the physical behaviour of the cloak structure which is analyzed using TCM. The TCM commercial software is used for the modal analysis of the structure to solve the generalized eigenvalue equation and the obtained result of the TCM analysis for the structure is represented by the plot of the characteristic angle with respect to frequency in figure 6.15:

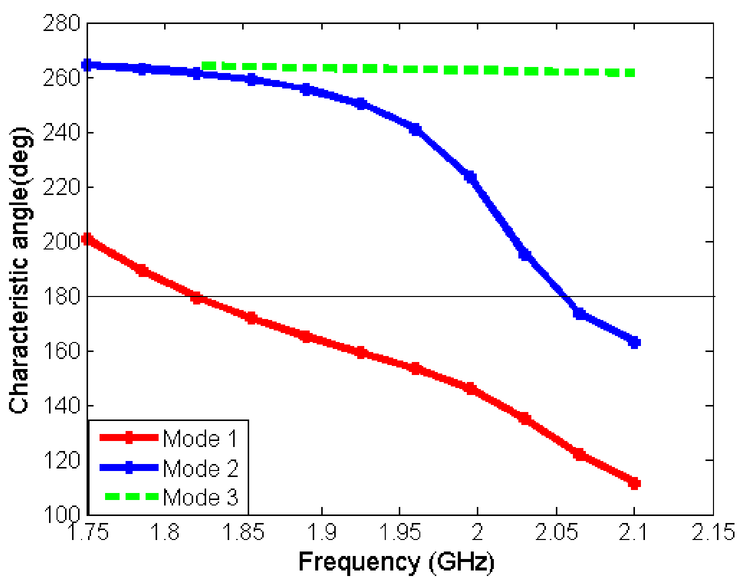

Figure 6.15: Characteristic angle against frequency of cloak structure.

In figure 6.15, mode 1 in red and mode 2 in blue resonate at 1.84 GHz and 2.06 GHz respectively because they cross 180° at those frequency points. They go from storing electric energy to resonating and storing magnetic energy. Mode 3 in green store electric energy throughout the considered frequency band since it stay above 180°. The introduction of the cloaked obstacle introduce a new resonant mode while the fundamental mode which is of the UMTS antenna also become resonant. The shift in the resonant frequency of the fundamental mode from that of the UMTS antenna alone is due to the coupling with the cloaked obstacle. To understand how the different modes relate to the different structure, the modal far-fields are considered in figure 6.16:

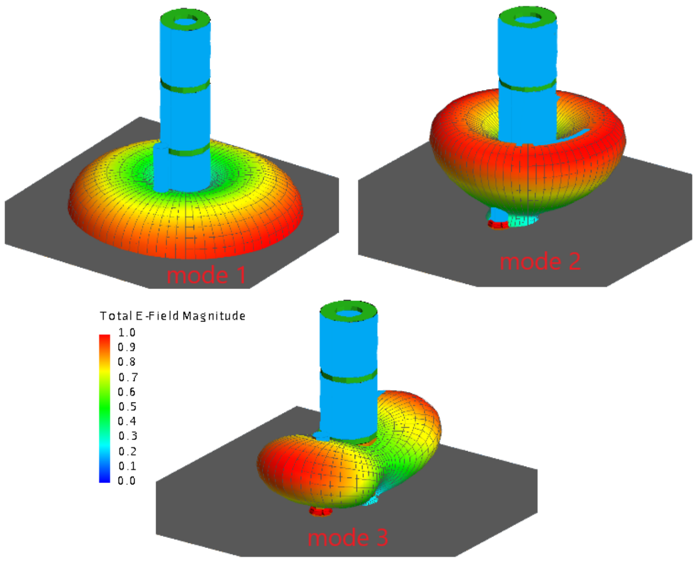

Figure 6.16: Modal far-field of cloak structure.

The far-field in figure 6.16 help to understand the evolution of the behaviour of the UMTS antenna and how the different modes relate to the different structures. Mode 1 have the pattern of a monopole similar to the UMTS antenna alone however the frequency is shifted to 1.84 GHz because of the coupling to the LTE antenna and the cloak structure. Mode 2 have a pattern which can be attributed to the combination of the LTE antenna and cloak structure. This combination cause a resonance at 2.06 GHz. Mode 3 have a similar pattern to one of the degenerate modes of the cloak structure alone. Therefore mode 1 is the mode of the UMTS antenna, mode 2 is the mode of the LTE antenna when the cloak is placed around it and mode 3 is the mode of the cloak structure.

To get more clarity, the modal stored energy of the cloak structure derived using the formulation in chapter 3 is presented with the graph of normalized $(\mathrm{W_m} - \mathrm{W_e})$ against frequency in figure 6.17.

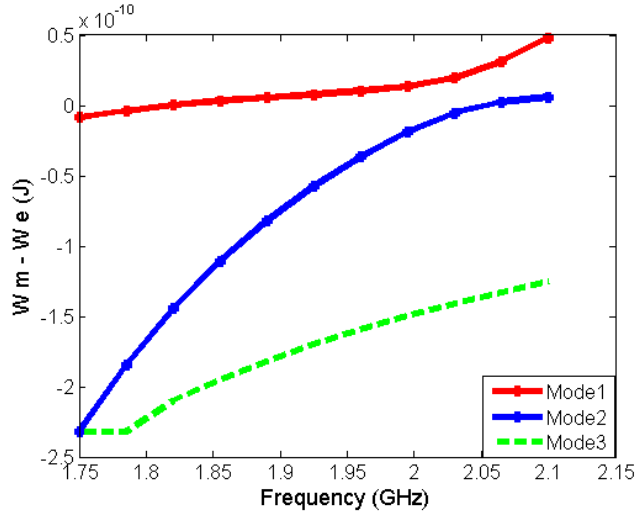

Figure 6.17: Normalized $(\mathrm{W_m - W_e})$ of cloak structure.

The curve in figure 6.17 represent the dominant modal stored energy of the configuration that have the UMTS antenna in the presence of a cloaked LTE antenna . Mode 1, mode 2 and mode 3 are represented by the red, blue and green curve respectively. They provide the same qualitative stored energy conclusion similar to the characteristic angle curve. The modal surface current can also provide similar qualitative stored energy analysis. Mode 1 and mode 2 are resonating modes which store electric energy before resonance and magnetic energy after resonance. The magnetic energy of mode 1 after its resonance at 1.84 GHz couples significantly to the electric energy of mode 2 before its resonance at 2.06 GHz. On the other hand, mode 3 stores electric energy throughout the considered frequency band. In contrast to the characteristic angle and modal stored energy which provide only qualitative stored energy information, the modal stored energy value can be extracted from the $\mathrm{W_m - W_e}$ curve.

The compensation of energy between mode 1 and mode 2 can be observed by the inter-modal coupling analysis. The $|\mathrm{M_{ij}}|$ is evaluated using the formulation given in chapter 4 and the result is shown in figure 6.18:

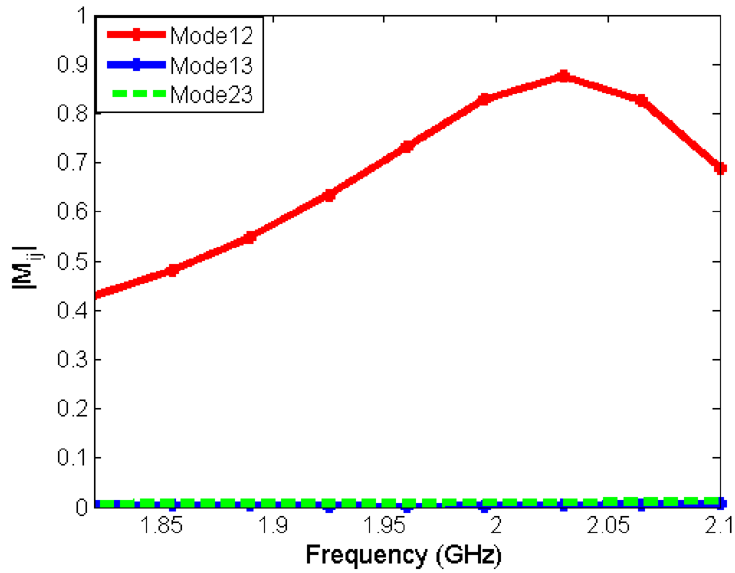

Figure 6.18: $|M_{ij}|$ of cloak structure.

The result displayed in figure 6.18 show how the different modes relate with each other. The coupling between mode 1 and mode 2 shown in red has the highest coupling since the coupling is significant where $|M_{ij}|$ is above 0.7. Therefore the coupling is significant between 1.95 GHz and 2.1 GHz which are within the UMTS frequency band. The coupling between the other modes (i.e mode 1 and mode 3 in blue and mode 2 and mode 3 in green are insignificant since their $|M_{ij}|$ value is zero.

One can conclude that the new resonant mode which couple with the resonance of the UMTS antenna is responsible for enhancing the performance of the UMTS antenna to the point that its performance are almost similar to its free space performance. The magnetic energy of the UMTS antenna and the electric energy of the cloaked LTE antenna interact to eliminate stored energy within the frequency band of 1.95 GHz and 2.1 GHz hence causing the UMTS antenna to resonate and perform almost like its free space operation.

6.4.1.5 Results

Further insight into the effect of the cloak structure is observed by comparing the reflection co-efficient of the UMTS antenna when it operate alone to the scenario when it operate in the presence of an LTE antenna and also in the presence of a cloaked LTE antenna. The radiation far-field pattern also provide insight into the functioning of the UMTS antenna in the different scenarios.

The structure is analyzed using the full wave simulation and the result of the reflection co-efficient of the different scenario is presented in figure 6.19:

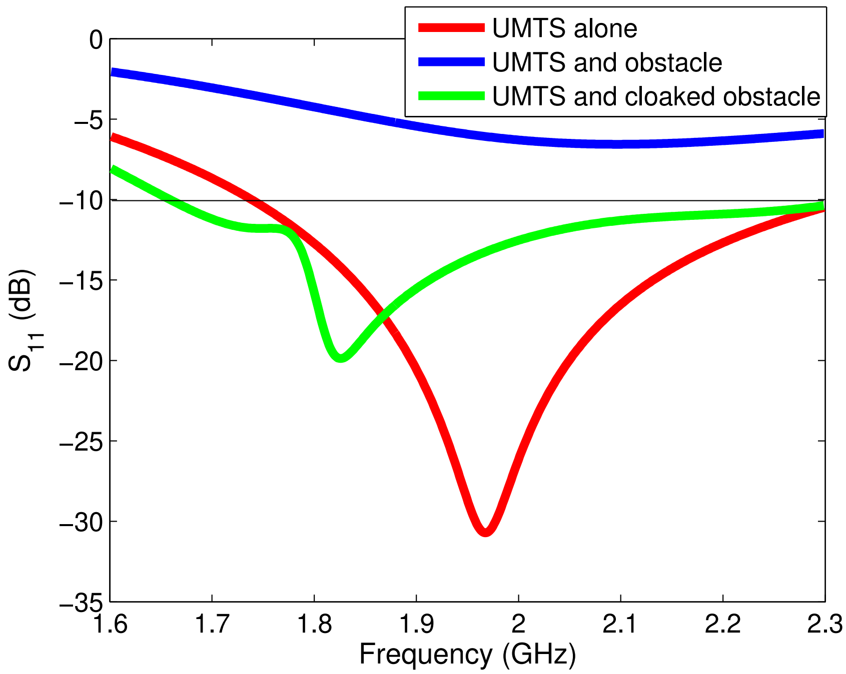

Figure 6.19: Reflection co-efficient results of the different scenario of the UMTS antenna.

The result in figure 6.19 confirm that the cloak restore the performance of the UMTS antenna. When the LTE is introduced in the presence of the cloak, the antenna is mismatched. The introduction of the cloak hide the LTE antenna such that the cloak operates almost like it is in free space. This same conclusion can also be derived using the radiation pattern parameter shown in figure 6.20:

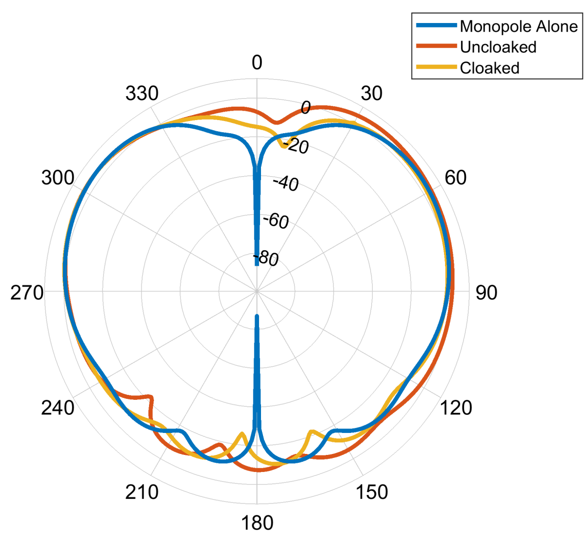

Figure 6.20: Radiation pattern results of the different scenario of the UMTS antenna.

The result in figure 6.20 also show that the introduction of the cloak hide the LTE antenna such that the cloak operates almost like it is in free space. The radiation pattern is restored to the the case of the UMTS operating in free space as compared to the blockage issue faced by the introduction of the uncloaked LTE antenna in the presence of the UMTS antenna.

6.4.2 Cloaking of an active antenna in the presence of an obstacle

Active cloaking of an antenna involve cloaking a radiating antenna. In literature, active cloaking is often implemented on two close-by antennas when both of them operate at close frequency range [226, 227] however because of the physical limitation to cloaking, the cloak is designed outside the operating frequency of the antenna structure because according to the fundamental theory of cloaking and the energy conservation principle, an antenna cannot transmit or receive electromagnetic wave if it is cloaked at its own resonant resonant frequency [236]. Although in [228], the cloaking of an antenna at its operating frequency was achieved where the cloak is only switched on when the incoming signal is a pulse signal.In an application where the properties of the obstacle in an antenna vicinity is known but the degree of freedom for modification is only permitted on the already existing antenna, one can follow a similar principle of designing metamaterial-inspired antenna and the radiating properties of the obstacle can be exploited by a cloaked antenna to enhance the performance of the antenna.

In this section, we investigate a scenario of two rectangular strip dipole antenna. One of the antenna radiate while the other antenna which is the obstacle is not excited and therefore does not radiate. This scenario is an inversion of the passive cloaking where instead of the cloak placed around the obstacle, it is rather placed around the antenna. The obstacle is also designed such that if excited its resonance frequency is close to that of the radiating antenna so that its radiating properties can be exploited as compared to the case of passive cloaking where the frequency of operation of both the antenna and the obstacle are far apart [9].

6.4.2.1 Analysis of the dipole antenna operating alone

It is important to understand the properties of the active antenna to get a clearer understanding of how the cloak affect its performance. The radiation properties of the antenna help in providing information for the optimization of the cloak design. The antenna used is a strip dipole, fed at the centre with a discrete port and resonating at 3.45 GHz. The antenna and its dimension is shown in figure 6.21:

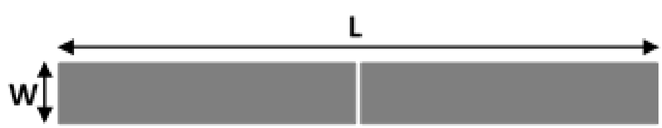

Figure 6.21: Active dipole antenna with dimensions: L = 38.8 mm, W = 4 mm.

The structure is analyzed to understand its physical behaviour between the frequency range of 2 GHz and 4 GHz. The TCM commercial software FEKO [189] is used for the modal analysis of the structure to solve the generalized eigenvalue equation and the obtained result of the TCM analysis for the structure is represented by the plot of the characteristic angle with respect to frequency for the first four modes in figure 6.22:

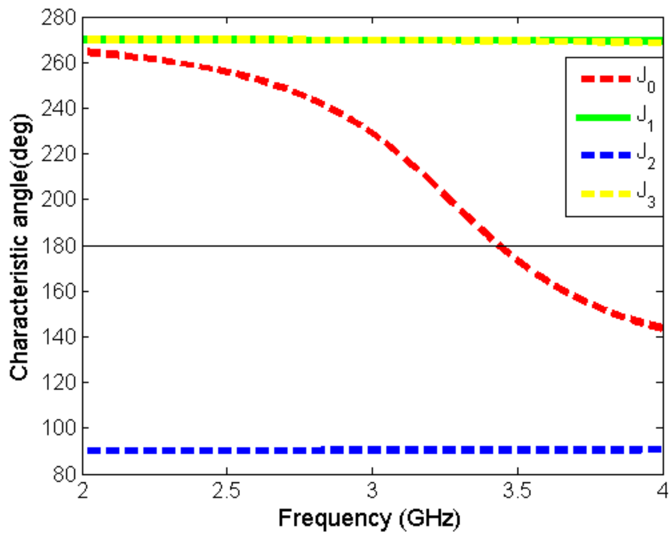

Figure 6.22: Characteristic angle against frequency of active dipole antenna.

In figure 6.22, information on the resonance of the structure can be derived. Only J_0 in red resonate at 3.5 GHz where it cross the 180°. J_1 in green and J_3 in yellow both store electric energy since they remain above 180° throughout the considered frequency band. J_2 in blue store magnetic energy throughout since it stay below 180° throughout the considered frequency band. Therefore J_0 is the resonant mode while J_1, J_2 and J_3 are high order non-radiating modes. The behaviour of this antenna can be better visualized using the modal far-field in figure 6.23:

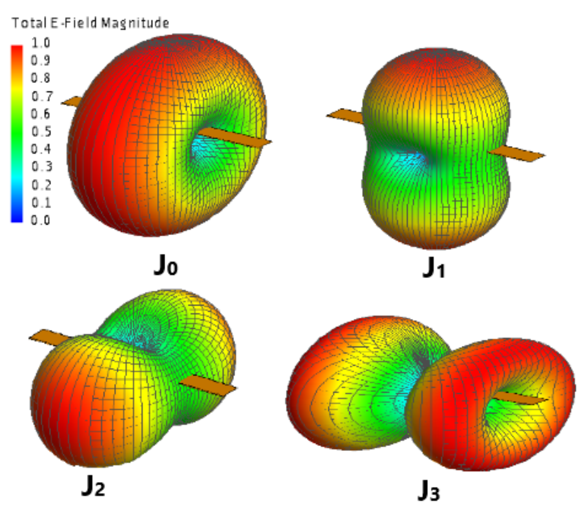

Figure 6.23: Modal far-field of active dipole antenna.

The far-field in figure 6.23 show that while J_0 have the pattern of a dipole, J_1, J_2 and J_3 have different far-field patterns which will help us understand the evolution of the radiation properties of the antenna when an obstacle or a cloak is placed within its vicinity. Since J_0 is the resonant mode, its far-field radiation pattern will be the dominant behaviour of the antenna. The near-field behaviour of the structure using modal stored energy also provide insight into the properties of the antenna.

The modal stored energy of the active antenna derived using the formulation in chapter 3 is presented with the graph of normalized $(\mathrm{W_m} - \mathrm{W_e})$ against frequency in figure 6.24.

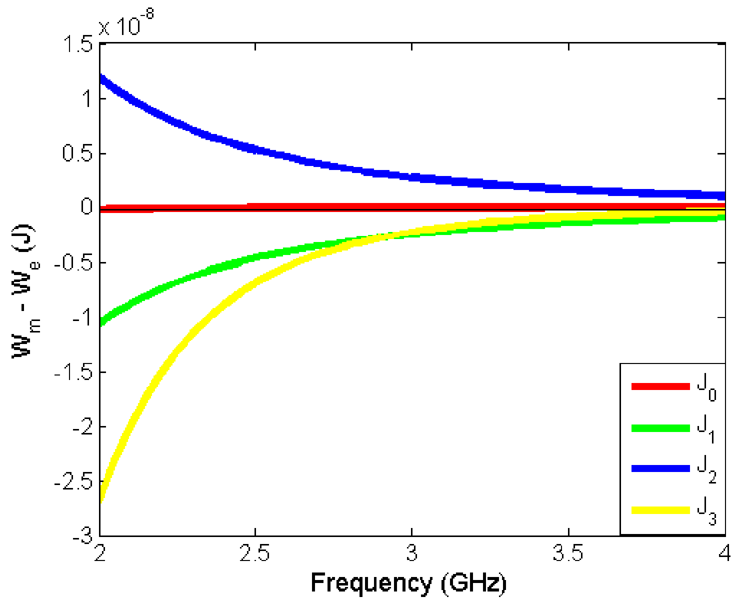

Figure 6.24: Normalized $(\mathrm{W_m} - \mathrm{W_e})$ of active dipole antenna.

The curve in figure 6.24 represent the dominant modal stored energy of the dipole antenna. J_0, J_1, J_2 and J_3 are represented by the red, green, blue and yellow curve respectively. They provide the same qualitative stored energy conclusion similar to the characteristic angle curve. J_0 have no stored energy at 3.5 GHz which is resonance however J_1 and J_3 both store electric energy while J_2 stores magnetic energy. In contrast to the stored energy information derived from the characteristic angle curve which are qualitative, the quantitative modal stored energy value can be extracted from the $(\mathrm{W_m} - \mathrm{W_e})$ curve.

When an obstacle is placed in the vicinity of the the dipole antenna, the antenna encounter blocking issues which affect the impedance matching and the far-field radiation pattern.

6.4.2.2 Analysis of the active dipole antenna in the presence of an obstacle

In the design, the obstacle placed in close proximity to the active dipole antenna is a passive dipole structure with no excitation. The use of excitation on the passive dipole will further deteriorate the performance of the active antenna making it difficult to recover the radiation properties. The aim is to excite the obstacle as a parasitic element to exploit its radiation properties. The active antenna in the presence of the obstacle and its dimension is shown in figure 6.25:

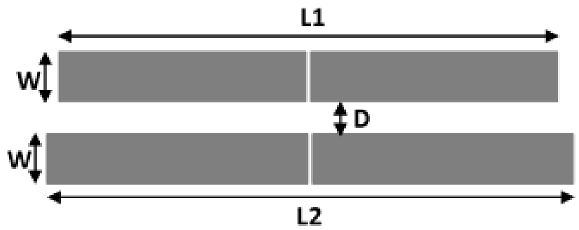

Figure 6.25: Active dipole in the presence of obstacle: L1 = 38.8 mm, W = 4 mm, L2 = 41.4 mm.

Just as was done for the analysis of the active antenna alone, the antenna in the presence of the obstacle is analyzed. The distance D between the active dipole antenna and the passive dipole structure is $\frac{\lambda}{10}$ where λ is the wavelength of the antenna. The TCM analysis for understanding the physical behaviour is done between the frequency range of 2 GHz and 4 GHz to cover similar frequency band for the active antenna analysis. The TCM commercial software is used for the modal analysis to solve the generalized eigenvalue equation and the obtained result of the TCM analysis for the structure is represented by the plot of the characteristic angle with respect to frequency in figure 6.26:

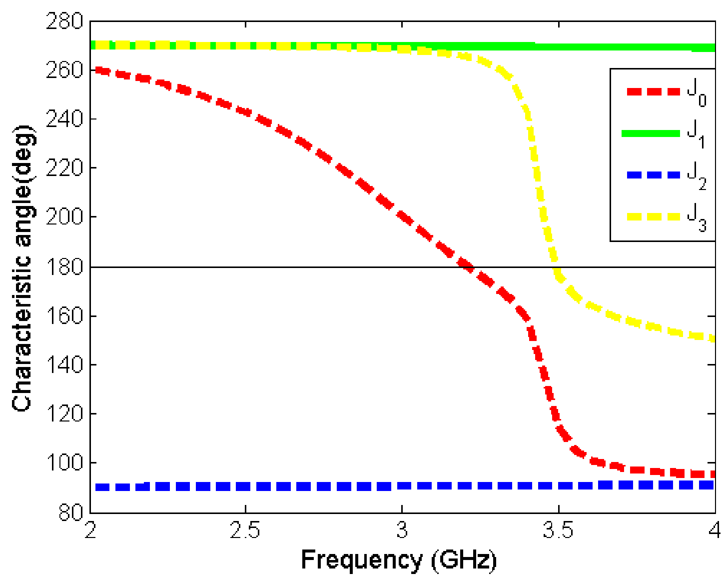

Figure 6.26: Characteristic angle against frequency of active antenna in the presence of an obstacle.

In figure 6.26, J_0 and J_3 in red and yellow resonate at 3.35 GHz and 3.56 GHz respectively because they cross the 180° at this frequency point. J_3 is the mode of the active antenna shifted up to a higher frequency because of the coupling to the obstacle and J_0 is the resonant mode of the obstacle. J_1 in green store electric energy and J_2 in blue store magnetic energy throughout the considered frequency band. Since the obstacle is a resonant structure and would radiate, J_0 and J_3 having similar radiation pattern will couple together and distort the radiation properties of the active dipole antenna hence the blocking issue. The obstacle having its resonant mode as the fundamental mode also mean that its radiation properties will be dominant. The behaviour of the active dipole antenna in the presence of the passive dipole obstacle can be better visualized using the modal far-field in figure 6.27:

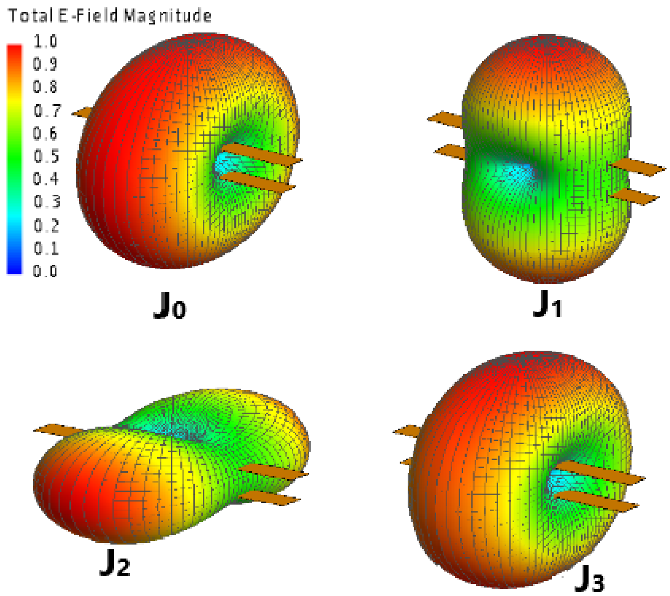

Figure 6.27: Modal far-field of the active antenna in the presence of a passive dipole structure.

The far-field in figure 6.27 show that J_0 and J_3 have similar pattern which is of a dipole antenna. J_1 and J_2 have pattern similar to that of J_1 and J_2 of the active antenna alone. The obstacle affect the active antenna and appear as J_3 hence the similarity in the radiation pattern of J_0 and J_3 indicate that both structure will radiate simultaneously when excited creating a highly directive radiation pattern rather than the omini-directional pattern of a dipole. The far-field is chosen to be displayed instead of the surface current to allow for better understanding of the evolution of the antenna radiation properties. It is clear that while the resonant mode of the active antenna alone remain, a new resonance which can be attributed to the obstacle also appear within the considered frequency band. The modal stored energy could also provide quantitative information on the near-field behaviour of the structure.

The modal stored energy of the active dipole antenna in the presence of the passive dipole structure is derived using the formulation in chapter 3 and it is presented with the graph of normalized $(\mathrm{W_m} - \mathrm{W_e})$ against frequency in figure 6.28.

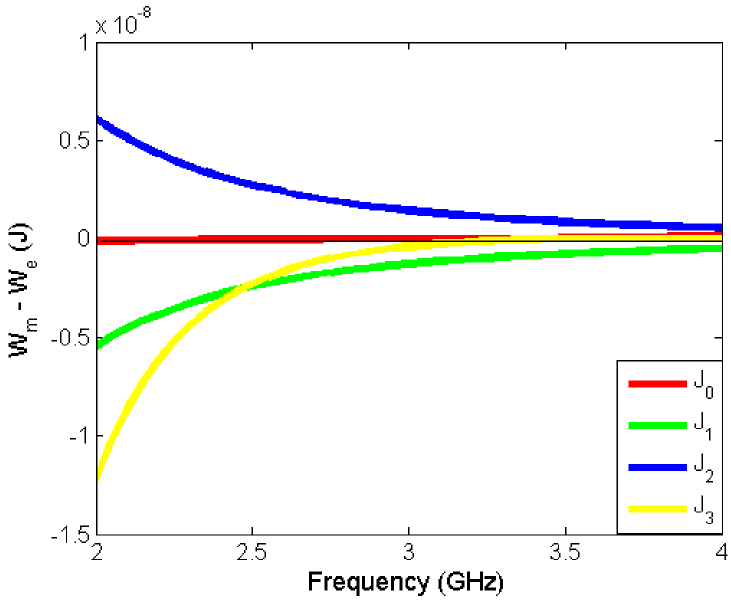

Figure 6.28: Normalized ($\mathrm{W_m - W_e}$) of the active antenna in the presence of an obstacle.

The curve in figure 6.28 represent the quantitative modal stored energy of the active dipole antenna in the presence of the passive dipole structure. J_0, J_1, J_2 and J_3 are represented by the red, green, blue and yellow curve respectively. They provide the same qualitative stored energy conclusion similar to the characteristic angle curve. J_1 and J_3 have no stored energy at 3.35 GHz and 3.56 GHz respectively because they are the resonance however J_1 store electric energy and J_2 store magnetic energy throughout the considered frequency band. In contrast to the characteristic angle that give qualitative modal stored energy insight, the modal stored energy value can be extracted from the $\mathrm{W_m - W_e}$ curve.

6.4.2.3 Analysis of the cloaked antenna structure

Generally, the design of mantle cloaks are based on the surface impedance of the antenna and the cloaks are placed around the obstacle [9] however in this case, the cloak is going to be placed around the active antenna and designed based on the surface impedance properties of the passive dipole structure. The cloak used is based on the design found in [226] and it is optimized to fit our application. It consist of three vertical strip lines placed on a dielectric substrate of ϵ_r 11. The cloaked antenna structure and its dimension is shown in figure 6.29:

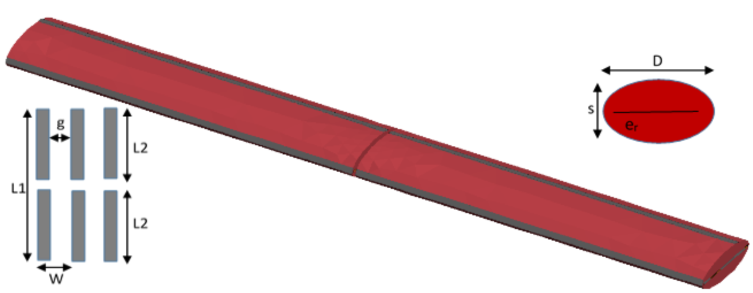

Figure 6.29: Cloaked dipole antenna with dimensions: L1 = 38.8 mm, L2 = 19.4 mm, g = 2.99 mm, W = 3.289 mm, D = 4.4 mm, s = 1.833 mm and e_r = effective permittivity = 11.

The cloaked antenna is analyzed using TCM to gain insight into its radiation properties and how the cloak affect its performance. The analysis is done between the frequency range of 2.5 GHz and 3 GHz to cover the resonant frequency of the antenna after the introduction of the cloak around it. The TCM commercial software is used for the modal analysis of the structure to solve the generalized eigenvalue equation and the obtained result of the TCM analysis for the structure is represented by the plot of the characteristic angle with respect to frequency in figure 6.30:

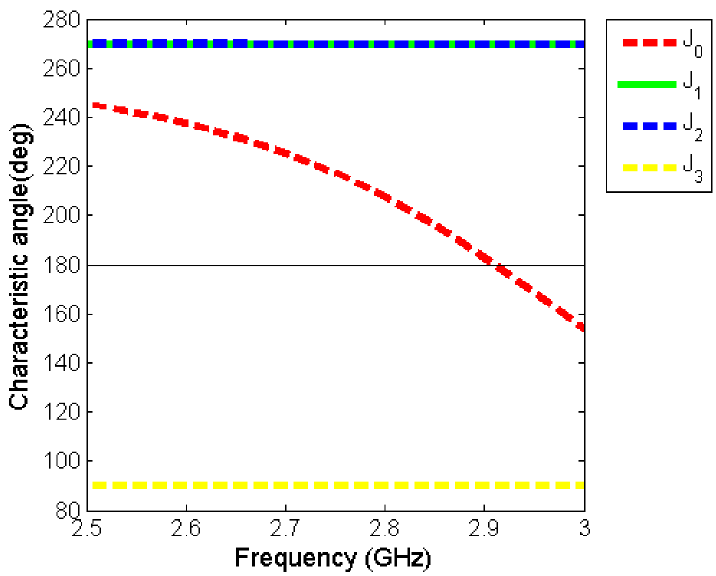

Figure 6.30: Characteristic angle against frequency of cloaked dipole antenna.

In figure 6.30, J_0 in red is the only mode that cross 180° at 2.9 GHz hence its the only resonant mode. J_1 in green, J_2 in blue and J_3 in yellow all store energy. J_1 and J_2 store electric energy throughout since they stay above 180° throughout the considered frequency band and J_3 store magnetic energy because it remain below 180° throughout the considered frequency band. The resonance frequency of the fundamental mode for the antenna is shifted down from 3.54 GHz to 2.9 GHz because of the cloak structure. The behaviour of this cloaked active antenna can be better visualized using the modal far-field in figure 6.31:

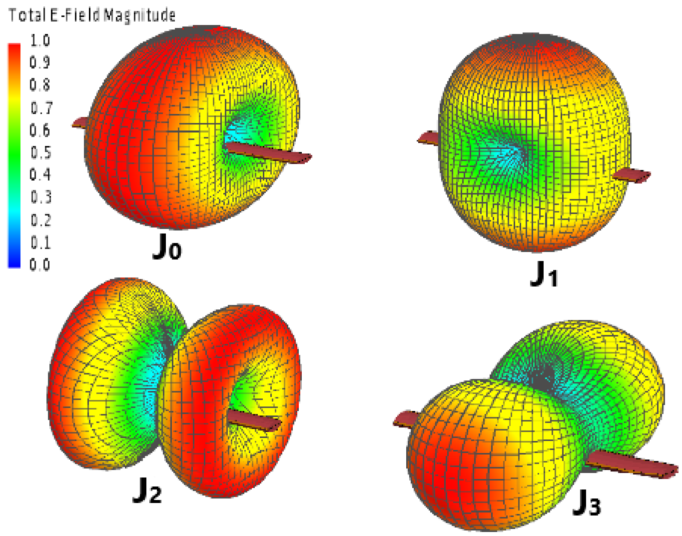

Figure 6.31: Modal far-field of cloaked dipole antenna.

The far-field in figure 6.31 show that J_0 and J_1 are similar to the J_0 and J_1 radiation pattern of the dipole alone, J_2 and J_3 radiation pattern is different and is due to the effect of the cloaking structure on the antenna. Although the pattern of the resonant mode is similar to that of the antenna operating alone, the effect of cloaking on mode J_2 and J_3 is seen on the overall radiation pattern of the cloaked antenna since the dielectric nature of the cloak impacts the radiation efficiency. The near-field behaviour of the structure can be analyzed using the quantitative modal stored energy.

The modal stored energy of the cloaked antenna derived using the formulation in chapter 3 is presented with the graph of normalized $(\mathrm{W_m} - \mathrm{W_e})$ against frequency in figure 6.32.

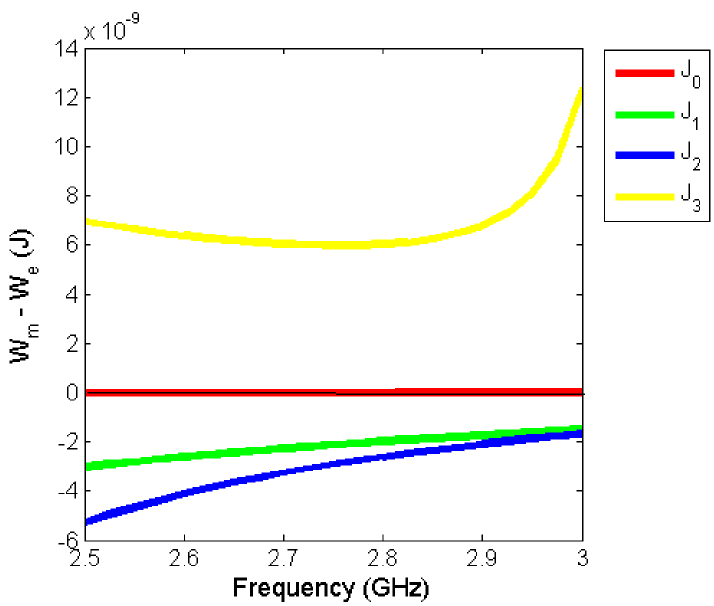

Figure 6.32: Normalized $(\mathrm{W_m} - \mathrm{W_e})$ of cloaked dipole antenna.

The curve in figure 6.32 represent the quantitative modal stored energy of the cloaked antenna structure. J_0, J_1, J_2 and J_3 are represented by the red, green, blue and yellow curve respectively. They provide the same qualitative stored energy conclusion similar to the characteristic angle curve. J_1 and J_2 store electric energy while J_3 store magnetic energy throughout the considered frequency band. J_0 has no modal stored energy at 2.9 GHz because it resonate at this frequency. In contrast to the characteristic angle which provide only qualitative stored energy information, the modal stored energy value can be extracted from the $\mathrm{W_m} - \mathrm{W_e}$ curve.

One can conclude that cloaking of an active antenna does not restore the performance of the antenna which is consistent with the physics for antenna cloaking however the radiation properties of the obstacle (i.e. the passive dipole structure) is exploited to restore the antenna radiation performance.

From the physical point of view, the current distribution on the dipole antenna is affected by the cloak and the radiation efficiency and matching of the antenna will remain affected. The radiation properties of the obstacle is therefore exploited to allow for a balanced current flow that would allow the antenna to perform efficiently.

Next, we consider the analysis of the cloaked dipole antenna in the presence of the passive dipole structure.

6.4.2.4 Analysis of the cloaked active antenna in the presence of obstacle

The cloaked antenna is placed in the vicinity of the obstacle at about $\frac{\lambda}{10}$ where λ is the wavelength of the active dipole element. The goal is to exploit the obstacle in enhancing the performance of the active dipole without modification to the obstacle. The configuration of the active dipole antenna in the presence of the passive dipole is shown in figure 6.33:

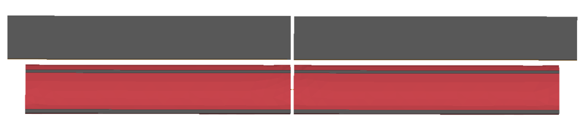

Figure 6.33: Cloaked active antenna in the presence of an obstacle.

The analysis is done within the frequency range of 2.8 GHz to 3.15 GHz to cover the known resonance of the dipole antenna of 2.9 GHz. The passive dipole affect the radiation properties of the cloaked active dipole which is analyzed using TCM. The TCM commercial software is used for the modal analysis of the structure to solve the generalized eigenvalue equation and the obtained result of the TCM analysis for the structure is represented by the plot of the characteristic angle with respect to frequency in figure 6.34:

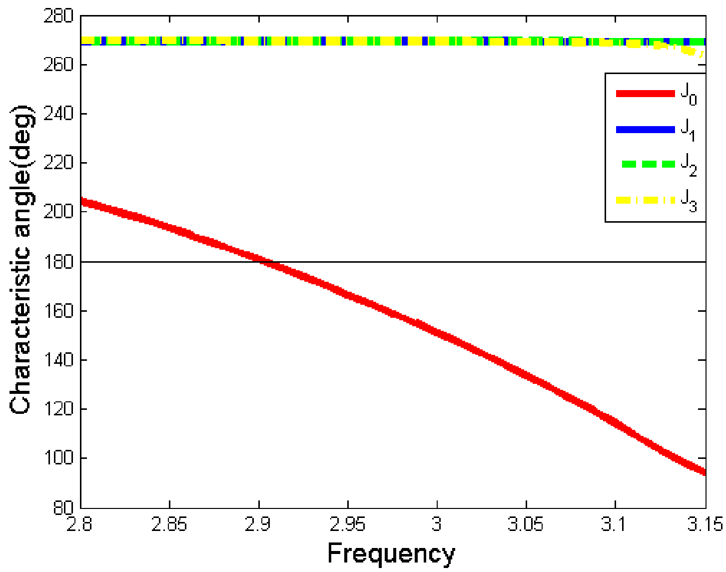

Figure 6.34: Characteristic angle against frequency of cloaked active antenna in the presence of an obstacle.

In figure 6.34, J_0 in red is the only resonant mode at 2.9 GHZ hence the introduction of the obstacle does not affect the resonant frequency of the antenna. The cloak prevent the active antenna from coupling with the obstacle. J_1, J_2 and J_3 in blue, green and yellow respectively all store electric energy throughout the considered frequency band because they stay above 180°. The resonant mode J_0 go from storing electric energy to resonance and storing magnetic energy. Interestingly, the introduction of the obstacle switch J_3 from storing magnetic energy to storing electric energy. To understand how the different modes interact and how the different elements affect the performance of the cloaked dipole antenna, the modal far-fields are considered in figure 6.35:

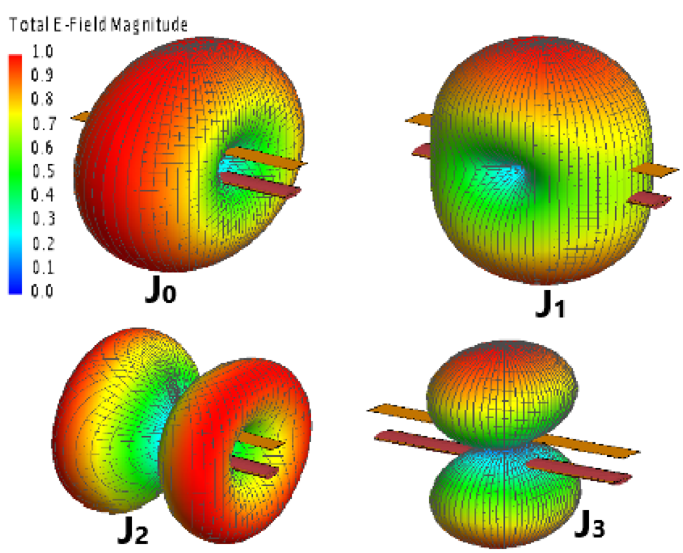

Figure 6.35: Modal far-field of cloaked active antenna in the presence of an obstacle.

The far-field in figure 6.35 provide insight into the evolution of the radiation properties of the antenna. The far-field behaviour of the first three modes, J_0, J_1 and J_2 have similar radiation pattern to that of the cloaked dipole antenna operating alone but the fourth mode J_3 which store magnetic energy change from radiating in the horizontal direction to radiating in the vertical direction. This is can be attributed to the effect of the obstacle on the cloaked dipole. J_3 modify the radiation property of the cloaked dipole such that the antenna has a good impedance matching and radiation characteristics.

To get more clarity, the modal stored energy of the cloaked dipole derived using the formulation in chapter 3 is presented with the graph of normalized $(\mathrm{W_m} - \mathrm{W_e})$ against frequency in figure 6.36.

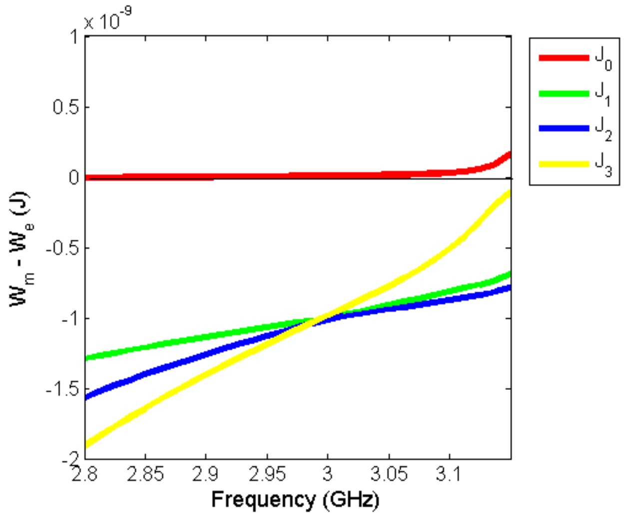

Figure 6.36: Normalized $(\mathrm{W_m} - \mathrm{W_e})$ of cloaked active antenna in the presence of an obstacle.

The curve in figure 6.36 represent the dominant modal stored energy of the configuration that has the cloaked dipole antenna in the presence of an obstacle (i.e. passive dipole). J_0, J_1, J_2 and J_3 are represented by the red, green, blue and yellow curve respectively. They provide the same qualitative stored energy conclusion similar to the characteristic angle curve. The modal surface current can also provide similar qualitative stored energy analysis. J_0 is the resonant mode which store electric energy before resonance and magnetic energy after resonance. The magnetic energy of J_0 after its resonance at 2.9 GHz couple significantly to the electric energy of J_3 between 2.9 GHz and 3.15 GHz. The other modes J_1 and J_2 store electric energy throughout the considered frequency band. In contrast to the characteristic angle and modal stored energy which provide only qualitative stored energy information, the modal stored energy value can be extracted from the $\mathrm{W_m} - \mathrm{W_e}$ curve.

The compensation of energy between J_0 and J_3 can be deduced from the inter-modal coupling analysis. The $|\mathrm{M_{ij}}|$ is evaluated using the formulation given in chapter 4 and the result is shown in figure 6.37:

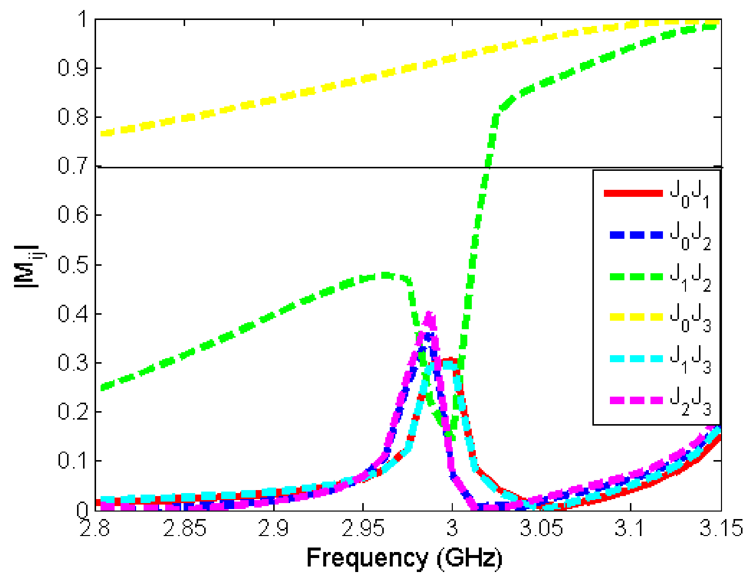

Figure 6.37: $|\mathrm{M_{ij}}|$ of cloaked active antenna in the presence of an obstacle.

The result displayed in figure 6.37 show how the different modes interact with each other. The coupling between J_0 and J_3 shown in yellow has the highest coupling since coupling is regarded as significant when $|\mathrm{M_{ij}}|$ is above 0.7. The coupling between J_0 and J_3 cover the entire band from 2.8 GHz to 3.15 GHz which is within the operating frequency band of the dipole antenna after cloaking. At 3 GHz there is also an interaction between the various modes because from the stored energy curve, all the modes cross each other at this frequency point but this interaction does not affect the performance of the antenna since it happens below the 0.7 threshold of the inter-modal co-efficient. The active dipole antenna also couple with the cloak which is evident from the interaction between J_1 and J_2 as the inter-modal coupling between this two modes goes above 0.7 after 3.02 GHz.

One can conclude that the obstacle couple to the cloaked antenna such that its radiation properties affect the performance of the cloaked dipole to enhance the radiation pattern and impedance matching. The coupling between the cloak structure and the dipole also affect the performance of the cloaked dipole at a higher frequency but limits the recovery of the radiation pattern.

6.4.2.5 Results

Further insight into the effect of the cloaked antenna is observed by comparing the reflection coefficient of the antenna when it operate alone to the scenario when it operate in the presence of the obstacle and also when it is cloaked in the presence of the obstacle. The radiation far-field pattern also provide insight into the functioning of the active dipole antenna in the different scenario.

The structure is analyzed using the full wave simulation and the result of the reflection co-efficient of the different scenario is presented in figure 6.38:

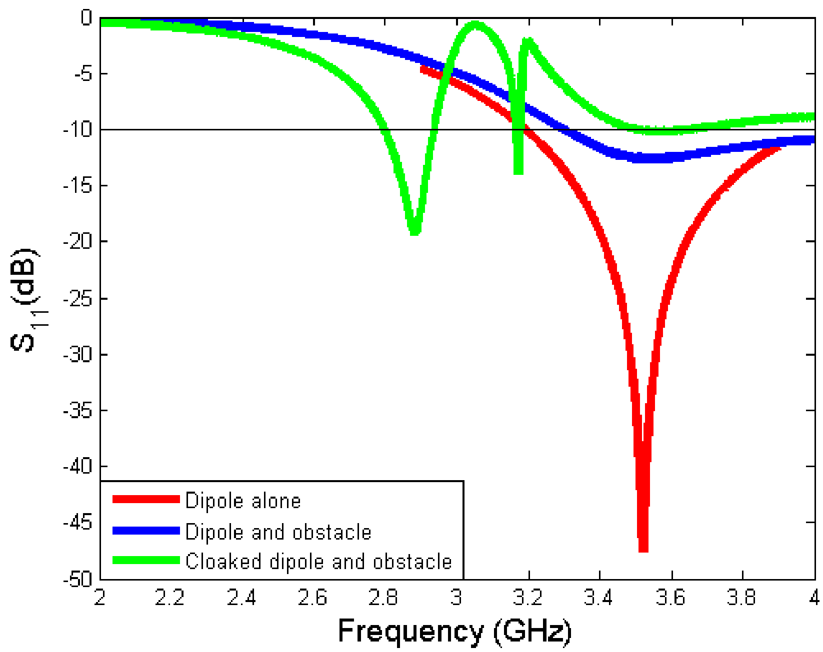

Figure 6.38: Reflection co-efficient result of the different scenario of the dipole antenna.

The result in figure 6.38 confirm that the presence of the obstacle affect the performance of the cloaked dipole. The frequency shift and reduced bandwidth is because of the cloak structure on the active element. Although the uncloaked dipole in the presence of the obstacle look slightly matched, the far-field radiation is distorted. The matching of the cloaked antenna in the presence of the obstacle at 3.2 GHz also has distorted far-field pattern. It is only at 2.9 GHz that the radiation pattern of the structure is improved. The radiation property can also be understood using the radiation pattern parameter shown in figure 6.39:

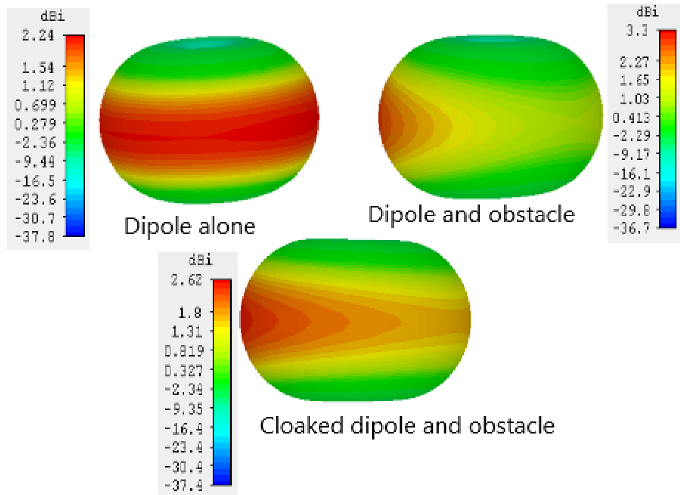

Figure 6.39: Radiation pattern results of the different scenario of the dipole antenna.

The result in figure 6.39 show that the introduction of the cloak on the active antenna improve the performance of the dipole although at a much lower frequency. This approach can be used for cloaking of antenna where there is a limited degree of freedom and the properties of the obstacle and antenna are known.

6.5 Conclusion

The proposed systematic method for enhancing the performance of antenna was applied in the analysis of cloaking design. A cloaking scenario from literature was used for the demonstration. It involve one UMTS monopole antenna whose performance is affected by an LTE antenna placed in its vicinity. The introduction of the cloak structure on the LTE antenna restores the performance of the UMTS antenna to its free space performance. The cloaking of an active dipole antenna was also demonstrated where the cloak leveraged on the radiation properties of the obstacle to enhance the performance of the antenna. The obstacle used in this case was a passive dipole since another active uncloaked dipole used as an obstacle will make the recovery of the antenna property more difficult.

The analysis based on the proposed method show that the cloak for passive cloaking is designed to have energies opposite to that of the antenna to be cloaked especially in its higher mode. Two degenerate modes of the antenna storing magnetic energy is compensated by two degenerate modes of the cloak structure storing electric energy and vice versa. Also, the combination of the obstacle and cloak provides a new resonant mode close to the resonance of the antenna to be cloaked. The two resonant mode couple together such that the electric energy of one compensates the magnetic energy of the other within the frequency band of interest. For cloaking of active antenna, the cloaked is designed to couple to the obstacle such that the cloaked antenna and the obstacle have compensating stored energies

Therefore, the proposed method can be applied in antenna cloaking application like sensor cloaking and satellite cloaking by using these principles derived from the analysis of this cloaking scenario. Further work will involving developing a generalized approach to cloaking of arbitrary structure for both passive and active cloaking.

Chapter 7

Conclusion and Future work

7.1 Main contributions of the thesis

The aim of the thesis was to define a systematic method for enhancing the performance of integrated electrically small antennas using TCM and metamaterial inclusion. This thesis work addressed the selection of metamaterial inclusions with modal stored energy and inter-modal coupling using the characteristic mode analysis in the design of integrated antennas. The main goal was to enhance the performance of these antennas with metamaterial when they are integrated into systems that degrade their performance.

The main contributions of this work include the following:

- **Identifying the factors that affect the performance on integrated antennas.** The major properties that determine the performance of an antenna and the conditions that affect its efficient operation were highlighted. A review of some of the techniques given in literature to enhance the performance of integrated antennas and their limitations were discussed.

- **Defining a method for classifying metamaterial inclusions based on modal stored energy evaluation.** In comparison to effective parameter method that use the far-field quantity for classifying metamaterials as electric or magnetic, the modal stored energy classification of metamaterials was used. It focused on the near-field quantity of the antenna and provided great insight useful for near-field application of metamaterial inclusions such as metamaterial-inspired antenna design. Furthermore a comparison between the modal stored energy method and the effective parameter method showed a good agreement in their qualitative analysis.

- **Evaluating the modal coupling interactions between antenna and metamaterial inclusions.** The modal coupling interaction derived with the inter-modal coupling co-efficient predicted which modes interact to significantly affect the overall performance of the system. It demonstrated how antenna's configuration and positioning with respect to metamaterial inclusion affect the system's performance.

- **A proposed method to designing metamaterial-inspired antenna based on modal stored energy evaluation and inter-modal coupling analysis.** A proof of concept on how the modal stored energy and inter-modal coupling analysis can be used in designing metamaterial-inspired antenna is demonstrated. The antenna consisted of a printed dipole antenna and a broadside-coupled split ring resonator (BC-SRR) and can be applied for railway communication. There is also a good agreement between simulation and measurement that validates the applied methodology.

- **Electromagnetic cloaking using the proposed systematic method of modal stored energy evaluation and inter-modal coupling analysis.** The modal stored energy and inter-modal coupling analysis is extended to electromagnetic cloaking of passive obstacles and active antennas. The modal stored energy analysis showed that a compensation of energy happens between the cloaked obstacle and the active antenna for passive cloaking or the cloaked antenna and the obstacle for active cloaking. The inter-modal coupling on the other had showed that a high coupling between the active antenna and the cloaked structure provided for the cloaking capability.

7.2 Limitation to proposed method

This thesis work heavily relies on the use of modal methods by applying the theory of characteristic modes. Although the theory of characteristic modes have been applied for a variety of electromagnetic application, the accuracy of the implementation of the presented method is dependent on the accuracy of the theory of characteristic modes. Therefore the proposed work in this thesis are limited by a variety of computational constraints some of which include:

- **Problem of modal tracking in complex structures:** TCM use the domain basis function for its method of moment (MoM) formulation which depends on frequency. For wide-band analysis, the characteristic mode analysis is performed for many sampling frequencies, the modes of one frequency is associated to another frequency and their relationship is determined by the correlation of their eigen-vector. Modal tracking is therefore important to sort the correct order of the modes at each frequency. Although there a various tracking algorithms [239–241], the accuracy of the modal tracking is linked to the meshing density hence a finer mesh will give a more accurate result. However, the more the number of sampling frequencies the more complex the tracking becomes.

- **Analysis of dielectric structure:** In comparison to PEC structures, TCM application for dielectrics are complicated and require the use of volume integral equation with large numbers of unknown. The surface electric current and magnetic currents are involved and depend on each other leading to computational complexity and appearance of nonphysical modes. PMCHWT integral equation [23, 242] is another method for analysis of dielectrics with TCM but its accuracy has not been validated for obtaining natural resonant frequencies and their corresponding modal fields [23].

- **Problem with analysis of large structures:** Large designs mean large surface area which would result to more number of unknowns and more computational complexity including longer run-time. Most TCM designs involving large scale size has often followed the principle of scaling [48] to get a physical insight into the behaviour of the structure.

7.3 Future work

The modal stored energy analysis concept has shown to be useful in simplifying the analysis of radiating structures while providing insight into its physical behaviour. This thesis work further open up an opportunity to analyse metamaterials in their near-field for electromagnetic applications. As a result of the interesting properties of metamaterials, its use in electromagnetic near-field application is on the increase especially in the THz range. Therefore it will be interesting to evaluate the modal stored energy of metamaterial inclusions of the THz frequency domain in future work. Furthermore the study of the use of stored energy method in the choice of metamaterials for other electromagnetic design applications including sensor design, active electromagnetic cloaking and antenna isolation are interesting areas to explore in future work. Already, the modal stored energy method is applied to optimize the performance of antenna thus, we are strongly confident that TCM based modal stored energy analysis will be a useful design tool in design application involving the use and selection of metamaterials.

Bibliography

[1] heynen, Electronic Components Blog, "Antonics multi-communication train and vehicle antennas, year = 2016, note = [Online; accessed April 15, 2020], url = http://www.alltronixin.com/high-tech-planar-antennas."

[2] S. Kibria, M. T. Islam, and R. Azim, "A heuristic approach to design broadband microstrip patch antenna," in *Conference: IIEEJ Image Electronics and Visual Computing Workshop*, vol. 6, 2015.

[3] Manpreet, Dhillon and Srikant Kumar, "Performance analysis and comparison of various rectenna based rf energy harvesting systems, year = 2017, note = [Online; accessed April 15, 2020], url = https://www.researchgate.net/profile/Manpreet$_D hillon6/publication/322509437/figure/fig15/AS:$ $668599723229224@1536418004899/Several - types - of - Antennas - 6.jpg.''$

[4] S. K. Behera and Y. Choukiker, "Design and optimization of dual band microstrip antenna using particle swarm optimization technique," *Journal of Infrared, Millimeter, and Terahertz Waves*, vol. 31, no. 11, pp. 1346–1354, 2010.

[5] H. N. Awl, Y. I. Abdulkarim, L. Deng, M. Bakır, F. F. Muhammadsharif, M. Karaaslan, E. Unal, and H. Luo, "Bandwidth improvement in bow-tie microstrip antennas: The effect of substrate type and design dimensions," *Applied Sciences*, vol. 10, no. 2, p. 504, 2020.

[6] A. Katyal and A. Basu, "Compact and broadband stacked microstrip patch antenna for target scanning applications," *IEEE Antennas and Wireless Propagation Letters*, vol. 16, pp. 381–384, 2016.

[7] Y. Zheng, A. Giere, H. Maune, M. Sazegar, and R. Jakoby, "Antenna bandwidth enhancement by ferroelectric tunable matching network," in *2008 Asia-Pacific Microwave Conference*. IEEE, 2008, pp. 1–4.

[8] A. Erentok and R. W. Ziolkowski, "Metamaterial-inspired efficient electrically small antennas," *IEEE Transactions on Antennas and Propagation*, vol. 56, no. 3, pp. 691–707, 2008.

[9] A. Monti, J. Soric, M. Barbuto, D. Ramaccia, S. Vellucci, F. Trotta, A. Alù, A. Toscano, and F. Bilotti, "Mantle cloaking for co-site radio-frequency antennas," *Applied Physics Letters*, vol. 108, no. 11, p. 113502, 2016.

[10] D. Ludick, E. Lezar, and U. Jakobus, "Characteristic mode analysis of arbitrary electromagnetic structures using feko," in *2012 International Conference on Electromagnetics in Advanced Applications*. IEEE, 2012, pp. 208–211.

[11] D. Tayli, M. Capek, L. Akrou, V. Losenicky, L. Jelinek, and M. Gustafsson, "Accurate and efficient evaluation of characteristic modes," *IEEE Transactions on Antennas and Propagation*, vol. 66, no. 12, pp. 7066–7075, 2018.

[12] M. Cabedo-Fabres, E. Antonino-Daviu, A. Valero-Nogueira, and M. F. Bataller, "The theory of characteristic modes revisited: A contribution to the design of antennas for modern applications," *IEEE Antennas and Propagation Magazine*, vol. 49, no. 5, pp. 52–68, 2007.

[13] C. A. Balanis, "Antenna theory: A review," *Proceedings of the IEEE*, vol. 80, no. 1, pp. 7–23, 1992.

[14] A. T. Mobashsher and A. Abbosh, "Reconfigurable water-substrate based antennas with temperature control," *Applied Physics Letters*, vol. 110, no. 25, p. 253503, 2017.

[15] H. Ma and H. D. Yang, "Miniaturized integrated folded helical antennas," in *2011 IEEE International Symposium on Antennas and Propagation (APSURSI)*. IEEE, 2011, pp. 753–756.

[16] S. H. He, W. Shan, C. Fan, Z. C. Mo, F. H. Yang, and J. H. Chen, "An improved vivaldi antenna for vehicular wireless communication systems," *IEEE Antennas and Wireless Propagation Letters*, vol. 13, pp. 1505–1508, 2014.

[17] F. Merli, L. Bolomey, E. Meurville, and A. Skrivervik, "Implanted antenna for biomedical applications," in *2008 IEEE Antennas and Propagation Society International Symposium*. IEEE, 2008, pp. 1–4.

[18] R. W. Ziolkowski, P. Jin, and C.-C. Lin, "Metamaterial-inspired engineering of antennas," *Proceedings of the IEEE*, vol. 99, no. 10, pp. 1720–1731, 2010.

[19] H. Boutayeb, P. R. Watson, L. Weishan, and T. Wu, "Dual polarized electronically steerable parasitic antenna radiator (espar)," Jun. 2 2020, uS Patent 10,673,140.

[20] M. Alibakhshikenari, M. Khalily, B. S. Virdee, C. H. See, R. A. Abd-Alhameed, and E. Limiti, "Mutual-coupling isolation using embedded metamaterial em bandgap decoupling slab for densely packed array antennas," *IEEE Access*, vol. 7, pp. 51 827–51 840, 2019.

[21] J. Hao, A. Djouadi, F. Rault, X. Tao, É. Lheurette, and L. Burgnies, "Multiresonant split ring resonator with meandered strips," *physica status solidi (a)*, vol. 217, no. 6, p. 1901017, 2020.

[22] N. Fernez, L. Burgnies, J. Hao, C. Mismer, G. Ducournau, D. Lippens, and É. Lheurette, "Radiative quality factor in thin resonant metamaterial absorbers," *IEEE Transactions on Microwave Theory and Techniques*, vol. 66, no. 4, pp. 1764–1772, 2018.

[23] Y. Chen and C.-F. Wang, *Characteristic modes: Theory and applications in antenna engineering.* John Wiley & Sons, 2015.

[24] M. H. Rabah, "Design methodology of antennas based on metamaterials and the theory of characteristic modes: application to cognitive radio," Ph.D. dissertation, Lille 1, 2015.

[25] Y. Haykir and O. A. Civi, "Characteristic mode analysis of unit cells of metal-only infinite arrays," *Advanced Electromagnetics*, vol. 8, no. 2, pp. 134–142, 2019.

[26] K. Schab, L. Jelinek, M. Capek, C. Ehrenborg, D. Tayli, G. A. Vandenbosch, and M. Gustafsson, "Energy stored by radiating systems," *IEEE Access*, vol. 6, pp. 10 553–10 568, 2018.

[27] M. Gustafsson and B. L. G. Jonsson, "Stored electromagnetic energy and antenna q," *arXiv preprint arXiv:1211.5521*, 2012.

[28] A. Michel, P. Nepa, M. Gallo, I. Moro, A. P. Filisan, and D. Zamberlan, "Printed wideband antenna for lte-band automotive applications," *IEEE Antennas and Wireless Propagation Letters*, vol. 16, pp. 1245–1248, 2016.

[29] J. Cui, A. Zhang, and X. Chen, "An omnidirectional multiband antenna for railway application," *IEEE Antennas and Wireless Propagation Letters*, vol. 19, no. 1, pp. 54–58, 2019.

[30] E. C. Neira, J. Carlsson, K. Karlsson, and E. G. Ström, "Combined lte and ieee 802.11 p antenna for vehicular applications," in *2015 9th European Conference on Antennas and Propagation (EuCAP).* IEEE, 2015, pp. 1–5.

[31] A. Abbadi, "Wireless sensors embedded in concrete," 2014.

[32] F. Merli, "Implantable antennas for biomedical applications," EPFL, Tech. Rep., 2011.

[33] M. A. B. Diez and S. Lindenmeier, "A highly efficient car2car-multiband rooftop automotive antenna," in *2015 IEEE International Symposium on Antennas and Propagation & USNC/URSI National Radio Science Meeting*. IEEE, 2015, pp. 1606–1607.

[34] J. K. Gamage, M. Engjom, and I. A. Jensen, "Design of a low profile multi-band antenna for vehicular communication system," in *2013 7th European Conference on Antennas and Propagation (EuCAP)*. IEEE, 2013, pp. 1273–1277.

[35] I. Goncharova and S. Lindenmeier, "A high efficient automotive roof-antenna concept for lte, dab-l, gnss and sdars with low mutual coupling," in *2015 9th European Conference on Antennas and Propagation (EuCAP)*. IEEE, 2015, pp. 1–5.

[36] D. V. Navarro-Mendez, L. F. Carrera-Suárez, D. Sánchez-Escuderos, M. Cabedo-Fabrés, M. Baquero-Escudero, M. Gallo, and D. Zamberlan, "Wideband double monopole for mobile, wlan, and c2c services in vehicular applications," *IEEE Antennas and Wireless Propagation Letters*, vol. 16, pp. 16–19, 2016.

[37] F. Ferrero, L. Lizzi, L. Jonsson, and L. Wang, "A two-element parasitic antenna approaching the minimum q-factor at a given directivity," *arXiv preprint arXiv:1705.02281*, 2017.

[38] Y. Hua, L. Huang, and Y. Lu, "A compact 3-port multiband antenna for v2x communication," in *2017 IEEE International Symposium on Antennas and Propagation & USNC/URSI National Radio Science Meeting*. IEEE, 2017, pp. 639–640.

[39] X. Chen, S. Zhang, and Q. Li, "A review of mutual coupling in mimo systems," *Ieee Access*, vol. 6, pp. 24 706–24 719, 2018.

[40] F. Hyjazie and H. Boutayeb, "Multi-band/wide band printed quad helical antenna," in *2020 14th European Conference on Antennas and Propagation (EuCAP)*. IEEE, 2020, pp. 1–3.

[41] A. K. Bhattacharyya, "Effects of finite ground plane on the radiation characteristics of a circular patch antenna," *IEEE transactions on antennas and propagation*, vol. 38, no. 2, pp. 152–159, 1990.

[42] E. Ebrahimi, O. Litschke, R. Baggen, and P. S. Hall, "Pattern control of uwb printed antenna on large ground plane," in *Proceedings of the 5th European Conference on Antennas and Propagation (EUCAP)*. IEEE, 2011, pp. 138–141.

[43] D.-H. Kwon and Y. Kim, "Suppression of cable leakage current for edge-fed printed dipole uwb antennas using leakage-blocking slots," *IEEE Antennas and Wireless Propagation Letters*, vol. 5, pp. 183–186, 2006.

[44] N. Koch, "Vehicular spoiler antenna for high data rate wlan," in *2015 Loughborough Antennas & Propagation Conference (LAPC)*. IEEE, 2015, pp. 1–4.

[45] A. Kwoczek, Z. Raida, J. Láčík, M. Pokorny, J. Puskelỳ, and P. Vágner, "Influence of car panorama glass roofs on car2car communication (poster)," in *2011 IEEE Vehicular Networking Conference (VNC)*. IEEE, 2011, pp. 246–251.

[46] J. S. Meiguni, M. Kamyab, and A. Hosseinbeig, "Effect of parasitic elements on spherical probe-fed antennas," in *2013 21st Iranian Conference on Electrical Engineering (ICEE)*. IEEE, 2013, pp. 1–4.

[47] M. F. Otero and R. G. Rojas, "Analysis and treatment of edge effects on the radiation pattern of a microstrip patch antenna," in *IEEE Antennas and Propagation Society International Symposium. 1995 Digest*, vol. 2. IEEE, 1995, pp. 1050–1053.

[48] Y. Chen and C.-F. Wang, "Hf band shipboard antenna design using characteristic modes," *IEEE Transactions on Antennas and Propagation*, vol. 63, no. 3, pp. 1004–1013, 2015.

[49] A. Monti, J. Soric, R. Fleury, A. Alù, A. Toscano, and F. Bilotti, "Mantle cloaking and related applications in antennas," in *2014 International Conference on Electromagnetics in Advanced Applications (ICEAA)*. IEEE, 2014, pp. 878–881.

[50] D. J. Kozakoff, *Analysis of radome-enclosed antennas*. Artech House, 2010.

[51] W.-J. Zhao, Y.-B. Gan, L.-W. Li, and C.-F. Wang, "Effects of an electrically large airborne radome on radiation patterns and input impedance of a dipole array," *IEEE transactions on antennas and propagation*, vol. 55, no. 8, pp. 2399–2402, 2007.

[52] Q. Wu, Y. Zhou, and S. Guo, "An l-sleeve l-monopole antenna fitting a shark-fin module for vehicular lte, wlan, and car-to-car communications," *IEEE Transactions on Vehicular Technology*, vol. 67, no. 8, pp. 7170–7180, 2018.

[53] C. Ryan Jr and F. Cain, "Techniques for estimating electromagnetic effectiveness of antennas in the presence of near-field obstacles," in *International Symposium on Electromagnetic Compatibility*, 1976, pp. 317–322.

[54] M. Geissler, M. Gehrt, D. Heberling, P. Waldow, and I. Wolff, "Investigations on radiation q of integrated handset antennas," in *IEEE Antennas and Propagation Society International Symposium. 2001 Digest. Held in conjunction with: USNC/URSI National Radio Science Meeting (Cat. No. 01CH37229)*, vol. 3. IEEE, 2001, pp. 54–57.

[55] K. Mohammadpour-Aghdam, R. Faraji-Dana, G. A. Vandenbosch, S. Radiom, and G. G. Gielen, "Physical bound on q factor for planar antennas," in *2011 41st European Microwave Conference*. IEEE, 2011, pp. 250–252.

[56] M. Zolghadri and C. Akyel, "Active q factor improvement of microstrip antenna," in *IMTC/99. Proceedings of the 16th IEEE Instrumentation and Measurement Technology Conference (Cat. No. 99CH36309)*, vol. 1. IEEE, 1999, pp. 134–138.

[57] H. A. Wheeler, "Fundamental limitations of small antennas," *Proceedings of the IRE*, vol. 35, no. 12, pp. 1479–1484, 1947.

[58] J. Rahola, "Effect of antenna q to the radiation efficiency of tunable antennas," in *The 8th European Conference on Antennas and Propagation (EuCAP 2014)*. IEEE, 2014, pp. 3285–3288.

[59] M. Gustafsson and S. Nordebo, "Optimal antenna currents for q, superdirectivity, and radiation patterns using convex optimization," *IEEE transactions on antennas and propagation*, vol. 61, no. 3, pp. 1109–1118, 2012.

[60] I. A. Tunio, Y. Mahe, T. Razban, and B. Froppier, "Study of impedance matching in antenna arrays due to total radiation," in *2019 13th European Conference on Antennas and Propagation (EuCAP)*. IEEE, 2019, pp. 1–5.

[61] S. Hwang and S.-Y. Hong, "A study of measurement the load impedance mismatch," in *2011 IEEE MTT-S International Microwave Workshop Series on Intelligent Radio for Future Personal Terminals*. IEEE, 2011, pp. 1–2.

[62] F. Meng, A. Van Bezooijen, and R. Mahmoudi, "A mismatch detector for adaptive antenna impedance matching," in *2006 European Microwave Conference*. IEEE, 2006, pp. 1457–1460.

[63] T. Dissanayake, K. P. Esselle, and M. Yuce, "Uwb antenna impedance matching in biomedical implants," in *2009 3rd European Conference on Antennas and Propagation*. IEEE, 2009, pp. 3523–3526.

[64] K. Ogawa, T. Takahashi, Y. Koyanagi, and K. Ito, "Automatic impedance matching of an active helical antenna near a human operator," in *33rd European Microwave Conference Proceedings (IEEE Cat. No. 03EX723C)*, vol. 3. IEEE, 2003, pp. 1271–1274.

[65] C. A. Balanis, *Antenna theory: analysis and design.* John wiley & sons, 2016.

[66] L. Aberbour, L. Laurent, I. Stefano, and L. V. UCL-Chairman, "" miniaturization of slot and planar monopole antennas: analytical approaches and experimental validation," Ph.D. dissertation, UCL-Université Catholique de Louvain, 2010.

[67] P. E. Law, *Shipboard antennas.* Artech House on Demand, 1986.

[68] V. Volski and G. Vandenbosch, "Radiation pattern of a microstrip antenna located on a finite size ground plane with small vertical wall at the edges," in *2001 Eleventh International Conference on Antennas and Propagation,(IEE Conf. Publ. No. 480)*, vol. 2. IET, 2001, pp. 619–622.

[69] S. R. Best, "The significance of ground-plane size and antenna location in establishing the performance of ground-plane-dependent antennas," *IEEE Antennas and Propagation Magazine*, vol. 51, no. 6, pp. 29–43, 2009.

[70] K.-L. Wong, *Compact and broadband microstrip antennas.* John Wiley & Sons, 2004, vol. 168.

[71] Q. Van den Brande, S. Lemey, S. Cuyvers, S. Poelman, L. De Brabander, O. Caytan, L. Bogaert, I. L. De Paula, S. Verstuyft, A. C. Reniers *et al.*, "A hybrid integration strategy for compact, broadband, and highly efficient millimeter-wave on-chip antennas," *IEEE Antennas and Wireless Propagation Letters*, vol. 18, no. 11, pp. 2424–2428, 2019.

[72] K. Mehzabin, A. U. Reza, M. A. Islam, and K. M. M. Haque, "Design and performance analysis of rectangular microstrip patch antenna (rmpa) based on 3 different substrates at 2.5 ghz," in *2017 IEEE International Conference on Power, Control, Signals and Instrumentation Engineering (ICPCSI).* IEEE, 2017, pp. 141–145.

[73] H. Liu, C. Yin, W. Gao, and Y. Sun, "Optimization and design of wideband antenna based on factor," *International Journal of Antennas and Propagation*, vol. 2015, 2015.

[74] X. Jin and M. Ali, "Embedded antennas in dry and saturated concrete for application in wireless sensors," *Progress in electromagnetics research*, vol. 102, pp. 197–211, 2010.

[75] H. Nornikman, B. H. Ahmad, M. A. Aziz, and H. Bakar, "Dual frequencies band and enhanced wideband effect of dual layer microstrip patch antenna with parasitic," in *Journal of Physics: Conference Series*, vol. 1049, no. 1. IOP Publishing, 2018, p. 012012.

[76] V. K. Singh, "Ka-band micromachined microstrip patch antenna," *IET microwaves, antennas & propagation*, vol. 4, no. 3, pp. 316–323, 2010.

[77] E. Ojefors, H. Kratz, K. Grenier, R. Plana, and A. Rydberg, "Micromachined loop antennas on low resistivity silicon substrates," *IEEE Transactions on antennas and propagation*, vol. 54, no. 12, pp. 3593–3601, 2006.

[78] J. Jayasinghe and D. Uduwawala, "Optimization of the performance of patch antennas using genetic algorithms," *Journal of the National Science Foundation of Sri Lanka*, vol. 41, no. 2, 2013.

[79] G.-H. Zhao, A.-G. Wang, W. Leng, B. Chen, and H. Chen, "Wideband internal antenna with coupled feeding for 4g mobile phone," *Microwave and Optical Technology Letters*, vol. 55, no. 3, pp. 513–516, 2013.

[80] G. Gampala, C. Reddy, D. Ludick, and P. Futter, "Systematic design of antennas using the theory of characteristic modes for mobile phone applications," in *2014 IEEE Antennas and Propagation Society International Symposium (APSURSI)*. IEEE, 2014, pp. 1421–1422.

[81] M. Gustafsson, D. Tayli, C. Ehrenborg, M. Cismasu, and S. Nordebo, "Antenna current optimization using matlab and cvx," *FERMAT*, vol. 15, no. 5, pp. 1–29, 2016.

[82] M. Capek, L. Jelinek, K. Schab, M. Gustafsson, B. Jonsson, F. Ferrero, and C. Ehrenborg, "Optimal planar electric dipole antenna," *arXiv preprint arXiv:1808.10755*, 2018.

[83] G. Moreno, H. Bernety, and A. B. Yakovlev, "Wideband elliptical metasurface cloaks in antenna technology," in *2017 IEEE International Symposium on Antennas and Propagation & USNC/URSI National Radio Science Meeting*. IEEE, 2017, pp. 69–70.

[84] F. Ohnimus, "Efficient integration of planar antennas considering electromagnetic interactions at board level," *Inst. Hochfrequenz- und Halbleiter-Systemtechnologien publications*, 2011.

[85] C. V. R. Sankar and P. Jayasree, "Design of planar and conformal microstrip patch antenna for avionics applications," *International Journal of Innovative Technology and Exploring Engineering*, 2019.

[86] W. Deal, Y. Qian, T. Itoh, and V. Radisic, "Planar integrated antenna technology," *Microwave Journal*, vol. 42, no. 7, pp. 128–137, 1999.

[87] J. L. Ethier, "Antenna shape synthesis using characteristic mode concepts," Ph.D. dissertation, Université d'Ottawa/University of Ottawa, 2012.

[88] J. A. Z. Luna, L. Dussopt, and A. Siligaris, "Hybrid on-chip/in-package integrated antennas for millimeter-wave short-range communications," *IEEE transactions on antennas and propagation*, vol. 61, no. 11, pp. 5377–5384, 2013.

[89] M. John and M. J. Ammann, "Antenna optimization with a computationally efficient multi-objective evolutionary algorithm," *IEEE transactions on antennas and propagation*, vol. 57, no. 1, pp. 260–263, 2009.

[90] M. Gujral, J. L.-W. Li, T. Yuan, and C.-W. Qiu, "Bandwidth improvement of microstrip antenna array using dummy ebg pattern on feedline," *Progress In Electromagnetics Research*, vol. 127, pp. 79–92, 2012.

[91] L. C. Paul, M. S. Hosain, S. Sarker, M. H. Prio, M. Morshed, and A. K. Sarkar, "The effect of changing substrate material and thickness on the performance of inset feed microstrip patch antenna," *American Journal of Networks and Communications*, vol. 4, no. 3, pp. 54–58, 2015.

[92] Z. Ying and P.-S. Kildal, "Improvements of dipole, helix, spiral, microstrip patch and aperture antennas with ground planes by using corrugated soft surfaces," *IEE Proceedings-Microwaves, Antennas and Propagation*, vol. 143, no. 3, pp. 244–248, 1996.

[93] Y. Sun, Z. N. Chen, Y. Zhang, H. Chen, and T. S. See, "Subwavelength substrate-integrated fabry-pérot cavity antennas using artificial magnetic conductor," *IEEE Transactions on Antennas and Propagation*, vol. 60, no. 1, pp. 30–35, 2011.

[94] P. Kumar and G. Singh, "Theoretical investigation of the input impedance of gap-coupled circular microstrip patch antennas," *Journal of Infrared, Millimeter, and Terahertz Waves*, vol. 30, no. 11, pp. 1148–1160, 2009.

[95] S. E. Sussman-Fort and R. M. Rudish, "Non-foster impedance matching of electrically-small antennas," *IEEE Transactions on Antennas and Propagation*, vol. 57, no. 8, pp. 2230–2241, 2009.

[96] P. Jin and R. W. Ziolkowski, "Broadband, efficient, electrically small metamaterial-inspired antennas facilitated by active near-field resonant parasitic elements," *IEEE Transactions on Antennas and Propagation*, vol. 58, no. 2, pp. 318–327, 2009.

[97] D. Kokotoff, R. B. Waterhouse, C. R. Birtcher, and J. T. Aberle, "Annular ring coupled circular patch with enhanced performance," *Electronics Letters*, vol. 33, no. 24, pp. 2000–2001, 1997.

[98] J. Zhong, A. Kiourti, and J. L. Volakis, "Increasing the efficiency of electrically small antennas across a large bandwidth using matching networks," in *2014 IEEE Antennas and Propagation Society International Symposium (APSURSI)*. IEEE, 2014, pp. 633–634.

[99] S. Shadrokh, Y. Yu, F. Jolani, and Z. Chen, "Use of compact lc resonant tank, resistor and frequency selective surface to construct a loaded planar dipole antenna for uwb radar and communication applications," in *2014 IEEE MTT-S International Microwave Symposium (IMS2014)*. IEEE, 2014, pp. 1–4.

[100] T. G. Spence and D. H. Werner, "A novel miniature broadband/multiband antenna based on an end-loaded planar open-sleeve dipole," *IEEE Transactions on Antennas and Propagation*, vol. 54, no. 12, pp. 3614–3620, 2006.

[101] P. R. Prajapati, "Multilayered circularly polarized microstrip antenna integrated with defected ground structure for wide impedance and axial ratio bandwidth," *Journal of Electromagnetic Waves and Applications*, vol. 30, no. 17, pp. 2256–2267, 2016.

[102] A. Sihvola, "Metamaterials in electromagnetics," *Metamaterials*, vol. 1, no. 1, pp. 2–11, 2007.

[103] A. Mithari and U. Patil, "Efficiency and bandwidth improvement using metamaterial of microstrip patch antenna," *International Research Journal of Engineering and Technology*, vol. 3, no. 4, 2016.

[104] Y. Dong and T. Itoh, "Metamaterial-based antennas," *Proceedings of the IEEE*, vol. 100, no. 7, pp. 2271–2285, 2012.

[105] P. Jin and R. W. Ziolkowski, "Multiband extensions of the electrically small, near-field resonant parasitic z antenna," *IET microwaves, antennas & propagation*, vol. 4, no. 8, pp. 1016–1025, 2010.

[106] Y.-F. Lin, C.-H. Chen, C.-T. Liao, C.-Y.-D. Sim, C.-C. Tseng, and H.-M. Chen, "Dual open-slot antennas integrated in metal frame and metal case of tablet computer for long-term evolution applications," *International Journal of RF and Microwave Computer-Aided Engineering*, vol. 29, no. 1, p. e21496, 2019.

[107] Z. N. Chen, Y. Juan, X. Qing, and W. Che, "Enhanced radiation from a horizontal dipole closely placed above a pec ground plane using a parasitic strip," *IEEE Transactions on Antennas and Propagation*, vol. 64, no. 11, pp. 4868–4871, 2016.

[108] B. Jonsson and M. Gustafsson, "Antenna q for small antennas with radiation constraints and perturbations," in *2015 9th European Conference on Antennas and Propagation (EuCAP)*. IEEE, 2015, pp. 1–3.

[109] A. Sarhadi, A. Hashemi, and H. Emami, "Optimization of q factor in complementary spiral resonator for rfid application," in *2013 21st Telecommunications Forum Telfor (TELFOR)*. IEEE, 2013, pp. 693–696.

[110] N. Zhu and F. Landstorfer, "Quality factor optimisation of coaxial resonators," *Electronics letters*, vol. 24, no. 14, pp. 862–863, 1988.

[111] M. Gustafsson, M. Cismasu, and B. L. G. Jonsson, "Physical bounds and optimal currents on antennas," *IEEE transactions on antennas and propagation*, vol. 60, no. 6, pp. 2672–2681, 2012.

[112] B. L. G. Jonsson and F. Ferrero, "On q-factor bounds for lossy embedded antennas in electrically small devices," in *2019 13th European Conference on Antennas and Propagation (EuCAP)*. IEEE, 2019, pp. 1–4.

[113] A. Taflove and S. C. Hagness, *Computational electrodynamics: the finite-difference time-domain method*. Artech house, 2005.

[114] E. M. Tentzeris, A. Cangellaris, L. P. Katehi, and J. Harvey, "Multiresolution time-domain (mrtd) adaptive schemes using arbitrary resolutions of wavelets," *IEEE transactions on microwave theory and techniques*, vol. 50, no. 2, pp. 501–516, 2002.

[115] N. Bushyager, M. Davis, E. Dalton, J. Laskar, and M. Tentzeris, "Q-factor prediction and optimization of multilayer inductors for rf packaging microsystems using time domain techniques," in *52nd Electronic Components and Technology Conference 2002.(Cat. No. 02CH37345)*. IEEE, 2002, pp. 1718–1721.

[116] M. Gustafsson, M. Capek, and K. Schab, "Tradeoff between antenna efficiency and q-factor," *IEEE Transactions on Antennas and Propagation*, vol. 67, no. 4, pp. 2482–2493, 2019.

[117] S. Clauzier, S. M. Mikki, Y. M. Antar, A. Sharaiha, and P. Pouliguen, "A method to obtain current distributions on small antennas with optimum directivity," in *2015 IEEE International Symposium on Antennas and Propagation & USNC/URSI National Radio Science Meeting*. IEEE, 2015, pp. 1406–1407.

[118] M. Gustafsson and B. L. G. Jonsson, "Antenna q and stored energy expressed in the fields, currents, and input impedance," *IEEE Transactions on Antennas and Propagation*, vol. 63, no. 1, pp. 240–249, 2014.

[119] R. L. Haupt and D. H. Werner, "Introduction to optimization in electromagnetics," 2007.

[120] Y. Rahmat-Samii and E. Michielssen, "Electromagnetic optimization by genetic algorithms," *Microwave Journal*, vol. 42, no. 11, pp. 232–232, 1999.

[121] C. Ehrenborg and M. Gustafsson, "Fundamental bounds on mimo antennas," *IEEE Antennas and Wireless Propagation Letters*, vol. 17, no. 1, pp. 21–24, 2017.

[122] L. Poli, G. Oliveri, F. Viani, and A. Massa, "Mt–bcs-based microwave imaging approach through minimum-norm current expansion," *IEEE transactions on antennas and propagation*, vol. 61, no. 9, pp. 4722–4732, 2013.

[123] L. Jelinek and M. Capek, "Optimal currents on arbitrarily shaped surfaces," *IEEE Transactions on Antennas and Propagation*, vol. 65, no. 1, pp. 329–341, 2016.

[124] L. Tenuti, G. Oliveri, F. Viani, A. Massa, A. Monti, F. Bilotti, and A. Toscano, "A system-by-design approach for the synthesis of multi-layer mantle cloaks," in *2015 IEEE International Symposium on Antennas and Propagation & USNC/URSI National Radio Science Meeting*. IEEE, 2015, pp. 59–60.

[125] G. Moreno, A. B. Yakovlev, H. M. Bernety, D. H. Werner, H. Xin, A. Monti, F. Bilotti, and A. Alu, "Wideband elliptical metasurface cloaks in printed antenna technology," *IEEE Transactions on Antennas and Propagation*, vol. 66, no. 7, pp. 3512–3525, 2018.

[126] A. Alu and N. Engheta, "Cloaking a sensor," *Physical review letters*, vol. 102, no. 23, p. 233901, 2009.

[127] A. Keivaan, M. H. Fakheri, A. Abdolali, and H. Oraizi, "Design of coating materials for cloaking and directivity enhancement of cylindrical antennas using transformation optics," *IEEE Antennas and Wireless Propagation Letters*, vol. 16, pp. 3122–3125, 2017.

[128] Y. Chen and C.-F. Wang, "Electrically small uav antenna design using characteristic modes," *IEEE Transactions on Antennas and Propagation*, vol. 62, no. 2, pp. 535–545, 2013.

[129] J. L. Ethier and D. A. McNamara, "Antenna shape synthesis without prior specification of the feedpoint locations," *IEEE Transactions on Antennas and Propagation*, vol. 62, no. 10, pp. 4919–4934, 2014.

[130] M. H. Rabah, D. Seetharamdoo, A. de Lustrac, and M. Berbineau, "Analysis of metamaterial inclusions for association with radiating elements using the theory of characteristic modes," in *The 8th European Conference on Antennas and Propagation (EuCAP 2014)*. IEEE, 2014, pp. 927–930.

[131] M. H. Rabah, D. Seetharamdoo, and M. Berbineau, "Analysis of miniature metamaterial and magnetodielectric arbitrary-shaped patch antennas using characteristic modes: Evaluation of the q factor," *IEEE Transactions on Antennas and Propagation*, vol. 64, no. 7, pp. 2719–2731, 2016.

[132] R. W. Ziolkowski, "Applications of metamaterials to realize efficient electrically small antennas," in *Antenna Technology: Small Antennas and Novel Metamaterials, 2005. IWAT 2005. IEEE International Workshop on.* IEEE, 2005, pp. 7–10.

[133] A. Monti, J. Soric, A. Alù, A. Toscano, and F. Bilotti, "Design of cloaked yagi-uda antennas," *EPJ Applied Metamaterials*, vol. 3, p. 10, 2016.

[134] B. Derat, A. Sharaiha, K. Mahdjoubi, and J.-C. Bolomey, "Discussion on the definition of the antenna radiation q," in *11th International Symposium on Antenna Technology and Applied Electromagnetics [ANTEM 2005].* IEEE, 2005, pp. 1–4.

[135] M. Capek and L. Jelinek, "The relation between fractional bandwidth and q factor," in *2015 IEEE International Symposium on Antennas and Propagation & USNC/URSI National Radio Science Meeting.* IEEE, 2015, pp. 858–859.

[136] J. C. Soric, A. Monti, A. Toscano, F. Bilotti, and A. Alù, "Dual-polarized reduction of dipole antenna blockage using mantle cloaks," *IEEE Transactions on Antennas and Propagation*, vol. 63, no. 11, pp. 4827–4834, 2015.

[137] S. Huang, J. Pan, and Y. Luo, "Study on the relationships between eigenmodes, natural modes, and characteristic modes of perfectly electric conducting bodies," *International Journal of Antennas and Propagation*, vol. 2018, 2018.

[138] R. Garg, P. Bhartia, I. J. Bahl, and A. Ittipiboon, *Microstrip antenna design handbook.* Artech house, 2001.

[139] S. Collardey, A. Sharaiha, and K. Mahdjoubi, "Evaluation of antenna radiation q using fdtd method," *Electronics Letters*, vol. 41, no. 12, pp. 675–677, 2005.

[140] R. Garbacz, "Modal expansions for resonance scattering phenomena," *Proceedings of the IEEE*, vol. 53, no. 8, pp. 856–864, 1965.

[141] R. Garbacz and R. Turpin, "A generalized expansion for radiated and scattered fields," *IEEE Transactions on Antennas and Propagation*, vol. 19, no. 3, pp. 348–358, 1971.

[142] R. Harrington and J. Mautz, "Theory of characteristic modes for conducting bodies," *IEEE Transactions on Antennas and Propagation*, vol. 19, no. 5, pp. 622–628, 1971.

[143] R. Harrington, J. Mautz, and Y. Chang, "Characteristic modes for dielectric and magnetic bodies," *IEEE Transactions on Antennas and Propagation*, vol. 20, no. 2, pp. 194–198, 1972.

[144] J. J. Adams and J. T. Bernhard, "A modal approach to tuning and bandwidth enhancement of an electrically small antenna," *IEEE Transactions on Antennas and Propagation*, vol. 59, no. 4, pp. 1085–1092, 2011.

[145] R. Martens, E. Safin, and D. Manteuffel, "Inductive and capacitive excitation of the characteristic modes of small terminals," in *2011 Loughborough Antennas & Propagation Conference*. IEEE, 2011, pp. 1–4.

[146] E. Antonino-Daviu, M. Cabedo-Fabres, M. Gallo, M. Ferrando-Bataller, and M. Bozzetti, "Design of a multimode mimo antenna using characteristic modes," in *Antennas and Propagation, 2009. EuCAP 2009. 3rd European Conference on.* IEEE, 2009, pp. 1840–1844.

[147] A. Araghi and G. Dadashzadeh, "Oriented design of an antenna for mimo applications using theory of characteristic modes," *IEEE Antennas and Wireless Propagation Letters*, vol. 11, pp. 1040–1043, 2012.

[148] R. Harrington and J. Mautz, "Computation of characteristic modes for conducting bodies," *IEEE Transactions on Antennas and Propagation*, vol. 19, no. 5, pp. 629–639, 1971.

[149] J.-F. Lin and Q.-X. Chu, "Extending bandwidth of antennas with coupling theory for characteristic modes," *IEEE Access*, vol. 5, pp. 22 262–22 271, 2017.

[150] G. A. Vandenbosch and J. Wang, "Recoverable energy and small antennas," in *2017 11th European Conference on Antennas and Propagation (EUCAP).* IEEE, 2017, pp. 1539–1541.

[151] L. J. Chu, "Physical limitations of omni-directional antennas," *Journal of applied physics*, vol. 19, no. 12, pp. 1163–1175, 1948.

[152] R. Collin and S. Rothschild, "Evaluation of antenna q," *IEEE Transactions on Antennas and Propagation*, vol. 12, no. 1, pp. 23–27, 1964.

[153] M. Capek, L. Jelinek, and G. A. Vandenbosch, "Stored electromagnetic energy and quality factor of radiating structures," *Proceedings of the Royal Society A: Mathematical, Physical and Engineering Sciences*, vol. 472, no. 2188, p. 20150870, 2016.

[154] D. Sarkar, S. M. Mikki, A. M. Alzahed, K. V. Srivastava, and Y. M. Antar, "New considerations on electromagnetic energy in antenna near-field by time-domain approach," in *2017 IEEE Applied Electromagnetics Conference (AEMC).* IEEE, 2017, pp. 1–2.

[155] X. Zheng, G. Vandenbosch, and V. Moshchalkov, "Recoverable energy of antennas," in *2016 International Conference on Electromagnetics in Advanced Applications (ICEAA)*. IEEE, 2016, pp. 845–847.

[156] K. Schab, L. Jelinek, and M. Capek, "Recoverable energy of dissipative electromagnetic systems," *arXiv preprint arXiv:1701.06313*, 2017.

[157] D. R. Rhodes, "Observable stored energies of electromagnetic systems," *Journal of the Franklin Institute*, vol. 302, no. 3, pp. 225–237, 1976.

[158] M. Capek, L. Jelinek, P. Hazdra, and J. Eichler, "The measurable q factor and observable energies of radiating structures," *IEEE Transactions on Antennas and Propagation*, vol. 62, no. 1, pp. 311–318, 2013.

[159] A. M. Alzahed, S. M. Mikki, and Y. Antar, "Stored energy in general antenna system: A new approach," in *2016 10th European Conference on Antennas and Propagation (EuCAP)*. IEEE, 2016, pp. 1–5.

[160] I. Semchenko, A. Balmakou, S. Khakhomov, and S. Tretyakov, "Stored and absorbed energy of fields in lossy chiral single-component metamaterials," *Physical Review B*, vol. 97, no. 1, p. 014432, 2018.

[161] P.-G. Luan, "Power loss and electromagnetic energy density in a dispersive metamaterial medium," *Physical Review E*, vol. 80, no. 4, p. 046601, 2009.

[162] M. Cismasu and M. Gustafsson, "Antenna bandwidth optimization with single frequency simulation," *IEEE Transactions on Antennas and Propagation*, vol. 62, no. 3, pp. 1304–1311, 2013.

[163] B. L. G. Jonsson, S. Shi, L. Wang, F. Ferrero, and L. Lizzi, "On methods to determine bounds on the q-factor for a given directivity," *IEEE Transactions on Antennas and Propagation*, vol. 65, no. 11, pp. 5686–5696, 2017.

[164] W. Wasylkiwskyj and W. Kahn, "Scattering properties and mutual coupling of antennas with prescribed radiation pattern," *IEEE Transactions on Antennas and Propagation*, vol. 18, no. 6, pp. 741–752, 1970.

[165] R. Marqués, F. Medina, and R. Rafii-El-Idrissi, "Role of bianisotropy in negative permeability and left-handed metamaterials," *Physical Review B*, vol. 65, no. 14, p. 144440, 2002.

[166] I. Gnanaharan and R. Anbazhagan, "Review on the design of the isolation techniques for uwb-mimo antennas," *Advanced Electromagnetics*, vol. 7, no. 4, pp. 46–70, 2018.

[167] K. R. Siarkiewicz and A. Adams, "Analysis and prediction of coupling between collocated antennas," in *1972 IEEE International Electromagnetic Compatibility Symposium Record.* IEEE, 1972, pp. 1–6.

[168] A. Raniszewski and P. Piasecki, "The investigation of mutual coupling effects on a large array antenna radiation pattern," in *2018 22nd International Microwave and Radar Conference (MIKON).* IEEE, 2018, pp. 52–56.

[169] D. Ramaccia, F. Bilotti, and A. Toscano, "Accurate analytical model of coupled omega particles for metamaterial design," in *2013 7th International Congress on Advanced Electromagnetic Materials in Microwaves and Optics.* IEEE, 2013, pp. 61–63.

[170] P. Liang and Q. Wu, "Characteristic mode analysis of antenna mutual coupling in the near field," *IEEE Transactions on Antennas and Propagation*, vol. 66, no. 7, pp. 3757–3762, 2018.

[171] S. Ghosal, R. Sinha, A. De, A. Chakrabarty, and H. Son, "Theory of coupled characteristic modes," *IEEE Transactions on Antennas and Propagation*, vol. 68, no. 6, pp. 4677–4687, 2020.

[172] D. Seetharamdoo, "Étude des métamatériaux à indice de réfraction négatif: paramètres effectifs et applications antennaires potentielles," Ph.D. dissertation, Rennes 1, 2006.

[173] A. Monti, A. Toscano, and F. Bilotti, "Metasurface mantle cloak for antenna applications," in *Proceedings of the 2012 IEEE International Symposium on Antennas and Propagation.* IEEE, 2012, pp. 1–2.

[174] B. Reinhard, K. M. Schmitt, V. Wollrab, J. Neu, R. Beigang, and M. Rahm, "Metamaterial near-field sensor for deep-subwavelength thickness measurements and sensitive refractometry in the terahertz frequency range," *Applied Physics Letters*, vol. 100, no. 22, p. 221101, 2012.

[175] W. Wang, F. Yan, S. Tan, H. Zhou, and Y. Hou, "Ultrasensitive terahertz metamaterial sensor based on vertical split ring resonators," *Photonics Research*, vol. 5, no. 6, pp. 571–577, 2017.

[176] S. M. Mikki and Y. M. Antar, "A theory of antenna electromagnetic near field—part i," *IEEE Transactions on Antennas and Propagation*, vol. 59, no. 12, pp. 4691–4705, 2011.

[177] A. D. Boardman and K. Marinov, "Electromagnetic energy in a dispersive metamaterial," *physical Review B*, vol. 73, no. 16, p. 165110, 2006.

[178] M. Capek, L. Jelinek, P. Hazdra, and J. Eichler, "The measurable q factor and observable energies of radiating structures," *IEEE Transactions on Antennas and Propagation*, vol. 62, no. 1, pp. 311–318, 2014.

[179] M. Capek and L. Jelinek, "Optimal composition of modal currents for minimal quality factor *q*," *IEEE Transactions on Antennas and Propagation*, vol. 64, no. 12, pp. 5230–5242, 2016.

[180] S. Tretyakov, "Electromagnetic field energy density in artificial microwave materials with strong dispersion and loss," *physics Letters A*, vol. 343, no. 1-3, pp. 231–237, 2005.

[181] W. X. Lim and R. Singh, "Universal behaviour of high-q fano resonances in metamaterials: terahertz to near-infrared regime," *Nano convergence*, vol. 5, no. 1, pp. 1–7, 2018.

[182] P. M. Ikonen and S. A. Tretyakov, "Determination of generalized permeability function and field energy density in artificial magnetics using the equivalent-circuit method," *IEEE transactions on microwave theory and techniques*, vol. 55, no. 1, pp. 92–99, 2007.

[183] G. W. Hanson and A. B. Yakovlev, *Operator theory for electromagnetics: an introduction*. Springer Science & Business Media, 2013.

[184] D. A. Powell, "Resonant dynamics of arbitrarily shaped meta-atoms," *Physical Review B*, vol. 90, no. 7, p. 075108, 2014.

[185] M. H. Rabah, D. Seetharamdoo, M. Berbineau, and A. De Lustrac, "New metrics for artificial magnetism from metal-dielectric metamaterial based on the theory of characteristic modes," *IEEE Antennas and Wireless Propagation Letters*, vol. 15, pp. 460–463, 2016.

[186] D.-W. Kim and S. Nam, "Systematic design of a multiport mimo antenna with bilateral symmetry based on characteristic mode analysis," *IEEE Transactions on Antennas and Propagation*, vol. 66, no. 3, pp. 1076–1085, 2017.

[187] M. Capek, P. Hazdra, and J. Eichler, "A method for the evaluation of radiation q based on modal approach," *IEEE Transactions on Antennas and Propagation*, vol. 60, no. 10, pp. 4556–4567, 2012.

[188] J. C. Rautio and R. F. Harrington, "An electromagnetic time-harmonic analysis of shielded microstrip circuits," *IEEE transactions on microwave theory and techniques*, vol. 35, no. 8, pp. 726–730, 1987.

[189] E. FEKO, "Simulation software," 2014.

[190] M. H. Rabah and D. Seetharamdoo, "Calculation of the total q-factor for electrically small antennas with metamaterials using characteristic modes," in *Antennas and Propagation (EuCAP), 2016 10th European Conference on.* IEEE, 2016, pp. 1–5.

[191] W. Pan, Y. Yan, Y. Ma, and D. Shen, "A terahertz metamaterial based on electromagnetically induced transparency effect and its sensing performance," *Optics Communications*, vol. 431, pp. 115–119, 2019.

[192] A. Hopper and R. Seviour, "Non-resonant metamaterials for high power vacuum electronics applications," in *2015 IEEE International Conference on Plasma Sciences (ICOPS).* IEEE, 2015, pp. 1–1.

[193] R. Liu, Q. Cheng, T. J. Cui, and D. R. Smith, "Broadband and low-loss non-resonant metamaterials," in *Metamaterials.* Springer, 2010, pp. 87–97.

[194] J. B. Pendry, A. Holden, D. Robbins, and W. Stewart, "Low frequency plasmons in thin-wire structures," *Journal of Physics: Condensed Matter*, vol. 10, no. 22, p. 4785, 1998.

[195] R. Martens, E. Safin, and D. Manteuffel, "Selective excitation of characteristic modes on small terminals," in *Proceedings of the 5th European Conference on Antennas and Propagation (EUCAP).* IEEE, 2011, pp. 2492–2496.

[196] E. Antonino-Daviu, M. Cabedo-Fabres, M. Sonkki, N. M. Mohamed-Hicho, and M. Ferrando-Bataller, "Design guidelines for the excitation of characteristic modes in slotted planar structures," *IEEE Transactions on Antennas and Propagation*, vol. 64, no. 12, pp. 5020–5029, 2016.

[197] H. Benosman and N. B. Hacene, "Design and simulation of double" s" shaped metamaterial," *International Journal of Computer Science Issues (IJCSI)*, vol. 9, no. 2, p. 534, 2012.

[198] X. Chen, T. M. Grzegorczyk, B.-I. Wu, J. Pacheco Jr, and J. A. Kong, "Robust method to retrieve the constitutive effective parameters of metamaterials," *Physical Review E*, vol. 70, no. 1, p. 016608, 2004.

[199] D. Smith, D. Vier, T. Koschny, and C. Soukoulis, "Electromagnetic parameter retrieval from inhomogeneous metamaterials," *Physical review E*, vol. 71, no. 3, p. 036617, 2005.

[200] D. Seetharamdoo, R. Sauleau, K. Mahdjoubi, and A.-C. Tarot, "Effective parameters of resonant negative refractive index metamaterials: Interpretation and validity," *Journal of applied physics*, vol. 98, no. 6, p. 063505, 2005.

[201] X. Chen, B.-I. Wu, J. A. Kong, and T. M. Grzegorczyk, "Retrieval of the effective constitutive parameters of bianisotropic metamaterials," *Physical Review E*, vol. 71, no. 4, p. 046610, 2005.

[202] D. Nyberg, P.-S. Kildal, and J. Carlsson, "Radiation q and radiation efficiency of wideband small antennas and their relation to bandwidth and cut-off of spherical modes," in *The Second European Conference on Antennas and Propagation, EuCAP 2007.* IET, 2007, pp. 1–6.

[203] H. Chen, G. Li, L. Han, Y. Zhou, Z. Zhou, X. Li, X. Weng, L. Zhang, D. Liang, J. Xie *et al.*, "Design of reducing mutual coupling in between two closely spaced dual-frequency antennas based on combined electromagnetic soft surfaces," *Applied Physics A*, vol. 124, no. 12, p. 811, 2018.

[204] R. Martin-Cuerdo, D. Segovia-Vargas, and M. Sierra-Perez, "Minimization of mutual coupling effects in eigenstructure algorithms based on modal analysis," in *IEEE Antennas and Propagation Society International Symposium. 1999 Digest. Held in conjunction with: USNC/URSI National Radio Science Meeting (Cat. No. 99CH37010)*, vol. 3. IEEE, 1999, pp. 1608–1611.

[205] P. Z. Petkov and P. S. Simon, "Antenna array with reduced mutual coupling between array elements," Jan. 3 2017, uS Patent 9,537,209.

[206] S. J. M. Rao, G. Kumar, and D. R. Chowdhury, "Near feild inductive coupling in terahertz metamaterials," in *JSAP-OSA Joint Symposia.* Optical Society of America, 2017, p. 7p_A409_10.

[207] Z.-J. Yang, Z.-S. Zhang, Z.-H. Hao, and Q.-Q. Wang, "Strong bonding magnetic plasmon hybridizations in double split-ring resonators," *Optics letters*, vol. 37, no. 17, pp. 3675–3677, 2012.

[208] X. He, L. Wang, J. Wang, X. Tian, J. Jiang, and Z. Geng, "Electromagnetically induced transparency in planar complementary metamaterial for refractive index sensing applications," *Journal of physics D: Applied Physics*, vol. 46, no. 36, p. 365302, 2013.

[209] M. H. Rabah, D. Seetharamdoo, R. Addaci, and M. Berbineau, "Novel miniature extremely-wide-band antenna with stable radiation pattern for spectrum sensing applications," *IEEE Antennas and Wireless Propagation Letters*, vol. 14, pp. 1634–1637, 2015.

[210] N. Liu and H. Giessen, "Coupling effects in optical metamaterials," *Angewandte Chemie International Edition*, vol. 49, no. 51, pp. 9838–9852, 2010.

[211] D. A. Powell, M. Lapine, M. V. Gorkunov, I. V. Shadrivov, and Y. S. Kivshar, "Metamaterial tuning by manipulation of near-field interaction," *Physical Review B*, vol. 82, no. 15, p. 155128, 2010.

[212] P. Liang, W. Su, and Q. Wu, "Characteristic mode analysis of near-field mutual coupling between wire and loop antennas," in *2016 Asia-Pacific International Symposium on Electromagnetic Compatibility (APEMC)*, vol. 1. IEEE, 2016, pp. 263–265.

[213] R. N'gongo and H. Baudrand, "A new approach for microstrip active antennas using modal fft-algorithm," in *IEEE Antennas and Propagation Society International Symposium. 1999 Digest. Held in conjunction with: USNC/URSI National Radio Science Meeting (Cat. No. 99CH37010)*, vol. 3. IEEE, 1999, pp. 1700–1703.

[214] Y. Liu, T. Chang, and A. E. Craig, "Coupled mode theory for modeling microring resonators," *Optical Engineering*, vol. 44, no. 8, p. 084601, 2005.

[215] S. Y. Elnaggar, R. J. Tervo, and S. M. Mattar, "Coupled mode theory applied to resonators in the presence of conductors," *IEEE Transactions on Microwave Theory and Techniques*, vol. 63, no. 7, pp. 2124–2132, 2015.

[216] K. R. Schab, J. M. Outwater, M. W. Young, and J. T. Bernhard, "Eigenvalue crossing avoidance in characteristic modes," *IEEE Transactions on Antennas and Propagation*, vol. 64, no. 7, pp. 2617–2627, 2016.

[217] P. Jin and R. W. Ziolkowski, "Multi-frequency, linear and circular polarized, metamaterial-inspired, near-field resonant parasitic antennas," *IEEE Transactions on Antennas and Propagation*, vol. 59, no. 5, pp. 1446–1459, 2011.

[218] D. Li, Z. Szabó, X. Qing, E.-P. Li, and Z. N. Chen, "A high gain antenna with an optimized metamaterial inspired superstrate," *IEEE transactions on antennas and propagation*, vol. 60, no. 12, pp. 6018–6023, 2012.

[219] S. Can, K. Y. Kapusuz, and A. E. Yılmaz, "An efficient metamaterial-inspired, electrically small antenna for ism band applications," in *2017 11th European Conference on Antennas and Propagation (EUCAP)*. IEEE, 2017, pp. 1122–1125.

[220] K. R. Dandekar and P. Mookiah, "Mimo antenna arrays built on metamaterial substrates," Sep. 16 2014, uS Patent 8,836,608.

[221] W. Krouka, S. Fenni, M. Challal, and R. Aksas, "Evaluation of polarization diversity antenna for wireless communication applications," in *2015 4th International Conference on Electrical Engineering (ICEE)*. IEEE, 2015, pp. 1–5.

[222] R. Martens and D. Manteuffel, "Systematic design method of a mobile multiple antenna system using the theory of characteristic modes," *IET Microwaves, Antennas & Propagation*, vol. 8, no. 12, pp. 887–893, 2014.

[223] M. H. Rabah, D. Seetharamdoo, M. Berbineau, and A. De Lustrac, "New metrics for artificial magnetism from metal-dielectric metamaterial based on the theory of characteristic modes," *IEEE Antennas and Wireless Propagation Letters*, vol. 15, pp. 460–463, 2015.

[224] J. García-García, F. Martín, J. Baena, R. Marques, and L. Jelinek, "On the resonances and polarizabilities of split ring resonators," *Journal of Applied Physics*, vol. 98, no. 3, p. 033103, 2005.

[225] J. C. Soric, R. Fleury, A. Monti, A. Toscano, F. Bilotti, and A. Alù, "Controlling scattering and absorption with metamaterial covers," *IEEE transactions on antennas and propagation*, vol. 62, no. 8, pp. 4220–4229, 2014.

[226] H. M. Bernety and A. B. Yakovlev, "Reduction of mutual coupling between neighboring strip dipole antennas using confocal elliptical metasurface cloaks," *IEEE Transactions on Antennas and Propagation*, vol. 63, no. 4, pp. 1554–1563, 2015.

[227] A. Monti, M. Barbuto, A. Alù, A. Toscano, and F. Bilotti, "Electromagnetic cloaking for antenna arrays," in *2018 IEEE International Symposium on Antennas and Propagation & USNC/URSI National Radio Science Meeting*. IEEE, 2018, pp. 909–910.

[228] S. Vellucci, A. Monti, M. Barbuto, A. Toscano, and F. Bilotti, "Waveform-selective mantle cloaks for intelligent antennas," *IEEE Transactions on Antennas and Propagation*, vol. 68, no. 3, pp. 1717–1725, 2019.

[229] W. X. Jiang, T. J. Cui, X. M. Yang, Q. Cheng, R. Liu, and D. R. Smith, "Invisibility cloak without singularity," *Applied Physics Letters*, vol. 93, no. 19, p. 194102, 2008.

[230] F. Qin, Z. Liu, Q. Zhang, H. Zhang, and J. Xiao, "Mantle cloaks based on the frequency selective metasurfaces designed by bayesian optimization," *Scientific reports*, vol. 8, no. 1, pp. 1–10, 2018.

[231] T. V. Teperik and A. de Lustrac, "Electromagnetic cloak to restore the antenna radiation patterns affected by nearby scatter," *AIP Advances*, vol. 5, no. 12, p. 127225, 2015.

[232] M. Bisht, V. P. Vinubhai, and K. V. Srivastava, "Analysis and realization of a wideband mantle cloak with improved cloaking performance," *Journal of Electromagnetic Waves and Applications*, pp. 1–14, 2020.

[233] G. Moreno, H. M. Bernety, and A. B. Yakovlev, "Reduction of mutual coupling between strip dipole antennas at terahertz frequencies with an elliptically shaped graphene monolayer," *IEEE Antennas and Wireless Propagation Letters*, vol. 15, pp. 1533–1536, 2015.

[234] A. Monti, M. Barbuto, A. Toscano, and F. Bilotti, "Nonlinear mantle cloaking devices for power-dependent antenna arrays," *IEEE Antennas and Wireless Propagation Letters*, vol. 16, pp. 1727–1730, 2017.

[235] Z. Hamzavi-Zarghani, A. Yahaghi, and L. Matekovits, "Electrically tunable mantle cloaking utilizing graphene metasurface for oblique incidence," *AEU-International Journal of Electronics and Communications*, vol. 116, p. 153080, 2020.

[236] F. Monticone and A. Alù, "Invisibility exposed: physical bounds on passive cloaking," *Optica*, vol. 3, no. 7, pp. 718–724, 2016.

[237] Y. R. Padooru, A. B. Yakovlev, P.-Y. Chen, and A. Alù, "Analytical modeling of conformal mantle cloaks for cylindrical objects using sub-wavelength printed and slotted arrays," *Journal of Applied Physics*, vol. 112, no. 3, p. 034907, 2012.

[238] A. Monti, J. C. Soric, A. Alù, A. Toscano, and F. Bilotti, "Anisotropic mantle cloaks for tm and te scattering reduction," *IEEE Transactions on Antennas and Propagation*, vol. 63, no. 4, pp. 1775–1788, 2015.

[239] B. D. Raines and R. G. Rojas, "Wideband characteristic mode tracking," *IEEE Transactions on Antennas and Propagation*, vol. 60, no. 7, pp. 3537–3541, 2012.

[240] M. Capek, P. Hazdra, P. Hamouz, and J. Eichler, "A method for tracking characteristic numbers and vectors," *Progress In Electromagnetics Research*, vol. 33, pp. 115–134, 2011.

[241] D. Ludick, U. Jakobus, and M. Vogel, "A tracking algorithm for the eigenvectors calculated with characteristic mode analysis," in *The 8th European Conference on Antennas and Propagation (EuCAP 2014)*. IEEE, 2014, pp. 569–572.

[242] D. Tihon, V. Sozio, N. Ozdemir, M. Albani, and C. Craeye, "Efficient numerical analysis of 3d periodic metamaterials: Multilayer approach and eigenmode analysis," in *2015 9th European Conference on Antennas and Propagation (EuCAP)*. IEEE, 2015, pp. 1–5.